

**Multidisciplinary Study of Geological
Processes on the North East Atlantic and
Western Mediterranean Margins**

Preliminary results of geological and geophysical investigations during
the TTR-9 cruise of *R/V Professor Logachev*
June-July, 1999

Editors: N.H. Kenyon
M.K. Ivanov
A.M. Akhmetzhanov
G.G. Akhmanov

The designations employed and the presentation of the material in this publication do not imply the expression of any opinion whatever on the part of the Secretariats of UNESCO and IOC concerning the legal status of any country or territory, or its authorities, or concerning the delimitation of the frontiers of any country or territory.

**For bibliographic purposes, this document
should be cited as follows:**

Multidisciplinary Study of Geological Processes on the
North East Atlantic and Western Mediterranean Margins
IOC Technical Series No. 56, UNESCO, 2000
(English)

Printed in 2000
by the United Nations Educational,
Scientific and Cultural Organization
7, place de Fontenoy, 75352 Paris 07 SP

Printed in UNESCO's Workshops
SC-2000/WS/56
© UNESCO 2000
Printed in France

TABLE OF CONTENTS

	page
ABSTRACT	iii
ACKNOWLEDGEMENTS	iv
INTRODUCTION	1
METHODS	5
I. FAEROE MARGIN (Leg 1)	9
I.1. Introduction	9
I.2. Mass flow studies	10
<i>I.2.1. Seismic and acoustic investigations</i>	10
<i>I.2.2. Core studies</i>	15
I.3. Current-induced bedform studies	21
<i>I.3.1. Acoustic investigations</i>	21
<i>I.3.2. TV-seabed inspection</i>	24
<i>I.3.3. Bottom sampling results</i>	24
I.4. Conclusions	25
II. ROCKALL TROUGH (Leg 1)	27
II.1. Geophysical surveying & geochemical analysis with respect to thermogenic gas escape north-east of George Bligh Bank	27
<i>II. 1.1. Introduction and background</i>	27
<i>II. 1.2. Results and discussion</i>	28
<i>II. 1.3. Summary</i>	34
II.2. Seabed geotechnical and biogeochemical survey in the eastern Rockall Trough	35
<i>II. 2.1. Introduction</i>	35
<i>II. 2.2. Results</i>	36
<i>II. 2.3. Summary</i>	40
III. PORTUGUESE MARGIN (Leg 2)	42
III.1. Introduction	42
III.2. Seismic and acoustic data	42
<i>III. 2.1. Area west of Porto</i>	42
<i>III. 2.2. Area west of Lisbon</i>	49
III.3. Bottom sampling	51

IV. GULF OF CADIZ/MOROCCAN MARGIN (Leg 2)	56
IV.1. Mud diapirism and mud volcanism study	56
<i>IV.1.1. Introduction and geologic setting</i>	56
<i>IV.1.2. Seismic data profiling</i>	57
<i>IV.1.3. Sidescan sonar data</i>	59
<i>IV.1.4. Bottom sampling results</i>	67
<i>IV.1.5. Conclusions</i>	73
IV.2. Mediterranean undercurrent short study	73
V. ALBORAN AND SOUTH BALEARIC BASINS (Leg 3)	76
V.1. Objectives and geological setting	76
V.2 Alboran basin (diapiric province)	79
<i>V.2.1. Seismic data</i>	79
<i>V.2.2. Sidescan sonar data</i>	82
<i>V.2.3. Bottom sampling results</i>	85
V.3 South Balearic basin: the Palomares and Mazarrón margins	91
<i>V.3.1. Seismic data</i>	91
<i>V.3.2. Sidescan sonar data</i>	95
<i>V.3.3. Bottom sampling results</i>	98
V. 4. Conclusions	99
REFERENCES	100
ANNEXE I: CORE LOGS	
ANNEXE II: LIST OF TTR-RELATED REPORTS	

ABSTRACT

A number of topics related to slope processes, tectonics, and diapirism in different locations on the North East Atlantic margin and in the Mediterranean Sea were the focus of investigations conducted during the 9th UNESCO/IOC cruise of RV *Professor Logachev*.

The new seismic data confirmed the presence of a buried slump complex of presumably Plio-Pleistocene age at the central western margin of the Faeroe-Shetland Channel, as was reported from the TTR8 cruise (Kenyon et al., 1999). The acoustic records and core data from Leg 1 of the TTR9 cruise proved that slope instability of the eastern Faeroe margin is more widespread than previously thought.

A wide range of mainly longitudinal current induced bedform types has been observed, representative of both low and high bottom current speed. A sandy top seen in all cores also confirms generally enhanced bottom current activity in the area. Further evidence for strong current activity is provided by the very coarse lag deposits found in the area of the steep escarpments in the southern part of the area. Investigations of these lag deposits showed a high percentage of non-basaltic material indicative of a non-Faeroes origin.

Studies on the Irish margin of the eastern Rockall Trough showed that the lower slope is dominated by canyon system channels with intervening seabed showing evidence of instability and contour-current activity. Moderate currents exist capable of limited seabed erosion in exposed places. The upper slope is subject to a much more rigorous current regime with no discernible preferred direction. The currents have eroded considerable quantities of the silty clay seabed to generate an upper (>c.30cm) layer of sandy gravel with common cobbles and occasional boulders causing a hazard to deployed equipment.

The existence of contourite deposits on the deep Portuguese margin west of Porto, one of the primary targets of the study during Leg 2, was not fully confirmed. Potential areas were only recognised north and west of the Vigo Seamount, and in the basin located between the continental slope and the Porto Seamount based on data collected from the 3.5 kHz profiler.

Acquisition of additional seismic and sidescan sonar data broaden the existing TTR8 OKEAN long-range sidescan sonar coverage and showed the development of the canyon system basinward. The Setubal canyon was found to be the most active conduit of terrigenous material to the Tagus abyssal plain.

Data collected during Leg 2 in the Gulf of Cadiz allowed identification of three regions of mud volcanism and diapirism: Western Moroccan Field (WMF), Middle Moroccan Field (MMF) and Eastern Moroccan Field (EMF). In the MMF, OREtech sidescan sonar data, grab samples and gravity core samples confirm the existence of two mud volcanoes, (Yuma and Ginsburg). Methane hydrates (clathrates) were recovered from Ginsburg. In the EMF, gravity core samples confirm the existence of three mud volcanoes (Kidd, Adamastor, TTR) and seismic and sidescan sonar data suggest that there are at least five more mud volcanoes and four diapiric ridges.

One underwater TV line obtained from the northeastern slope of the Gulf showed the character of the seabed within a contour current channel which is an active pathway for basinward sand transport.

During Leg 3, surveys in selected sectors of the Alboran and South Balearic basins in the Western Mediterranean Sea, a new mud volcano (Granada) associated with a mud diapir field was discovered on the Moroccan margin of the Alboran Sea.

OKEAN imagery obtained on the Balearic basin showed a variety of processes taking place. Basement outcrops, canyon systems and slope instability features were successfully mapped.

Samples of hard rocks dredged on some outcrops provided a valuable source of information on the age and origin of the basement in the Alboran and Balearic basins.

ACKNOWLEDGEMENTS

The ninth Training-Through-Research Cruise became a reality due to financial support from various sources, among which were: the Intergovernmental Oceanographic Commission (IOC) of UNESCO, the Faeroes GEM Network, STATOIL Exploration (Ireland) Ltd., STATOIL (UK) Ltd., Instituto Geologico e Mineiro (Portugal), Southampton Oceanography Centre (UK), the US Naval Research Laboratory, Instituto Andaluz de Ciencias de la Tierra (CSIC and University of Granada) through the Spanish government project MAR98-0981 (CICYT-CYTMAR), the Russian Ministry of Science and Technological Policy, the Polar Marine Geological Exploration Expedition of the Russian Ministry of Natural Resources and Moscow State University (Russia). Logistic support was provided by the Netherlands Institute for Sea Research.

A number of people from different organizations supported the Training-Through-Research Programme and were involved in the cruise preparation. The editors would like to express their gratitude for the contributions made by Prof. I. F. Glumov (Ministry of Natural Resources of the Russian Federation), Dr. P. Bernal (Executive Secretary, IOC), Dr. A. Suzyumov (UNESCO), and Mr. V. Zhivago (Ministry of Science and Technological Policy of the Russian Federation).

Credits also should be given to Dr. M. Rietveld of the Netherlands Institute for Sea Research and Prof. Dr. B. A. Sokolov (Moscow State University) for administrative support.

Thanks are due to the administration and staff of the Polar Marine Geological Exploration Expedition (St. Petersburg) for their co-operation and assistance with the cruise organization. Captain A. Arutyunov and the skilful crew of the R/V *Professor Logachev* are thanked for successfully carrying out the operations at sea.

Staff and students of the UNESCO-MSU Marine Geosciences Centre were very instrumental in processing the acoustic data and the preparation of figures.

INTRODUCTION

M. IVANOV, T. NIELSEN, N.H. KENYON, J. MONTEIRO, J. GARDNER AND M. COMAS

Since 1990, the Floating University programme of UNESCO/IOC continues to benefit from the advantages provided by combining the training of students and young scientists with the advanced research in the field of marine geosciences. The 9th Training-Through-Research Cruise took place onboard RV *Professor Logachev*, owned by the Ministry of Natural Resources of the Russian Federation. The large size of the ship and a wide range of equipment available onboard for marine geoscientists make her very suitable for the purposes of the TTR programme and this cruise was the fourth one that the programme has undertaken on this vessel. An international team of 82 scientists, post-graduate and undergraduate students, and technicians from 11 countries (Algeria, Denmark, Ireland, Italy, Morocco, the Netherlands, Portugal, Russia, Spain, UK and USA) was involved in studies of a number of topics related to slope processes, tectonics, and diapirism in different locations on the North East Atlantic margin and in the Mediterranean Sea (Fig. 1).

During the cruise, 55 single and multichannel seismic lines with a total length of 1500 km were shot simultaneously with the OKEAN sidescan sonar survey and 3.5 kHz hull-mounted profiling. The OREtech deep-towed system survey was conducted along nine lines with a total length of 110 km. A deep-towed TV system was used in seven runs with a total length of 20 km. A bottom sampling programme included 100 sampling sites.

The first half of Leg 1 of the cruise (June 10-28; Den-Helder - Porto) was devoted to investigations of southeastern Faeroe margin which continued the study of slope instability processes carried out here in 1998 during the TTR8 cruise. The other task was to study distribution of coarse-grained material and seabed processes related to the strong bottom current of the Norwegian Sea Overflow Water in the Faeroe-Shetland Channel. The second half of the leg was spent in the northern Rockall Trough where TTR conducted geophysical and geochemical surveys with respect to thermogenic gas escape north-east of George Bligh Bank. Another seabed geotechnical and biogeochemical survey was undertaken on the Irish margin.

During the first half of Leg 2 of the cruise (June 30 – July 16; Porto - Cadiz) TTR was working on the Portuguese continental margin where we were looking at the distribution of the contourites and sediment drifts west of Porto and continued the study of a canyon system west of Lisbon, began in 1998. The second half of the Leg was devoted to a study of the tectonic framework and evolution of the area to the west of the Strait of Gibraltar based on sidescan sonar imagery and ground-truthing information in the form of sediment cores as well as sub-bottom information for the mud volcanic structures in the Gulf of Cadiz.

Leg 3 (July 17 – July 27; Cadiz - Valencia) dealt with various scientific problems to be solved in the Alboran Sea and South Balearic basins. Among them were:

- Development of a mud-diapir province recognized from seismic profiling data in the West Alboran basin;

- The nature and age of volcanic edifices forming residual or structural highs within the Alboran basin;

- The nature and petro-structural characteristics of the basement of the Alboran basin;

- The geometry and kinematics of tectonic lineaments and their relationship with the seafloor morphology in actively deforming sectors in the eastern Alboran basin and western South Balearic basin

- Submarine channels, supposed to be related to the above mentioned lineaments, bedforms, sediment type, and slope stability;

The report presents a significant amount of data obtained during the cruise. Most of the interpretations are preliminary although part of the post-cruise work is also included.

Comprehensive reports from other TTR cruises are available within the series of UNESCO Reports in Marine Science (Nos. 56, 62, 64, 67 and 68) and IOC Technical Series (Nos. 48, 52 and 54). Scientific results of the cruise are partially presented in abstract books of the post-cruise meetings pub-

lished in UNESCO's *Marinf* series (Nos. 91, 94, 99, 100) and in IOC Workshop Report series (Nos. 129, 143, 168) (Annexe II).

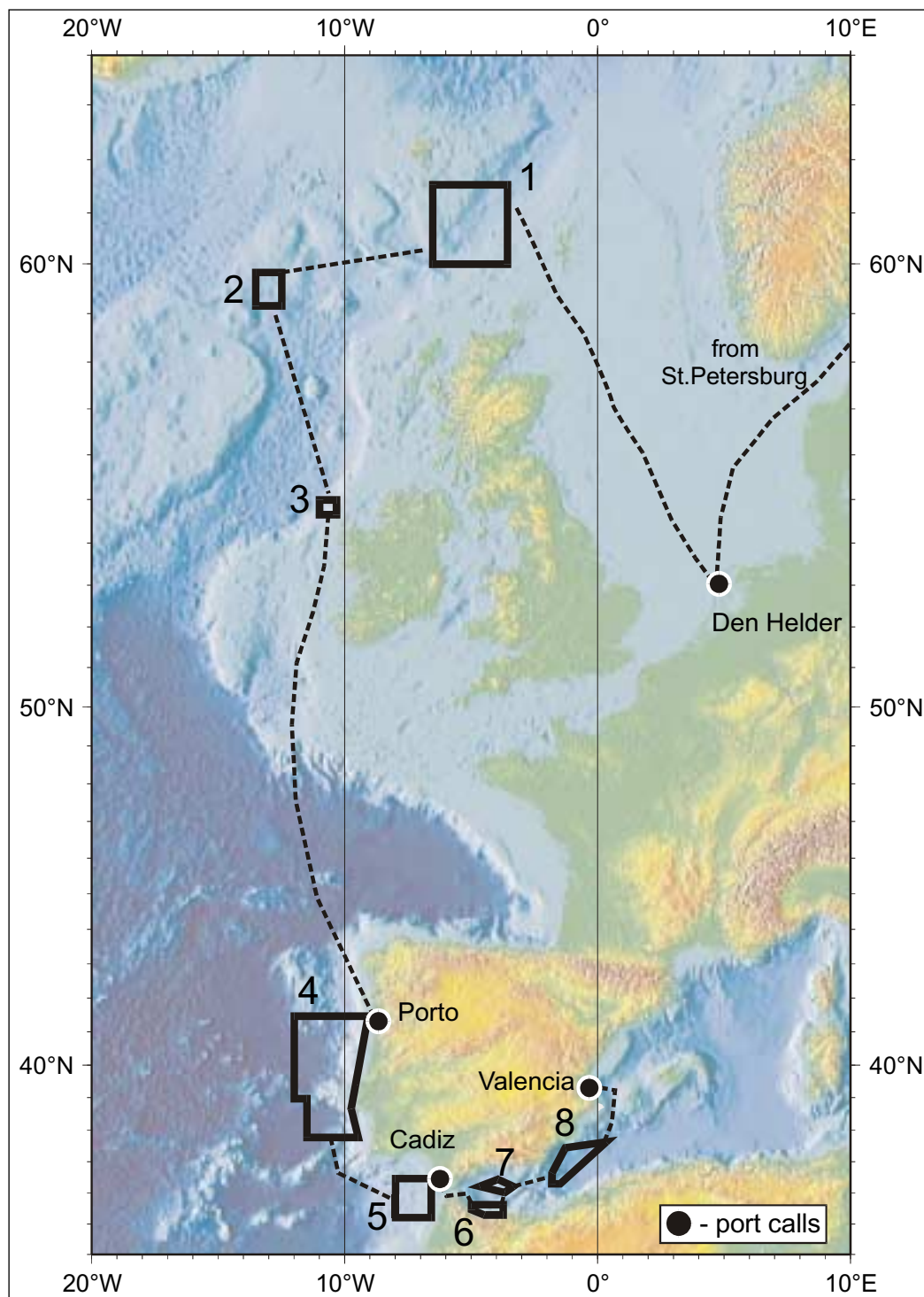


Figure 1. Location map of the TTR-9 cruise.

1 - Southeastern Faeroe Margin (Leg 1); 2 - Northern Rockall Trough (Leg 1); 3 - Eastern Rockall Trough (Leg 1); 4 - Portuguese margin (Leg 2); 5 - Gulf of Cadiz (Leg 2); 6,7 - Alboran Sea (Leg 3); 8 - Southern Balearic basin (Leg 3).

**List of the participants of the 9th Training-Through-Research international cruise
of the R/V *Professor Logachev* in the northeast Atlantic within the UNESCO/IOC
"Floating University" Programme, June 10 - July 27, 1999**

			Leg
ALGERIA	Lies Lakhal	Astrophysics, astronomy and geophysics research Centre (AAGRC), Bouzareah	3
DENMARK	Tove Nielsen*	Geological Survey of Denmark and Greenland (GEUS)	1
	Anders Madsen	University of Copenhagen	1
	Antoon Kuijpers	GEUS	1
	Trier Pedersen	GEUS	1
	Malene Rank	GEUS	2
IRELAND	Andy Wheeler*	University College, Cork	1
ITALY	Adriano Mazzini	University of Genoa	1
MOROCCO	Naima Hamoumi	Mohamed V University, Rabat	3
THE NETHERLANDS	Tine Svaerborg	Netherlands Institute for Sea Research (NIOZ)	1
	Robert Janus	Marine Geological Group, Utrecht	2
	Robin Koelewijn	Free University of Amsterdam	3
	Irene Zeldenrust	Free University of Amsterdam	3
	John Woodside	Free University of Amsterdam	3
PORTUGAL	Jose Monteiro*	Instituto Geologico e Mineiro	2
	Fatima Teixeira	Instituto Geologico e Mineiro	2
	Rosa de Freitas	University of Aveiro	2
	Francisco Teixeira	Instituto Geologico e Mineiro	2
	Tiago Cunha	Instituto Geologico e Mineiro	2
	Tiago Alves	University of Manchester	2
	Luis Pinheiro	Instituto Geologico e Mineiro	2
	Monica Felicio	University of Oporto	2
	Ana Hilario	University of Oporto	2
RUSSIA	Alexandr Arutyunov	Polar Marine Geological Exploration Expedition (PMGEE)	1 2 3
	Alexandr Zakharov	PMGEE	1 2 3
	Alexey Krotov	PMGEE	1 2 3
	Viktor Ivanov	PMGEE	1 2 3
	Alexandr Machulin	PMGEE	1 2 3
	Evgeny Samsonov	PMGEE	1 2 3
	Igor Tyunyak	PMGEE	1 2 3
	Gennady Antipov	PMGEE	1 2 3
	Irina Antipova	PMGEE	1 2 3
	Victor Sheremet	PMGEE	1 2 3
	Valentin Konfetkin	PMGEE	1 2 3
	Victor Sidorchuk	PMGEE	1 2 3

	Alexandr Plakhotnik	PMGEE	1 2 3
	Sergey Luybimov	PMGEE	1 2 3
	Alexandr Ivanov	PMGEE	1 2 3
	Alexandr Marakulin	PMGEE	1 2 3
	Vyacheslav Gladyshev	PMGEE	1 2 3
	Alexey Nazarov	PMGEE	1 2 3
	Alexandr Nescheretov	PMGEE	1 2 3
	Michael Ivanov	Moscow State University (MSU)	1 2 3
	Alexey Bobrov	MSU	1 2 3
	Alexandr Grachev	MSU	1 2 3
	Alexey Gongalsky	MSU	1 2 3
	Sergey Buryak	MSU	1 2 3
	Vasily Tokmenko	MSU	1 2 3
	Vladislav Malin	MSU	1 2 3
	Elena Zyrianova	MSU	1 2 3
	Pavel Shashkin	MSU	1 2 3
	Anna Volkonskaya	MSU	1 2 3
	Nikolay Amelin	MSU	1 2 3
	Evgeny Petrov	MSU	1 2 3
	Grigorii Akhmanov	MSU	1 2 3
	Andrey Akhmetzhanov	MSU	1 2 3
	Elena Kozlova	MSU	1 2 3
	Alexander Sautkin	MSU	1 2 3
	Alexey Sadekov	MSU	1 2 3
	Dmitry Ovsyannikov	MSU	1 2 3
	Ellina Suslova	MSU	1 2 3
	Alina Stadnitskaya	MSU	1 2 3
	Irina Belenkaya	MSU	1 2 3
	Dmitry Goncharov	MSU	1 2 3
	Yulya Volkova	VNII Okeanologiya, St. Petersburg	1 2 3
	Leonid Mazurenko	University of St. Petersburg	1 2 3
SPAIN	Asrarur Rahman Talukder	University of Granada	3
	Menchu Comas Minondo*	University of Granada	3
	Francisca Martinez Ruiz	University of Granada	3
	Juan-Manuel Fernandez Soler	University of Granada	3
	Juan Ignacio Soto Hermoso	University of Granada	3
	Jose Miguel Azanyin Hernandez	University of Granada	3
	Mario Sanchez Gomez	University of Granada	3
	Javier Prades Vilarroya	University of Granada	3
	Abel Zahinos Ruiz	University of Granada	3
	Guillermo Booth	University of Granada	3
	Jorge Gutierrez Meseguer	University of Granada	3
UK	Neil Kenyon*	Southampton Oceanography Centre (SOC)	2
	Marianthi Lavrentaki	SOC	2
	Najeeb Rasul	SOC	2
	Daniel Dixon	SOC	2
USA	Joan Gardner	US Naval Research Laboratory	2 3

- co-chief scientists

METHODS

VESSEL

The RV *Professor Logachev* is a Russian 104.5m marine geology research and survey vessel equipped with seismic and seabed sampling equipment. She is operated by the State Enterprise “Polar Marine Geological Exploration Expedition”, St. Petersburg. The vessel has: a draught of 6.66m, width of 16m, net tonnage of 1351 ton, displacement of 5700 ton and is powered by two 3500 hp diesel engines.

EQUIPMENT

Most of the equipment available onboard has been already described in details in the previous reports e.g. Kenyon et al. (1998). This chapter will give a brief overview of the methods used. Where some of the equipment was used for the first time a more detailed description is provided.

Seismic profiling was carried out simultaneously with OKEAN 10 kHz long-range sidescan sonar. Two seismic systems were used; a single-channel one was the same as in the 1998 cruise and a multi-channel system is described below. At selected areas where higher resolution of the seabed features was considered necessary, an OREtech deep-towed sidescan sonar operating at 30 or 100 kHz frequencies and equipped with a 5 kHz subbottom penetrating echosounder was employed. Bottom samples were retrieved using a large diameter gravity corer, PREUSSAG TV-controlled grab, a box corer and a dredge. Hull-mounted 3.5 kHz profiler was routinely used during most of the above operations with a continuous paper output and a selective recording of the digital data.

Navigation

A. WHEELER, G. ANTIPOV AND E. KOZLOVA

Positioning of the ship is acquired using an Ashtech GG24 GPS + GLONASS receiver. The use of both the GPS and GLONASS satellite configurations allows a far greater accuracy than is available from conventional GPS alone, with up to 60% greater satellite availability. Positions are calculated in real-time code differential mode with 5 measurements per second and an accuracy of +/- 35cm (75cm at 95% confidence limits) with optimal satellite configuration. Realistic positioning accuracy under normal satellite configuration for European waters is assumed as c. 5m. Positioning when the vessel is moving also utilises Doppler velocity determinations from the differential code signal to generate a vessel speed accuracy of 0.04 knot (0.1 at 95% confidence limits) with optimum satellite configuration.

The GPS + GLONASS receiver is located centrally on the vessel with accurate levelling to sampling and equipment deployment positions on the vessel allowing precise back navigation. Seabed sampling positions with the gravity corer, box corer and kasten corer is normally 5% of the accuracy of the vessel position due to their rapid deployment. OREtech sidescan, OKEAN sidescan, TV controlled grab and deep-tow video system are all fitted with a pinger allowing precise navigation between the vessel and sub-sea surface position. This is necessary as deep-towed equipment is subject to greater spatial differences with respect to the vessel. This underwater navigation is based on the Sigma-1001 hydroacoustic system. Four stationary aerials, spaced 14m apart, are hull mounted and receive acoustic signals from pingers attached to deployed equipment in short-base mode operating between 7-15 kHz. The signal emitted by the sub-surface pinger is tracked on board and accurate x,y positioning of the device relative to the vessel is computed taking into account vessel roll, trim and ship's speed. Accurate level of the GPS + GLONASS antennae with the hull mounted transducers allows precise positioning of deployed equipment. Error positioning of this method usually does not exceed 1-2% of water depth.

Multi-channel Seismic System

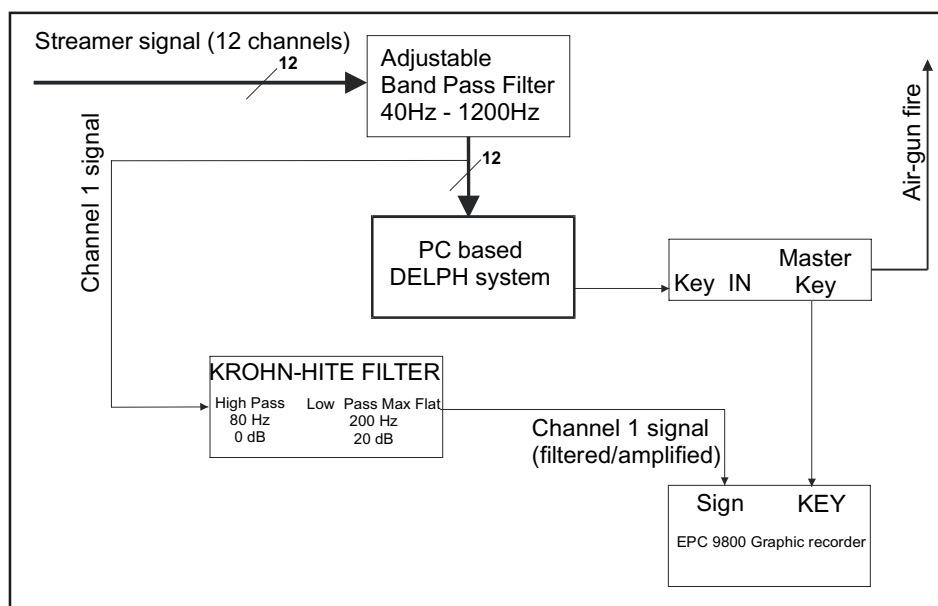
In the area west of Portugal both single-channel and multi-channel seismic reflection data was acquired, respectively using the on-board Russian system and the Dutch system of the Netherlands Institute of Applied Geoscience (TNO). Due to a signal amplification problem on the Dutch system, seismic data acquisition was only possible from line PSAT 103 onwards. For the same reason, the Russian system was used from line PSAT 103 to line PSAT 108, being replaced by the Dutch system onwards until the conclusion of the survey on the western Portuguese Margin. A mixed solution was considered using the Russian airgun with the Dutch acquisition system, but this solution was soon abandoned due to differences on the frequency ranges of the airgun source. The Russian airgun produces low frequency sound waves, ranging around 100 Hz, not appropriate for the Dutch acquisition system, with consequent losses for the overall resolution of the obtained data. This report describes the configuration of the Dutch system as the Russian system is described elsewhere

Equipment Configuration

R. JANUS, F. TELXEIRA

A summarised description of the seismic equipment is presented below.

Power Supply: A current stabiliser of high quality with galvanic isolation is used. This system is based on a 220/220V transformer and adjacent coils/ capacitors, assuring the elimination of unwanted



Block-diagram showing the mulichannel seismic data acquisition system

components of the normal electricity network on the ship.

Sound Source: The energy source consisted of a TEXAS INSTRUMENTS sleeve-gun with an air chamber of 10 cubic-inches, working with a total air-pressure of 120 bar.

Receivers: A 12-channel *streamer* with 150 m length and a channel spacing of 12.5 m was used on the survey. Initially, the *streamer* was placed at a depth of 2.5 m, using a hydrodynamic controlling system attached to the *streamer* (birds). An extreme high level of ship's noise was introduced into the *streamer* through the 150 m towing cable.

Filters: The band-pass used for the 12 channels on the analogic filter was 40 Hz to 1200 Hz. The low-cut frequency of the filter is established in order to eliminate the very low-frequency noise components (10 to 20 Hz) derived from voltage generated by acceleration of the hydrophone elements. The anti-alias filtering is automatically assured by the DPS in relation to the pre-established sample frequency. This way, the DPS produces an analogic filtering with a high-cut similar to 1/3 of the sample

frequency. This assures that the higher signal frequency will be inferior to the Nyquist frequency.

Data Acquisition System Elics/Triton DELPH: The sampling and digital record of the data was made by the DELPH system, constituted by S/W running on a PC computer with Windows 95, and a full-length Signal Processing Board (DSP) installed on the PC. To allow the simultaneous signal acquisition of all the streamers' 12 channels, two additional boards with six input connectors each are installed on the PC. These assure the interface between the seismic acquisition channels and the DSP of the DELPH program. The data can be saved in the PC internal hard disk or on compatible *Exabyte 8500* drive. Alternatively, an external JAZ drive with a SCSI interface can be also used. The acquisition process timing (*sleeve-gun* shot, EPC key, oscilloscope triggering) is controlled by the DELPH program. The PC signal is transmitted into a separate equipment unit that triggers the sleeve-gun (24 V) and EPC (5 V) with the appropriate signal.

Acquisition and Data Recording

Data Recording: At the same moment as it is acquired, the data is simultaneously printed on a thermic EPC 9800 recorder and saved in a digital format in the PC hard disk drive, or using any of the JAZ or *Exabyte* tape drives. During the survey, due to reading problems on the Exabyte drive, the data was temporarily saved in the hard disk and later recorded on JAZ drives. In order to obtain multiple copies of the seismic lines, assuring a backup version of each line in case of problems, the files were systematically saved on CD-ROM.

Main Parameters: A sampling frequency of 2000 Hz was used for a sampling window of 2 seconds. The main parameter controlled by the DELPH is the *Acquisition Delay* that should be adjusted in relation to the sea-bottom depth variations. Other parameters like the *Display Gain* for each channel, the AGC (*Automatic Gain Control*) and the *Cut-Off Frequencies* of the digital filter are pre-established and unchanged during the acquisition. The scale and the delay on the EPC recorder must be changed according to the depth variations. The signal obtained from the *streamer's* channel 1 was immediately used after the pre-filtering/analogic amplification and extra amplification to give the signal to the EPC recorder. Due to this fact, the amplitude of the received signal on this channel is usually attenuated. Using a superior value of display gain in this channel solved the problem.

Digital Filters: The band-pass used on the DELPH filter ranged from 40 Hz to 320 Hz. This frequency range was pre-established after the first acquisition tests, when it was verified that *low-pass cut-off filter* values above 320 Hz resulted in a substantial increase of the noise. On the other hand, the *high-pass cut-off filter* is not useful in eliminating the low-frequency components, it being necessary to use a pre-filtering with the analogue filter. With the selected parameters, the 50Hz component derived from the alternating electric current used by the seismic equipment was not eliminated, as can be seen on the recorded signal.

Seismic Data Processing

L. PINHEIRO

Whilst on board, all the Dutch seismic lines were processed using only one of the 12 channels, because of lack of time and disk space (failure of an external hard disk). Only one portion of line PSAT117 was fully processed, using the 12 available channels. For this line, both a stacked section and an F-K constant velocity migrated section were obtained, in which the signal-to-noise ratio and the quality of the final section were significantly improved. All the seismic lines will be fully processed at the Marine Geology Department of the Mining and Geological Institute, after the cruise. All the seismic data was processed on a Power-PC, using the SPW software (from Parallel Geoscience Corporation).

The processing sequence for the single channel data consisted of amplitude recovery by spherical divergence correction and Butterworth bandpass filtering. The bandpass filtering applied was generally between 80 and 200 Hz. Spectral whitening was also applied to compress the source wavelet and to compensate for different wavelength attenuation. However, the quality of the sections was not

improved, even after bandpass filtering, partially because of the poor signal-to-noise ratio of some of the seismic data..

Sampling Tools

Gravity cores

Coring was performed using two gravity corers: a c. 800 kg gravity corer with an internal diameter of 13.2 cm capable of retrieving 2.5 m of sediment and a 6 m long, c. 1500 kg one with an internal diameter of 14.7 cm.

One half of the opened core was described on deck paying particular attention to changes in lithology, colour and sedimentary structures. All colours relate to Munsell Colour Charts. The other half was measured for changes in magnetic susceptibility using a Bartington Instruments Magnetic Susceptibility meter with a MS2E1 probe. Magnetic susceptibility reflects the ease with which a material can be magnetised. This property is most strongly influenced by grain-size, heavy mineral content and is inversely related to carbonate content and diagenetic ferric mineral reduction.

Samples were also taken for coccolith and micropalaeontological assays from smear slides. This was done to generate a preliminary chronostratigraphy for the cores.

Box-cores

Box cores were taken using a Reineck box-corer with a 50 cm x 50cm x 50 cm box capable of retrieving 185kg of sample. Lowering and retrieving operations are taken using a hydraulic A-shaped frame with a lifting capacity of 2 tonnes.

Kasten Cores

Where retrieval of bottom sediments was not possible using the gravity corer or box corer due to large pebbles on the seabed and equipment loss, a kasten corer was used. This has internal dimensions of 0.39 m x 0.39 m x 1.80 m and is capable of retrieving a variety of sediments in an undisturbed form. When the corer was open, the surface of the core was photographed and then the sub-sampling procedure was employed. As with the box-cores, the opened core was described on deck paying particular attention to changes in lithology, colour and sedimentary structures.

Deep-tow video imagery

The deep-tow video system is housed within an open frame based on an OREtech design. It contains deep-sea pressure housings with electronic equipment such as a TV camera, lights and external storage batteries as well as an echo sounder and pinger for navigation purposes. The system produces colour images and is towed 2-8m above the seabed. The system uses a conventional SONY CCD-TR 640 E camera. The video was recorded in Video 8XR format (PAL mode).

I. FAEROE MARGIN (Leg 1)

I.1. INTRODUCTION

T. NIELSEN AND A. KUIJPERS

The western margin of the Faeroe-Shetland Channel area has been the subject of several geological investigations in the last decade. These studies have, however, mainly concentrated on the deeper geological structures (e.g. Boldreel and Andersen, 1993), while fewer studies have been directed towards the younger and upper parts of the geological strata (e.g. Waagstein and Rasmussen, 1975; Nielsen et al. 1981).

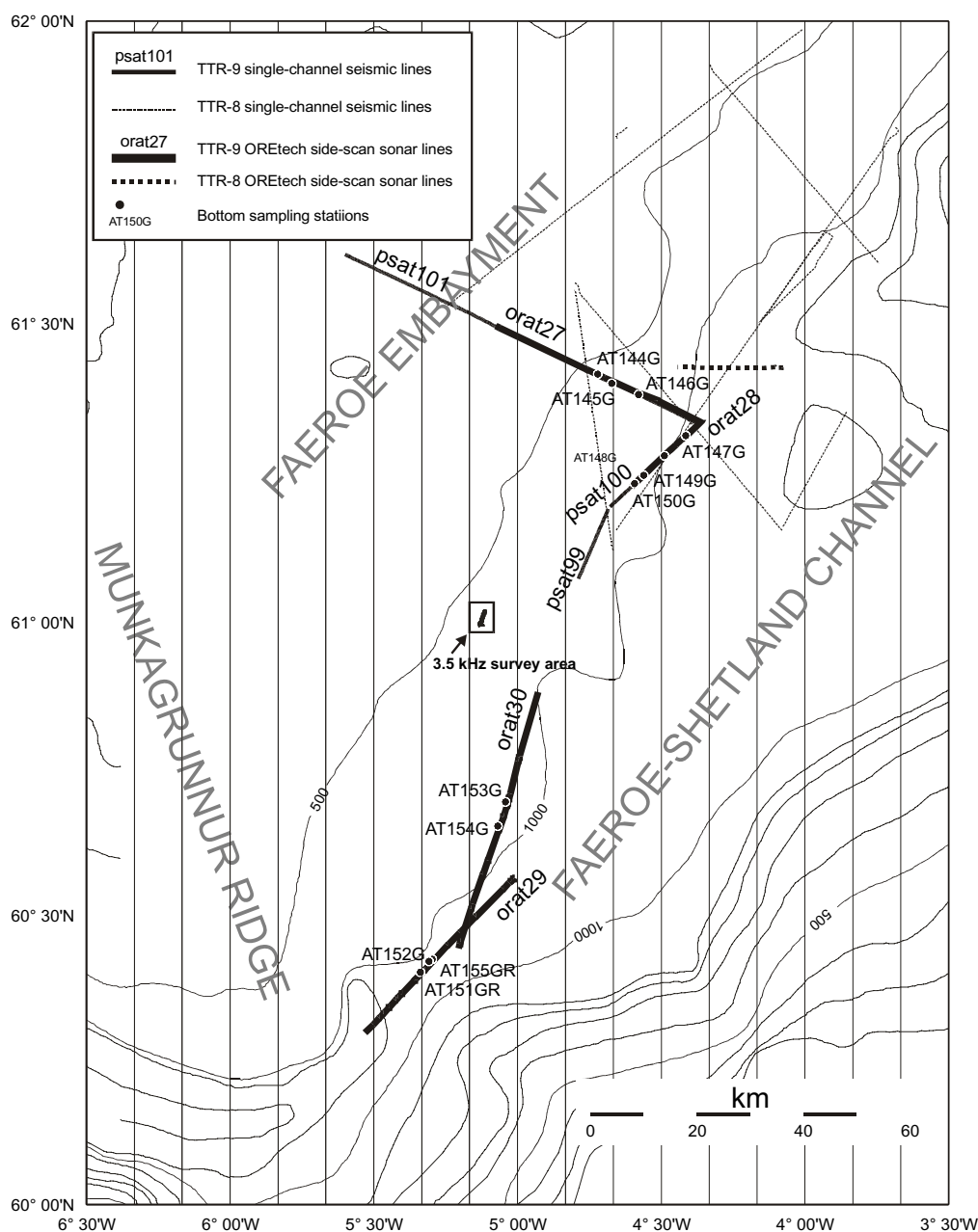


Figure 2. Track chart of the seismic and acoustic lines, also showing the location of the sediment sampling stations as well as regional setting of the southeastern Faeroe margin study area.

Although the Faeroe-Shetland Channel forms one of the main gateways for deepwater exchanges between the Nordic Seas and the North Atlantic Ocean (Hansen and Østerhus, 2000), very few studies have concentrated on current-induced bedforms in the area. For this purpose the western margin of the channel is of particular interest, as strong bottom currents transporting “Norwegian Sea Overflow Water” (NSOW) are known to run southwards along this margin.

The western margin of the Faeroe-Shetland Channel had been generally inferred to be stable, and no indications of slope instability were publicly reported until 1998 when several generations of mass flow deposits were described from the western margin of the channel during the TTR8 cruise.

The aim of the TTR9 investigations in the Faeroe-Shetland Channel (Fig. 2) was thus two-fold: 1) to further elucidate the mass flow deposits and their origin, and in particular to date the latest slope instability event on the western margin; and 2) to study current-induced bedforms in general, and more specifically at the southern outlet of the channel.

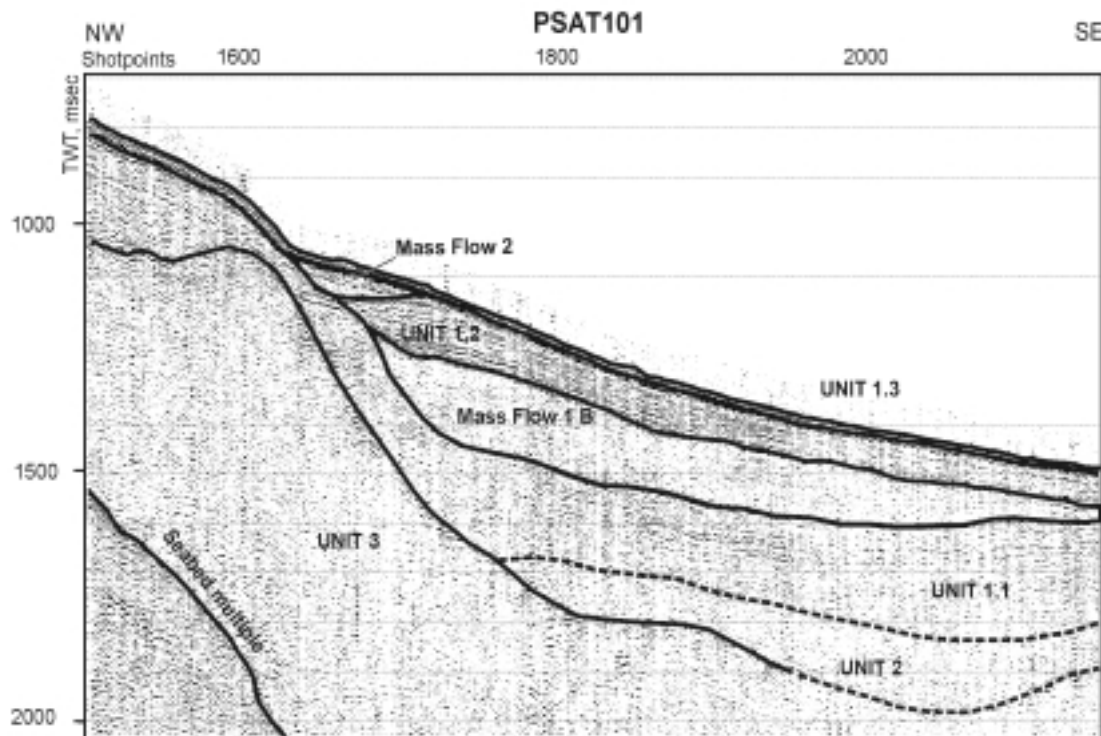
1.2. MASS FLOW STUDIES

1.2.1. Seismic and acoustic investigations

Seismic data

A. MADSEN, T. SVAERBORG, T. NIELSEN, A. VOLKONSKAYA, S. BURYAK

As a supplement to the TTR8 seismic survey carried out in 1998 in the central sector of the western margin of the Faeroe-Shetland Channel, 3 additional seismic lines with a total length of c. 90 km were run (Fig. 2), labelled PSAT-99, PSAT-100 and PSAT-101. A set-up similar to that of the 1998 seismic survey was used, i.e. a single channel airgun system, a shot interval of 10 sec, and an average survey speed of 6 knots. Processing included trim statics, before deconvolution and band-pass filter-



ing. Figure 3. Fragment of PSAT-101 showing the seismic expression of the western slope and basin of the Faeroe-Shetland Channel with Units 1, 2 and 3. The more transparent units are interpreted as different mass wasting events (Mass Flow 1 and 2).

Line PSAT- 99 and line PSAT- 100 were run in a SW direction, roughly parallel to the depth contours, at water depths in excess of 1000 m. Line PSAT-101 was run in a ESE direction, starting in the channel at c. 1100 m water depth and ending on the Faeroe shelf at c. 350 m water depth.

Three major seismic units were identified, labelled Unit 3 to 1 from below. Unit 1 was divided into six subunits, Unit 1.1 to 1.4, and Mass Flow 1 and Mass Flow 2 (Fig. 3).

Unit 3 forms the acoustic basement and is defined by a medium to strong amplitude reflector, which is continuous and undulating. The reflector has only been observed in the basin and on the slope, and could not be recognised on the shelf due to low penetration. Internal reflectors are either not visible or chaotic. Depth to the top of Unit 3 is between 1100-1200 ms TWT below sealevel on the slope, and dips eastward into the basin to 1900 ms TWT. At the intersection between PSAT- 99 and 100, Unit 3 forms a local high. Towards SSW on line PSAT- 99 in the basin area, the depth to the top of the unit shallows (1400 ms TWT), and comes close to the seabed.

The undulating nature of Unit 3 is thought to be the result of folding in relation to the Oligocene deformation phase proposed by Boldreel and Andersen (1993). The unit is found in the whole of the study area and is thought to be regional. It is tentatively given a Late Eocene-Oligocene age.

Unit 2 is recognised in the basin area, where it forms a partial fill of the surface of Unit 3. The top reflector of Unit 2 is slightly undulating and continuous, and of medium to high amplitude. It appears to have the same shape as the basal reflector. The internal reflector pattern on PSAT- 99 shows continuous parallel reflectors that are slightly undulating. However, on PSAT- 100 and 101 they appear more chaotic and transparent. On PSAT- 99 the internal reflectors onlap onto the topmost Unit 3 reflector, where this unit domes up and comes close to the seabed (Fig. 4). The unit is thickest in the basin (250 ms TWT) and thins out toward the slope.

Unit 2 is thought to be of Miocene age and is only distributed in the channel area. This is the

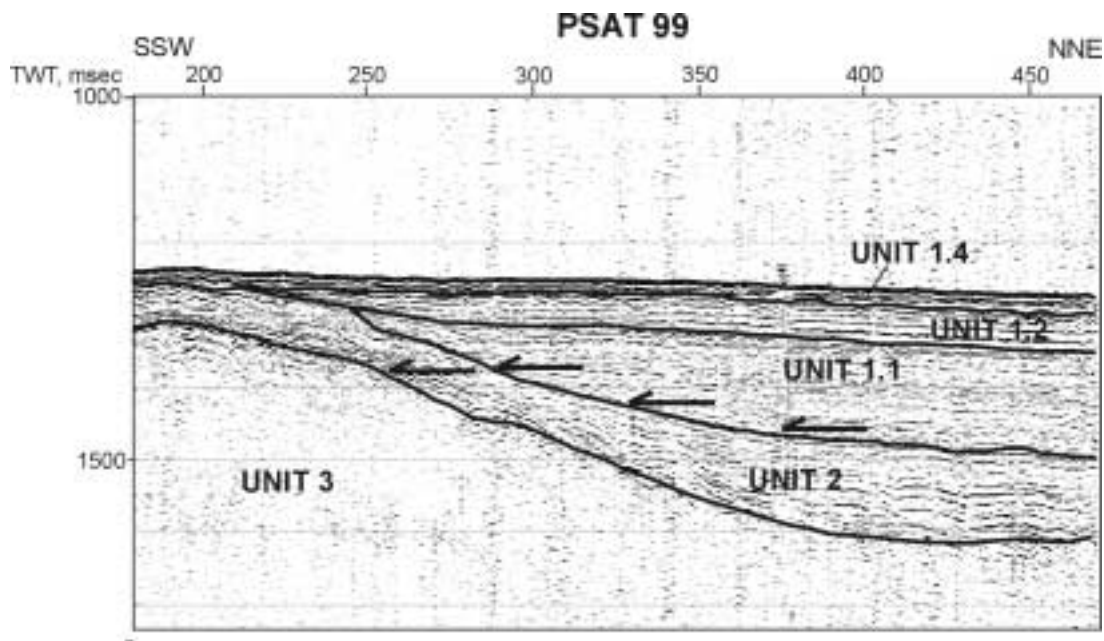


Figure 4. SSW end of PSAT-99 showing onlap of reflectors of Unit 2 and Unit 1.1 onto the high area of Unit 3.

result of the underlying Unit 3's topography that seems to have controlled the subsequent sedimentation. On PSAT- 99 the overlying units onlap onto Unit 2 creating an unconformity. This unconformity is likely to be coincident with a widespread unconformity seen in the surrounding area (Stoker, 1995; Kenyon et al., 1999), and is interpreted as a result of compression having occurred during the middle or late Miocene (Boldreel & Andersen, 1993).

Unit 1.1 fills the basin formed by Unit 2 and drapes the slope (Fig. 3). The unit differs from the surrounding units by its strong, continuous and parallel internal reflector pattern, which onlaps the top of Unit 2 on PSAT- 99 (Fig. 4). Here the unit also thins out and disappears. On PSAT- 101 the internal reflectors onlap Unit 3. The maximum thickness of 400 ms TWT of Unit 1.1 is located close to the steep part of the slope.

Mass Flow 1 is recognised on the seismic by a transparent to chaotic internal reflection configuration. The unit has a maximum thickness of 150 ms TWT and has a lens shaped geometry, which thins out toward the slope. On PSAT- 100 an internal, high amplitude reflector is observed, which separates Mass Flow 1 into two minor units, *Mass Flow 1A* and *1B* (Fig. 5). Towards the SE the unit thins out (17:20 on PSAT- 100).

Unit 1.2 has strong continuous and parallel internal reflectors. It overlies the Mass Flow 1 unit

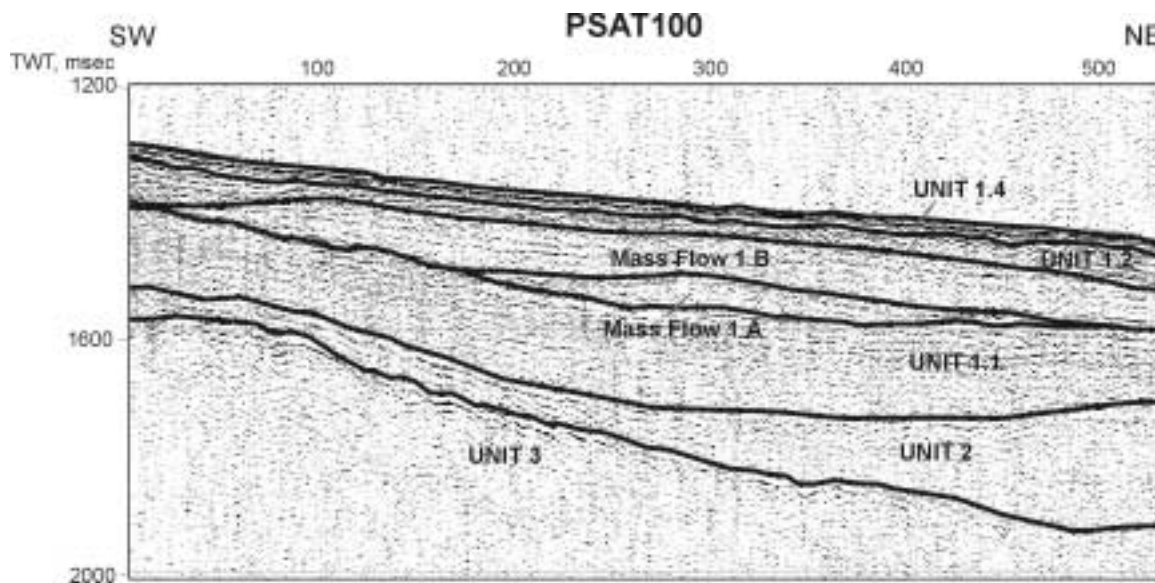


Figure 5. PSAT-100 showing the separation of the lens shaped Mass Flow 1 into events 1A and 1B.

on PSAT- 100 and 101, and Unit 1.1 on PSAT- 99, where it thins out toward the SSW (Fig. 4). The unit has an average thickness of 50-80 ms TWT.

Mass Flow 2 is recognised as a small transparent unit at the foot of the steep slope (Fig. 3). It has a lensoid shape with a maximum thickness of 50 ms TWT. A strong reflector bounds the top of Mass Flow 2. This reflector is the base of Unit 1.4.

Unit 1.3 is only recognised on the shelf on PSAT- 101. The base of this unit is not observed due to lack of penetration. Internally the unit appears transparent, but some weak, steeply dipping reflectors are observed. The tops of these reflectors show truncation. Toward the slope the dipping reflectors disappear, and the reflector pattern changes to a transparent configuration.

Unit 1.4 is the uppermost unit and is present in the whole of the study area. On the shelf it is c. 50 ms TWT thick, though the base of the unit is difficult to pick. On the slope and in the channel area the unit becomes thin (<20 ms TWT), and is often hidden by a strong seabed reflector which bounds the top of the unit. This seabed reflector shows an uneven nature on the shelf, but becomes more continuous downslope into the channel.

Unit 1 is considered to have a Pliocene to Recent age. Unit 1.1 is thought to be of Early Pliocene age. Post-dating Unit 1.1 are erosive debris flows, Mass Flow 1A and Mass Flow 1B. The triggering event of these two debris flows has not been determined, but is here interpreted to be associated with the onset of glacial conditions. Thus, the complete Mass Flow 1 unit is here attributed to the late Pliocene (Kenyon et al., 1999). Unit 1.2 post-dates Mass Flow 1 and is therefore thought to have a

Pleistocene age. Mass flow 2 is bedded in Unit 1.2 and is therefore thought also to be of Pleistocene age. The dipping reflectors of Unit 1.3 are thought to be associated with a prograding wedge system deposited during the Plio-Pleistocene period. As Unit 1.4 overlies the other subunits of Unit 1 and forms the seabed, it is thought to be of Pleistocene to Recent age. The minor mass wasting deposit (Mass Flow 2) found within Unit 1.4, indicates that the slope has been unstable also during the Pleistocene/Holocene period. The undulating nature of the seabed reflector on the shelf is interpreted as the result of iceberg ploughmarks (Kenyon et al., 1999).

OREtech sidescan sonar and onboard subbottom profiler data

T. NIELSEN, A. KUIJPERS, AND M. IVANOV

Repeating seismic line PSAT- 100 and 101, two lines were run using the OREtech deep tow sidescan sonar (ORAT-27 & 28) concurrently with the 3.5 kHz onboard subbottom profiler (PRAT-27 & 28). A range of 2 x 500 m and a frequency of 100 kHz was used for the sidescan sonar. Line ORAT-27/PRAT-27 was run in a ESE direction, starting on the Faeroe shelf at about 260 m water depth and ending in the Faeroe-Shetland Channel at about 1100 m water depth. Line ORAT-28/PRAT-28 was run in SW direction, roughly parallel to the depth contours, in water depths in excess of about 1000 m (Fig. 1).

The presence of widespread iceberg ploughmarks on the shelf down to more than 400 m water depth is indicated by a criss-cross backscatter pattern on the sidescan sonar image of line ORAT-27 (Fig. 6). In the same area the subbottom profile PRAT-27 shows no acoustic penetration and a rough and irregular seabed reflector. Further down the track the seabed smooths out and at the same place the gradient of the slope slightly increases.

The first clear evidence of downslope mass flow processes is observed on ORAT-27 at c. 20:00 GMT (Fig. 7) by virtue of a relatively high and variable backscatter pattern. A specific feature is an up to more than 100 m wide, downslope slightly sinuous channel, which may be a turbidity current path-

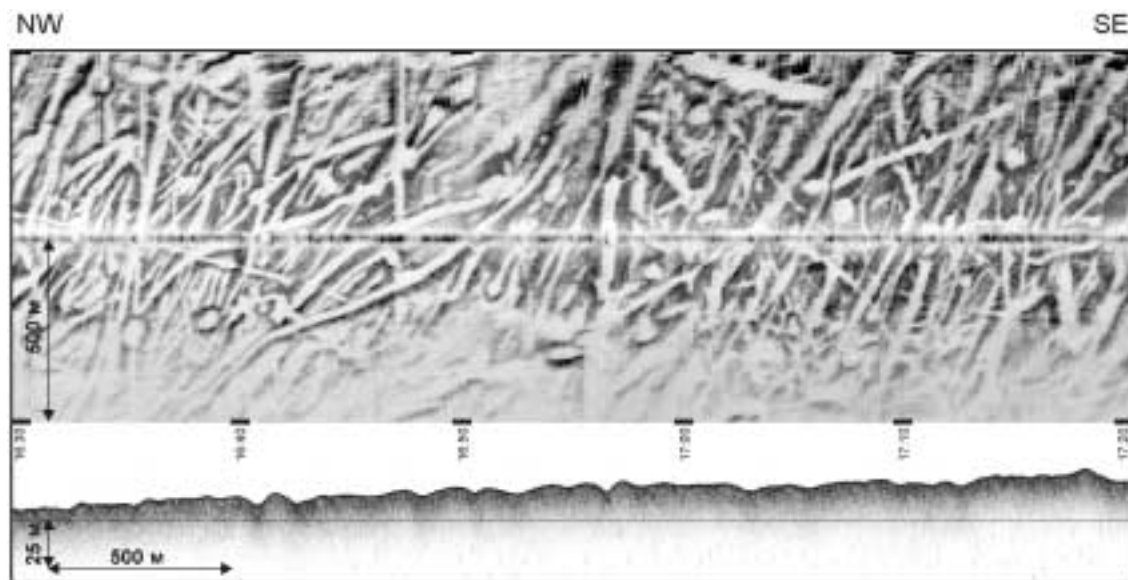


Figure 6. Fragment of OREtech line ORAT-27 and 7 kHz subbottom profiler records showing criss-cross pattern of iceberg ploughmarks on the shelf.

way (Fig. 7). A series of isolated small channels of similar dimension to this one, have also been found on the opposite slope of the Faeroe-Shetland Channel (Kenyon, 1987). In the area of mass flow deposits the onboard profiler record PRAT-27 shows no, or weak, penetration and a seabed morphol-

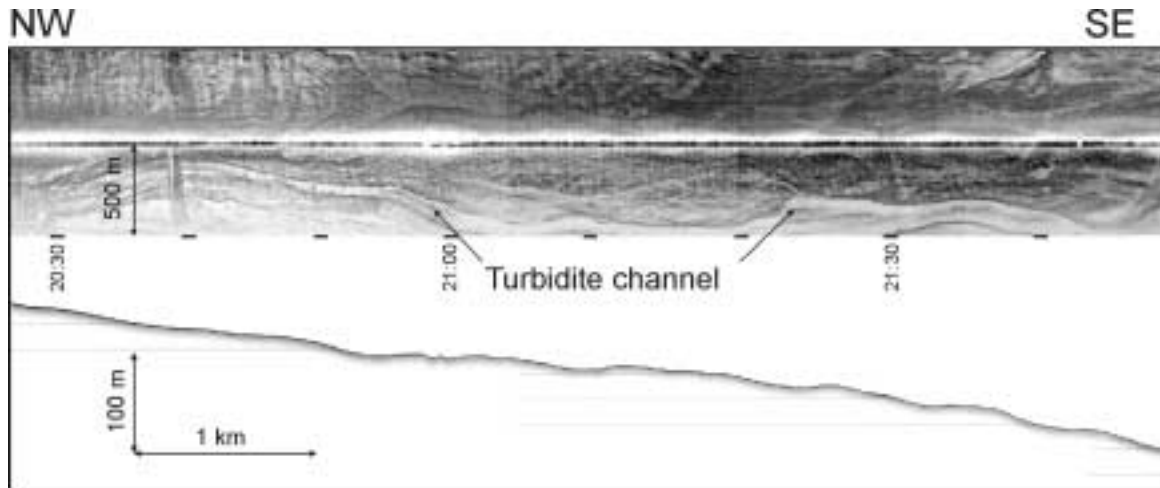


Figure 7. Sidescan sonar record and 7 kHz profile from ORAT-27 showing mass flow features and a presumed turbidite channel (low backscattering) on the slope.

ogy characterised by low relief, mound-like structures. The mass flow features extend down to c. 21:50 GMT, where the sidescan image reveals an area of relatively low backscattering sediments, and where the onboard profiler record shows acoustically laminated sediments with a thin surficial unit and a flat seabed. At about 23:30 GMT a gradual increase of backscattering occurs, and this may indicate the transition to generally coarser, or more compacted sediments. The backscatter pattern here also suggests some weak, unidentified seabed features with a predominantly NE-SW direction. Distinct black specks with little or no acoustic shadow also occur in this area, and may indicate patches of coarser material.

Line ORAT-28 was run in a SW direction, i.e. at a wide angle with respect to the transport direction of the mass flows. The sidescan record shows medium backscattering with very little variation along the line. Black specks, similar to those observed on the last part of line ORAT-27, occur frequently and randomly along the line. Narrow stripes of slightly stronger backscattering are visible from the beginning of the line until about 10:00 GMT. They display two dominant directions; one is WNW-

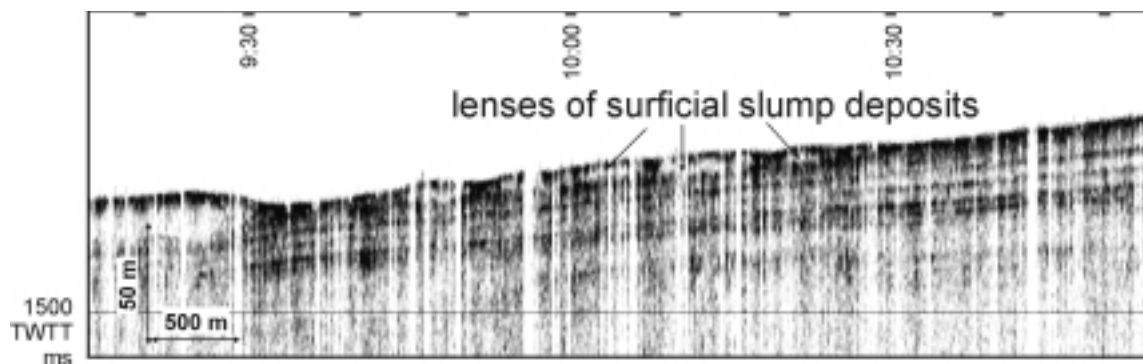


Figure 8. Fragment of 3.5 kHz hull-mounted profiler line PRAT-28 showing thin lenses of acoustically transparent surficial slump deposits overlying laminated sediments. The lens on the left appears to have an erosive base.

ESE and the other more W-E. These directions suggest a relation with the transport direction of the mass flows. The presence of slump deposits in the area is documented by the subbottom profile PRAT-28, which displays a wavy seabed morphology along most of the line until 10:30 GMT. The individual mass flow deposits are characterised by thin, acoustically transparent units of limited extent (Fig. 8). These look like the crosssections of glacial debris flows as described by, for instance, Vorren et al (1998). The sidescan sonar imagery from the last part of the line, from 11:00 GMT, shows a more uni-

form backscatter pattern with less frequent black specks. This is an area without superficial slump deposits, where the subbottom profiler reveals a seabed of laminated sediments (Fig. 8)

Line ORAT-30/PRAT-30 is located in the southern sector of the western margin of the Faeroe-Shetland Channel (Fig. 2). The line was run parallel to the depth contours in a SSW direction, in water depths in excess of 950 m. A frequency of 100 kHz and a 2 x 500 m range was used for the sidescan sonar, and a 3.5 kHz frequency for the onboard subbottom profiler.

From the start of the line until c. 8:00 GMT the onboard profiler record shows a flat seafloor. Hereafter until ca 18:00 GMT an undulating and up-doming relief appears. In the first part of the line until c. 13:00 GMT the profiler record shows penetration up to ca 20 ms, but apart from a few channel-like infills, no distinct layering is visible. This structureless character of the sub-seabed, together with the slightly elevated relief, was interpreted as providing evidence for the presence of mass flow deposits in this area. Hereafter and until c. 18:00 GMT penetration is less, but more continuous layering is observed and the seafloor is smooth.

The sidescan sonar record shows a generally low backscattering, which gradually increases along the line towards 18:00 GMT. The backscattering is relatively uniform, with frequent and random occurrence of black specks, with no visible acoustic shadow. These specks are similar to those observed on line ORAT-27 and ORAT-28, and are likewise expected to represent patches of coarser material. Although line ORAT-30 shows no clear indications of mass flow deposits, the similarity with ORAT-28 lead us to conclude that this may be an effect of wide angle between the ship's course and the transport direction of the mass flows.

1.2.2. Core studies

A. MAZZINI, T. PEDERSEN, A. KUIJPERS, G. AKHMANOV, A. AKHMETZHANOV, A. STADNITSKAYA, E. KOZLOVA, L. MAZURENKO, A. SAUTKIN, D. OVSYANNIKOV, A. SADEKOV, I. BELENKAYA, YU. VOLKOVA, E. SUSLOVA, AND D. GONCHAROV

Introduction

The Faeroe-Shetland Channel was sampled in two main areas (Fig.2). Seven gravity cores in the northern area (cores AT-144G - AT-150G), and 2 gravity cores in the central area (AT-153G - AT-154G). The total sediment recovery in this area was c. 30 m.

Technical information about the site parameters and their sedimentological, acoustic and geological characteristics are summarized in the Tables 1 and 2.

Figures 9 and 10 show a schematic illustration of the seabed along line ORAT-27 and the along slope transect of ORAT-28, respectively, together with the core sites and magnetic susceptibility trends.

Core No	Date	Time. GMT	Latitude	Longitude	Cable length. m	Depth. m	Recovery. cm
TTR9-AT144G	15.06.99	07:04	61° 24. 975'	04° 43. 280'	575	575	174
TTR9-AT145G	15.06.99	09:05	61° 24. 054'	04° 40. 307'	695	695	259
TTR9-AT146G	15.06.99	11:53	61° 22. 956'	04° 34. 731'	867	863	309
TTR9-AT147G	15.06.99	14:25	61° 18. 819'	04° 24. 896'	1063	1059	Unopened
TTR9-AT148G	15.06.99	16:14	61° 16. 794'	04° 29. 365'	1045	1043	349
TTR9-AT149G	15.06.99	18:18	61° 14. 850'	04° 33. 635'	1035	1032	384
TTR9-AT150G	15.06.99	19:22	61° 14. 006'	04° 35. 574'	1020	1020	420
TTR9-AT151GR	17.06.99	21:40	60° 24. 172'	05° 20. 287'	-	1196	0.5 tons
TTR9-AT152G	18.06.99	00:20	60° 25. 483'	05° 17. 837'	1060	1047	cc
TTR9-AT153G	19.06.99	02:02	60° 41. 692'	05° 02. 512'	925	916	405
TTR9-AT154G	19.06.99	03:49	60° 39. 226'	05° 04. 111'	923	910	330
TTR9-AT155GR	19.06.99	08:34	60° 25. 303'	05° 18. 464'	-	1050	0.5 tons

Table 1. General information on the cores sampled on the southeastern Faeroe margin.

Core No	Geographical Setting	Sedimentary Summary	Instrumentation	Acoustic Characteristics
TTR9-AT-144G	Upper part of the slump (at 20:10 on 3.5 kHz profiler ORAT-27)	174 cm of sediments consist of sand, sandy silty clay and silty clay rich in shell fragments	OREtech sidescan sonar; 3.5 kHz profiler; Single channel high resolution seismic system	Gentle slope, transparent layer at seafloor
TTR9-AT-145G	Upper part of the slump/ channel setting (at 21:02 on ORAT-27)	259 cm of sediments consist of sand, sandy silty clay and silty clay	OREtech sidescan sonar; 3.5 kHz profiler; Single channel high resolution seismic system	Channel complex with low backscatter in the medium backscatter, slump area
TTR9-AT-146G	Mid part of the slump (at 22:00 on ORAT-27 3.5 kHz profiler)	309 cm of sand, sandy silty clay and silty clay	OREtech sidescan sonar; 3.5 kHz profiler; Single channel high resolution seismic system	Layered, gentle slope
TTR9-AT-147G	Lower part of the slump (at 05:20 on ORAT-28 3.5 kHz profiler)	Unopened in liner	OREtech sidescan sonar; 3.5 kHz profiler; Single channel high resolution seismic system	Low relief, positive topography
TTR9-AT-148G	Lower part of the slump (at 07:56 on ORAT-28 3.5 kHz profiler)	Alternation of sandy clay, silty clay, clay and marl	OREtech sidescan sonar; 3.5 kHz profiler; Single channel high resolution seismic system	Small lens of recent slump
TTR9-AT-149G	Lower part of the slump (at 10:30 on ORAT-28 3.5 kHz profiler)	Alternation of sandy clay, silty clay, clay and marl, with the layers of debris flow	OREtech sidescan sonar; 3.5 kHz profiler; Single channel high resolution seismic system	Flat seabed with small lens of recent slump above subparallel layering
TTR9-AT-150G	Distal part of the slump/hemi-pelagic setting (at 11:20 on ORAT-28 3.5 kHz profiler)	Alternation of sandy clay, silty clay, clay and marl, with the layers of debris flow	OREtech sidescan sonar; 3.5 kHz profiler; Single channel high resolution seismic system	Flat seabed with subparallel layering
TTR9-AT-151GR	Lower part of slope of the deep (strong bottom current) (at 09:20 on ORAT-29)	Half tons of dropstones in mud matrix	OREtech sidescan sonar; 3.5 kHz profiler	Moderate backscatter – bedrock on the sidescan sonar image, steep slope on the 3.5 kHz profiler
TTR9-AT-152G	Slope of the deep (strong bottom current) (at 08:37 on ORAT-29)	Small amount of poorly sorted sand and gravel	OREtech sidescan sonar; 3.5 kHz profiler	Moderate backscatter – bedrock with sand waves on the sidescan sonar image, slope
TTR9-AT-153G	Distal part of the slump; area with the strong bottom current (at 12:07 on ORAT-30 3.5 kHz profiler)	Few cm of sediments consist of sand, sandy silty clay and silty clay with a debris flow	OREtech sidescan sonar 100 kHz; 3.5 kHz profiler	Moderate backscatter with subparallel lines on the sidescan sonar image, flat seabed
TTR9-AT-154G	Distal part of the slump; area with the strong bottom current (at 13:55 on ORAT-30 3.5 kHz profiler)	Few cm of sediments consist of sand, sandy silty clay and silty clay with a debris flow	OREtech sidescan sonar 100 kHz; 3.5 kHz profiler	Moderate backscatter with subparallel lines on the sidescan sonar image, flat seabed
TTR9-AT-155GR	The same as TTR9-AT152G	Half tons of dropstones in mud matrix	OREtech sidescan sonar; 3.5 kHz profiler	Moderate backscatter – bedrock with sand waves on the sidescan sonar image, slope

Table 2. Sedimentological, acoustic and geological characteristic of sampling stations on the southeastern Faeroe margin.

Sedimentological description and magnetic susceptibility

Core AT-144G: The target was to collect information from the area immediately below the lower limit of the iceberg ploughmarks, where the sidescan sonar records show the first indications of

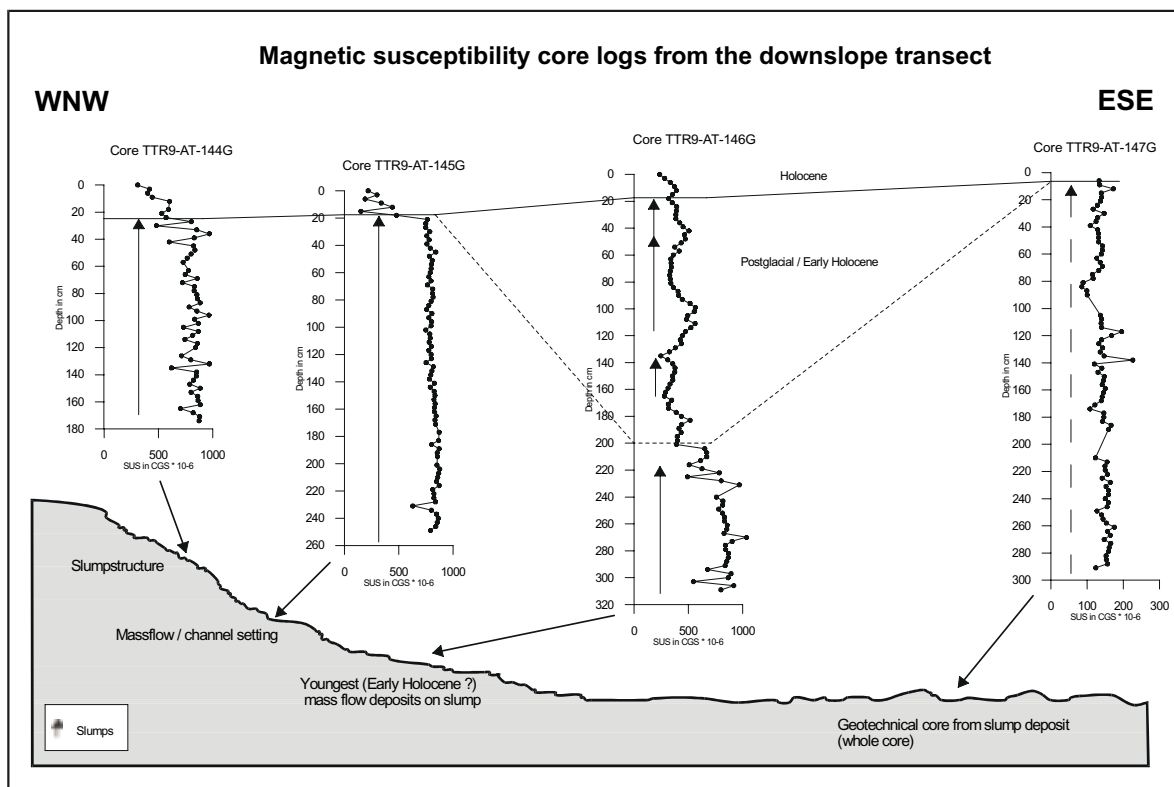


Figure 9. Magnetic susceptibility core logs from the downslope transect of line ORAT-27. Mass flow deposits are indicated by a vertical arrow

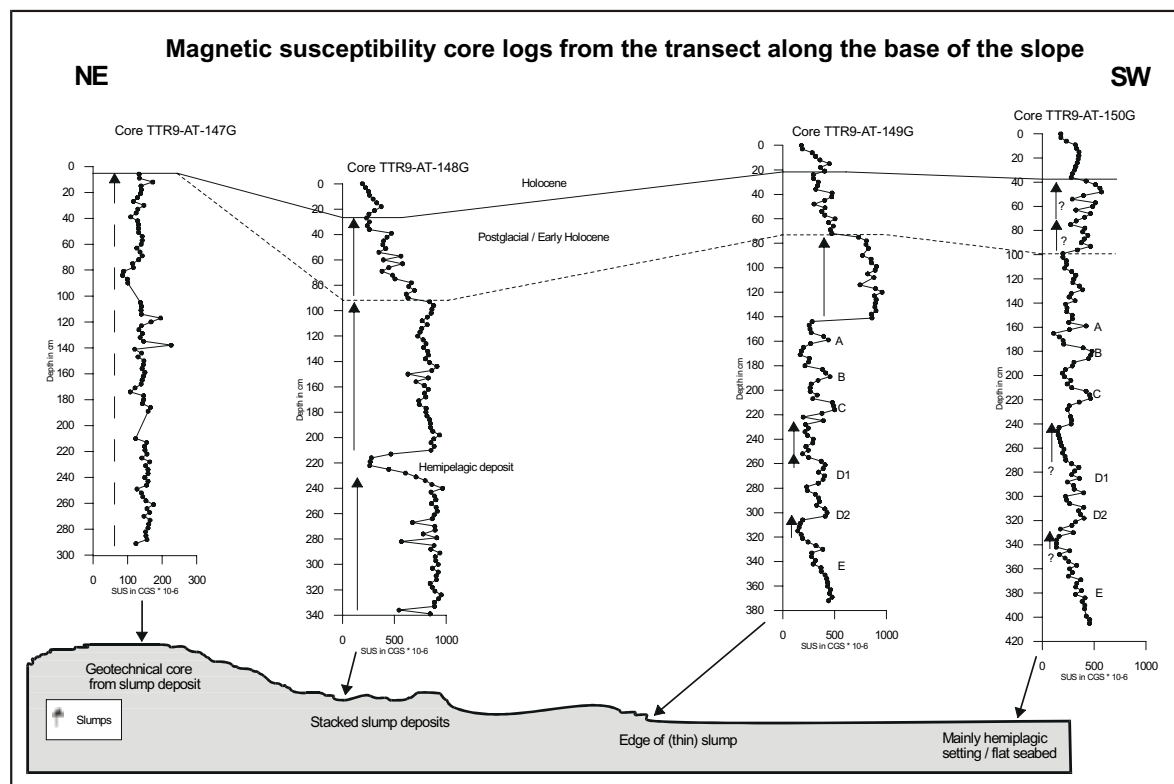


Figure 10. Magnetic susceptibility core logs from the alongslope transect of line ORAT-28. Mass flow deposits are indicated by a vertical arrow

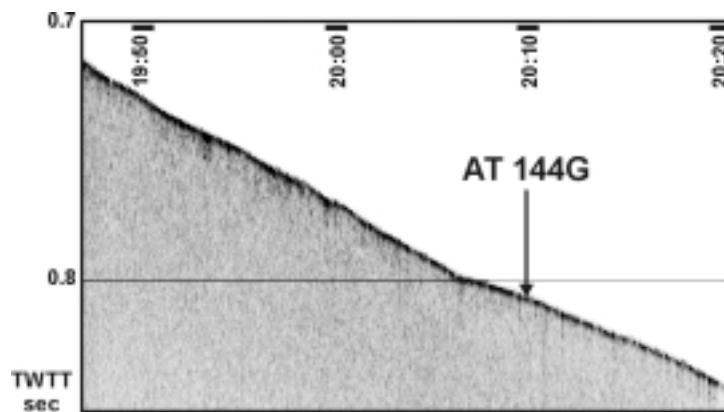


Figure 11. Location of the site AT-144G on the hull-mounted 3.5 kHz profiler record.

the core shows high values, but with a more uneven pattern compared to the other profiles. This could be explained as a result of less sorted sediment here than farther down the slope.

Core AT-145G: This core was taken in order to determine the characteristics of the sediments present in the channel observed on the sidescan sonar records (Fig. 12). The recovery is comparable with AT-144G. The top 18 cm is an oxidized layer of coarse sand containing centimetre sized clasts with the lithology grading to a sandy silty clay towards the bottom. The remaining core consists of silty clay

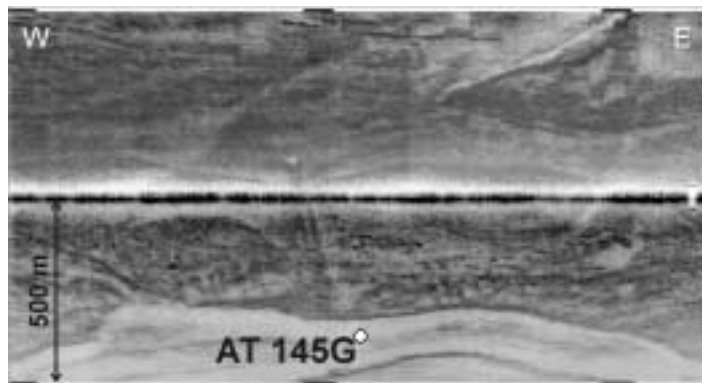


Figure 12. Fragment of ORAT-27 sonograph with sampling site AT-145G.

mass flow (ORAT-27) and where the 3.5 kHz profiler showed weak sub-bottom reflections (Fig. 11). This core had 19 cm of coarse sand in the uppermost part with small clasts of different lithologies. Towards the bottom of the sandy layer the sediment is less oxidized and finer grained (19-28 cm). Below a sharp contact at 28 cm, the remaining core is homogeneous and structureless. Stones of different lithologies and sizes, as well as shell fragments, are variously distributed throughout the whole unit (mud flow deposit). The magnetic susceptibility of this part of

the core shows high values, but with a more uneven pattern compared to the other profiles. This could be explained as a result of less sorted sediment here than farther down the slope.

Core AT-146G: The target was to determine the sediment characteristics in the area of weak backscattering seen on the sidescan sonar. The coring site was selected where the hull-mounted pinger indicated the presence of a thin (several ms) cover of surficial sediment unit,

overlying weak parallel internal reflectors. The 305 cm long core has an upper 3 cm of water saturated brownish fine sands with a clayey admixture. Between 3 and 128 cm the colour is more greyish, the grain size becomes silty clay with no structures visible and the foram content decreases towards the bottom (different stages of mud flow deposit). From 128 down to 171 cm the silty clay shows evidence of bioturbation and shell fragments (mud flow deposit). From 171 to 227 cm irregularly shaped patches of sandy/silty sediment are variously distributed in the silty clay where the lower part of the interval is more clayey. From 227 cm to the bottom, the core consists of dark grey silty clay with abundance of shell fragments and centimetre sized clasts (glacial mud flow deposit).

Core AT-147G: The aim of this core was to collect mass flow sediments for determining sediment physical properties. The site was selected on top of a positive seabed topography associated with assumed slump deposits. The core was cut in sections of 1 m length with four sections recovered, the last one of 43 cm long. Each one was sealed with wax and stored at c. 4°C for subsequent geotechnical analyses for the GEM consortium of offshore companies. Measurements of magnetic susceptibility

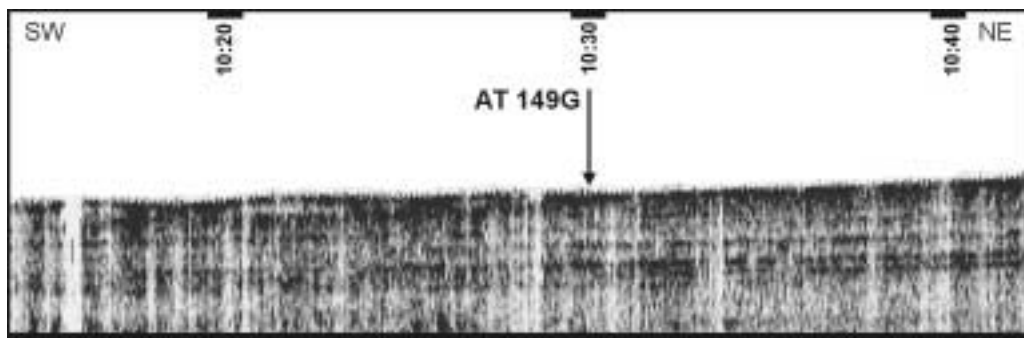


Figure 13. Fragment of 3.5 kHz hull-mounted profiler PRAT-28 with sampling site TTR9 AT-149G. The core was taken from small lens of surficial slump above subparallel layering.

ty were made from the outside of the plastic liner. The log has uniform shape consistent with a slump deposit.

Core AT-148G: The coring station appears on the 3.5 kHz profile to be the site of various generations of mass flow deposits. The top layer of 17 cm of brownish coarse sand with high clayey admixture is intercalated with an oxidized clayey layer (9-14 cm). From 17 to 28 cm there is a structureless clayey layer whose colour changes from brownish to greyish towards the bottom. From 28 to 99 cm is a unit of silty clay with lumps of lighter, finer and water saturated sediment; towards the bottom the coarse terrigenous admixture increases (mud flow deposit). From 99 to 220 cm a unit of dark grey silty clay with stones and shell fragments (mud flow deposit) is followed by a small interval (220-235 cm) of light marl with foraminifera and bioturbation on the lower boundary (hemipelagic). The hemipelagic unit could have been deposited at a time when the channel was temporarily abandoned. The rest of the core consists of structureless silty clay containing stones and shell fragments chaotically distributed (mud flow deposit).

Core AT-149G: The target was to penetrate assumed superficial slump deposits and reach the underlying sediments as seen on the pinger records (Fig. 13). The upper section (0-13 cm) comprises brownish coarse sand with a clayey admixture that is fining downward to a more sandy clay sediment and becomes more consistent. The lower unit (13-78 cm) consisted of a greyish structureless silty clay with randomly distributed shell fragments. A stiffer layer of clay between 78 and 80 cm could indicate an hemipelagic event. From 80 to 149 cm an homogeneous layer of dark grey silty clay contains numerous clasts chaotically distributed (mud flow deposit). The following unit (149-219 cm) comprises bioturbated and structureless brownish marl rich in foraminifera (hemipelagic deposition) with an intercalation of an irregular sandy layer between 167 and 170 cm. The interval 219-308 cm includes dark grey silty clay with possible mud flow between 219 and 236 cm, and with some bioturbation structures below (hemipelagic). Two sandy layers (between 308-311cm and between 340-342cm) are packing a unit of clayey structureless sediment. The rest of the core showed silty clay coarsening downward with chips of dark silty clay and light grey water saturated clay. Clasts are also visible in this layer (possible mud flow)

Core AT-150G: This coring station attempted to sample the outcropping stratified sediment unit shown on the hull-mounted pinger. The core contains a very thin layer (0-3 cm) of brownish coarse sand on the top that fines downward (3-9 cm) with irregular boundaries becoming more greyish in colour and bioturbated between 9 and 13 cm. Similar to AT-149G the remaining core consists of alternations of darker silty clay, containing millimetric grains, and lighter clay with a higher foraminifera concentration. A few stones are randomly distributed, although mainly concentrated in the darker layers, while most of the core shows the effects of bioturbation, especially between 84 and 100 cm. Two main mud flows can be recognized; between 53 and 74 cm and between and between 95 and 100 cm. The magnetic susceptibility correlation between AT-150G and AT-149G is indicated in the Fig. 10. The interval from 100-40 cm has uniform low values, and cannot be correlated to AT-149G. A reason for this could be, that this part of AT-149G has been eroded by the slump from 140-80cm. The postglacial deposits below the Holocene unit can also be correlated to the postglacial unit of core AT-149G

and AT-148G. The trend of the basal unit of AT-149G and AT-150G shows decreasing values. This pattern could be interpreted as a Bond cooling cycle (Moros et al., 1997; Broecker 1994), which indicates a general cooling event of the global climatic record.

Core AT-153G: The coring sites AT-153G and AT-154G were selected in order to determine the character of the sediments present in morphological highs, where the hull-mounted pinger penetrated, but did not reveal subbottom reflection. The top 10 cm of this core consists of a brown water-saturated silty marl overlying a 2 cm thick greenish fine sand. These upper sediments overlie mainly bioturbated silty clays and clayey sands. The silty clays are usually structureless and coloured brown, greenish, light grey or medium grey. These changes are marked by sharp boundaries and may be separated by coarse sands (26-30 cm) or sandy clays (48-56 cm) especially in the upper levels. In the middle of the core, the silty clays show distinct burrows on a centimetre scale that are usually filled by more silt-rich units with a higher foram concentration. The bioturbated debrite(s) extends from 66 to 248 cm. The magnetic susceptibility logs show occasional negative excursions, related to the presence of the larger clasts. The underlying unit (248-217 cm) represents a return to light grey silty clays (hemipelagic). A large clast is present at 277 to 280 cm. Below 300 cm more stones are apparent including another large clast at 345 to 352 cm. A fining upward sandy silt layer is also apparent between 311 and 316 cm. The lowermost silty clays down to 406 cm shows some mottling/bioturbation. For both the coring stations (AT-153G and AT-154G) the debris flow deposit observed in the upper part of the cores immediately underlies a short interval of markedly higher magnetic susceptibility values. This suggests an age of the debris flow event, which probably pre-dates the Last Glacial Maximum. Apart from the short intervals characterised by minor mass flow deposits, the regularly decreasing magnetic susceptibility values near the bottom of core AT-153G may tentatively be related with a Bond climate cooling cycle (Oxygen Isotope Stage 3?).

Core AT-154G: The top 10 cm of this core is marked by fining upwards coarse grained sand with several gravel-size clasts and clasts of stiff sandy clay. A large dropstone (8 cm x 12 cm) is present at the base of this interval. The underlying sediments (12-35 cm) are represented by structureless sandy silty clays with varying admixtures of sandy material and are brown, grey, or greenish. Stones are present throughout. Between 35 cm and 156 cm a silty clay unit is present enriched with a number of clasts of greenish grey clay (mud flow), with an interval of sandy silty clay containing clasts and bioturbations filled with sand between 137 and 156 cm. This last interval is interpreted as a debrite. Underlying this unit, structureless or intensely bioturbated grey silty clays are present. Between 173 and 184 cm a bioturbated grey clayey layer had been interpreted as a turbidite as is the silty clay layer between 226 and 271 cm. Suspected debrites revealing large sandy filled burrows and with stones occur between 295 cm and the base of the core.

Discussion

In summary, all cores retrieved contain mass flow deposits (Figs 9 and 10). These deposits form the main sediment type in the cores AT-144G to AT-148G as well as in core AT-153G and 154G. In core AT-149G, but in particular in core AT-150G, hemipelagic intervals are more common. Furthermore, all cores taken in the area display a top unit with a fine sand cover (< 20 cm), clearly indicating current-induced reworking.

The majority of the slumps were found in the glacial deposits. Indications were also found for postglacial slumping in cores number AT-146G, AT-148G, AT-149G and AT-150G. Slump structures were found not only on the slope but also out on the flat seabed.

Comparing the northern mass flow area with the central one (cores AT-153G and 154), it may tentatively be concluded that the episode of mass flow activity in the northern area postdates the debris flow event recorded in the cores AT-153G and 154. Moreover, we may assume a different, more southern, source for this debris flow.

The stones observed in all the cores have a basaltic lithology with only rare exceptions. This could indicate that the clasts were transported by mud flows from the Faeroe Islands rather than by ice rafting.

I.3. CURRENT-INDUCED BEDFORM STUDIES

I.3.1. Acoustic investigations

T. NIELSEN, A. KUIJPERS, N. KENYON, M. IVANOV AND A. AKHMETZHANOV

Apart from the line ORAT-27/PRAT-27, which was run in an ESE direction, i.e. approximately perpendicular to the Faeroe Platform slope, the other three deep-tow sidescan sonar and subbottom profiler tracks (ORAT-28 to 30/PRAT-28 to 30) were run more or less parallel to the channel axis in depths of about 1000 m. (Fig. 2). Only on line ORAT-29 was a sidescan sonar frequency of 30 kHz and 2 x 1000 m range used. The other lines were run with 100 kHz and a 2 x 500 m range.

The sonograph of line ORAT-27 shows well-defined and continuous iceberg ploughmarks with clearly expressed preferred orientation along the slope at water depths of between about 400 m and 550m (Fig. 14), with somewhat weaker developed similar bedforms extending down to nearly 650 m. The preferred orientation of the bedforms suggest iceberg transport by along slope flowing Norwegian Sea Overflow Water. At the ESE end of line ORAT-27, and on line ORAT- 28, where water depth is around 1000 m, no firm evidence of current-induced bedforms is found.

Line ORAT-30 gets progressively deeper to the south and nearer to the centre of the channel. At its northern end only weakly developed minor current lineations are observed. After a more elevated area associated with the presence of mass flow deposits, where current-induced features are virtually

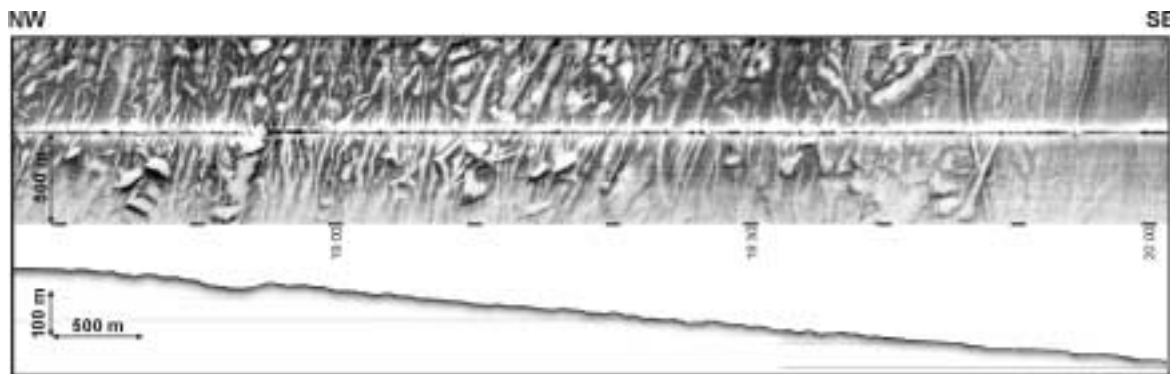


Figure 14. Fragment of OREtech line ORAT-27 and 7 kHz subbottom profiler records showing preferred orientation of ploughmarks due to iceberg transport by an along slope flowing current.

absent, better defined, shorter, current lineations appear. The sonographs further indicate a clear change in the bottom current direction from about 170 degrees to about 220 degrees, which may be attributed to the effect of the topography on the currents. In the same place, weakly developed large-scale backscattering features occur, that also have a current-parallel direction.

Further to the south on line ORAT-30 large stones and boulders are visible on the seabed, and associated with them are well-developed comet marks, up to 300 m long, that extend to the south of these obstacles (Fig. 15).

Further down the track of line ORAT-30, longitudinal bedforms are replaced by extensive fields of small sand waves with a wavelength of up to 25 m (Fig. 15). Here, a surficial sediment unit which was several meters thick at the beginning of line ORAT-30, pinches out. Further south, the transverse bedforms display arrangements in longitudinal bands, after which they are gradually replaced by well-defined, long current lineations and sand streaks (Fig 16).

At water depths of about 1000 m lines ORAT-29 and ORAT-30 cross two escarpments located on the upstream sides of two very large enclosed deeps that are found in the southern part of the Faeroe-Shetland Channel, where it nearly reaches its most restricted cross-section. The shapes of the escarpments are presumably caused by the presence of a particularly resistant horizon that has been an

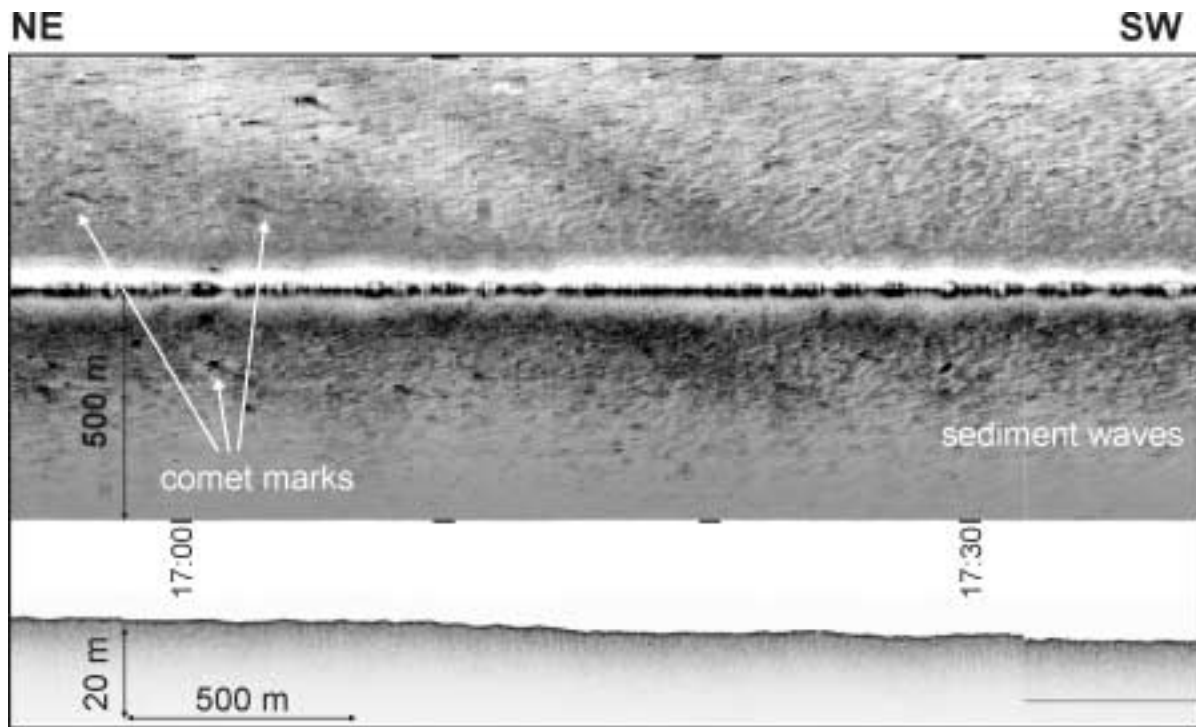


Figure 15. Sidescan sonar record from line ORAT-30 showing the transition from a comet mark bedform domain to an environment characterised by the occurrence of megaripples and sediment waves more to the south.

obstacle to flow through the Faeroe-Shetland Channel for a considerable time. Erosion due to turbulence created by the scarps is believed to have maintained these giant scour holes, possibly over a very long period of time. Here the sonograph from line ORAT-30 shows a very strong backscattering seabed, with only few areas with well-defined current lineations. The latter pattern is also seen in the sonograph from line ORAT-29, that shows similarly very strong backscattering and a few areas with

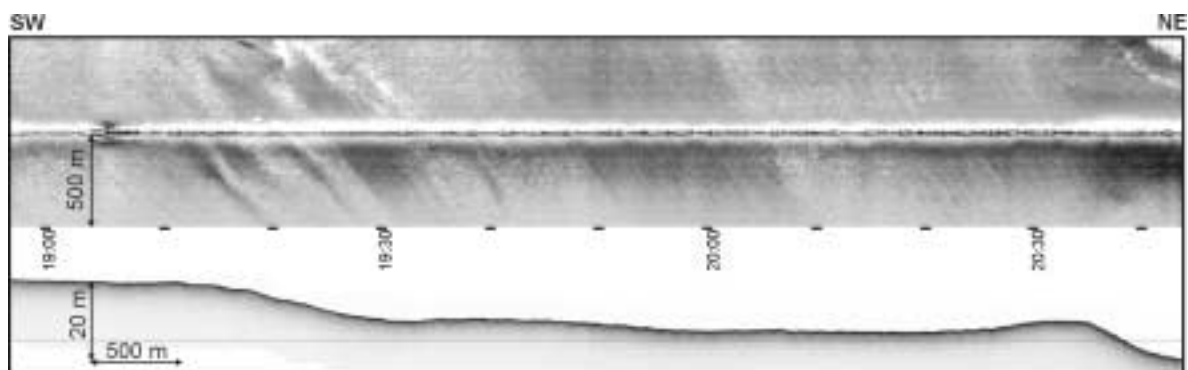


Figure 16. Fragment of OREtech line ORAT-30 and 7 kHz subbottom profiler record showing pattern of longitudinal bedforms with sand ribbons and other longitudinal bedforms.

well-defined current lineations occurring in association with both the escarpments.

Notable is the loss of bottom trace and the strong acoustic distortions that occurred when the deep-tow vehicle was towed over the escarpment. Sudden, and strong instability of the tow-fish can be attributed to strongly turbulent high-energy bottom currents over this area.

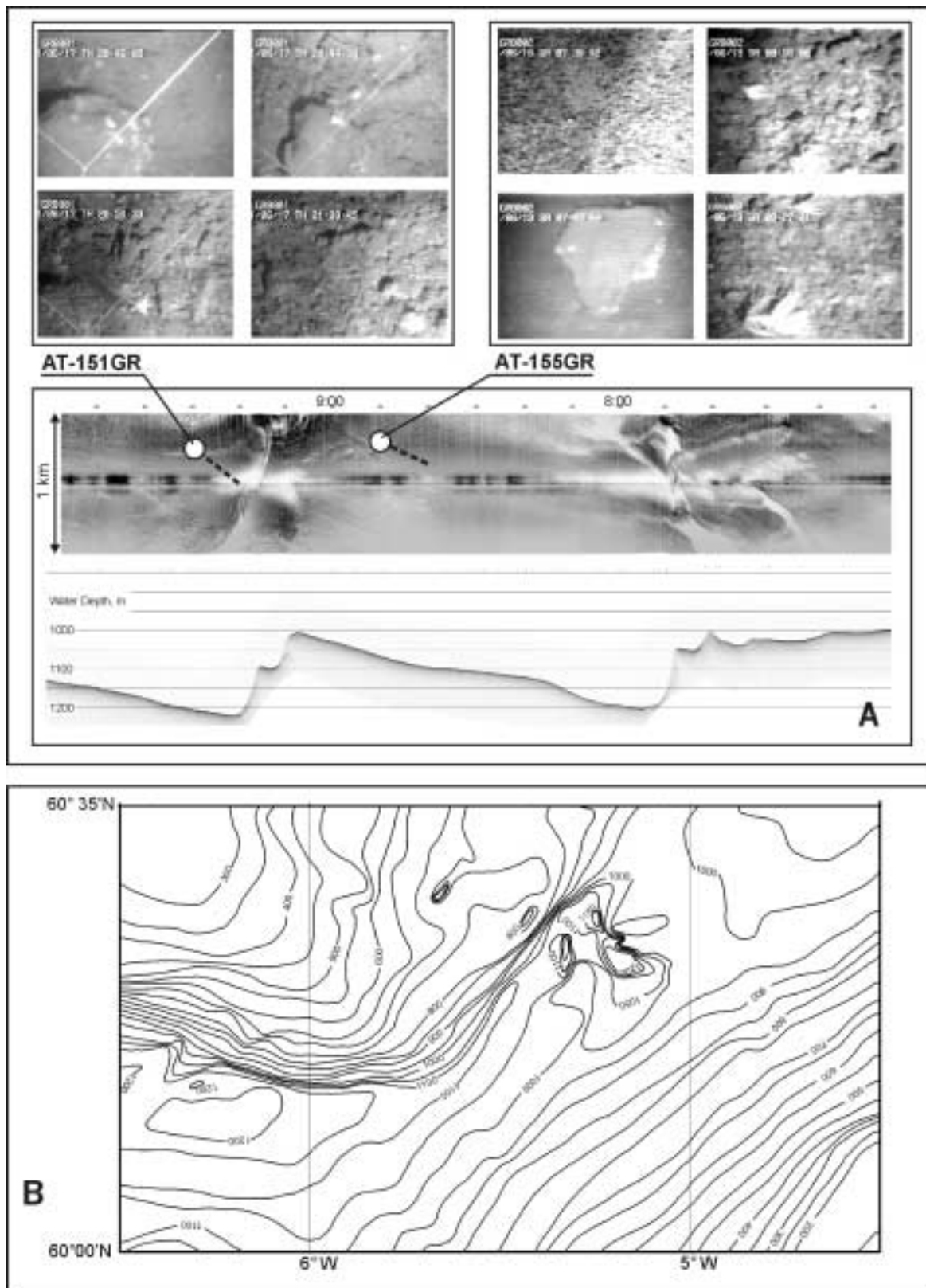


Figure 17. **A** - Sidescan sonar record of the southernmost escarpment (line ORAT-29), and stills from TV grab sampling sites illustrating the coarse character of the seabed sediments; **B** - Bathymetry compiled by N.H. Kenyon from data available to Southampton Oceanography Centre.

I.3.2. TV-seabed inspection

T. NIELSEN, A. KUIJPERS AND P. SHASHKIN

The TV-recordings from the two sites near the escarpment (stations AT-151GR, AT-155GR, Fig. 17) clearly demonstrate the coarse character of the substrate in these areas characterised on the sonographs by very strong backscattering (Fig. 17). The seabed mainly consists here of lag sediment of medium to coarse sand and gravel, with frequent pebbles, stones and cobbles. The TV records showed occasional boulders. The maximum boulder size recorded was up to nearly a metre. A maximum boulder size in this order of magnitude is also indicated by the deep-tow sidescan sonar records from the area. The largest boulder sampled by the grab had dimensions of 33 x 22 x 19 cm.

From the TV recordings (Fig. 17) it appears that areas with a more sandy substrate alternate with a coarse seabed. The sandy areas may be from the less reflective sand streaks and other current-parallel features observed on the sonographs. It should be noted that the TV records showed the presence of abundant benthic fauna, with filter feeder tentacles clearly indicating the direction of the strong, southerly current.

I.3.3. Bottom sampling results

A. MAZZINI, G. AKHMANOV, D. OVSYANNIKOV, A. SADEKOV, A. KUIJPERS, T. NIELSEN, A. AKHMETZHANOV, A. STADNITSKAYA, E. KOZLOVA, L. MAZURENKO, A. SAUTKIN, I. BELENKAYA, YU. VOLKOVA, E. SUSLOVA, AND D. GONCHAROV

Sedimentological description

The TV-grab was used at two sites in the immediate vicinity of the southernmost escarpment. The sites were selected just downslope of the escarpment (AT-151GR) and on the rising seafloor just north of the escarpment (AT-155GR).

Grab AT-151GR: A relatively small amount of material was recovered with this grab (approximately 0.4 m³). It mainly consists of drop stones of different sizes (up to about 30cm diameter) and degrees of roundness. The sediment is mainly brownish coarse sandy sediment with foraminifera and a clayey admixture. Various organic species are also observed: sponges, Echinodermata, Hydrozoa, Bryozoa, and worms. The drop stones recovered were subdivided into main groups according to their lithology, grain size and degree of metamorphism. Further study will produce a better classification of these samples. Two thirds of the grab recovery were randomly selected and sieved. The fraction with size greater than 1 cm was classified as below. Tables were produced of clast classification that show the measurement of the long/short axis and the degree of roundness for each clast:

Sedimentary rocks with low metamorphism

Although different rocks are recognised, this group is subdivided into two other main subgroups according to the grain size defined from simple observation.

Sandy sized- Except for one big clast (18x13 cm), greyish and well rounded, the rest of them have a mainly brownish to yellowish grey colour. Their size varies from 2 cm up to 8 cm approximately and the roundness from well rounded to angular, with some flattened and more metamorphosed.

Silty sized- These are mainly greyish, subrounded and angular samples with a size of up to 13 cm. Two samples, finely grained and non-metamorphosed, were taken for dating. A couple of samples show fine laminations of finer sediment.

Sedimentary rocks with high metamorphism

Samples are subdivided into three main subgroups according to the grain size and the rate of metamorphism.

Gravel sized -Samples of different colours, mainly reddish, have from well rounded to subrounded form. Centimetre sized minerals (quartz, feldspar, others) and gravels of different lithology in coarse sand matrix.

Sandy sized –Many large specimens were recovered. The colour varied from reddish to brownish. Most of the samples are rounded.

Silty sized- Apart from one rounded sample, the rest are smaller and are mainly flattened. Generally the samples have a greyish colour and a couple of them have visible fine laminations.

Chert -From rounded to angular shape with different colours (brownish, reddish and greenish), and a few of them with structures of lamination.

Quartzite -Variously coloured (mainly reddish) and shaped, the largest of them up to 5 cm. Many of them are unexpectedly well rounded. No structures and textures are visible

Schist - Mainly angular samples, the colour varies from grey to mainly dark grey. Some clasts are greenish. Typical schist structures are often seen.

Gneiss -Mainly grey clasts of different roundness, from angular to very well rounded, composed of mica, quartz and feldspar grains, fine crystalline to medium crystalline, with typical gneiss structure.

Basalt -The samples are mainly dark grey, very dark grey and greyish brown with the size varying from 1 cm up to 20 cm, roundness is variable, mainly subangular and angular form. Very micro-crystalline or crypto-crystalline. Some clasts show remains of a hexagonal column that is typical for basalt. Some of the clasts have a zoolitic crust on the surface.

Granites - The clasts are rather variable in size, of pinkish brown and light grey colour, fine to coarse crystalline, composed of quartz, feldspar, mica, and others are structureless. The rocks represented are from very “fresh” to rather altered.

Core AT-152G: The position of this coring station is the same as that of TV grab sample AT-155GR. Approximately 20 cm³ of sediment were recovered; it consists of coarse sand, poorly sorted with clayey admixture and gravels and clasts (up to 5 cm) of different lithologies.

Grab AT-155G: Approximately 1m³ of sediment is recovered. The majority consists of drop stones of different size (from centimetric and up to 40 cm) and different lithology. The roundness also varies from angular to well rounded, although the bigger clasts are mostly rounded and sub-rounded. The clasts are mixed with coarse sand with a clayey admixture, also gravels and millimetric grains of different lithologies are found. The fauna sampled is very similar to that described for the sampling station AT-151GR but without any exemplar of Echinodermata. Because of the similarities of the recovery, for the lithological description of the drop stones, refer to the paragraph for station AT-151GR.

The variety of lithologies of the drop stones recovered indicates that the source area isn't restricted just to the Faeroe Islands but involves a wider area. Also the roundness of many samples indicates a long transport history before the final deposition.

I.4. CONCLUSIONS

T. NIELSEN, A. KUIJPERS, M. IVANOV

The new seismic data confirmed the presence of a buried slump complex of presumably Plio-Pleistocene age at the central western margin of the Faeroe-Shetland Channel, as was reported from the TTR8 cruise (Kenyon et al., 1999). Furthermore, the new seismic data yield evidence for a younger, minor slump unit, which is thought to be of Pleistocene age. There was also a surficial slump

detected during the TTR8 cruise. The new acoustic data show that these surficial deposits can be traced as far upslope as 400m water depth. The preliminary investigations of cores taken from this slump suggest that the latest, large-scale mass flow event occurred around the last glacial maximum (18-20,000 yrs. BP). Minor mass-flow activity may have occurred also in postglacial/early Holocene times. The acoustic records and core data from this cruise prove that slope instability of the eastern Faeroe margin is more widespread than previously thought.

A wide range of mainly longitudinal current induced bedform types, together with some sand wave fields, has been observed, representative for both medium and high bottom current speed. A sandy top seen in all cores, confirms the generally enhanced bottom current activity in the area.

Further evidence for strong current activity is provided by the very coarse lag deposits found in the area of the deeps and steep escarpments in the southern part of the area. Investigations of these lag deposits showed a high percent of non-basaltic material indicative of a non-Faeroese origin.

II. ROCKALL TROUGH (Leg 1)

II.1. GEOPHYSICAL SURVEYING & GEOCHEMICAL ANALYSIS WITH RESPECT TO THERMOGENIC GAS ESCAPE NORTH-EAST OF GEORGE BLIGH BANK

A. WHEELER AND TTR9 SHIPBOARD SCIENTIFIC PARTY

II. 1.1. Introduction and Background

The objective of this study is the acquisition and analysis of samples to test whether there is thermogenic gas escape north-east of George Bligh Bank. Sub-bottom profiler lines (pinger) also generated valuable information with respect to the location and surface expression of faults and shallow gas bodies. Existing data regarding seabed properties in this area is limited, with the exception of some confidential commercial seismics.

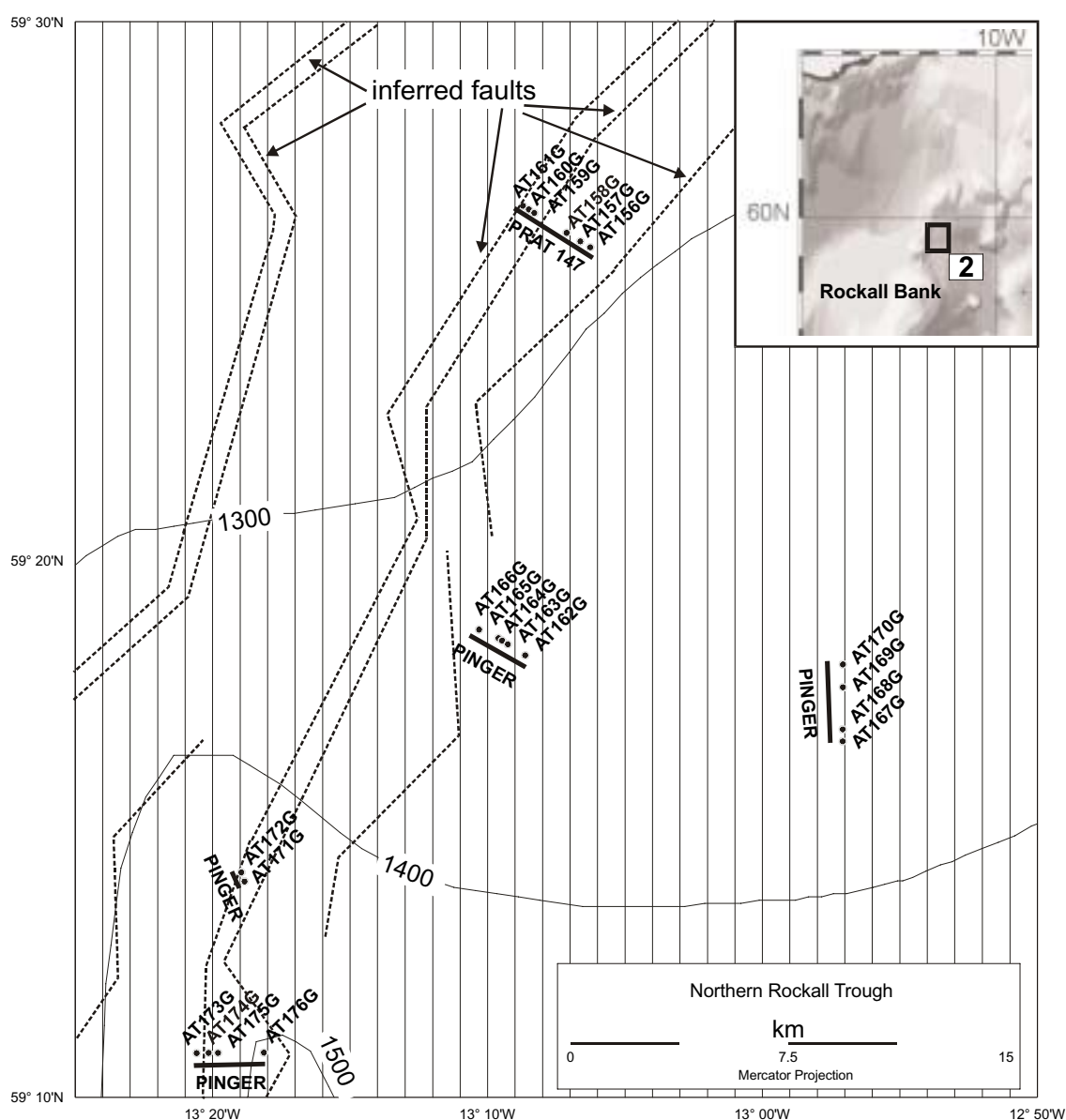


Figure 18. Bathymetric map of area NE of George Bligh Bank showing core locations and sub-bottom profiler lines.

The study area is to the northeast of George Bligh Bank on the western margin of Rockall Trough. The George Bligh Bank is the southernmost of the seamounts that bound the northern Rockall Trough and, together with the Faeroes platform, separate the Rockall Trough from the Norwegian Sea. The George Bligh Bank lies immediately north of the Rockall Bank and at the northern end of Hatton basin. Thus, the area of investigation lies between a number of oceanographic provinces.

The Norwegian Sea Overflow Water enters the North Atlantic through the Faeroe Bank Channel and some of it enters the Rockall Trough over the Wyville Thomson Ridge (Hansen and Østerhus, 2000). Some of this outflow water is deflected southwards to flow along the western margin of Rockall Trough. These waters, and other waters deflected around northern Rockall Trough, are assumed to have generated contourites as imaged by commercial seismic investigations (A Kuipers, *pers. comm.*). These waters generate the spectacular contourite formation known as the Feni Ridge, to the south of the study area, that bounds the eastern side of Rockall Bank. At the northern limit of the Feni Ridge, immediately south of the study area, the seabed is dominantly erosive implying substantial bottom current accelerations as the currents are deflected around the George Bligh and Rockall Banks. Existing bathymetry (Fig. 18) reveals a gently sloping plateau in the northern part of the area running into a deep in the south-west. This deep is the start of a moat bounding the George Bligh Bank due to currents accelerating around this obstruction.

II.1.2. Results and Discussion

Core descriptions

Details of core locations and retrieval are summarised below in Table 3. Core locations are also presented in Fig. 18.

Core descriptions are provided in full for each core in conjunction with an age appraisal based on coccolith micropalaeontological identifications. Sub-bottom profile imagery for some core sites are

Core No.	Date	Time, GMT	Latitude	Longitude	Cable length, m	Depth, m	Recovery, cm
TTR9 AT-156G	20.06.99	21:51	59°25.8201	13°06.2809	1322	1320	132
TTR9 AT-157G	20.06.99	23:11	59°25.9262	13°06.6177	1323	1315	189
TTR9 AT-158G	21.06.99	00:11	59°26.0675	13°07.1372	1323	1312	200
TTR9 AT-159G	21.06.99	01:50	59°26.4597	13°08.2859	1310	1304	192
TTR9 AT-160G	21.06.99	02:49	59°26.5242	13°08.5036	1315	1304	200
TTR9 AT-161G	21.06.99	03:44	59°26.5835	13°08.7452	1308	1299	199
TTR9 AT-162G	21.06.99	10:10	59°18.2571	13°08.6231	1388	1375	182
TTR9 AT-163G	21.06.99	11:09	59°18.4493	13°09.2891	1380	1375	198
TTR9 AT-164G	21.06.99	12:03	59°18.5103	13°09.4917	1379	1374	187
TTR9 AT-165G	21.06.99	12:51	59°18.5688	13°09.6316	1378	1375	196
TTR9 AT-166G	21.06.99	13:44	59°18.7267	13°10.3348	1378	1374	197
TTR9 AT-167G	21.06.99	15:58	59°16.6551	13°02.8841	1403	1395	193
TTR9 AT-168G	21.06.99	23:31	59°16.8713	13°02.8666	1400	1395	200
TTR9 AT-169G	22.06.99	00:36	59°17.6544	13°02.9136	1400	1389	189
TTR9 AT-170G	22.06.99	01:35	59°18.0749	13°02.9202	1390	1388	191
TTR9 AT-171G	22.06.99	05:01	59°14.2105	13°18.9569	1416	1409	189
TTR9 AT-172G	22.06.99	06:06	59°14.0358	13°18.8255	1422	1418	200
TTR9 AT-173G	22.06.99	07:41	59°10.8115	13°20.5633	1535	1530	200
TTR9 AT-174G	22.06.99	08:40	59°10.8246	13°20.1637	1542	1536	222
TTR9 AT-175G	22.06.99	09:40	59°10.8421	13°19.8270	1544	1535	196
TTR9 AT-176G	22.06.99	10:54	59°10.8389	13°18.1543	1500	1488	196

Table 3. General information on the cores sampled in the George Bligh Bank area.

also presented in Figures 19, 20 and 21.

Gravity cores AT-156G to AT-170G are all comparable. These cores are characterised by an

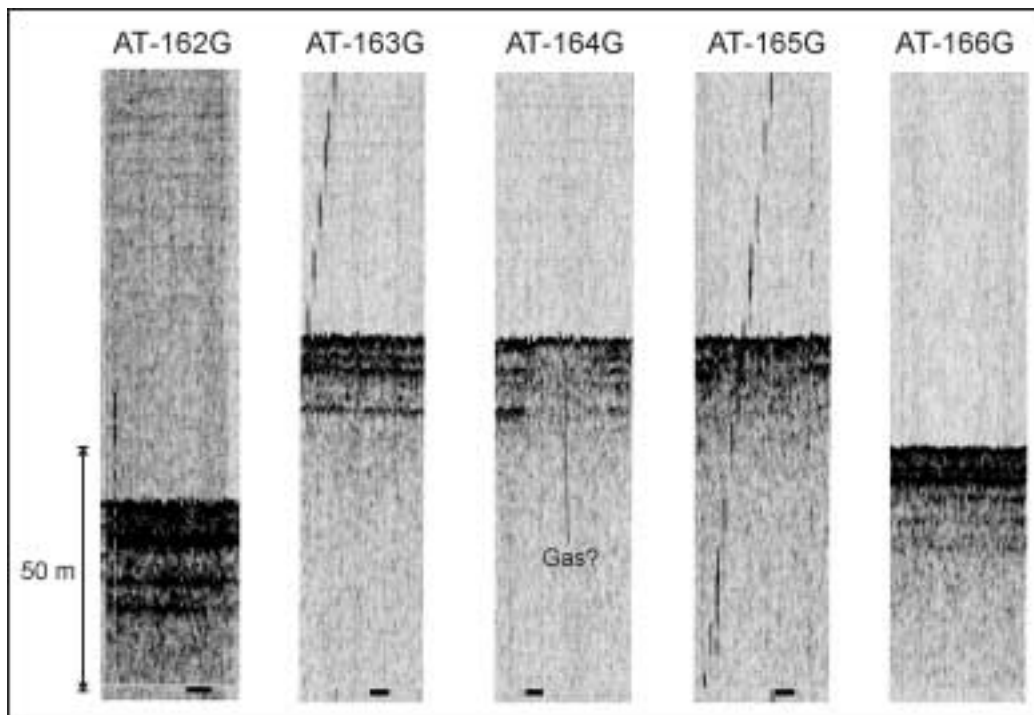


Figure 19. 3.5 kHz sub-bottom profiler (pinger) imagery of core sites AT-162G to AT-166G.

upper layer of often water-saturated and oxidised foram-rich marl. This is usually of Holocene age (>10ka) and represents a period of increased basal current strength and pelagic biological activity. This interval varies in thickness but usually comprises the upper 20 cm.

This layer overlies darker silty clays of glaciomarine origin that are usually bioturbated, both by small scale vertical burrows and larger horizontal burrows, suggesting background sluggish basal current activity during oxygen isotope stage 2 and 3. These cores usually contain forams, sandy admixtures and dropstones (due to the ablation of ice-bergs), shell fragments and organic inclusions. Organic content is moderate and reduced conditions in the core favour organic preservation. Burrows are often filled with coarser material and are occasionally the site of preferential mineralisation and/or organic preservation. An association between preserved organics, mineralisation and thermogenic gas seepage cannot be confirmed although organic chemical processes are active within these surface layers.

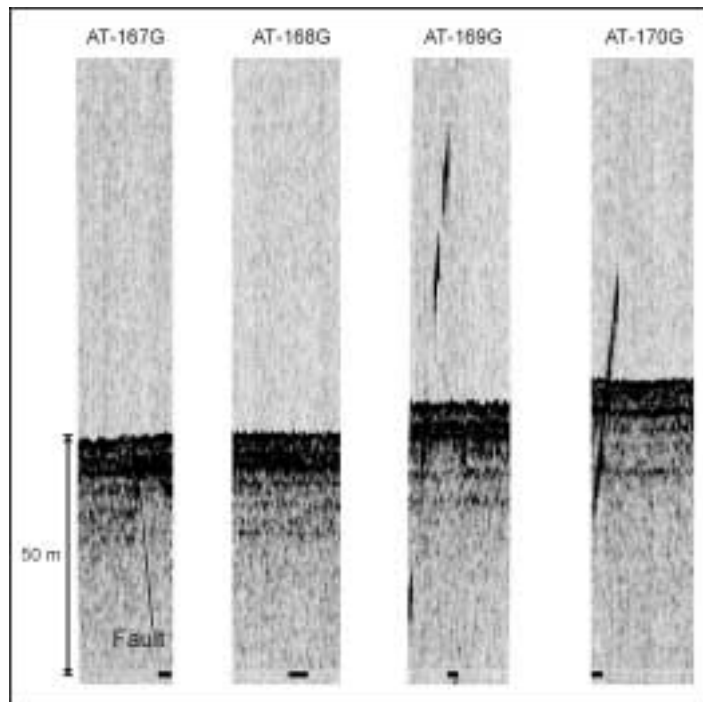


Figure 20. 3.5 kHz sub-bottom profiler (pinger) imagery of core sites AT-167G to AT-170G.

These cores usually contain forams, sandy admixtures and dropstones (due to the ablation of ice-bergs), shell fragments and organic inclusions. Organic content is moderate and reduced conditions in the core favour organic preservation. Burrows are often filled with coarser material and are occasionally the site of preferential mineralisation and/or organic preservation. An association between preserved organics, mineralisation and thermogenic gas seepage cannot be confirmed although organic chemical processes are active within these surface layers.

Cores AT-162G to AT-170G are from well-stratified sediment with some indication of possible sub-surface gas on the profiler images, especially at core sites AT-164G and AT-167G, the latter being also associated

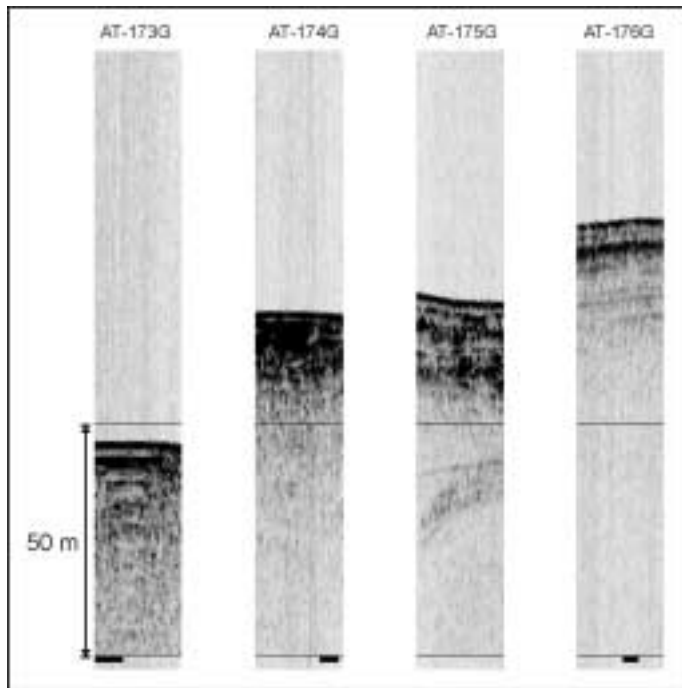


Figure 21. 3.5kHz sub-bottom profiler (pinger) imagery of core sites AT-173G to AT-176G.

with a near-surface fault (Figs 19 and 20).

Magnetic susceptibility profiles are presented for these cores in Figs. 22 to 24. These profiles show no coherent pattern downcore and magnetic susceptibility cannot be used as a correlation tool. Characteristic low magnetic susceptibility values associated with the Holocene are indistinct, possible due to bioturbation effects. Individual peaks in magnetic susceptibility probably reflect the presence of dropstones.

Cores AT-171G to AT-176G produce a different stratigraphy strongly affected by downslope processes and slope instabilities on the edge of the moat of the George Bligh Seamount. Both AT-171G and AT-172G show coccolith assemblages suggesting either very high Holocene sedimentation rates in this area (due to preferential sedimentation on the edge of the moat) or sequences where

glacial sedimentation is absent due to down-slope movement. Magnetic susceptibility profiles from these cores (Fig. 25) are also indistinct.

Cores AT-173G to AT-176G also give indications of variations in sedimentation rate as well as

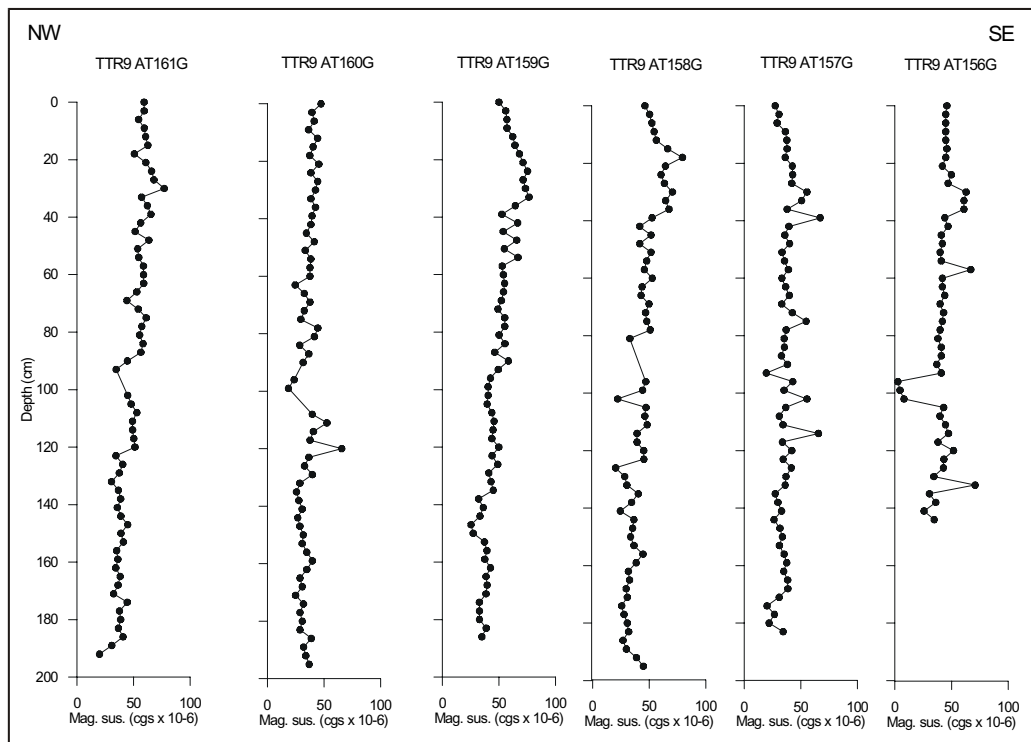


Figure 22. Magnetic susceptibility profiles from cores AT-156G to AT-161G.

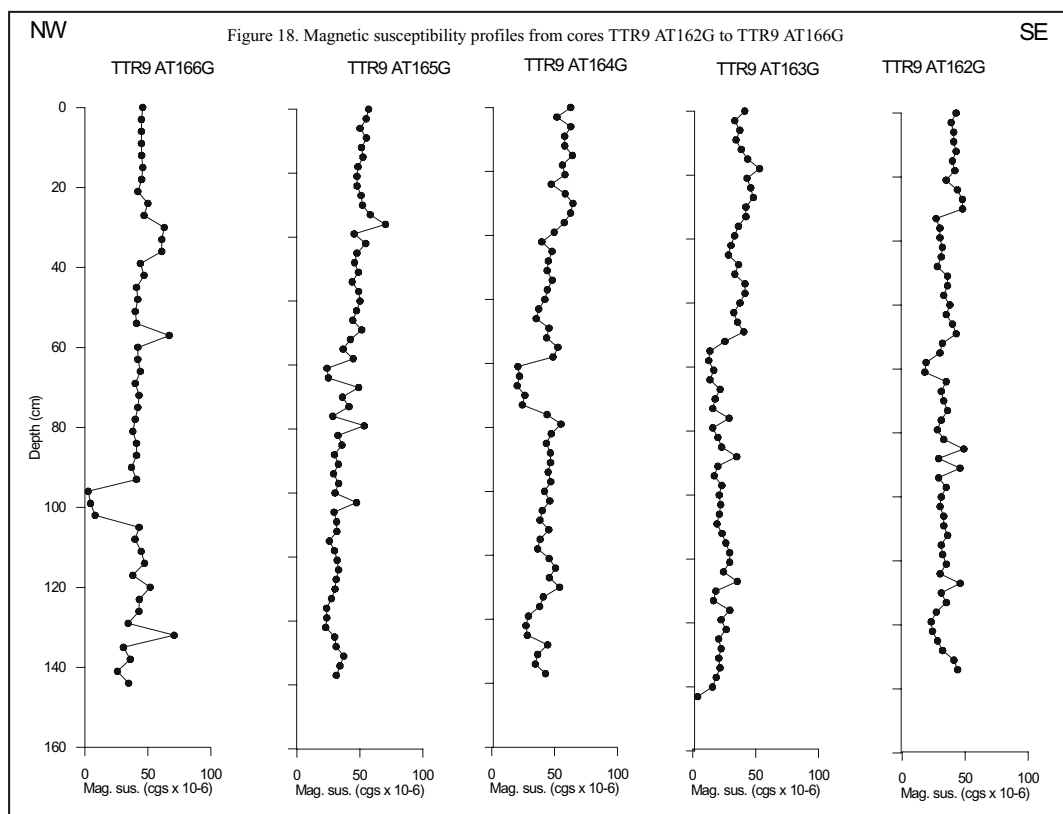


Figure 23. Magnetic susceptibility profiles from cores AT-162G to AT-166G.

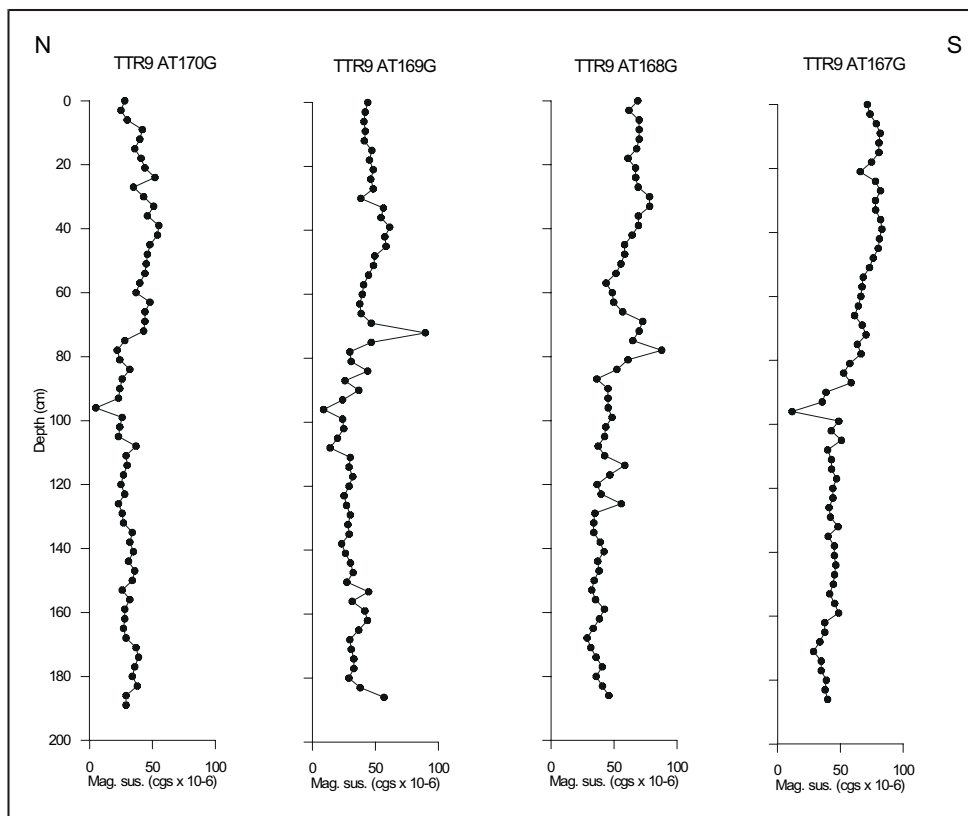


Figure 24. Magnetic susceptibility profiles from cores AT-167G to AT-170G.

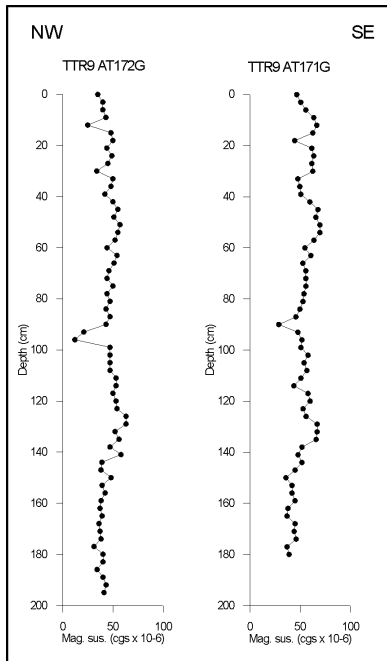


Figure 25. Magnetic susceptibility profiles from cores AT-171G to AT-172G.

preserving glacial turbidity events suggesting slope instabilities in this area. The area also preserved diatomite layers, suggesting either locally specific oceanographic conditions which facilitate diatom-blooms and/or variations in basal current activity, facilitating differential sedimentation of diatom tests.

Sub-bottom profiler imagery for these core sites (Fig. 21) shows a less well-stratified seabed. Caution should be used when interpreting these profiles due to the effects of vessel manoeuvring whilst coring.

Magnetic susceptibility profiles from these cores show some differences (Fig. 26). The diatomite in AT-174G is distinct at the top of the profile with decreasing values representative of reductive diagenetic reactions. The diatomite at the top of AT-175G is also apparent overlying a distinct unit with relatively high magnetic susceptibility values, suggestive of an increase in magnetic grain-size or clastic content.

Sub-bottom profiler record

3.5kHz and 4.5kHz sub-bottom profiler records were taken during the course of the survey and are dis-

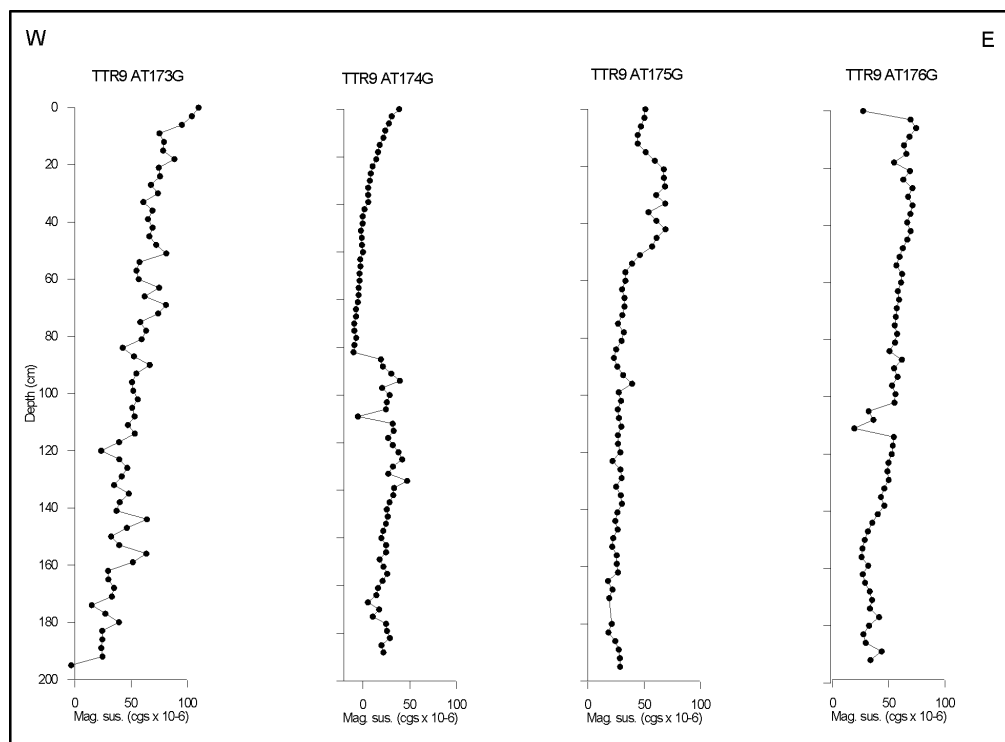


Figure 26. Magnetic susceptibility profiles from cores AT-173G to AT-176G.

cussed below. The records are not back-navigated and are presented against a linear timescale with geographic fixes corresponding to sample stations.

Line PRAT- 147 is a 3.5kHz pinger record run in a northwesterly direction over the seabed downslope of AT-156G (18:47 GMT) and upslope of AT-161G (19:37 GMT) (Figure 27). The profile

shows a mean penetration depth of c. 20 msec. with medium to strong reflectors 3 to 4 msec. below the seabed reflector. The seabed is flat, though a small increase in topography is seen toward the north-west. The profile shows several bright-spots indicative of sub-surface gas accumulations. Two main

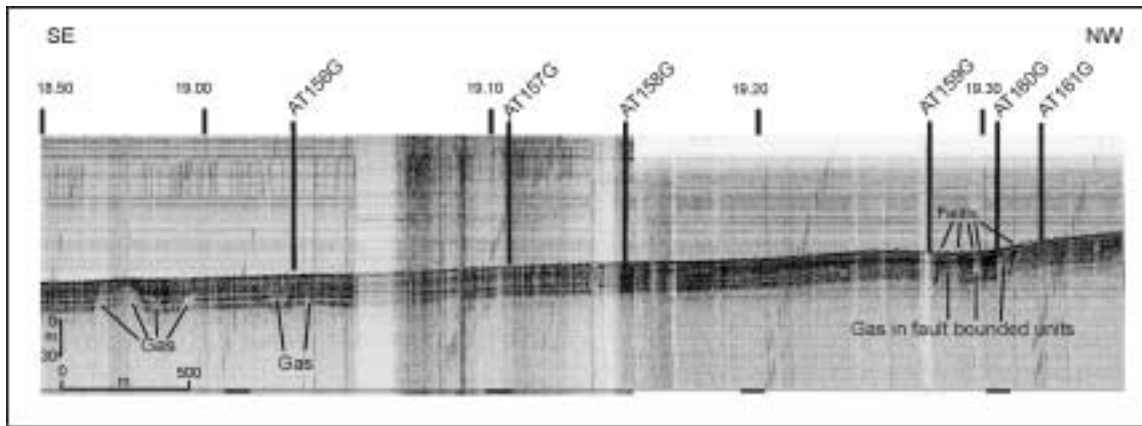


Figure 27. PRAT-147 subbottom profiler line (3.5 kHz pinger) showing shallow gas and associated faults in the vicinity of AT-156G to AT-161G sample stations.

clusters of bright-spots were imaged: downslope of AT-156G and in the vicinity of AT-159G to AT-161G. The latter cluster is fault bounded.

Figure 28 shows a 3.5kHz pinger line taken in transit between AT-166G and AT-167G. The profile shows two strong reflectors including the seabed reflector. From 14:20 GMT to 15:15 GMT the seabed is irregular with some possible faults associated with depressions. Weak indications of steep

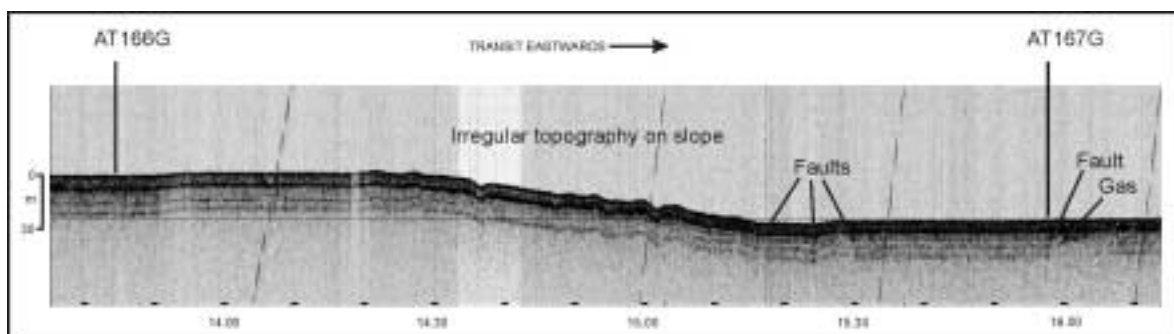


Figure 28. 3.5 kHz sub-bottom profile (pinger) between coring station AT-166G and AT-167G showing evidence of near-surface faulting and shallow gas. Note profile plotted against shiptime not distance. Approximate distance from AT-166G to AT-167G = 11.7 km.

fault traces can be seen at 15:11, 15:19, 15:27 and 15:31 GMT. Although it is probable that the irregular topography is entirely due to the presence of fault scarps on the seabed (see below), it is not possible to say whether downslope processes or sediment waves are also a contributing factor in this area. From 15:00 GMT, the topmost 10 msec. has an increasing number of internal reflectors.

Figure 29 shows a 3.5kHz pinger record from between AT-170G and AT-172G. The section reveals a high density of faults (c. every 400 m) whose surface expression generates an undulating topography. The irregular topography is seen as a southerly continuation of the irregular topography imaged further north (Figure 28). In this case, the irregularity is clearly structurally controlled. A faulted block is seen from 4:00 to 4:06 GMT, which has an offset on each side of 5 msec. At 4:20 GMT, a fault trace with c. 5 msec. offset is also seen. There is some slight evidence of near surface gas.

Figure 30 shows a 3.5kHz pinger record from the transit between AT-172G and AT-173G, which is run in a southerly direction. The sediments are well stratified and reveal a more steeply dipping seabed as the moat of the George Bligh Bank is encountered. There is evidence for possible slumping on the upper slope, with a thickening and disturbance of the stratified sediment.

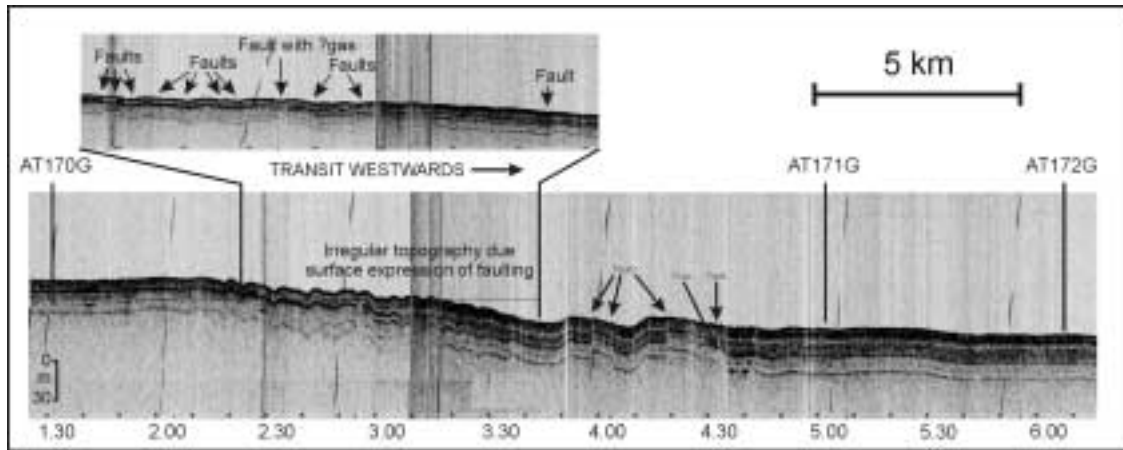


Figure 29. 3.5 kHz sub-bottom profile (pinger) between coring station AT-170G and AT-172G, showing evidence of near-surface faulting and shallow gas. Note profile plotted against shiptime not distance.

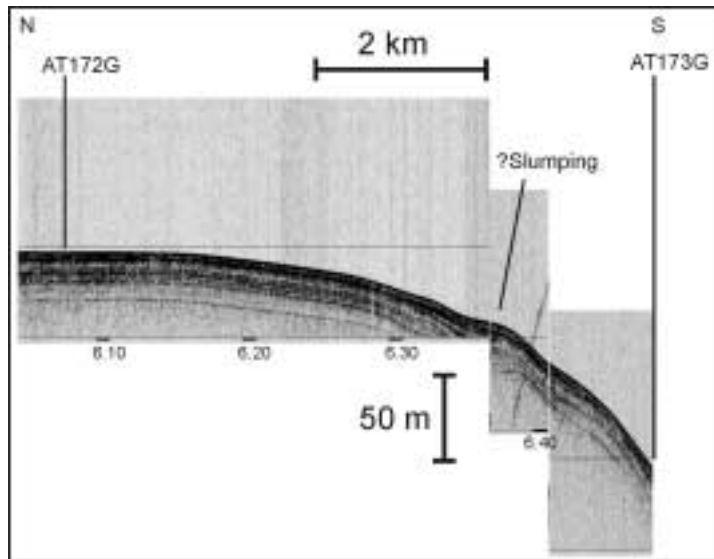


Figure 30. 3.5 kHz sub-bottom profile (pinger) between coring station AT-172G and AT-173G. Note profile plotted against shiptime not distance.

II.1.3. Summary

The results of geophysical surveying suggest the presence of shallow bodies of gas within the upper 30 m of the sediment column as well as near-surface faults. Near-surface faulting, presumably related to the reactivation of deeper structures, occurs in the sampled areas on the plateau although it is more intense in non-sampled intervening areas where the seabed is more disturbed by fault scarps.

Shallow gas bodies imaged by the geophysics are sometimes coincident with faulting, with fault planes forming a boundary to the gas bodies. This is suggestive of a mechanism whereby thermogenic gas is migrating to the surface along deeper fault planes.

In the southern part of the surveyed area, a deep is encountered with no evidence of faulting or gas bodies although there is evidence of slope instability.

All cores sampled Holocene (>10kyrs) and older glaciomarine sediments (>75kyrs). Sediments on the plateau showed characteristic background sedimentary sequences, whereas samples from the deep revealed evidence of slope instabilities (minor submarine avalanches) and localised concentrations of siliceous microflora implying a change in background biological environmental conditions.

II.2. SEABED GEOTECHNICAL AND BIOGEOCHEMICAL SURVEY IN THE EASTERN ROCKALL TROUGH

A. WHEELER AND TTR9 SHIPBOARD SCIENTIFIC PARTY

II.2.1 Introduction

Environmental parameters, sedimentary processes and seabed facies were studied on the Irish margin of the eastern Rockall Trough between 54°40'N and 55°00' N and between 10°30'W and 11°05'W where water depths range from 350 m to 2600 m. This area is of interest to Statoil Exploration (Ireland) Ltd. and partners where it is speculated that four separate hydrocarbon reservoirs exist: Kilkenny, Glendalough, Inishmor & Ceide. This study forms part of an environmental baseline and reconnaissance investigation in these hydrocarbon exploration areas. Further to these objectives, the acquisition of seabed samples, underwater video lines and sub-bottom profiler imagery provide interesting data with respect to current dynamics and local morphological features.

Existing public-domain data in this area is limited although extensive confidential commercial seismics exists. Released industrial seismics show the area to be underlain by collapsed fault blocks. Overlying these faulted blocks is a succession of sedimentary units capped by a regional unconformity. Some of the major faults show evidence of potentially breaking the surface on the upper slope and may mark the head of slumped units. Downslope, sedimentary packages imply contourite deposition

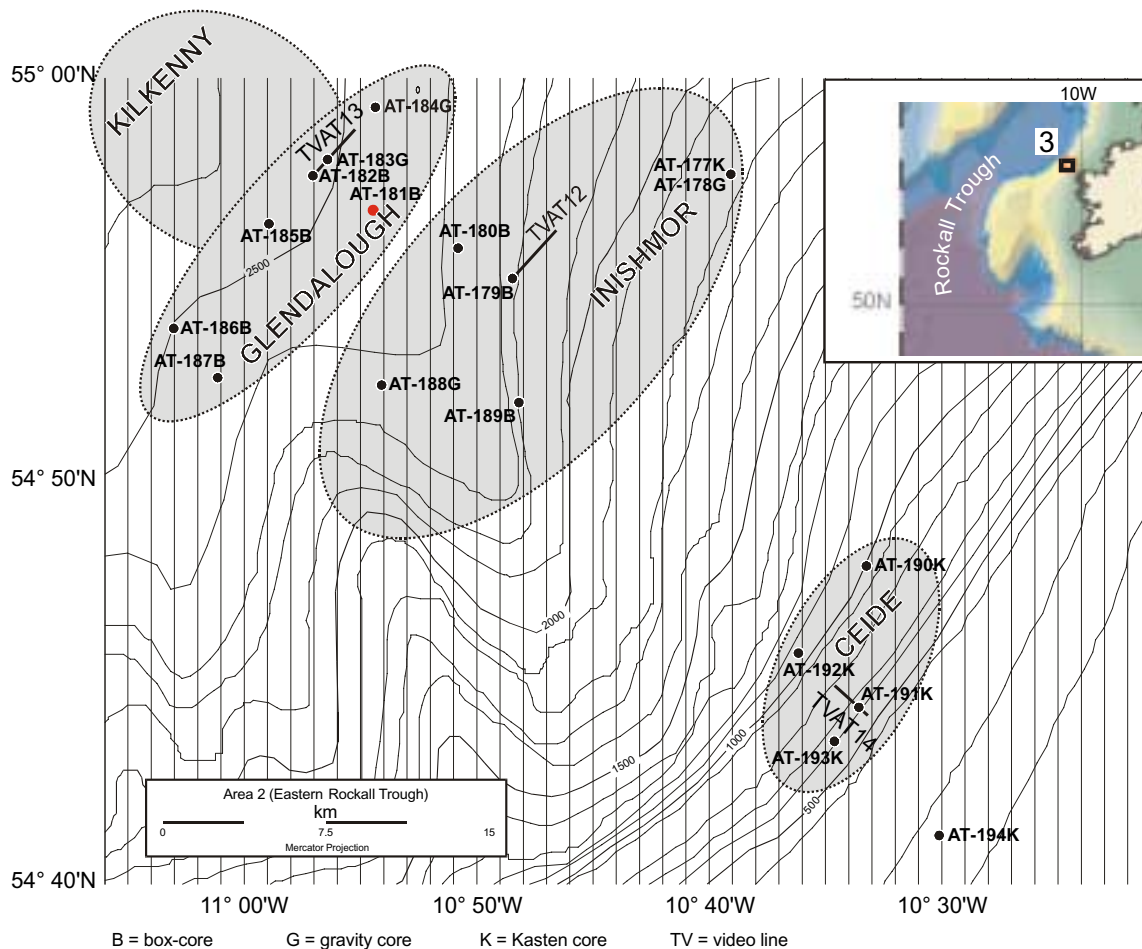


Figure 31. Location map showing prospect areas, core locations and underwater video-lines.

and slumping.

Existing bathymetric data (Figure 31) shows a continental margin (extending from the 400 m isobath to the 2600 m isobath) that becomes progressively gentler with depth. Between 2400 m and 1400 m, deflections in the bathymetric contours imply the presence of submarine canyons, an assumption that is confirmed by the sub-bottom profiler imagery. Confidential TOBI sidescan sonar data was taken in this area in waters deeper than 1000 m.

In addition to Statoil (Ireland)'s primary requirements, the sampling strategy also concentrated in the lower part of the suspected canyon features with attempts to quantify sediment facies, assess sediment mobility, instability, current strength and direction. Further sampling was concentrated on the upper slope with a view to assessing current activity along and across the slope as well as to assessing any slope instabilities.

II.2.2. Results

Core descriptions

The core location and details are presented in Figure 31 and Table 4.

Three different types of sampling gear were used depending on the nature of analyses that were to be performed on the sample. The box corer provides shallow retrieval but a relatively undisturbed sample and gravity cores provide deeper penetration. At site AT190K the box-core was lost on the seabed, probably because a boulder ensnared it. The cobbly nature of the seabed precluded the use of the gravity corer and sampling continued with a kasten corer that provided limited samples.

Descriptions of core profiles are presented in Table 5. Note that descriptions of gravity cores are

Core No	Date	Time, GMT	Latitude	Longitude	Depth m	Recovery
TTR9-AT177K	22.06.99	15.41	54°57.6262°	10°38.1243°	1689	20 cm
TTR9-AT178G	23.06.99	17.10	54°57.5952°	10°38.1191°	1689	160 cm
TTR9-AT179B	24.06.99	03.34	54°55.0367°	10°47.4696°	2082	24 cm
TTR9-AT180B	24.06.99	06.24	54°55.8049°	10°49.8134°	2217	24 cm
TTR9-AT181B	24.06.99	08.22	54°56.7562°	10°53.4681°	2334	30 cm
TTR9-AT182B	24.06.99	10.30	54°57.5893°	10°56.0642°	2414	31 cm
TTR9-AT183G	24.06.99	12.01	54°57.9939°	10°55.4344°	2439	164 cm
TTR9-AT184G	24.06.99	13.38	54°59.2885°	10°53.3618°	2503	142 cm
TTR9-AT185B	24.06.99	22.38	54°56.4042°	10°57.9706°	2563	21 cm
TTR9-AT186B	25.06.99	00.58	54°53.8016°	11°02.0542°	2587	29 cm
TTR9-AT187B	25.06.99	04.42	54°52.5942°	11°00.1656°	2517	26 cm
TTR9-AT188G	25.06.99	07.32	54°52.4664°	10°53.0724°	2354	185 cm
TTR9-AT189B	25.06.99	09.43	54°52.0148°	10°47.2130°	2244	36 cm
TTR9-AT190K	25.06.99	19.48	54°47.9403°	10°32.2317°	734	c.10 cm
TTR9-AT191K	25.06.99	16.45	54°44.4073°	10°32.5720°	622	30 cm
TTR9-AT192K	25.06.99	18.00	54°45.7313°	10°35.1378°	1037	c.10 cm
TTR9-AT193K	25.06.99	20.59	54°43.5743°	10°33.5820°	593	c.10 cm
TTR9-AT194K	25.06.99	21.55	54°41.3658°	10°29.0990°	209	c.10 cm

Table 4. General information on the cores sampled in the eastern Rockall Trough.

not provided as these were unopened to ensure that the geotechnical properties of the core were preserved.

In summary, cores AT177K to AT189B reveal silty foraminiferal marls overlying grey silty clay. The upper marl is 10-30 cm thick and probably of Holocene age (less than 10,000 BP). This is possibly associated with an increase in current speeds during the Holocene following the retreat of the gla-

Core No	Depth, bsf	Description
TTR9-AT177K	0-20 cm	Light brownish grey foraminiferal ooze with fine sand, structureless, homogenous, very well sorted, clayey admixture.
TTR9-AT179B	0-1cm	Light brown and oxidised silty marl with forams.
	1-24cm	Pale grey silty marl with forams. Structureless.
TTR9-AT180B	0-5cm	Light brown and oxidised with large burrow.
	5-24cm	Pale grey silty marl with forams.
TTR9-AT181B	0-8cm	Light brown silty marl with sharp basal contact.
	8-30cm	Grey silty clay with dropstones and burrow.
TTR9-AT182B	0-15cm	Silty foraminifera marl with dropstones and burrows. Oxidised.
	15-31cm	Greyish brown silty clay, bioturbated at top otherwise structureless. <i>Zoophycos</i> .
TTR9-AT185B	0-5cm	Brownish marl with forams. Structureless. Soupy for upper 2cm.
	5-21cm	Greyish marl with forams. Structureless.
TTR9-AT186B	0-10cm	Brownish marl with forams. Structureless. Soupy for upper 5cm.
	10-29cm	Greyish marl with forams, some bioturbation.
TTR9-AT187B	0-15cm	Sandy silty marl with black grit.
	15-26cm	Grey silty clay with <i>Zoophycos</i> .
TTR9-AT189B	0-3cm	Brown oxidised silty marl.
	3-36cm	Structureless grey silty marl.
TTR9-AT191K	Bulk	Coarse sand with clasts of various rock types. Interstitial clays and shell fragments. Clasts up to c.10cm diameter. Becoming sandy clay with depth.
TTR9-AT192K	Bulk	Coarse sand with centimetre sized clasts of various rock types. Shell fragments also present.
TTR9-AT193K	Bulk	Coarse sand with clasts of various rock types and sizes. Shell fragments and clayey admixture present. Fining downward to silty clay.

Table 5. Lithological description of cores collected in the eastern Rockall Trough.



Figure 32. Coarse-grained sediments recovered at site AT-194B.

cial ice caps and an increase in planktonic biological activity. Underlying this upper unit are glacio-marine silty clays with dropstones from icebergs and burrows. This unit probably continues for several metres.

Cores AT190K to AT194K provided very little retrieval but reveal a sandy gravel surface layer to the seabed overlying glacial marine silty clays. The upper gravelly layer also contains large boulders (Fig. 32). This layer probably formed due to an increase in Holocene current strengths that have eroded the silty clays but left a >c.30cm lag of stones that were too heavy to move.

Sub-bottom profiler record

The sub-bottom profiler was run throughout coring operations to provide a context for the coring sites. It provides valuable information with respect to morphological features imaged during transit between core stations and adds details to the existing bathymetry and TOBI sidescan sonar data. The record is not navigated and interpretations at core sites need to be cognizant of the fact that the

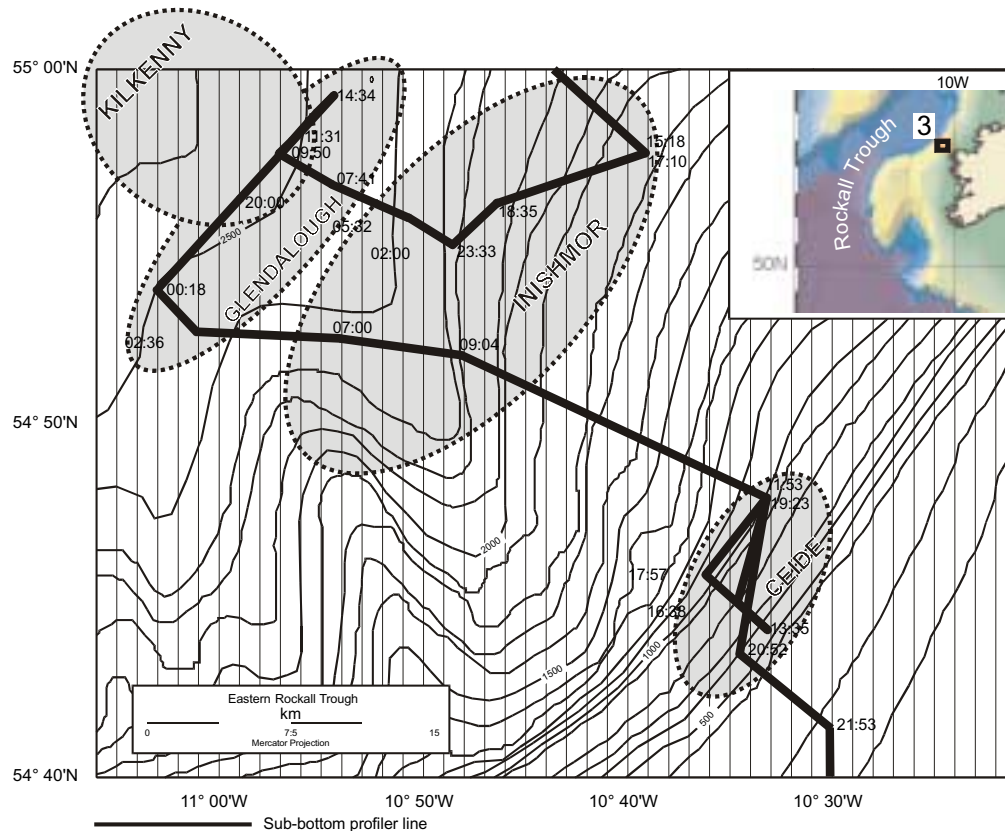


Figure 33. Location map showing the 3.5 kHz subbottom profiler cruise track.

ship is maneuvering, turning and/or stationary.

The track of the sub-bottom profiler line is shown in Figure 33.

Video Descriptions

Three video lines were shot in the area, one for each prospect area. Summaries of the video lines are presented below with images from the videos presented in Figures 21 - 23. The location of the video lines is presented in Figure 31. Identifications of animals from the video allow for a preliminary qualitative macrofaunal appraisal (Table 6-8).

TVAT12 - Inishmor

This video line runs from 54° 56.258'N / 10° 45.538'W to 54° 54.930'N / 10° 47.641'W in water depths of c.2200 m (see Fig. 34 for details). The video line starts at the edge of a channel and shows a hemipelagic covering of silty mud with patches of sand. This implies that there are currents operating in the channel but these are not strong enough to cause erosion or produce mobile bedforms. As the edge of the channel is encountered, the current speed increases and the substrate is littered with dropstones and the degree of bioturbation decreases. The abundance of dropstones is probably a result of the erosion of fine material. This area also supports a large diversity of brittlestars. As the video line proceeds past the edge of the channel it enters an area of extreme topographic irregularity that produces a large amount of side-echoes on the sub-bottom profiler. The seabed in this area is swept by relatively weak currents with a bioturbated muddy substrate dominating. As the video line proceeds to shallower water depths, the seabed again becomes exposed to currents and brittlestars and patchy sands again become apparent. The transition between all four zones is transitional.

Macrofauna	Abundance
<i>Holothuridea</i> indet. (sea cucumber)	common
Unidentified fish	common
cf. <i>Centroseymnus coelolepis</i> (Portuguese dogfish / Siki)	common
cf. <i>Macrourid</i> sp. (Grenadier)	common
cf. <i>Brevivaja</i> sp. (ray)	common
cf. <i>Opisthoteuthis</i> sp. (squid)	rare
cf. <i>Plinthaster</i> sp. (starfish)	common
Sea pens	common
<i>Ophiuroidea</i> indet. (brittlestar)	common

Table 6. Qualitative macrofaunal appraisal from Inishmor.

4.3.2.TVAT13 - Glendalough

This video lines runs from 54° 58.701'N / 10° 54.173'W to 54° 57.312'N / 10° 56.538'W at water depths of c.2500m. It also starts on the edge of a channel and proceeds up the edge of the channel onto a plateau with hemipelagics, and eventually onto a high before heading down into an adjacent channel. A similar facies to TVAT12 is encountered with stronger currents dominant in the channel and the channel edge, muddy sediment present away from the channel and indications of stronger currents on the pelagic high. Fauna also includes brittle stars, sea cucumbers, fish and a squid.

Macrofauna	Abundance
<i>Holothuridea</i> indet. (sea cucumber)	common
cf. <i>Zooaster</i> sp. (starfish)	abundant
cf. <i>Plinthaster</i> sp. (starfish)	rare
<i>Asteroidea</i> indet.	common
<i>Pyenogonid</i> indet.	rare
Unidentified fish	common
Unidentified shrimp	common
Tripod fish	common
<i>Notacanth</i>	common
cf. <i>Centroseymnus coelolepis</i> (Portuguese dogfish / Siki)	common
cf. <i>Benthoctopus</i> sp. / cf. <i>Bathypopus</i> sp. (octopus)	rare

Table 7. Qualitative macrofaunal appraisal from Glendalough / Kilkenny.

TVAT14 - Ceide

This video line runs from 54° 45.682'N / 10° 32.500'W to 54° 44.655'N / 10° 32.526'W and proceeds upslope at an angle from c.780 m to c. 680 m. The orientation of this line was changed from that proposed due to the direction of swell and increasing weather conditions. The line was also terminated after 1600 m due to equipment failure.

The entire line is characterised by the same facies, which consists of a coarse grained sand with large clasts. A significant number of these boulders are up to 20 cm in diameter or larger. Most of the fields of view show some large clasts. The area is obviously scoured by strong currents that are removing finer material but there are no indications of current-induced, sedimentary bedforms. The fauna observed on the line were also symptomatic of a high current regime including brittle-stars, sea urchins, large anemones attached to some of the boulders, crabs and several species of fish. There is

Macrofauna	Abundance
<i>Gastropoda</i> indet.	common
Hermit crab	common
cf. <i>Cidaris</i> sp. (echinoid)	common
<i>Unidentified fish</i>	common
<i>Helicolonius dactylopteris</i>	rare
cf. <i>Hydrolagus mirabilis</i>	common
cf. <i>Chimera monstrosa</i>	common
<i>Asterodea</i> indet. (starfish)	rare
cf. <i>Pseudarchaster</i> sp.	rare
<i>Artinaria</i> indet. (anemone)	rare
<i>Holothuridea</i> indet. (sea cucumber)	rare

Table 8. Qualitative macrofaunal appraisal from Ceide.

no evidence of cold water corals.

II.2.3. Summary

Findings are summarised below with respect to each of these prospect areas.

Inishmor

The seabed topography in the Inishmor area is dominated by the lower part of a submarine canyon system and, on the adjoining slope, hummocky topography probably caused by slope instability. The area is swept by moderate along-slope currents (producing patchy sands) that are more intense on topographic highs and canyon sides where some seabed erosion is apparent.

Sediments in this area are composed mainly of silty clays overlain by a variable thickness (c.20 cm) of marl composed principally of tests of planktonic foraminifera. The seabed supports a deep sea fauna dominated by polychaete worms and bivalves. Brittle stars and fish are also seen.

Glendalough including part of Kilkenny

The seabed topography in this area of deeper water suggests broad shallow canyon mouths opening onto the continental rise. A similar current regime exists for this area as with the Inishmor area and many of the attributes are the same. Sediments are again composed of silty clays overlain by a variable thickness of marl. Similarly, the seabed supports a deep sea fauna dominated by polychaete worms and bivalves with brittle stars and fish.

Ceide

The Ceide area is considerably up-slope from the other areas (upper continental slope to shelf break) and subjected to a much more rigorous current regime. Current activity shows no preferred discernible orientation and has prevented deposition or eroded finer sediments and generated an upper (>c.30cm thick) layer of sandy gravel with cobbles and occasional boulders. This area proved difficult to survey with large boulders offering a hazard to deployed equipment.

Biologically, the area supports a worm- and molluscan-dominated fauna with the presence of fish and encrusting bryozoa. No evidence of deep-water coral was detected, although no systematic search for these organism was performed (note that this area was not covered by the TOBI survey) and environmental conditions would favour deep-water corals.

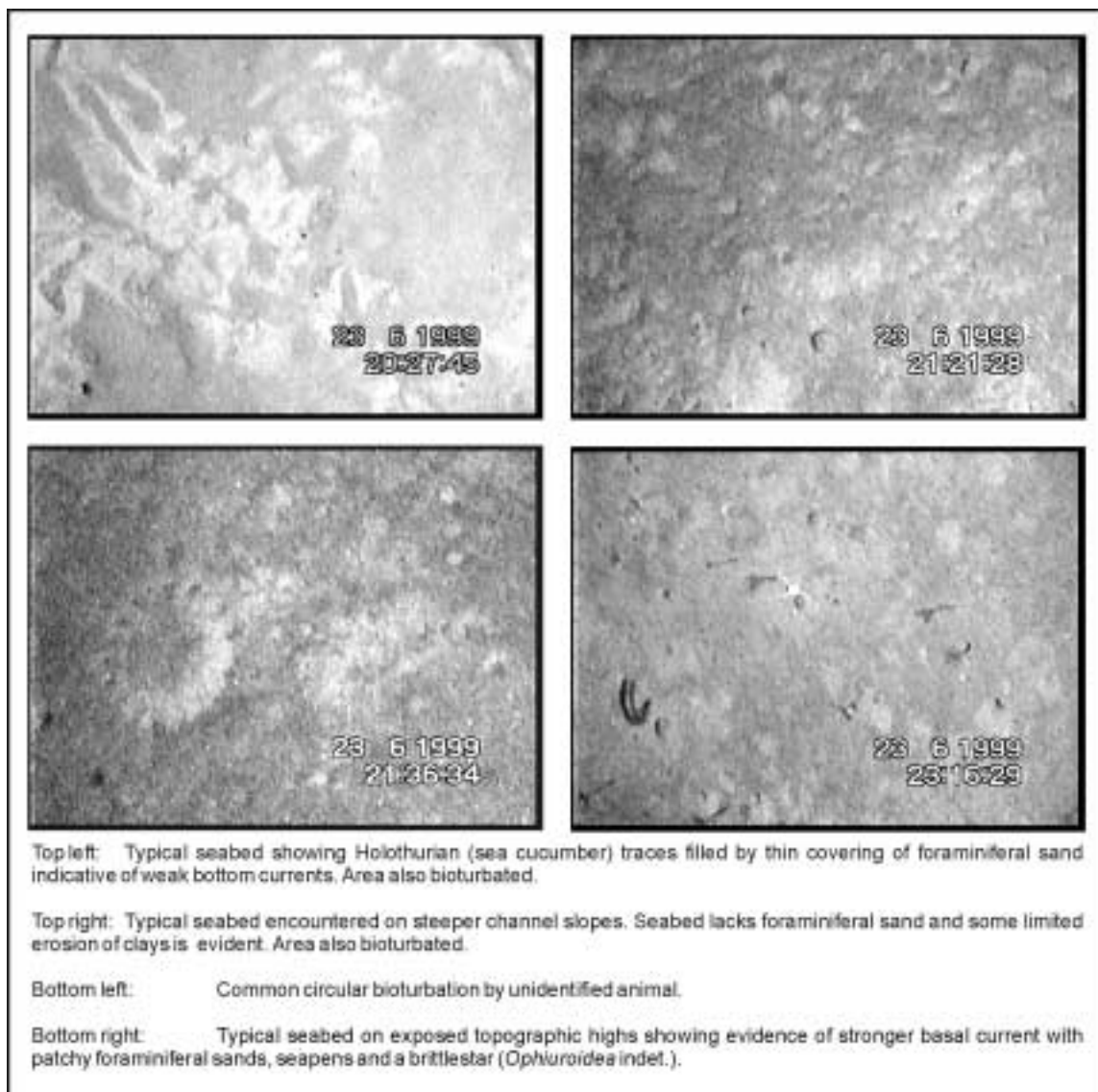


Figure 34. Video stills from TVAT-12 (Inishmor area).

III. PORTUGUESE MARGIN (Leg 2)

III.1. INTRODUCTION

J. MONTEIRO AND N. H. KENYON

The aim of the work west of Portugal was to use seismic as the primary tool, accompanied by long range sidescan sonar and hull mounted high resolution seismic, to investigate processes of sedimentation and tectonics in two areas. There were two seismic systems used. A Dutch system, not available during other legs of TTR-9, is described in the “Methods” section, as are details of the processing of the seismic data. In northwest Portugal, offshore of the Minho and Beira littoral, it was proposed to investigate any contourite deposits. These were expected to be at depths of less than 1500 m, influenced mainly by the Mediterranean outflow water as found further to the south e.g. Abrantes et al. (1998), and at depths greater than 1500m influenced by a proposed deep boundary current e.g. Gardner and Kidd (1987). The area was mainly east of the Vigo Seamount and around the Porto Seamount. On the best available bathymetry (Fig. 35) there are several elevated features alternating with the deeper areas of the Aveiro and Porto canyon systems and the Dom Carlos valley. Further south, in the area offshore of Estremaduras, we aimed to extend the survey begun during TTR8, which used seismic and OKEAN long range sidescan sonar to map the canyoned slope leading down to the Tagus abyssal plain. It was also intended to take cores from areas of presumed high sedimentation rate, on the outer shelf area adjacent to the Tagus River, for future palaeoceanographic and geochemical studies.

III.2. SEISMIC AND ACOUSTIC DATA

III.2.1. Area west of Porto

Seismic data

T. ALVES, J. MONTEIRO, L. PINHEIRO, S. BURYAK, A. VOLKONSKAYA

In the northern area, 14 seismic lines (PSAT-103 to PSAT-116) were obtained. Due to equipment problems with the Dutch system, the planned PSAT-102 line was not acquired. Similar data acquisition problems were solved with the use of the on-board Russian acquisition equipment on the lines PSAT-103 to PSAT-108. On remaining seismic lines (PSAT-109 to PSAT-119), in both areas, the Dutch system was used with satisfactory results.

Three seismic lines from the northern area were interpreted: PSAT-104, PSAT-106 and PSAT-114. In the southern area, the line PSAT-117 was selected for interpretation. On the lines PSAT-104 and PSAT-106, the seismic units recognised by Mougénot et al. (1986) were used in the interpretation (Fig. 36). However, their use was limited due to the shallow penetration depth. The deeper seismic units are oftentimes masked by non-coherent reflections derived both by acoustic noise and attenuation of the seismic waves at depth. A summary of the seismic stratigraphy of the surveyed area is presented below (modified from Mougénot et al. 1986):

Unit 1a (Quaternary?): The base of Unit 1a is characterised by a medium to low amplitude reflector, sub-parallel to the sea floor. Low to medium-amplitude internal reflectors are visible, occasionally with mounded geometries. Thickness varies between 50 ms and 180 ms.

Unit 1b (Upper Eocene to Quaternary): The base of Unit 1b is hardly distinguishable on the interpreted seismic lines, in part due to the low amplitude internal reflectors presented by the underlying Unit 2. Unit 1b is transparent with occasional non-continuous isolated internal reflectors. Thickness varies from 400 ms to 500ms.

Unit 2 (Senonian to Middle Eocene): The base of Unit 2 is characterised by downlap/baselap

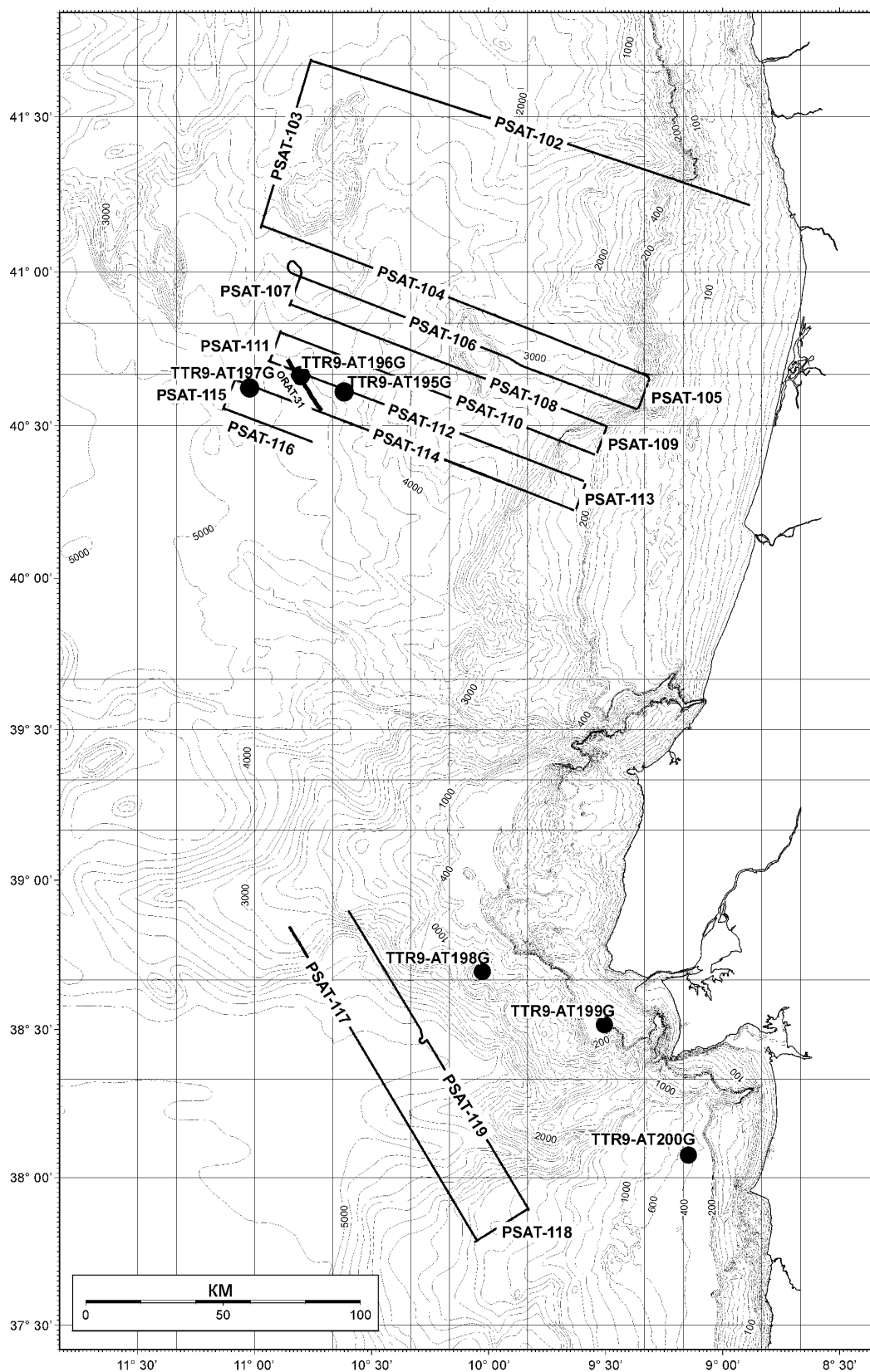


Figure 35. Location map of the studied areas offshore Portugal.

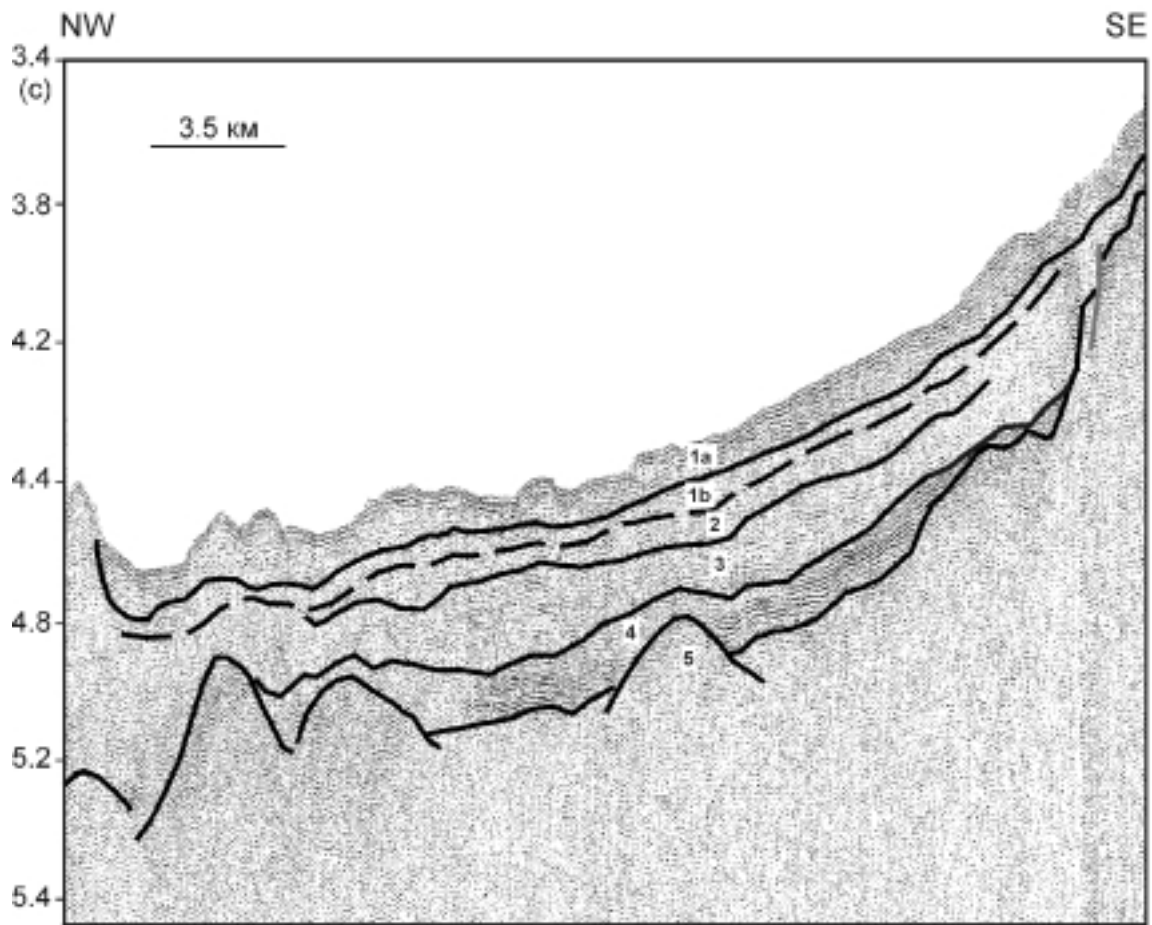


Figure 36. Fragment of seismic line PSAT 104. Major seismic units recognised in the area are shown.

onto a high to medium amplitude irregular surface. The unit presents moderate local deformation (folding). Low to medium amplitude internal reflectors are visible. Thickness varies between 60 ms and 200 ms.

Unit 3 (Albian to middle Cenomanian): The base of Unit 3 is irregular, characterised by onlap close to the recognised diapiric structures. Internally, Unit 3 shows high to medium amplitude reflectors. Thickness varies from 150 ms to 200ms. Moderate deformation (folding) is seen.

Unit 4 (Hauterivian to Aptian): The base of unit 4 is marked by an irregular surface showing onlap and downlap. The unit presents considerable localised growth and high to medium amplitude internal reflectors.

Unit 5 (early Cretaceous): The base of Unit 5 is marked by an irregular surface presenting onlap. The unit shows low to medium amplitude internal reflectors. Thickness is variable but difficult to measure due to the low definition that the Unit presents in depth.

Structurally, the area is characterised by the existence of two fault-bounded structures, Vigo and Porto Seamounts. The structures form positive features on the northwestern Iberian Margin, along with the Galicia Bank and Vasco da Gama seamounts, visible both on seismic and sidescan sonar. In the area between the two main structures two distinctive basins occur. The wider basin is coincident with the Dom Carlos valley, a major pathway for sediments from the Aveiro-Porto-Vigo canyon system and from the Valle-Inclan region, distributing turbiditic-type deposits onto the Iberia abyssal plain. A narrower basin is visible between the Porto Seamount and the continental slope, considered by Mougén et al. (1986) as the southernmost part of a major Mesozoic basin (Inner Galicia basin) located between the Galician Bank and the continental shelf of northwest Iberia. The shelf edge and slope areas mark the easternmost boundary of the surveyed area.

The existence of salt structures in the area between the Porto Seamount and the Portuguese shelf was mentioned by Mougenot et al. (1986). In the zone between Dom Carlos valley and the Vigo seamount deep structures with a similar seismic character could be recognised. However, due to the poor resolution of the lines in depth, it was impossible to obtain unquestionable proof of the existence of salt diapirs in the area west from Porto Seamount. Uplifted basement blocks can also produce a similar seismic character difficult to distinguish from real salt diapirs, especially when the resolution of the lines gradually decreases with depth, as in this case.

Apart from the two seamounts, all the main geomorphological features appear to be fault-bound. The seismic data confirms this assumption, already suggested on bathymetric data and on the 3.5 kHz profiles. In the Dom Carlos valley a fault-scarp is visible on both sidescan sonar and seismic data. The fault clearly dissects the Tertiary deposits, with Units 1 and 2 showing a considerable reduction of thickness inside the valley. This might be due to later erosion or non-deposition of Tertiary deposits inside the valley, with subsequent preservation, without erosion, of the Units 1 and 2 west of the fault. The sharp geometry and the Units' relative displacement on the adjacent hangingwall and footwall zones of the fault, indicate a possible late Tertiary (Miocene?) age for the fault movement. However, in accord with the structural pattern in the studied area, this feature may constitute an early Cretaceous fault reactivated during late Tertiary times.

OKEAN and OREtech sidescan sonar data

N. H. KENYON, J. MONTEIRO, P. SHASHKIN, M. IVANOV

Fourteen lines were run on the margin west of central Portugal (Fig. 35). The longer lines were even numbered, PSAT-102 to PSAT-116, the odd numbered lines (PSAT-103 to PSAT-115) were the shorter connecting lines on the shelf and at the distant side of the survey. PSAT-102 ran westwards to the north of Vigo Seamount. PSAT-103 ran southwards, just west of Vigo Seamount, and the remainder were run 12 km apart in order to give as near complete sidescan coverage as possible. In shallow

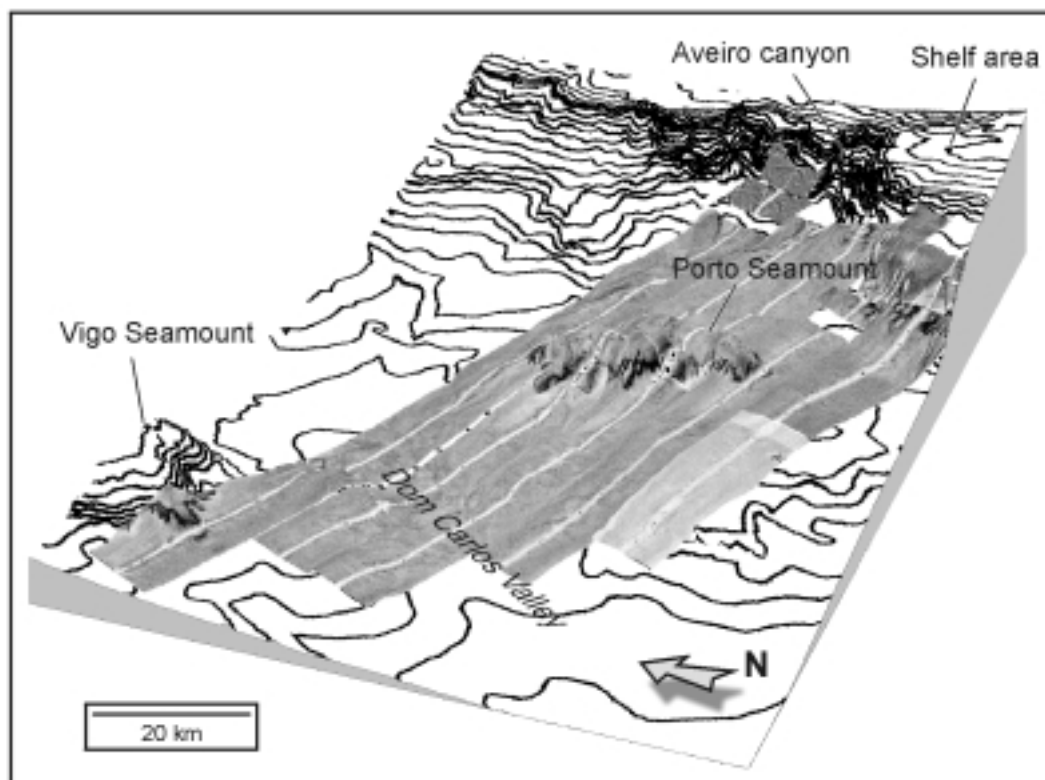


Figure 37. Perspective view of the OKEAN mosaic of the main survey area west of Porto.

shelf areas the shorter range of 3.6 nm was used and in deeper areas, PSAT-116 and part of PSAT-12, a range of 28 km was used. Only one deep towed line was obtained (ORAT-31). This was a crossing of the east side of the Dom Carlos Valley where prolonged echoes had been seen on the hull mounted 3.5 kHz profiler. There were some subbottom reflectors that appeared to be eroded as the axis of the valley was crossed. The quality of the deep towed sidescan image was poor. This was attributed to strumming in the wire due to the long length of cable out.

The OKEAN image (Fig. 37) show that the shelf has a slightly higher overall backscatter strength than the sedimented parts of the deep margin, in keeping with it having coarser surface sediments. The slope is steep with many short canyons starting at a depth of about 500m. The head of Aveiro Canyon has an amphitheatre shaped head. Only the Porto and Aveiro Canyons can be seen on the OKEAN beyond the foot of the slope. They both have near straight channels, as does the Dom Carlos Valley into which they flow, which is typical for canyon fed systems on steep margins (Clark et al., 1996) although the extreme straightness of these channels may be due to fault guidance. The straight, parallel, NE-SW trending lineations that mark the thalweg of the lower reaches of the Dom Carlos Valley have also been seen on the GLORIA sonographs (Roberts and Kidd, 1984).

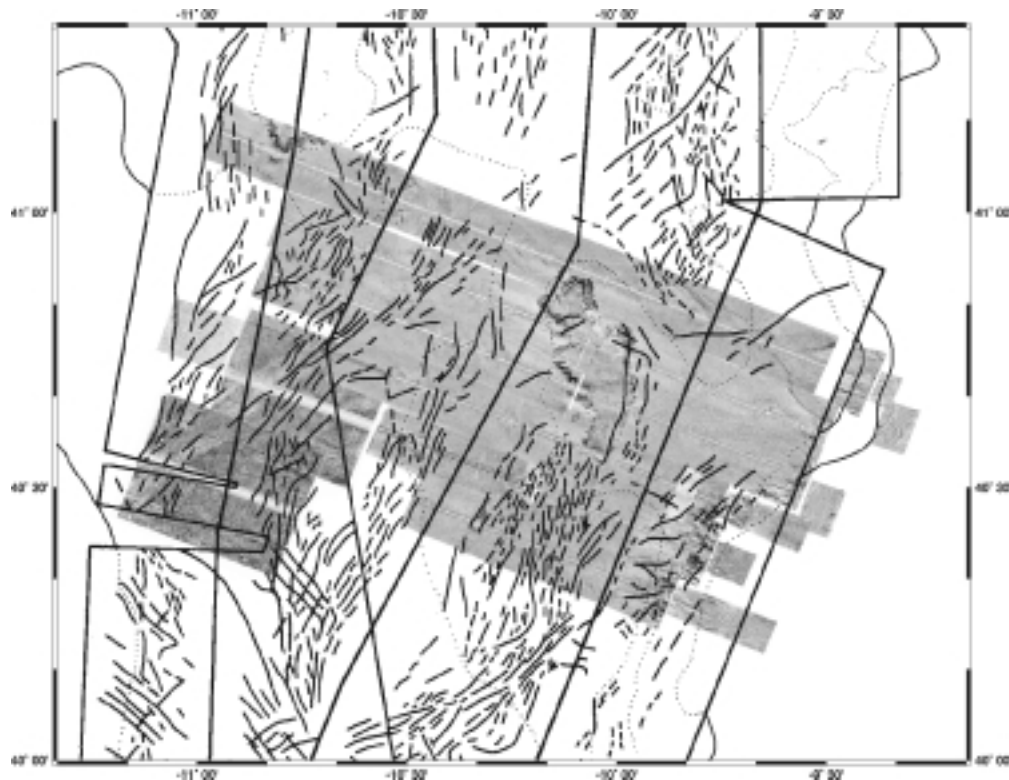


Figure 38. Trends of feature mapped from early GLORIA sidescan sonar data. (Roberts and Kidd, 1984) compared with the area of the OKEAN survey. Later analysis of the same GLORIA data by Gardner and Kidd (1987) differentiated channel associated features from other lineations thought to be sediment waves. The Dom Carlos Valley trend is well seen, but most other features on GLORIA were not present on OKEAN or on the 3.5 kHz profiles.

Amongst tectonic features on the sidescan mosaic, the most prominent are the bounding scarps of the non-magnetic seamounts (Fig. 37). These are rather jagged in plan view, without a well developed system of downslope gullies. Some have round headed embayments. The edges have been described by Mougénou et al. (1984, 1986) from a Seabeam swath bathymetry and a GLORIA survey. Something of the overall, relatively straight, fault bounded nature of the scarps on Porto Seamount, with their abrupt changes of trend, can be seen in places. There is also a small seamount that is direct-

ly crossed west of Vigo Seamount on PSAT-103. We also map the northern end of a long, narrow, NNE trending ridge, seen also on the GLORIA survey (Gardner and Kidd 1987). The ridge is about 1000m high where it was crossed. Another place where rock outcrop is mapped is an easterly dipping scarp, bounding the west side of the Dom Carlos Valley. This also trends NNE, the dominant trend in this part of Iberia. Three narrow, parallel lineaments are mapped to the NW of the Porto Seamount and trend NW. As there is little or no penetration of surface sediment seen on the 3.5 kHz profiles from here they are assumed to be structural features. Mougenot (1985) has a NE trending scarp at this location.

Most of the broad continental rise that we map has relatively low backscatter of sound and is relatively featureless on the OKEAN records. In the same area the GLORIA survey seemingly shows extensive, near ubiquitous, fields of bedforms with various trends (Fig. 38). They are interpreted as sediment waves, presumed to be contour current formed deep sea mud waves (Gardner and Kidd 1987). As our lines have 3.5 kHz profiles accompanying them, we can map where there are any potential mud waves. There are no wavy bedforms in many of the places where the GLORIA mapping claims them to be. Some of the most featureless ground seen on 3.5 kHz profiles has bedforms marked on the GLORIA interpretation. We conclude that it is unlikely that there are sediment waves in the area. Long range sidescan sonar has successfully mapped mud waves trends elsewhere, such as on the Blake Bahama Outer Ridge and the Feni Ridge, but neither GLORIA nor OKEAN seem to have convincingly mapped the trends here. There is a faintly seen west-east lineation on PSAT-102, in an area of possible mud waves north of Vigo Seamount. However the GLORIA interpretation for the supposed mud waves trends in this area is dominantly north-south.

3.5 kHz hull mounted pinger profiles

An excellent data set was collected with the 3.5 kHz profiler along all of the lines in the area (Fig. 35). The initial printing of the profiles is greatly exaggerated and so, as an aid to interpretation,

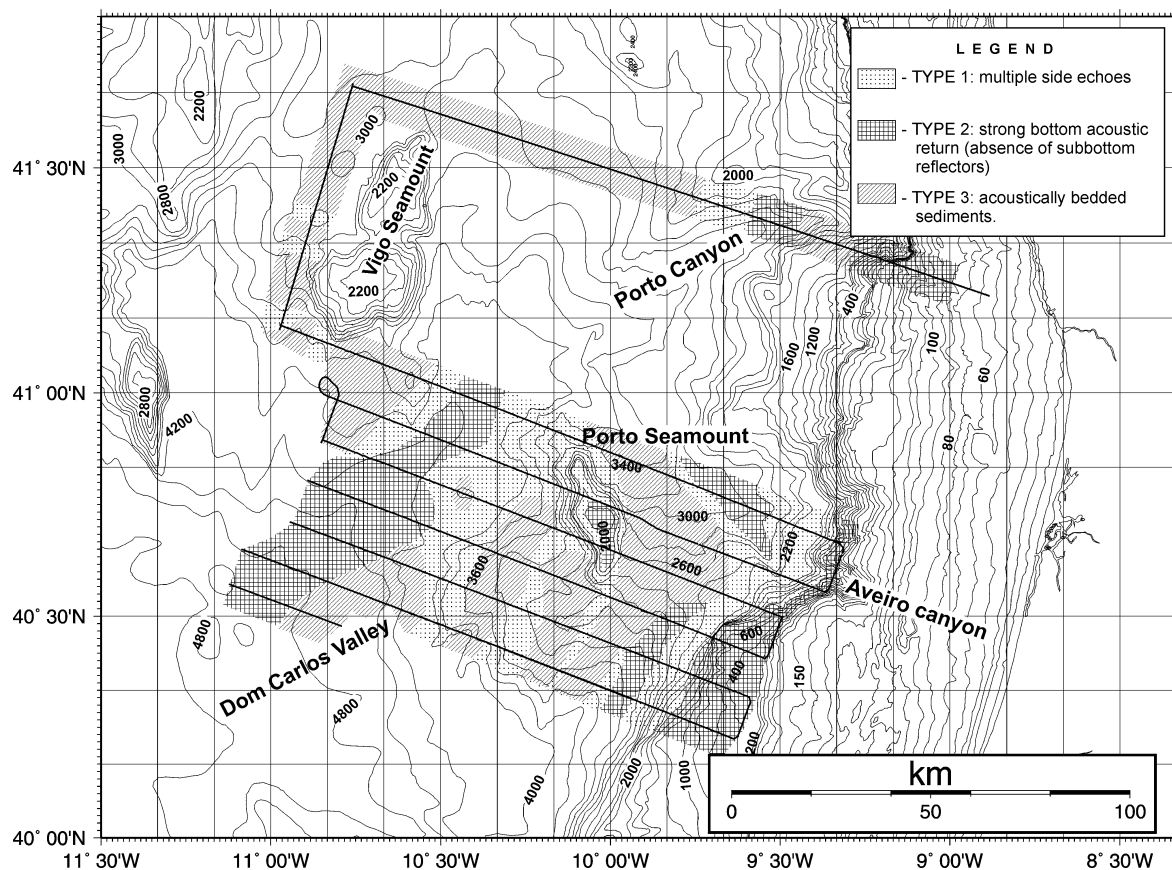


Figure 39. Map of echo character from analysis of the 3.5 kHz profiles.

a second copy was produced at a lower exaggeration and printed to the same length.

A map of the echo character on the margin was made following the principles introduced by Damuth et al., (1988) but modified for the local circumstances (Fig. 39). The echo character was divided into readily mappable types (Fig. 40).

Type 1. Steep slopes or other areas of hyperbolic echoes where no penetration could be detected. These occur on the continental slope, on the edges of the seamounts and other rock outcrops, on the margins of channels and extensively west of the Porto Seamount, where the seafloor does not have an overall steep gradient but is generally rugged. Little depth of soft sediment is expected in these areas.

Type 2a. Single echo, either narrow or prolonged, no subbottoms. This is found on the outer shelf, in the axis of channels and on the southern crossing of the top of Porto Seamount. It is expected that where this type is found there will be relatively coarse sediments near or on the seafloor and indeed there are coarse sediments mapped on the outer shelf (Vannev and Mougénot, 1990). In the Dom Carlos Valley axis there appears to be some erosion at the place where core AT-197 was taken.

Type 2b. Single or prolonged echo with some limited subbottom reflectors. This is found on the mid-shelf sediment body and on the gently sloping floor of the Dom Carlos Valley outside of the thalweg. Some coarse sediments would be expected. Thin sands were found in a core from a Type 2b area.

Type 3a. Continuous parallel bedded, not wavy, good penetration. Found in elongate areas surrounding Porto Seamount. These belts trend mainly NNE-SSW and tend to occur on the very slightly higher ground on which the Porto Seamount is located. Sediments are expected to be fine grained.

Type 3b. Wavy, continuous parallel bedded, good penetration. These occur in some relatively limited areas near Porto Seamount but the best development of them is NE and NW of Vigo Seamount. Mougénot (1985) maps them as “Distal accumulations”. They are expected to be fine grained. These could consist mainly of hemipelagic drape over underlying irregular, possibly faulted relief or could be contourites formed into mud waves. If they are mud waves then they are not very regular bedforms and do not have any consistent asymmetry.

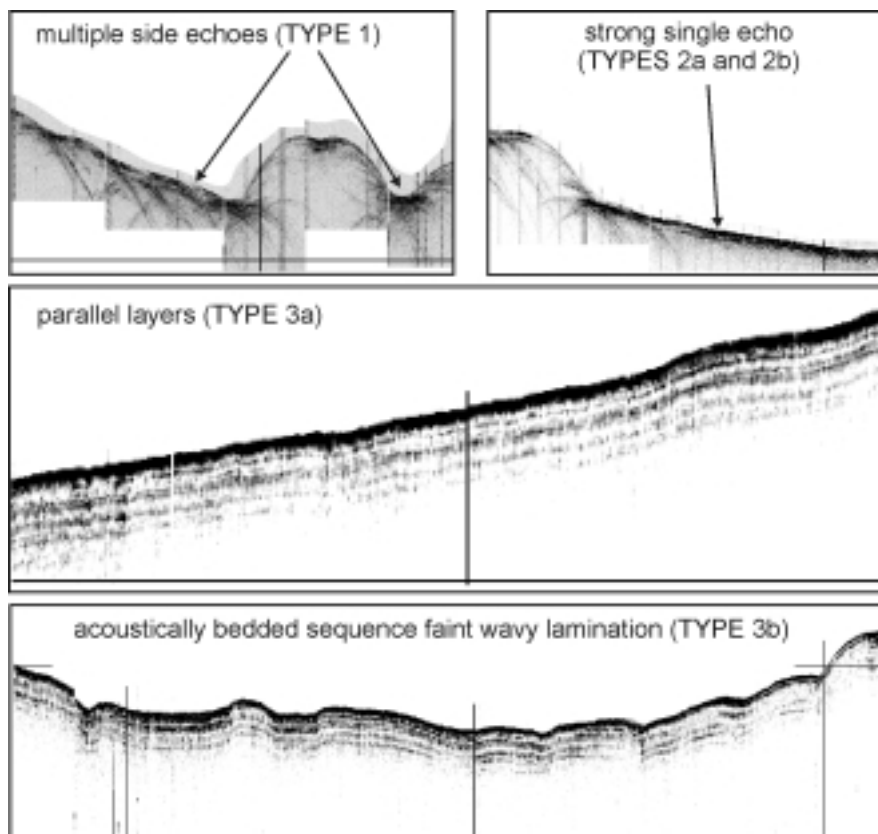


Figure 40. Examples of the echo character types mapped from 3.5 kHz profiles on the margin west of Porto. Note: images are not at the same scale.

Summary

One of the aims of the survey was to investigate possible drifts ornamented with mud waves that are believed to be due to a deep boundary current flowing northwards along the Iberian Margin at depths below 1500 m. The seismic profiles produced no firm evidence for drifts. There are bodies of sediment, having a sheet like appearance, a generally north-south orientation and that lie in slightly elevated positions, that could be drifts. However there is no telling evidence of contourite drift geometry. The typical seismic characteristics of drifts may not be seen because they are bounded by the pathways of erosional turbidity currents. Moats around the seamounts are proposed by Gardner and Kidd (1987). There is not enough evidence in this survey to confirm whether there is a consistent pattern of moat development. Nor is there any good evidence for contourite mud waves. The hull mounted 3.5 kHz profiles show that there are places where wavy bedded sediments occur. The waves are not regular and neither are they asymmetrical, as would be expected in a relatively strong contour current or from moulding by overbank turbidity currents. The OKEAN data set is of generally good quality, made in favourable weather, and has had some preliminary digital enhancement but there is no evidence for trends at the wavelength of these wavy features on the OKEAN data.

Many of the potential sediment waves mapped by an early GLORIA survey are considered to be spurious observations as they occur in places with no sediment penetration on 3.5 kHz profiles or with no wavy bedding. However some of the wavy bedding that is seen on profiles from this survey could be mud waves due to a weak contour current that flowing in either a northerly or a southerly direction. Cores need to be taken from the areas of wavy bedding and studied in order to solve this problem.

III.2.2. Area west of Lisbon

Seismic data

T. ALVES, J. MONTEIRO, L. PINHEIRO, S. BURYAK, A. VOLKONSKAYA

This was one of the sites of the TTR8 cruise, where seismic study was undertaken in 1998. Further work on the canyon system was one of the objectives for this year. Three seismic lines (PSAT-117 to PSAT-119) were executed along with OKEAN sidescan sonar.

The poor penetration revealed by the seismic data conditioned the interpretation of the surveyed area. Lines PSAT-118 and PSAT-119 were not interpreted for this reason. In essence, only the deposits filling the Lisbon and Setúbal Canyons in the studied area could be analysed. Here the sediment packages are very heterogeneous in character. A thin package with irregular internal reflectors is underlain by a unit showing wavy-hummocky internal character in the Lisbon Canyon (line PSAT-117). Towards

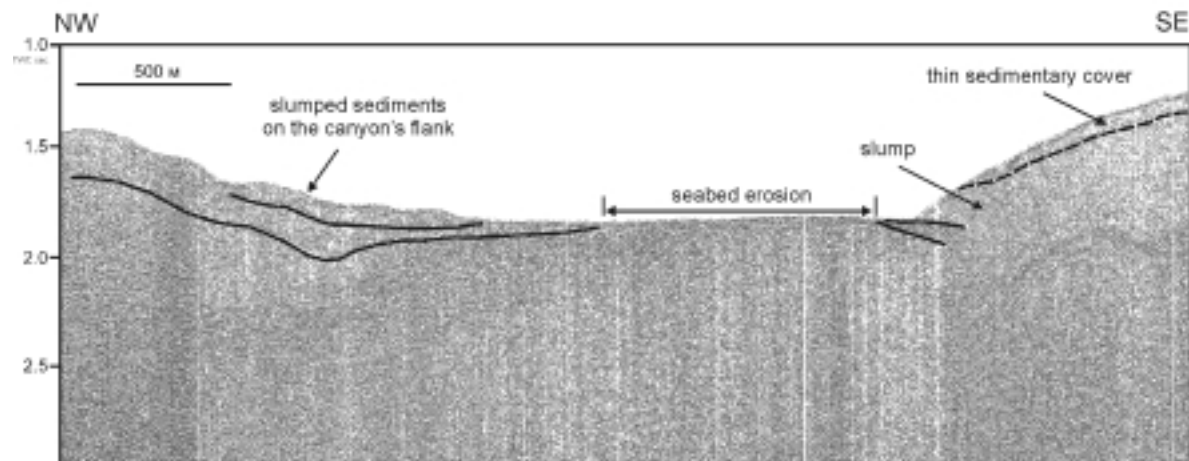


Figure 41. Fragment of seismic line PSAT-117 running across Setubal canyon.

the continental slope and the Afonso de Albuquerque Plateau, the same units change laterally into a homogeneous and thick package with medium to high amplitude sub-parallel internal reflectors. The seismic character of the sedimentary units is again hardly identified in the Setúbal Canyon (Fig. 41). On the slope area adjacent to the Setúbal Canyon, a homogeneous package composed of sub-parallel medium amplitude internal reflectors is visible. The homogeneous character of the package suggests the existence of contouritic deposits in the area, as seen at similar depths west off Lisbon (Kenyon et al., 1999).

Structurally, the study area does not show the same density of structures observed offshore Porto, partially because of the lower density of data. Nevertheless, the slope area is dissected by several gullies and minor canyons which seem to follow the dominant northeast to southwest and north-northeast to south-southwest fault trends recognised onshore in the Central Lusitanian basin. Another major feature is the Afonso de Albuquerque Plateau, a prominent anticline southerly bounded by a reverse fault, possibly the offshore extension of the Setúbal-Arrábida Fault that bounds the Arrábida Chain onshore. The same structural character is seen on the zone south of the Afonso de Albuquerque Plateau, towards the Setúbal Canyon and in the adjacent slope area.

OKEAN sidescan sonar data

N. H. KENYON, J. MONTEIRO, P. SHASHKIN, M. IVANOV

Two lines (PSAT-118 and PSAT-119) were run to extend the coverage of the canyoned slope west of Lisbon that was obtained in TTR8 (Kenyon et al., 1999). The area covered is the base of the slope which is crossed by sediment pathways fed by the two main canyon systems, the Lisbon Canyon and its tributaries and the Setubal Canyon (Fig. 42). There is a canyon cutting through the southern flank of the Estremadura Spur that is about 300 m deep, where crossed, and flat floored. It appears to stop at the foot of the slope. The canyons on the steep slope off Lisbon have strongly backscattering

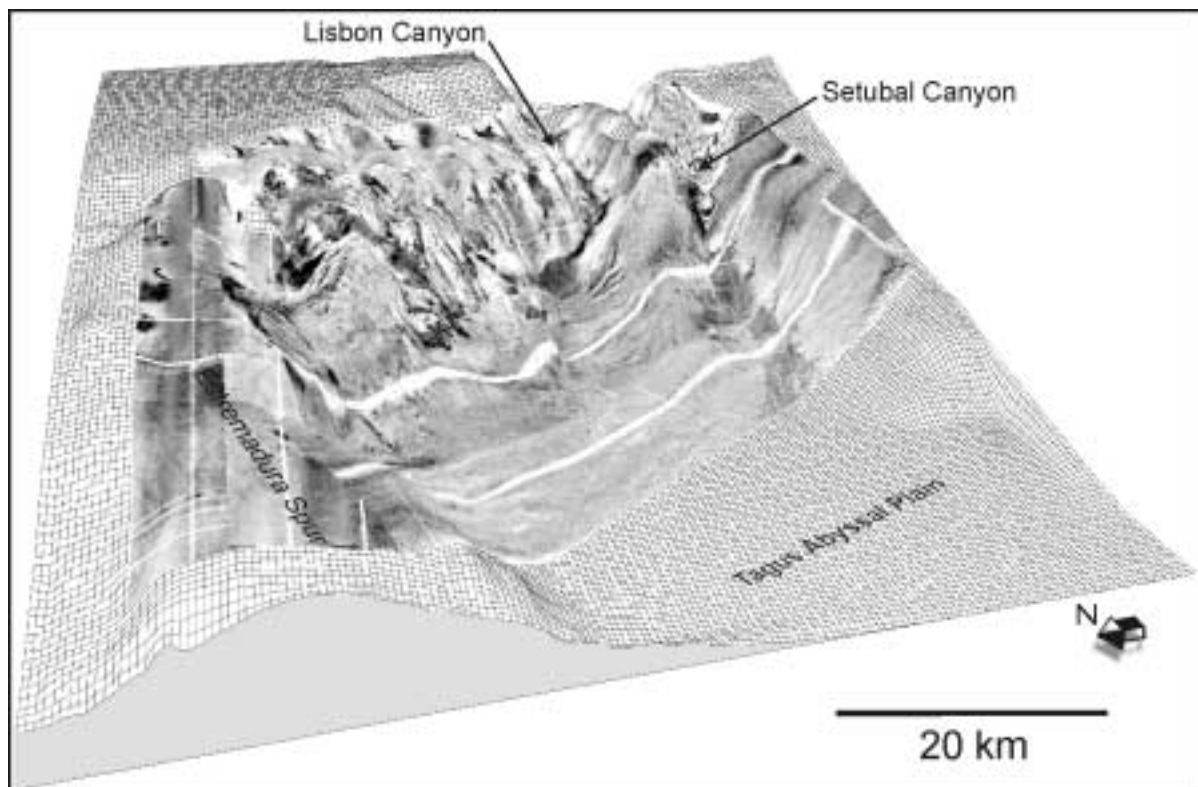


Figure 42. Perspective view of the OKEAN mosaic of the survey area west of Lisbon.

floors but these cannot be traced far beyond the foot of the slope. The Lisbon Canyon turns sharply to the right, steered by an upstanding ridge, before resuming its course to the west. The Setubal Canyon makes a sharp twist at a depth of about 3000 m. The westward extension which separates the two main canyons is mapped on both OKEAN lines and is seen to have secondary channels running down from its crest both to the Lisbon Canyon and to the Setubal Canyon. Both canyons have relatively flat floors but the Lisbon Canyon is much wider than the Setubal Canyon. The Lisbon Canyon also has much weaker backscattering than the Setubal Canyon. High backscattering on canyon floors has been shown to mean that there is little pelagic sediment at the seafloor and that there are scour holes and/or gravel ripples (e.g. Limonov et al., 1995). Just before we see the last of the Setubal Canyon pathway it seems to be spreading out into a funnel shaped mouth, a common characteristic of submarine canyons e.g. Kenyon and Millington (1995).

The canyon on the Estremadura Spur is fairly straight and runs NE-SW. This is in keeping with the trend found in other canyons mapped on TTR8. It is believed to show structural control by major faults.

3.5 kHz hull mounted pinger profiles

Two profiles, PRAT-117 and PRAT-119, accompany the two OKEAN and seismic lines. The ridge to the south of the study area has continuous, parallel bedded reflectors with the best penetration in the area. The sediments are believed to be a part of a contourite drift. There are prolonged echoes in the floor of the two main canyons but the echoes from the Lisbon Canyon have some subbottom reflections whereas those from the Setubal Canyon do not.

III.3. BOTTOM SAMPLING

Sediment cores

F. TEIXEIRA, G. AKHMANOV, A. AKHMETZHANOV, A. STADNITSKAYA, E. KOZLOVA, L. MAZURENKO, A. SAUTKIN, D. DIXON, D. OVSYANNIKOV, A. SADEKOV, N. RASUL, I. BELENKAYA, YU. VOLKOVA, E. SUSLOVA, AND D. GONCHAROV

In the northern part of the study area west of Porto (Fig. 35), 3 coring attempts were made but only 2 cores were recovered. The first one, AT-195G, from the broad Dom Carlos Valley, west of Porto Seamount and another, AT-197G, east of Vasco da Gama Seamount, at the deepest part of the basin, on the continental rise. The AT-196G was meant to sample the channel of Dom Carlos Valley.

In the southern part of the study area west of Lisbon (Fig. 35), AT-198G was taken on the upper slope southwest of Estremadura Spur in order to continue the investigation of sediment characteristics begun where the TTR8 studies took place, last year. Two more cores were collected: AT-199G in a flat area west of Lisbon canyon and AT-200G south of Setúbal canyon, both places with high sedimentation rates, according to studies of previous seismic reflection profiles.

The full log description was made by the sedimentological team and core logs are provided in

Core No	Date	Time GMT	Latitude	Longitude	Cable length, m	Depth, m	Recovery, cm
TTR9-AT-195G	05.07.99	16.36	40°36.982	10°36.517	4540	4469	73
TTR9-AT-196G	05.07.99	20.27	40°40.174	10°47.736	4735	4625	-
TTR9-AT-197G	06.07.99	23.52	40°37.757	11°00.754	4880	4800	103
TTR9-AT-198G	08.07.99	20.20	38°41.846	10°01.820	1070	1045	276
TTR9-AT-199G	08.07.99	23.23	38°31.148	09°30.583	144	143	122
TTR9-AT-200G	09.07.99	02.32	38°04.804	09°08.978	505	502	31

Table 9. General information on the cores sampled on the Portuguese margin.

Core No	Geographical Setting	Instrumentation	Acoustic Characteristics
TTR9-AT-195G	Slope above the Dom Carlos Valley (at 09:48 on 3.5 kHz profiler PSAT-112)	OKEAN long range side-scan sonar; 3.5 kHz profiler; Single channel high resolution seismic system.	Subparallel layering in the upper part of 3.5 kHz profiler
TTR9-AT-196G	Near axis of the Dom Carlos Valley to the west of Porto Seamount (at 08:15 on 3.5 kHz profiler PSAT 112)	OKEAN long range side-scan sonar; 3.5 kHz profiler; Single channel high resolution seismic system.	Subparallel layering and transparent lens in the upper part of 3.5 kHz profiler
TTR9-AT-197G	Dom Carlos Valley. East of Vasco da Gama Seamount (at 06:20 on 3.5 kHz profiler PSAT 114)	OKEAN long range side-scan sonar; 3.5 kHz profiler; Single channel high resolution seismic system, ORETech side-scan sonar.	Bottom of the Valley with rough topography
TTR9-AT-198G	Upper slope to southwest of Estremadura Spur, flat area between canyons with high sedimentation rate	TTR-8 OKEAN long range side-scan sonar; 3.5 kHz profiler;	
TTR9-AT-199G	Flat area west of Lisbon Canyon	-	-
TTR9-AT-200G	Upper continental slope to the south of Setubal Canyon	-	-

Table 10. Sedimentological, acoustic and geological characteristics of sampling stations on the Portuguese margin.

Annexe I. The main sampling site parameters and sedimentological, acoustic and other relevant information are summarized in Tables 9 and 10. A generalized description of core logs is given below.

In the northern area, the core AT-195G (Fig. 43) consisted of light brown and grey marl and carbonate clay intercalated with numerous thin layers of silt, sand and gravel deposited by gravity flows. Core AT-196G recovered only a small fragment of light brown marl in the core-catcher, suggesting a hard substratum covered with only a thin veneer of carbonate pelagic sediments. The core AT-197G recovery was 103 cm. Its upper interval (0-23 cm bsf) consisted of light brown pelagic marl, intensively bioturbated and with abundant planktonic foraminifers. The middle part of the core (23-57 cm bsf) showed evidence for intensive slumping represented by dislocated marly sediments as well as by lenses of silt and sand of initially turbidite origin. The lowermost interval (57-103 cm bsf) was composed of rhythmic thin intercalations of light grey marl (normally graded by foraminiferal content and

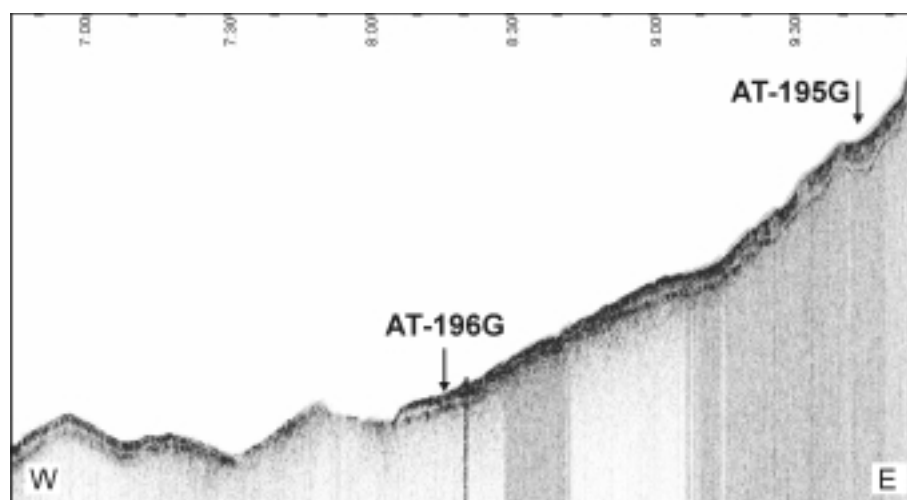


Figure 43. 3.5 kHz profiler record across Dom Carlos valley flank with sampling stations indicated. Possible erosion by turbidity currents is seen west of AT-196G.

slight changes in colour) and grey silty clay (normally graded by silty admixture content), implying deposition from distal terrigenous and carbonate gravity flows.

In the Lisbon area, the longest core recovered, AT-198G, had generally muddy sediment. Numerous lenses of silty and fine grained sandy material as well as normal and inversely graded horizons were observed throughout the core, suggesting possible deposition from contour currents. Finally, the two last cores, AT-199G and AT-200G, were rich in silty, sandy layers with well sorted sand, mixed with fine dark minerals and with sedimentary structures implying a river material supply, perhaps from the River Tagus. The upper intervals of AT-199G contained abundant inclusions of anthropogenous/technogenous character – plastic film, rope fragments, etc.

In general, sediment bottom sampling on the Portuguese margin showed a predominance of terrigenous sedimentation in all studied areas.

In the area west of Porto sediments, which can be interpreted as contour current deposits, were not recovered. The cores were characterized by a prevalence of turbiditic and mass-wasting deposits, erosion was possible in some places.

In the area west of Lisbon contourites were cored in depths of about 1000 m, that might correspond with a contribution from the Mediterranean Outflow, known to act at this depth (Abrantes et al., 1998). The Tagus river supplies a large volume of terrigenous material and its anthropogenous and technogenous supply has become more significant recently.

Biology

A. HILÁRIO, M. FELÍCIO, R. FREITAS

Bottom sediment and biological samples were collected throughout the second Leg for study at the University of Aveiro and the University of Porto, where all the species will be identified and related to their ecology. The specimens were taken from the surface of the cores and from the dredge material, as indicated below on their respective description. The biological samples were preserved in Formaldehyde and a preliminary classification was produced.

Core AT-203G/208G

Abundant specimens of Phylum *Pogonophora* were found. Thirteen specimens (5 from AT-203G and 8 from AT-208G) with up to approximately 5 cm of length and 0.5 mm of thickness were collected. Some of them were red and others white/grey.

Core AT-207G

In this core a tube from a specimen, presumably a *Pogonophora* was found. This tube is 3 cm long and 1mm thick.

Core AT-212G

Several specimens of corals – *Lophelia pertusa* (Pallas) (Phylum *Cnidaria*) were collected.

Core AT-215G/216G

These cores had a high abundance of corals. *Lophelia pertusa* was collected in both cores. Another specimen, collected from core AT-216G, is presumed to belong to a distinctive specie.

Grab AT-209GR

Several species were collected from this grab sample: one bivalve (Phylum *Molusca*); one specimen that cannot be readily identified but is presumed to be a *Pogonophora*; one sponge (Phylum *Porifera*, Class *Desmospongiae*); two worm tubes and four small (up to 1mm diameter) cirripedia (Phylum *Arthropoda*, Class *Crustacea*). The last three specimens were found attached to sampled rocks.

Grab AT-218GR

The most abundant groups were *Pogonophora* and *Cnidaria*. Fourty specimens of Phylum *Pogonophora* were collected. These can be up to 30 cm long and 0.5 mm thick. Some are red in colour and others white/grey. Two different species of corals belonging to Phylum *Cnidaria* were collected: *Lophelia pertusa* and another specie not yet identified. Small sponges (Phylum *Porifera*, Class *Desmospongiae*) were found attached to rocks. One shell of a bivalve and one *Polychaeta* (Phylum *Annelida*) were also found.

Surficial clay mineral assemblages

D. DIXON

The top 0-1 cm or 0-2 cm of surficial sediment was sampled from each core which had a satisfactory sediment recovery. These samples were placed in separate beakers, then treated using standard techniques. The samples were treated with 1M acetic acid and subjected to ultrasonic agitation to remove carbonate, washed by the stir, settle, and decant method, dispersed with sodium hexametaphosphate, allowed to settle under gravity according to Stokes' law to separate the <2 μm fraction, magnesium saturated, washed by centrifugation, smeared onto labelled glass slides, and allowed to dry in air.

The air dried samples were scanned using an X-ray diffractometer (XRD), through the angles of 2-17°. After the air dried samples had been run, the slides were placed into a glycolating (vapour) oven overnight at 55°C (this dispels all the water from the clay and replaces it with Ethylene Glycol). After glycolating, the slides were scanned in the XRD from an angle of 2-40° and then placed into a 375°C oven overnight. After baking at 375°C, the slides were run again in the XRD from 2-17°. Following this, the slides were placed in a 550°C oven for 6-12 hours (any longer and the slides would deform and melt) and run again in the XRD from 2-17°.

CLAY PERCENTAGES (areas)				CLAY MINERAL RATIOS (peak heights)				
	Sm	Ill	K+C		Sm/Ill	K+C/Ill	Sm/K+C	Ill/Sm+K+C
AT-195G	31.23	47.80	20.97	AT-195G	0.65	0.97	0.67	0.62
AT-197G	34.25	47.59	18.16	AT-197G	0.62	0.75	0.83	0.73
AT-198G	33.82	45.53	20.65	AT-198G	0.74	1.04	0.72	0.56
AT-199G	49.97	35.92	14.11	AT-199G	1.49	0.96	1.55	0.41
AT-200G	35.81	53.17	11.02	AT-200G	0.86	0.65	1.33	0.66

Sm = Smectite

Ill = Illite

K + C = Kaolinite + Chlorite

Figure 44. Clay Mineral Data: Percentages calculated from XRD peak areas of the three most abundant clay.

The peak area values of the XRD graphs are subjected to a peak intensity correction before they can be represented: Smectite/3, Illite/1, and (Kaolinite+Chlorite)/2. The peak area values are used for determination of total clay mineral percentages, and the peak height values (measured direct from the graph) are used for determining clay mineral ratios within a single sample (Fig. 44).

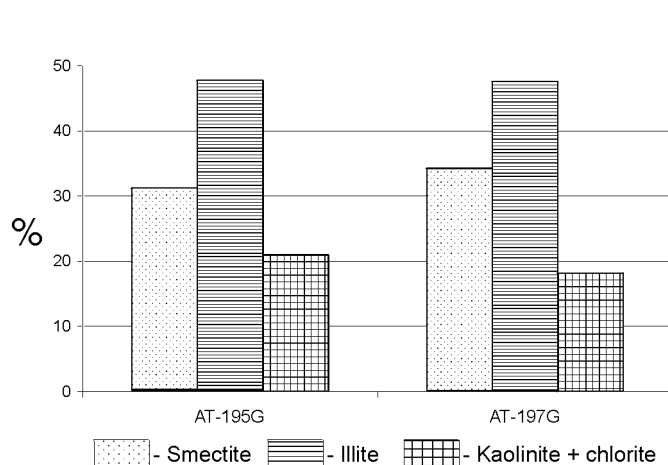


Figure 45. Clay mineralogy of the cores taken from Dom Carlos Valley.

Dom Carlos Valley

Of the three cores taken in the Dom Carlos Valley, two were sampled: AT-195G and AT197G. Both cores are almost identical in a clay mineralogy context (Fig. 45). Spatially, the two cores are within 30 km of each other at the distal end of a turbidity current pathway, with a height difference between the two sites of just over 300 m.

Biscaye (1965) calculated the relative abundances for the main clay mineral groups in the recent Atlantic sediments, and stated that the most recent Atlantic deep sea clay is detritus from the continents. Biscaye also states that

the formation of minerals *in situ* on the ocean bottom is relatively unimportant in the Atlantic.

The percentages of illite and kaolinite+chlorite from the two cores both fall in to the predicted categories for the Northeast Atlantic as set out by Biscaye (1965).

Lisbon and Setubal canyons

The mineralogy of the three cores taken in this area varies remarkably (Fig. 46). The control on variability is waterdepth, core AT-198G was 1040 m deep, core AT-199G was 143 m deep and core AT-200G was 500 m deep. Cores AT-198G and AT-200G are in the path of the Mediterranean Outflow Water (MOW), but core AT-199G is too shallow to feel its influence.

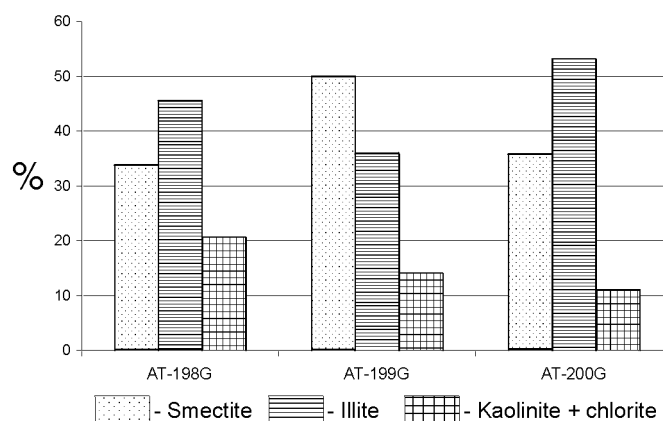


Figure 46. Clay mineralogy of the cores taken from the area west of Lisbon.

Core AT-199G is directly opposite the Tagus Estuary mouth and shows an elevated smectite content (50%) and a reduced illite (14%) content in comparison with the other two cores (about 30% for smectite and about 20% for illite). This suggests that the Tagus estuary drains from a highly smectitic source. According to data from Mougenot (1985), the smectitic core (AT-199G) is situated in a prograding shelf sequence.

Cores AT-198G and AT-200G are situated at the very limit of noticeable MOW influence along the Portuguese margin, hence they exhibit a normal Atlantic clay signature.

IV. GULF OF CADIZ/MOROCCAN MARGIN (Leg 2)

IV.1. MUD DIAPIRISM AND MUD VOLCANISM STUDY

IV.1.1. Introduction and geologic setting

J. GARDNER

Complex interactions between the Iberian and African plates since the Triassic in the Gulf of Cadiz, Alboran Sea and adjacent Moroccan continental margin have created an interesting puzzle for both sedimentologists and structural geologists. The Marine Physics Branch of the Naval Research Laboratory (USA) in cooperation with the Hawaii Mapping Research Group (HMRG) and the Naval Oceanographic Office (NAVOCEANO) conducted a sidescan sonar and multibeam bathymetry survey of the Gulf of Cadiz and Western Moroccan continental margin in 1992. Several seafloor structures believed to be methane hydrate related mud volcanoes were identified during the cruise. Similarly, the Institute of Oceanographic Sciences (UK) mapped part of the same area with GLORIA long range sidescan sonar in 1979 and identified circular features on the seabed. Further subbottom information and groundtruthing was needed to better understand the genesis and development of these structures.

Data collected during Leg 2 has provided additional critical scientific information. Over 550 km

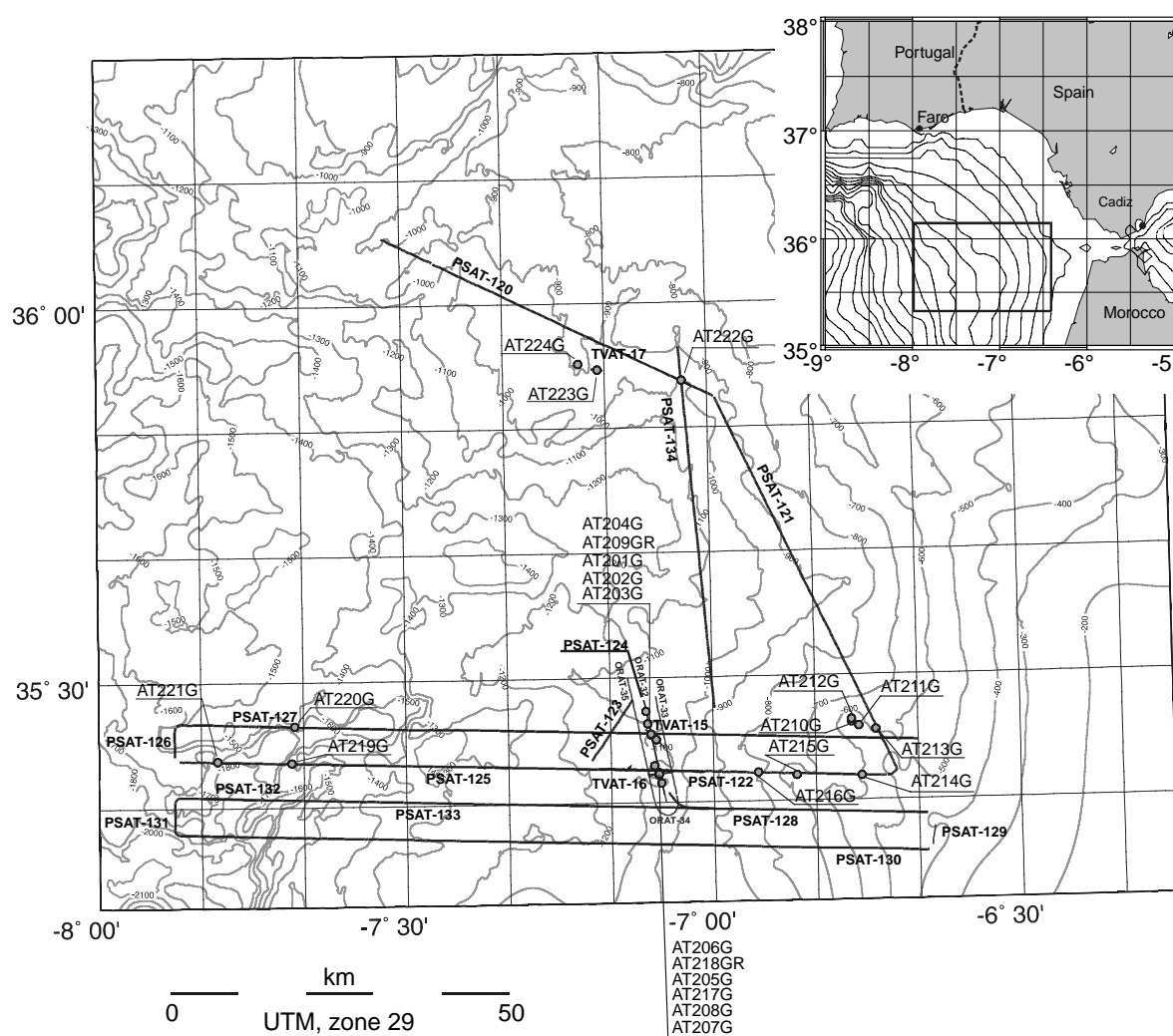


Figure 47. Gulf of Cadiz working area location map. Bathymetry after Gardner (2000).

of single channel seismic and 3.5 kHz subbottom profiler data, 15,000 km² of OKEAN 9 kHz sidescan sonar and 160 km² of OREtech 30 kHz sidescan sonar data were collected in the area of interest (Fig. 47). Ground-truthing information for the sidescan was obtained from nineteen gravity cores, 2 grab samples and 6 hours of video imaging.

Three regions of mud volcanism and diapirism were identified during the cruise. We refer to them as the Western Moroccan Field (WMF), Middle Moroccan Field (MMF) and Eastern Moroccan Field (EMF) for simplicity. In the WMF the diapiric structures are represented by long, sinuous ridges on the seafloor. Sedimentary basins have formed adjacent to these ridges. In the MMF, OREtech sidescan data, grab samples and gravity core samples confirm the existence of two mud volcanoes, (Yuma and Ginsburg). Methane hydrate (clathrates) were recovered from Ginsburg. In the EMF, gravity core samples confirm the existence of 3 mud volcanoes (Kidd, Adamastor, TTR) and seismic and sidescan sonar data suggest that there are at least 5 more mud volcanoes and 4 diapiric ridges.

The Gulf of Cadiz and Western Moroccan margin have undergone several episodes of extension and compression since the Triassic (Wilson et al., 1989; Dewey et al., 1989; Srivastava et al., 1990 and Maldonado et al., 1999). The Atlantic and Mediterranean basins were connected by straits and deep basins which developed between an autochthonous calcareous margin to the north, which extended into southern Portugal and an allochthonous terrigenous margin to the south, which developed around tectonically controlled morphological highs (Sanz de Galdeano and Vera, 1992; Rodero et al., 1999). Westward movement of the Gibraltar arc during the Late Tortonian caused the Gulf of Cadiz to form as a forearc basin (Maldonado and Comas, 1992). Olistostrome emplacement occurred as a result of the westward migration of the Gibraltar arc resulting in accretionary wedge type deposition and deformation of sediments. This olistostrome and accretionary wedge are derived from sediments from the southern Iberian and northern African margins of the Tethys (Blankenship, 1992; Flynn et al., 1996; Maldonado and Somoza, 1997; Maldonado et al., 1999). Rapid subsidence of the basin occurred during the Late Messinian and the early Pliocene as a result of basin extension (Flynn et al., 1996; Maldonado et al., 1999). This subsidence allowed thick depositional sequence development along the margin and turbidite deposition in the deep NE-SW trending basins (Rodero et al., 1999). Messinian tectonism re-established a gateway from the Atlantic to the Mediterranean via the Strait of Gibraltar which significantly changed sediment deposition patterns in the Gulf of Cadiz. In the Early Pliocene, deposition was influenced both by extensional collapse of the basin and diapiric activity (Rodero et al., 1999; Maldonado et al., 1999). Basement subsidence rates decreased rapidly from the Late Pliocene to Quaternary which, along with eustatic sea-level changes, affected sediment deposition in the foredeep basins of the Gulf of Cadiz (Rodero et al., 1999).

IV.1.2. Seismic Data Profiling

J. GARDNER, M. RANK, T. ALVES, L. PINHEIRO, A. VOLKONSKAYA, S. BURIK, E. ZYRYANOVA, AND
E. PETROV

Fourteen seismic lines were completed in the Gulf of Cadiz/Morocco Margin survey area. Twelve of the lines collected data in the mud volcano/diapir area of interest south of 35° 30'N and west of 6° 30' E (Fig. 47). Lines PSAT-122, 125-133 were run parallel to each other in an east-west direction. Another four lines were orientated NW-SE or NE-SW.

We have no deep core log data to correlate seismic units within our survey so our interpretation is very general. The quality of the seismic data is average to poor due to problems with the streamer. Rodero et al. (1999) have published seismic facies for Quaternary deposition in an area of the Gulf of Cadiz which is to the northeast of our study area and we have relied heavily on their interpretations to guide us in our stratigraphic interpretation. Based on their research, we are relatively confident that we are resolving nothing older than Quaternary aged sediments in the study area. Structures we have interpreted as being mud volcanoes or diapirs occur in all of the seismic profiles and disturb or cut through all the seismic units in most cases. Several diapiric bodies and mud volcanoes were seen to disrupt,

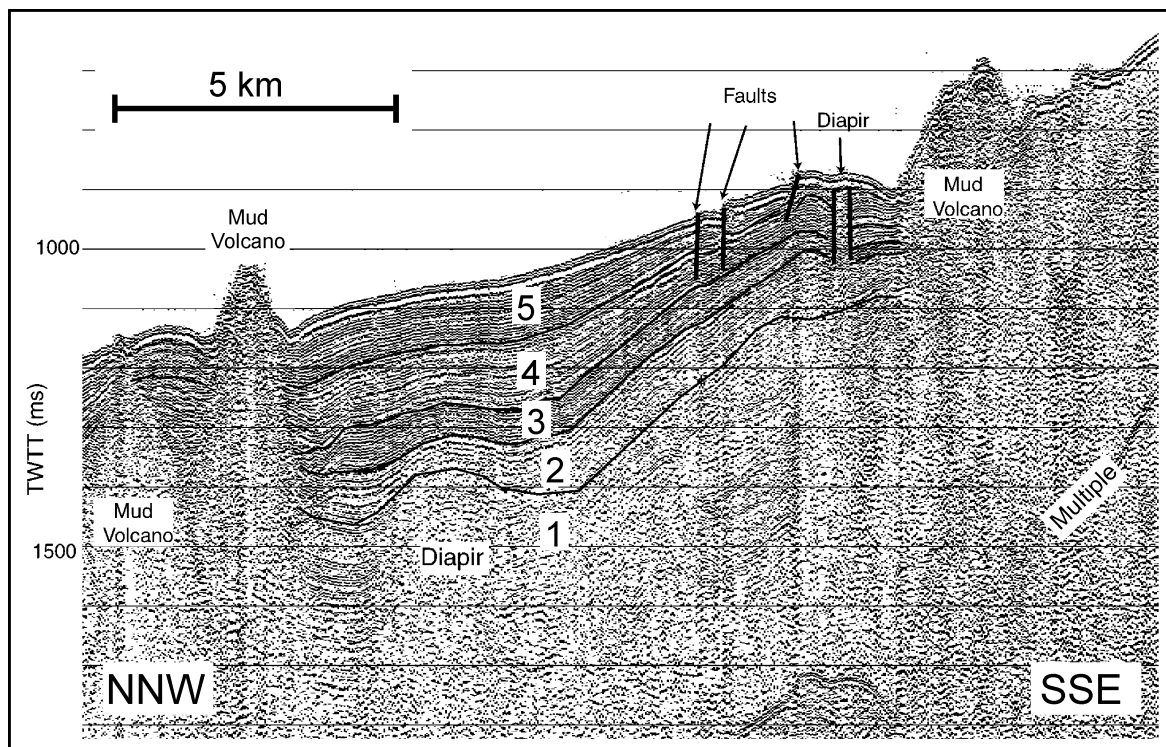


Figure 48. Fragment of seismic line PSAT 121 showing mud volcanoes, diapirs and minor faulting within Quaternary stratigraphic units.

interfere or control the general sedimentation pattern.

Unit 1: The base of seismic unit 1 is not identifiable (Figs. 48 and 49). In a couple of the profiles the unit thickness is at least 150 msec TWTT. The unit is characterised by a weak internal reflection pattern with only a few coherent reflectors.

Unit 2: Unit 2 is characterized by stronger reflectors than seen in Unit 1 but weaker than those resolved in the overlying units (Figs 48 and 49). The lower part of the unit often exhibits broken reflectors which form an undulating pattern. A thickness of 70-100 msec TWTT is relatively consistent in the majority of the profiles.

Unit 3: Unit 3 consists of strong coherent parallel reflectors which are closely grouped. Its thickness is about 50 msec TWTT.

Unit 4: Unit 4 (Figs 48 and 49) is a package of relatively coherent reflectors which are sometimes discontinuous and are spaced further apart than Units 3 or 5. The base and top of Unit 4 is marked by a strong reflector. The unit reaches a maximum thickness of 100 msec, which sometimes thins to about 50 msec adjacent to mud volcano/diapir features (Figure 48) and thickens to 200 msec in high deposition regions (Figure 49). The internal reflection pattern is characterised by parallel but discontinuous reflectors.

Unit 5: The uppermost unit is traceable within the whole area and shows only minor variations in thickness. The maximum thickness has been interpreted to be 60-80 msec TWT. The internal reflection pattern is characterised by relatively strong and coherent reflectors.

Faulting: Reverse, normal and antithetic faulting is observed in some of the profiles. Very little displacement occurs and the faults are confined to the uppermost Quaternary units (Fig. 48). We suspect that diapir/mud volcano emplacement may cause more extensive faulting but the poor quality and resolution of the seismic precludes us from confirming this hypothesis.

Diapirs and Mud Volcanoes:

Diapirs and mud volcanoes appear as domed features with no coherent seismic reflectors. Converging reflectors, slight thinning and upflank drag of the stratigraphic units are associated with most of the diapirs and mud volcanoes. In addition, some of the volcanoes have downward dipping

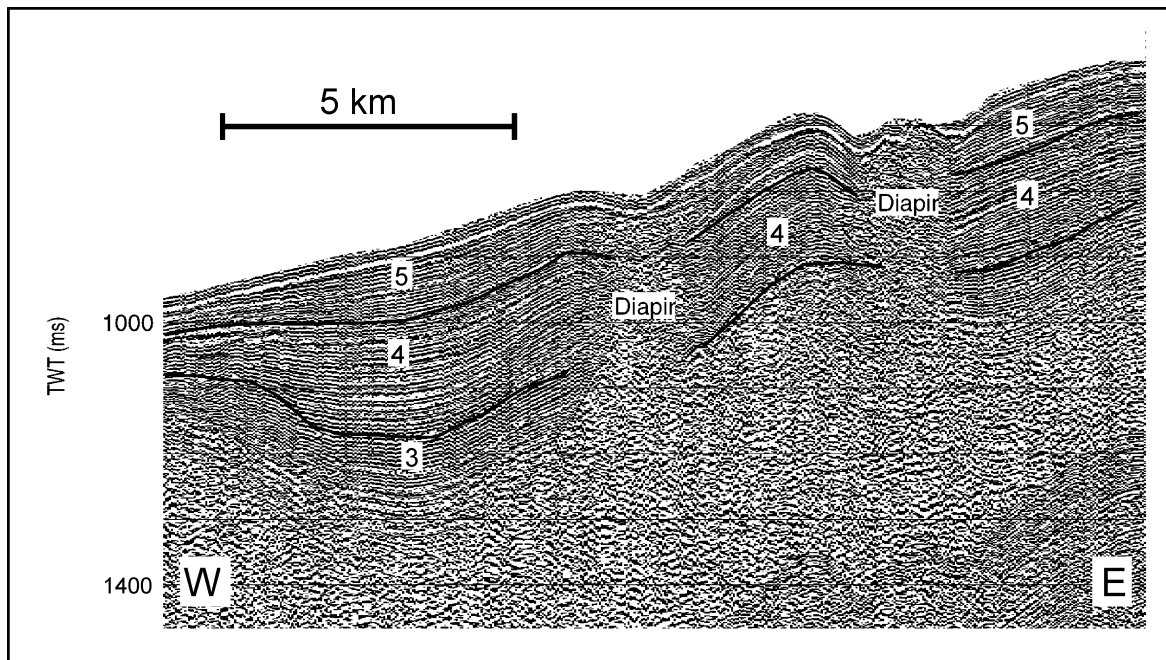


Figure 49. Fragment of seismic line PSAT 130 showing mud diapirs.

beds adjacent to them suggesting possible collapse. In most cases, the diapirs and mud volcanoes disturb adjacent stratigraphic units suggesting that they are relatively recent features.

Conclusions

Despite the quality of the seismic profiles, several important observations can be made in the study area:

1. Diapiric and mud volcanic events post date the deposition of the sediments and are recent events (Holocene to recent). We have relied heavily on the work of Rodero et al. (1999) to determine the age of the stratigraphic units effected by the diapirs and mud volcanoes. We resolve nothing older than Quaternary sequences in our seismic lines.
2. Thinning of stratigraphic units on approaching the diapirs and volcanoes and upflank drag of adjacent beds could be due to syndeposition or deformation during emplacement.
3. Lack of deformation or thinning of beds adjacent to some of the diapirs and mud volcanoes could indicate that emplacement occurred along fractures or faults that are unresolvable in our seismic sections.
3. Downward dipping reflectors adjacent to diapirs and mud volcanoes could be due to lack of sedimentation (current erosion) or collapse due to subsidence. This type of collapse structure or “moat” surrounding the mud volcano has been observed around similar mud volcanoes (e.g. the Haakon Mosby Mud volcano) in the Arctic.

IV.1.3. Sidescan Sonar Data

J. GARDNER, P. SHASHKIN

Eastern Moroccan Field (EMF)

The EMF is characterized by a grouping of at least seven mud volcanoes (Fig. 50), three of which have been confirmed by gravity core data. Two of the unconfirmed mud volcano structures appear to have either large flow structures associated with them or are diapiric ridges or fractures

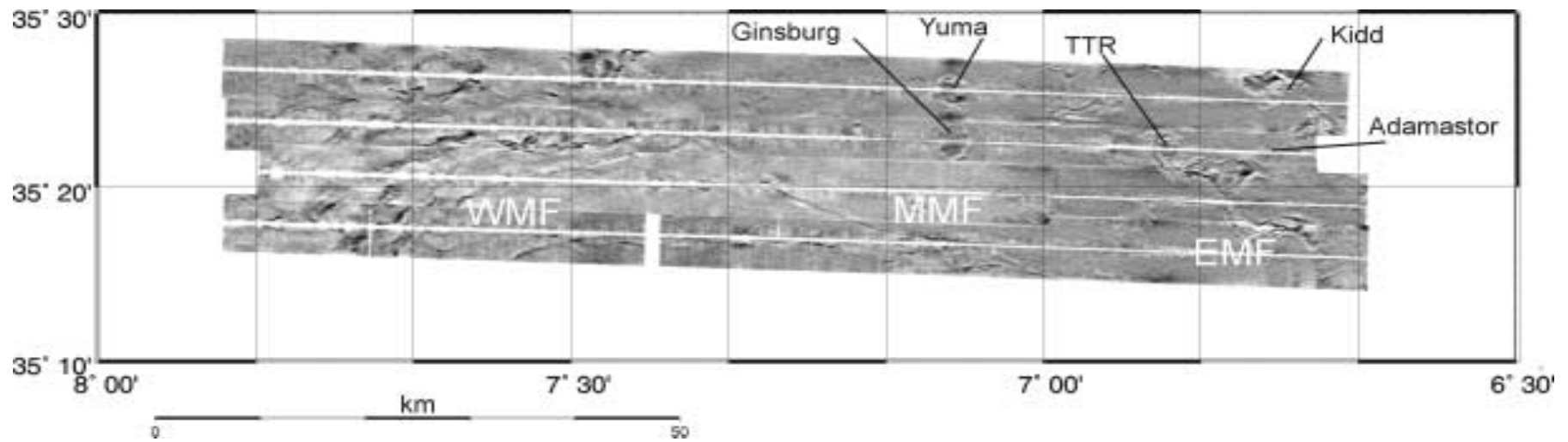


Figure 50. OKEAN 9 kHz sidescan sonar mosaic of the Moroccan mud volcano fields: Western Moroccan Field (WMF), Middle Moroccan Field (MMF) and Eastern Moroccan Field (EMF). High backscatter is dark and low backscatter is light.

where mud seepages or flows have occurred. These features tend to line up in a NW-SE direction which is roughly the present direction of tectonic compression in this region (Maldonado et al. 1999).

Figure 51(A) shows OKEAN sidescan data of two mud volcanoes; one which we have named Kidd in memory of Professor Robert Kidd and the other is unnamed since we were unable to obtain a gravity core confirming that it is a mud volcano. Both features are circular and return high backscatter. Kidd is approximately 4 km in diameter and the unnamed volcano is 5 km in diameter. Figure 51(B) is the single channel seismic line collected over these two features. No coherent reflectors can be seen under the two features which are characteristic for mud volcanoes or salt domes. This mud volcano is covered by a very thin layer of sand underlain by mud breccia. Both Kidd mud volcano and the unnamed volcano disturb adjacent Quaternary age units thus emplacement of these structures is believed to have occurred during Holocene to Recent time.

Figure 52 (A) is an OKEAN line of Adamastor, TTR and an unnamed mud volcano. Both Adamastor and TTR are relatively circular structures that are approximately 2 km in diameter and return high backscatter. The unnamed mud volcano is about 4 km in diameter and also circular with high backscatter. The name Adamastor was given to the easternmost mud volcano in the EMF by the Portuguese scientists and students who participated on Leg 2 of TTR9. Adamastor was a monster who guarded the seas. The mud volcano TTR was given its name in recognition of all the students who have participated in past and present TTR cruises. Figure 52 (B) is the seismic profile of all three mud volcanoes. Note that the unit reflectors adjacent to the volcanoes are bent upwards in all cases suggesting drag during emplacement. Both TTR and Adamastor are covered by a thin veneer of hemipelagic sediments which contain *Pogonophora* tube worms similar to those found on some other mud volcanoes

e.g. the Haakon Mosby mud volcano in the Arctic (Vogt et al, 1999). Below the hemipelagic sediment in TTR is a silt layer with coral branches suggesting that this volcano may at one time have been inhabited by corals. Below this unit is the mud breccia unit which is indicative of mud volcanism in this region. Adamastor lacks the calcium carbonate layer seen in TTR and its hemipelagic layer is underlain by mud breccia. The upper layers of the unnamed mud volcano appear to be carbonate reef related. We were unable to get a deeper core sample of this mud volcano which we are confident would have revealed that the coral rich layers are underlain by mud breccia similar to what was cored on TTR. All three volcanoes disturb Quaternary stratigraphic units so it can be surmised that they were emplaced sometime after the Quaternary (Holocene to Recent).

Figure 53 (A) is an OKEAN image of what could possibly be diapiric ridges or mud volcanoes. We were unable to gravity core these features to confirm that they were mud related features but, based on the seismic returns in Figure 53 (B), we are confident that they are related to the other mud volcanoes in the area. These features resemble the diapiric ridges described in the north-

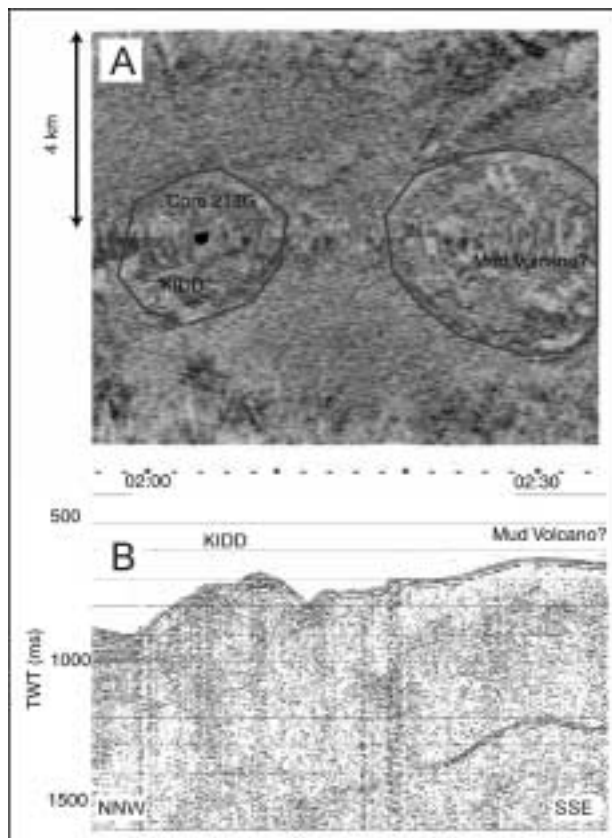


Figure 51. A - OKEAN sidescan image of an unconfirmed mud volcano and Kidd mud volcano; B - Seismic profile along centre line of OKEAN image.

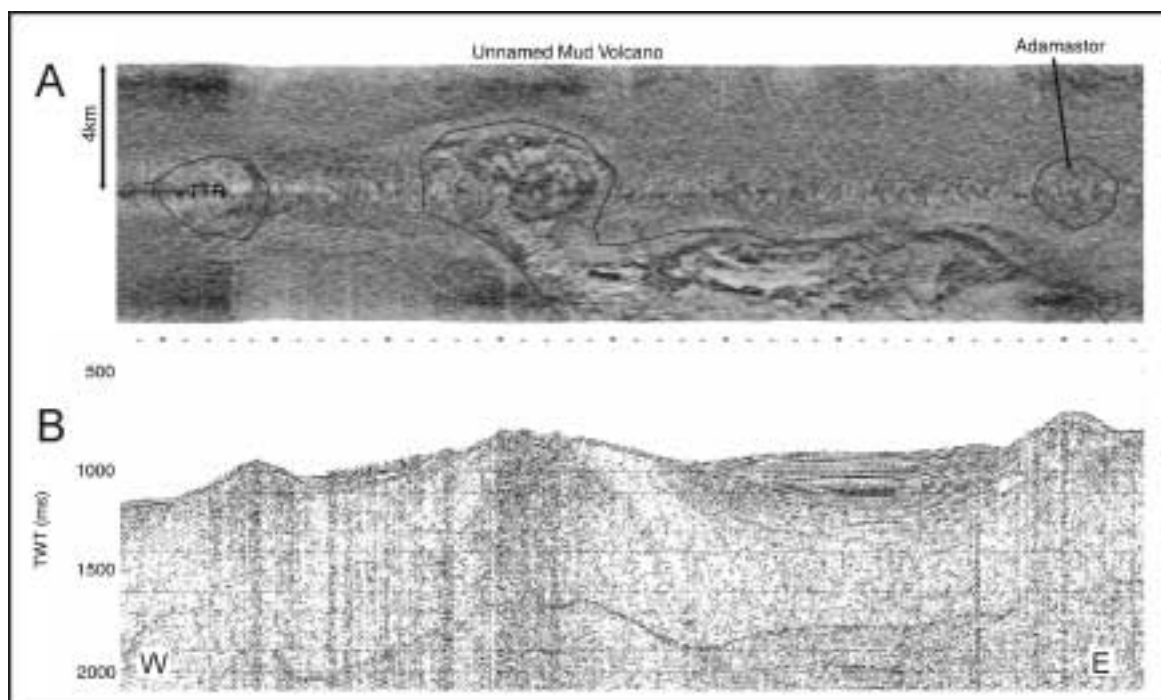


Figure 52. A - Interpreted OKEAN sidescan sonar image of mud volcanoes; B - Seismic profile through the centre line of OKEAN image.

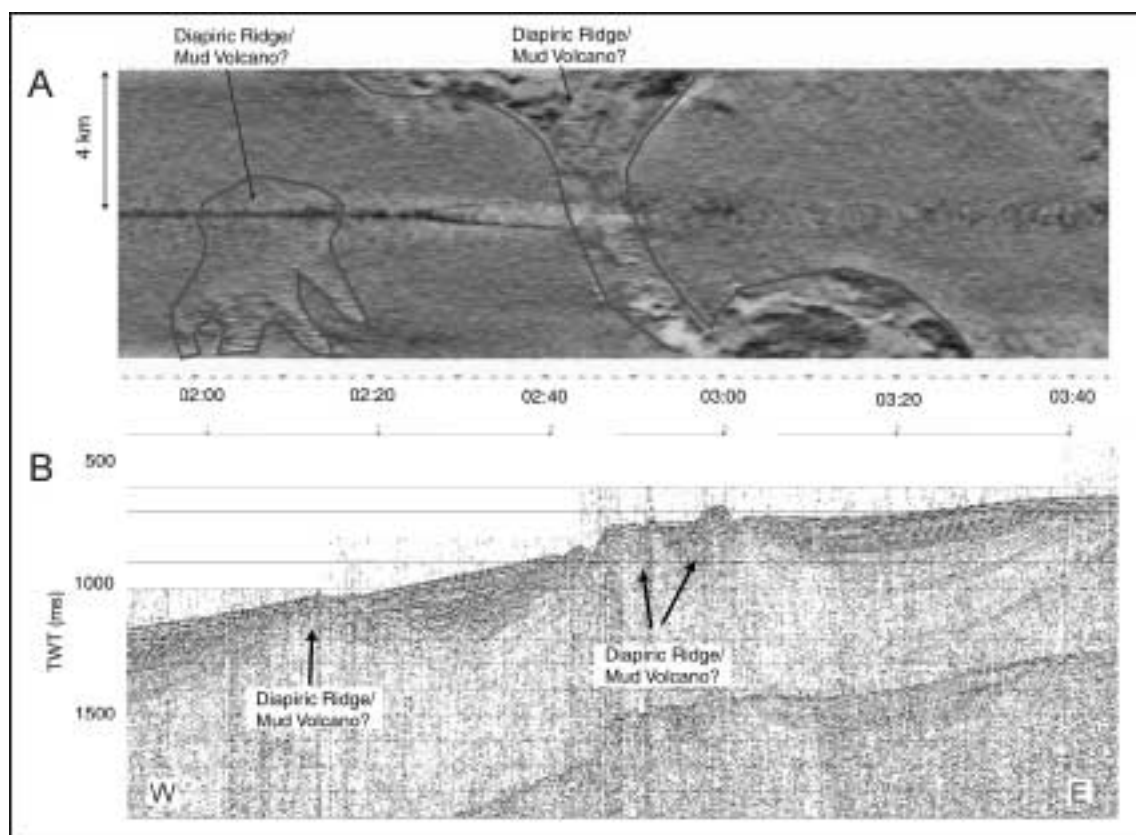


Figure 53. A - Interpreted OKEAN sidescan image of presumed diapiric ridges/mud volcanoes; B - Seismic profile through the centre line of OKEAN image.

ern part of the Gulf of Cadiz by Maldonado et al. (1999) and Rodero et al. (1999). We suspect that these features are fault controlled based on their linear shape and NW-SE orientation. Figure 54 (A and B) are OKEAN and seismic lines of the larger of the two diapiric ridges in this region. Note in Figure 54 (B) the extensive deformation of the stratigraphic units adjacent to the diapirs.

The Middle Moroccan Field (MMF)

This part of the study area was the main focus of the survey. Two circular high backscatter structures, approximately 4 km in diameter with more than 200 m of bathymetric relief, had been identified on 12 kHz sidescan sonar and 6.5 kHz GLORIA data. Confirmation that these features were mud volcanoes was accomplished through collection of OREtech deep tow 30 kHz sidescan sonar data (Fig. 55), seismic data, gravity core data, grab sampling and video camera imagery collected during TTR9 Leg 2. The OREtech 30 kHz data (Figure 56) revealed a northern mud volcano with three separate

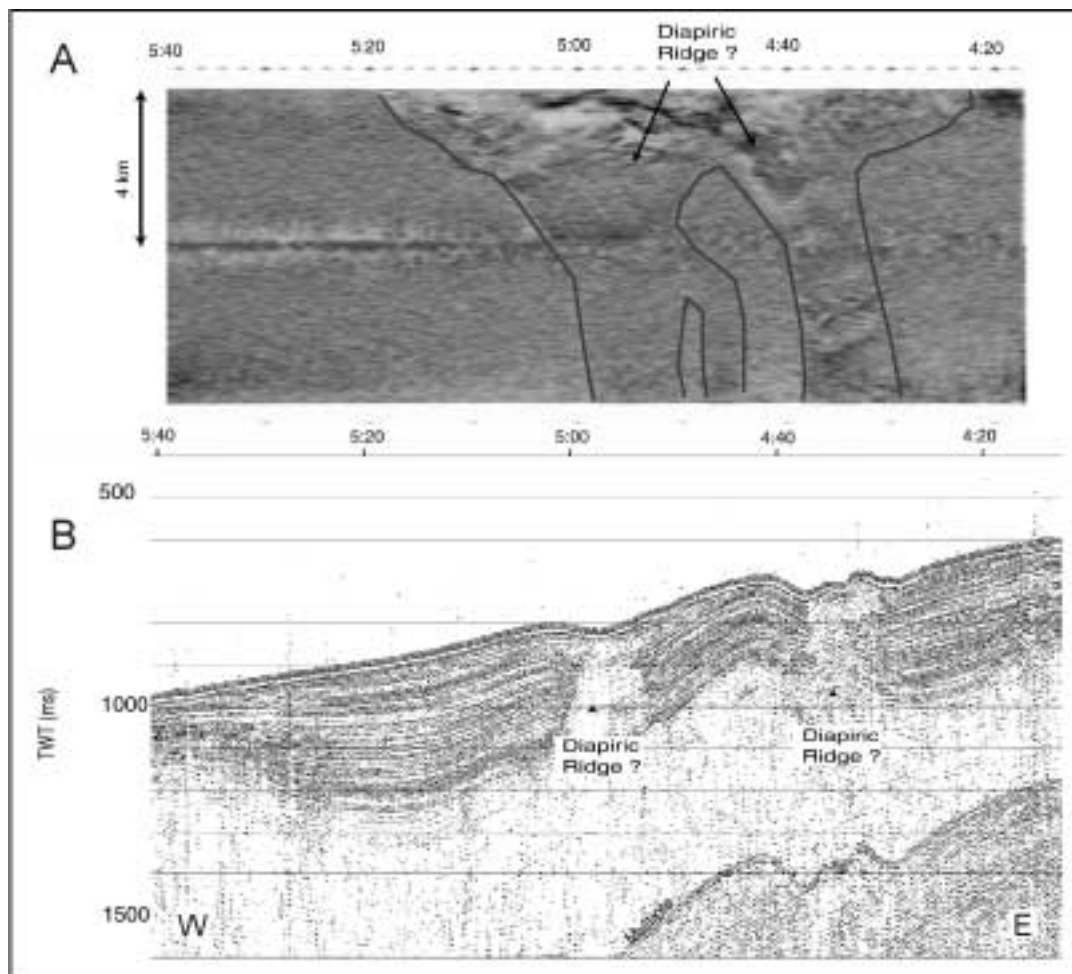


Figure 54. A - Interpreted OKEAN sidescan sonar image of diapiric ridges; B - Seismic profile of diapiric ridges.

domes. This volcano was given the name Yuma after J. Gardner birthplace. The central dome is surrounded by high backscatter concentric circles which radiate out from the center of the volcano in relatively equal increments. These circles appear to be small ridges or fractures on the OREtech subbottom profiler records. There are two smaller domes, one of which falls directly below the nadir of the sidescan, where no backscatter return can be collected, therefore it is only visible on the subbottom profile and the other is southeast of the main central dome. Both the central and southeastern domes

were cored. The main dome had a thin veneer of marl on top of a gas saturated clay layer. The smell of H_2S was strong throughout this core. The smaller dome lacked the marl and clay layer and consisted of mud breccia with a strong H_2S smell. The difference in the backscatter levels of the two domes (the smaller dome having a higher overall level of backscatter) can be attributed to the lack of a fine marl and clay layer overlying the mud breccia. The mud breccia is coarse and contains clasts which are good point scatterers for the acoustic signal.

The second volcano, which is located to the southeast of Yuma, is identical in size and bathymetric relief. It has been named Ginsburg after the late Dr. Gabriel Ginsburg who dedicated his life to studying mud volcanoes. Ginsburg (Fig. 57) has one central dome which is surrounded by concentric high backscatter circles similar to those seen on Yuma. Gravity cores taken in the central dome yield-

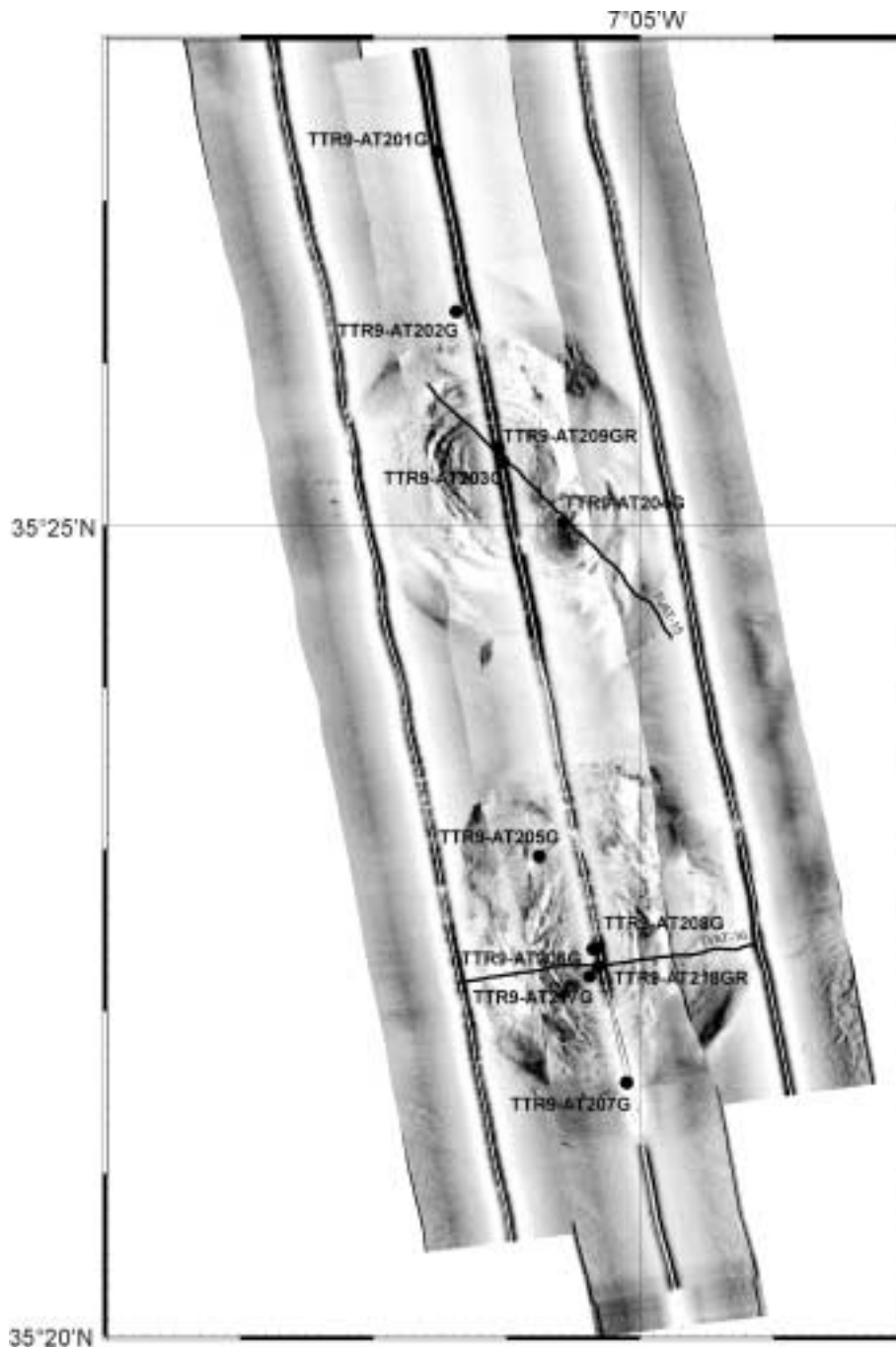


Figure 55. 3 lines of OREtech 30 kHz sidescan sonar from MMF. Core sites and track of the bottom towed video camera are shown.

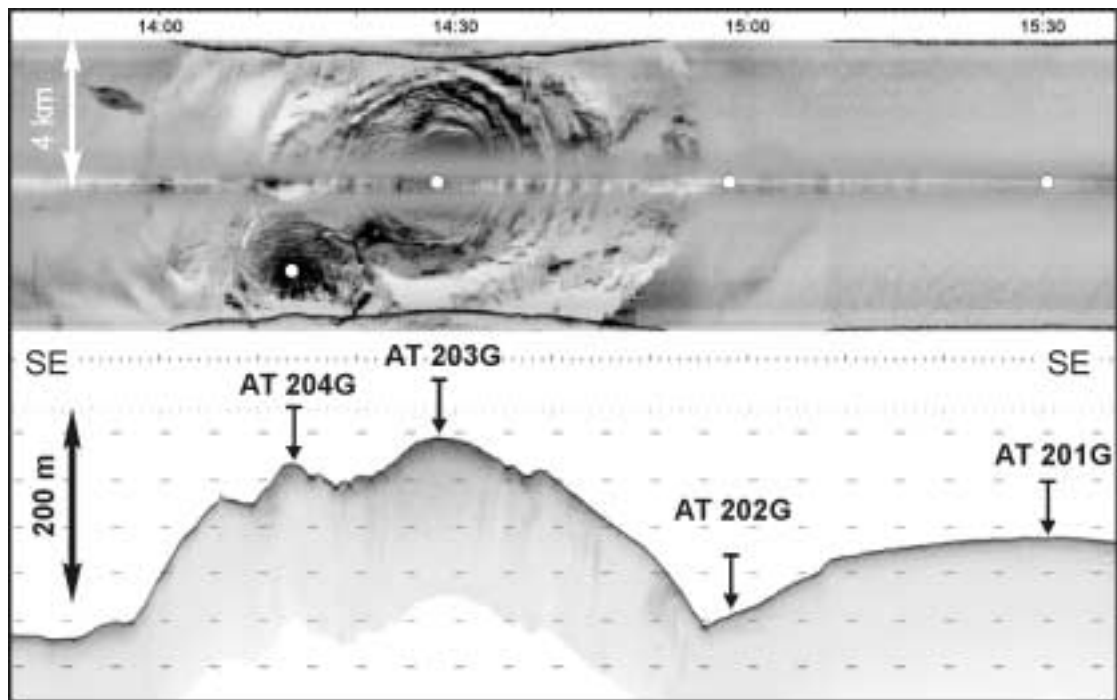


Figure 56. OREtech sidescan sonar image and subbottom profile of Yuma mud volcano.

ed a thin layer of marl rich with foraminifera and *Pogonophora* tube worms. Underlying this layer is a thick mud breccia layer which had a strong H_2S smell. Gas hydrate crystals (clathrates) were found 150 cm from the top of the core.

The seismic characteristics of Yuma (Fig. 58) are similar to other mud volcanoes in the region; no coherent reflectors under the mud volcano and stratigraphic units adjacent to the mud volcano are disturbed by the structure. In this case, the beds are bent downward suggesting that possible subsidence

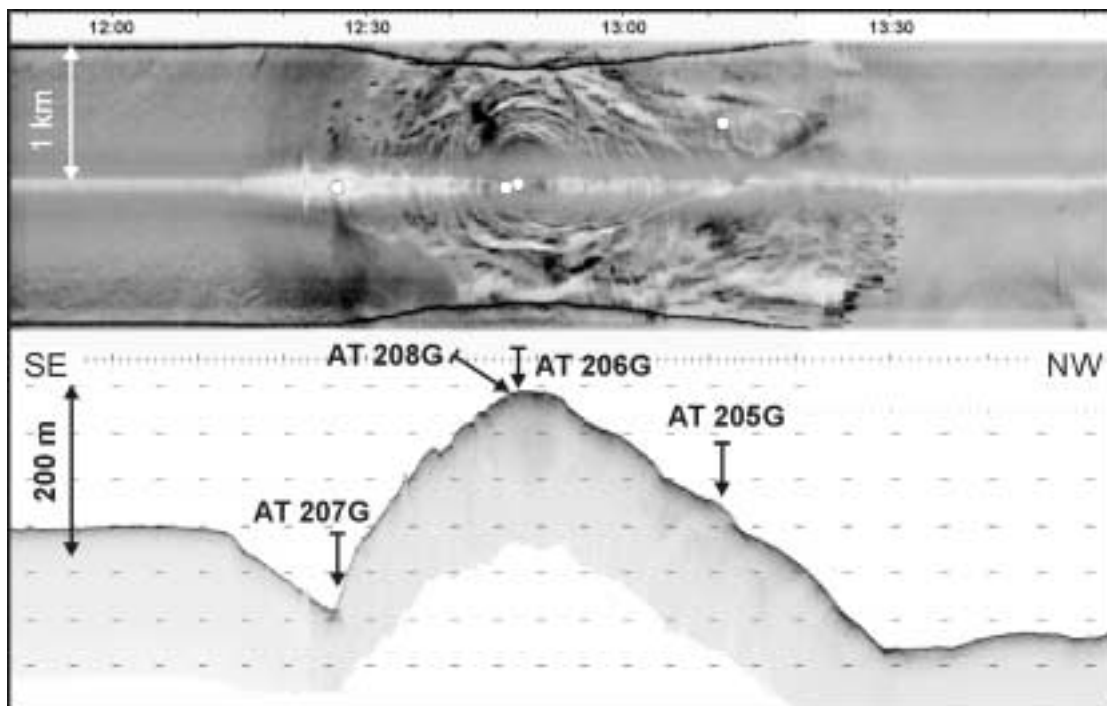


Figure 57. OREtech sidescan image and subbottom profile of Ginsburg mud volcano.

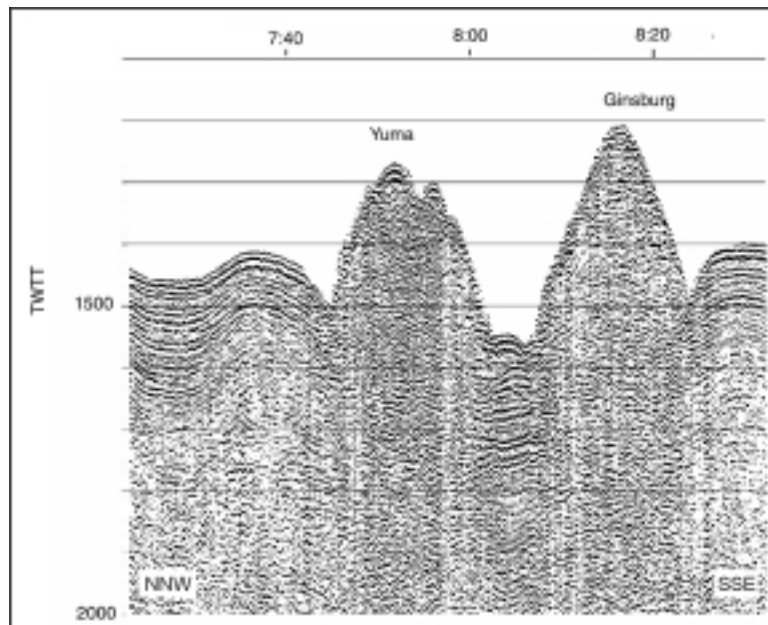


Figure 58. Seismic profile of Yuma and Ginsburg mud volcanoes.

of the volcano has/is taking place. The seismic profile of Ginsburg (Fig. 58) also shows no coherent reflectors below the volcano and shows downward bending of adjacent stratigraphic units suggesting subsidence.

The Western Moroccan Field (WMF)

This part of the study area was the most intriguing and baffling. Bathymetric data collected in 1992 by the U.S. Naval Research Lab (NRL) indicated that this region has several steep ridges trending NE-SW which interfinger with small basins. In the OKEAN sidescan sonar data (Fig. 50) there are high backscatter linear features trending NE-SW that are slightly sinuous and coincide with the ridges

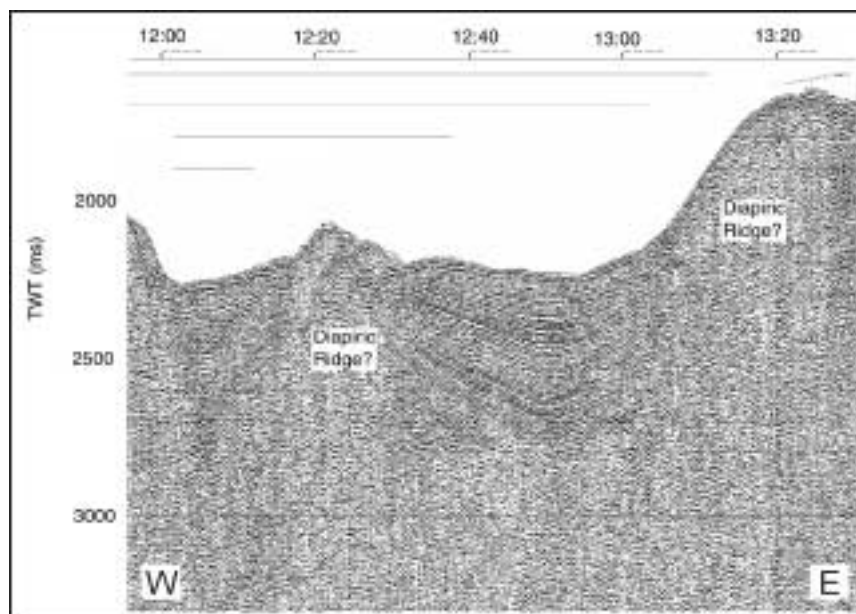


Figure 59. Seismic data of diapiric ridges and sediment basins in the Western Moroccan Field (WMF).

observed in NRL's bathymetric data. The seismic data for this region is of poor quality due to poor weather but one relatively good section of PSAT-127 (Fig. 59) indicates that these ridges may be diapirs. There are few coherent reflectors below these ridges and the adjacent stratigraphic units appear to be disturbed by the ridges. Gravity coring on two of these features yielded brown marl rich in foraminifers with some indication of past slumping events (see core logs 219G and 221G in annexe) but no indication of mud related volcanism. Are these pressure ridges caused by NW directed tectonic compression? Are they fractures or faults that have mud or gas related material which we failed to core in our few attempts? Multichannel seismic and more extensive gravity coring is needed to answer these questions.

IV.1.4. Bottom Sampling Results

G.AKHMANOV, A. AKHMETZHANOV, A. STADNITSKAYA, E. KOZLOVA, L. MAZURENKO, F. TEIXEIRA, A. SAUTKIN, D. DIXON, D. OVSYANNIKOV, A. SADEKOV, N. RASUL, I. BELENKAYA, YU. VOLKOVA, E. SUSLOVA, AND D. GONCHAROV

The main purpose for bottom sampling in the Gulf of Cadiz area was to check assumed mud volcanic features expressed in the seafloor topography and characterized by particular backscattering patterns. The bottom sampling followed surveys with air gun seismic and long range OKEAN and high resolution, deep towed OREtech sidescan sonar systems, which led to recognition of several sub-circular dome-like structures in the MMF and the EMF and several elongated ridges in the WMF. A total of 22 stations, 20 by gravity corer (total recovery was 26.85 m) and 2 by TV-controlled grab system, were sampled to clarify their origin (Fig. 47). The main sampling site parameters and sedimentological and acoustic settings are summarized in Tables 11 and 12. Core logs are given in Annexe I.

A great variety of sediment types were recovered and described, implying a superposition of different depositional environments in this region of very complex geology and hydrology.

Facies I:

In all cores, with the exception of AT-204G, the uppermost unit is represented by light brown marl very rich in planktonic foraminifera. The unit is extremely water-saturated in its upper part, intensively bioturbated throughout, structureless, and with an irregular lower boundary. The unit thickness varies in different cores from about 3 to up to 50 cm. It overlies older pelagic sediments or mud volcanic deposits and extends through the whole study area, suggesting carbonate pelagic sedimentation as the most recent dominant depositional process and a high productivity of foraminifers.

Facies II:

The cores taken on the flanks of mud volcanoes of the Middle (AT-201G, AT-202G, AT-207G), the Eastern (AT-210G, AT-211G, AT-212G) and the Western Moroccan Fields (AT-220G, AT-221G) recovered clayey and carbonate-clayey pelagic units coloured grey and brownish grey, depending on the different proportion of carbonate. The sediments were enriched in planktonic foraminifera and very fine grained terrigenous admixtures, whose amount varied with Pleistocene climatic fluctuations in the region. In most cores this facies is structureless and intensively bioturbated, apart from the lower part of AT-201G, where thin planar lamination is observed. In some cores burrows are large, up to 7 cm, and filled with soupy water-saturated mud enriched in foraminifera and terrigenous grains due to selective filtration of host sediments by burrowing endobenthic organisms. This facies implies pelagic deposition in the deep open sea, at a distance from the continent, with an intermittent supply of fine grained terrigenous material into the basin, controlled by eustatic sea-level changes.

Facies III:

Core AT-219G, taken on a small ridge in the Western Moroccan Field, recovered a thick interval of redeposited sediments, mostly of mass-wasting deposits (slumps and debris flows) with characteristic structures. The unit is represented by brown marl rich in planktonic foraminifera and by several oxidized layers. The materials are lithologically identical to Facies I which may imply recently active mass-wasting associated with upgrowth of the ridge that the core was taken from. A diapiric ori-

Core No	Date	Time. GMT	Latitude	Longitude	Cable length, m	Depth, m	Recovery, cm
TTR9-AT-201G	11.07.99	08.44	35°27.305	07°06.518	1090	1064	239
TTR9-AT-202G	11.07.99	09.58	35°26.320	07°06.378	1175	1147	205
TTR9-AT-203G	11.07.99	10.54	35°25.391	07°06.026	980	964	142
TTR9-AT-204G	11.07.99	11.45	35°25.019	07°05.575	980	983	134
TTR9-AT-205G	11.07.99	13.05	35°22.957	07°05.756	1060	1040	91
TTR9-AT-206G	11.07.99	13.47	35°22.385	07°05.351	928	912	165
TTR9-AT-207G	11.07.99	14.33	35°21.561	07°05.101	1160	1140	89
TTR9-AT-208G	11.07.99	15.27	35°22.392	07°05.321	935	911	138
TTR9-AT-209GR	11.07.99	18.28	35°25.481	07°06.065	963	960	2 tons
TTR9-AT-210G	12.07.99	22.37	35°26.212	06°46.469	525	517	138
TTR9-AT-211G	12.07.99	23.21	35°25.889	06°45.778	555	540	62
TTR9-AT-212G	13.07.99	00.39	35°26.437	06°46.464	530	503	94
TTR9-AT-213G	13.07.99	01.46	35°25.603	06°44.104	506	502	39
TTR9-AT-214G	13.07.99	11.35	35°21.924	06°45.553	520	511	149
TTR9-AT-215G	13.07.99	13.36	35°22.017	06°51.899	600	596	30
TTR9-AT-216G	13.07.99	14.47	35°22.289	06°55.622	730	721	180
TTR9-AT-217G	13.07.99	21.18	35°22.217	07°05.377	930	918	112
TTR9-AT-218GR	13.07.99	23.42	35°22.277	07°05.312	933	907	2 tons
TTR9-AT-219G	14.07.99	16.45	35°23.550	07°41.167	1560	1508	304
TTR9-AT-220G	14.07.99	18.38	35°26.500	07°40.858	1556	1504	106
TTR9-AT-221G	14.07.99	20.36	35°23.736	07°48.408	1760	1682	155
TTR9-AT-222G	15.07.99	12.36	35°53.749	07°02.441	900	879	151

Table 11. General information on the cores sampled in the Gulf of Cadiz.

gin for the ridge is assumed on the basis of geophysical data.

Facies IV:

In the lower part of AT-202G, taken from the outer slope of the Yuma mud volcano rim (Fig. 56), another type of redeposition is represented by two graded thin laminae of marl with abundant very fine grained terrigenous admixture and high foraminiferal content. Normal grading, sharp lower and transitional upper boundaries imply their deposition as turbidites. The lithological composition of the laminae suggests that pelagic material was redeposited by local inter-basinal gravity flows. The trigger mechanism for these gravity flows might be recent processes of growth or collapse of mud volcanoes located nearby.

Facies V:

Cores AT-220G and AT-221G, taken from small ridges in the Western Moroccan Field, were very similar in lithology and contained light brown intervals (10-20 cm bsf in AT-220G; 25-45 cm bsf in AT-221G) of semi-lithified, intensively oxidized, lumpy/cloddy marl enriched in foraminifers. This interval is interpreted as formed in response to abrupt changes in depositional environments in the region, perhaps analogous to hard-grounds.

Facies VI:

Most cores contained mud volcanic deposits. In the MMF they are in AT-203G and AT-204G, taken from the main crater and from the small south-eastern crater of the Yuma mud volcano respectively (Fig. 56), in AT-205G, taken from mud flow on the slope of the Ginsburg mud volcano and in AT-206G, AT-208G, and AT-217G, taken from its main crater (Fig. 57); in the EMF they are in AT-213G, taken from the Kidd mud volcano crater, in AT-214G, taken from the Adamastor mud volcano crater, in AT-216G, taken from the TTR mud volcano and in the northern part of the study area in AT-222G from the crater of the St. Petersburg mud volcano.

Mud volcanic deposits (mud breccias) from the different sites are essentially of similar lithology. They are grey and greenish grey, very poorly sorted, sandy, silty clay, matrix-supported, with large quantity of sub-angular rock fragments up to 35 cm in size. Various sandstones, marlstones, and claystones, consolidated to a different degree, are the predominant lithologies among rock fragments from the mud breccia. Each mud breccia flow is structureless, with sharp lower and upper boundaries. The uppermost layer, immediately below the pelagic veneer, is commonly oxidized and brownish in colour.

Core No	Geographical Setting	Instrumentation	Acoustic Characteristics
TTR9-AT-201G	Plain to the north of Yuma mud volcano (at 15:30 on the ORAT-32)	OKEAN long range sidescan sonar; 3.5 kHz profile; Single channel high resolution seismic system, OREtech sidescan sonar.	Low backscatter on the OREtech image, subparallel layering on 3.5 kHz record
TTR9-AT-202G	Gentle slope on northern flank of the Yuma mud volcano (at 14:59 on the ORAT-32)	OKEAN long range sidescan sonar; 3.5 kHz profile; Single channel high resolution seismic system, OREtech sidescan sonar.	Low backscatter on the OREtech image, subparallel layering on 3.5 kHz record
TTR9-AT-203G	Main crater of the Yuma mud volcano (at 14:29 on the ORAT-32)	OKEAN long range sidescan sonar; 3.5 kHz profile; Single channel high resolution seismic system, OREtech sidescan sonar.	High backscatter on the OREtech image, cone structure on the 3.5 kHz profile
TTR9-AT-204G	Small crater of the Yuma mud volcano (at 14:10 on the ORAT-32)	OKEAN long range sidescan sonar; 3.5 kHz profile; Single channel high resolution seismic system, OREtech sidescan sonar.	High backscatter on the OREtech image
TTR9-AT-205G	Mud flow of the Ginsburg mud volcano (at 13:12 on the ORAT-32)	OKEAN long range sidescan sonar; 3.5 kHz profile; Single channel high resolution seismic system, OREtech sidescan sonar.	High backscatter on the OREtech image
TTR9-AT-206G	Crater of the Ginsburg mud volcano (at 12:49 on the ORAT-32)	OKEAN long range sidescan sonar; 3.5 kHz profile; Single channel high resolution seismic system, OREtech sidescan sonar.	High backscatter on the OREtech image, cone structure on the 3.5 kHz profile
TTR9-AT-207G	Southern slope of the Ginsburg mud volcano (at 12:27 on the ORAT-32)	OKEAN long range sidescan sonar; 3.5 kHz profile; Single channel high resolution seismic system, OREtech sidescan sonar.	Moderate backscatter on the OREtech image
TTR9-AT-208G	Crater of the Ginsburg mud volcano (at 12:49 on the ORAT-32)	OKEAN long range sidescan sonar; 3.5 kHz profile; Single channel high resolution seismic system, OREtech sidescan sonar.	High backscatter on the OREtech image, cone structure on the 3.5 kHz profile
TTR9-AT-209GRAB	Crater of the Yuma mud volcano (at 14:28 on the ORAT-32)	OKEAN long range sidescan sonar; 3.5 kHz profile; Single channel high resolution seismic system, OREtech sidescan sonar.	High backscatter on the OREtech image, cone structure on the 3.5 kHz profile
TTR9-AT-210G	Southern flank of assumed mud volcano in the Eastern Moroccan Field (PSAT-121)	OKEAN long range sidescan sonar, 3.5 kHz profile	High backscatter on the sonar image
TTR9-AT-211G	Southern flank of assumed mud volcano in the Eastern Moroccan field (PSAT-121)	OKEAN long range sidescan sonar, 3.5 kHz profile	High backscatter on the sonar image
TTR9-AT-212G	Northern flank of assumed mud volcano in the Eastern Moroccan Field (PSAT-121)	OKEAN long range sidescan sonar, 3.5 kHz profile	High backscatter on the sonar image
TTR9-AT-213G	Crater of the Kidd mud volcano (PSAT-121)	OKEAN long range sidescan sonar; 3.5 kHz profile	High and moderate backscatter on the sonar image, cone structure on the 3.5 kHz profile
TTR9-AT-214G	Crater of the Adamastor mud volcano (PSAT-122)	OKEAN long range sidescan sonar; 3.5 kHz profile; Single channel high resolution seismic system.	High and moderate backscatter on the sonar image, cone structure on the 3.5 kHz profile
TTR9-AT-215G	Crater of assumed mud volcano in the Eastern Moroccan Field (PSAT-122)	OKEAN long range sidescan sonar; 3.5 kHz profile; Single channel high resolution seismic system.	High and moderate backscatter on the sonar image

Table 12. Acoustic and geographical characteristic of sampling stations in the Gulf of Cadiz.

Core No	Geographical Setting	Instrumentation	Acoustic Characteristics
TTR9-AT-216G	Crater of the TTR mud volcano (PSAT-122)	OKEAN long range sidescan sonar; 3.5 kHz profile; Single channel high resolution seismic system.	High and moderate backscatter on the sonar image, cone structure on the 3.5 kHz profile
TTR9-AT-217G	Crater of the Ginsburg mud volcano (ORAT-32)	OKEAN long range sidescan sonar; 3.5 kHz profile; Single channel high resolution seismic system, OREtech sidescan sonar.	High backscatter on the OREtech image, cone structure on the 3.5 kHz profile
TTR9-AT-218GRAB	Crater of the Ginsburg mud volcano (ORAT-32)	OKEAN long range sidescan sonar; 3.5 kHz profile; Single channel high resolution seismic system, OREtech sidescan sonar.	High backscatter on the OREtech image, cone structure on the 3.5 kHz profile
TTR9-AT-219G	Ridge in the Western Moroccan field (at 6:27 on the PSAT-125)	OKEAN long range sidescan sonar; 3.5 kHz profile; Single channel high resolution seismic system	High and moderate backscatter on the sonar image
TTR9-AT-220G	Ridge in the Western Moroccan Field (at 11:50 on the PSAT-127)	OKEAN long range sidescan sonar; 3.5 kHz profile; Single channel high resolution seismic system	High and moderate backscatter on the sonar image
TTR9-AT-221G	Ridge in the Western Moroccan Field (at 9:25 on the PSAT-125)	OKEAN long range sidescan sonar; 3.5 kHz profile; Single channel high resolution seismic system	High and moderate backscatter on the sonar image
TTR9-AT-222G	Crater of the St.-Petersburg mud volcano (PSAT-134)	OKEAN long range sidescan sonar; 3.5 kHz profile; Single channel high resolution seismic system.	High backscatter on the sonar image, cone structure on the 3.5 kHz profile

Table 12 (*Continuation*). Acoustic and geographical characteristic of sampling stations in the Gulf of Cadiz.

Mud breccia, recovered in the MMF from the Yuma and Ginsburg mud volcanoes (cores AT-203G, AT-204G, AT-205G, AT-206G, and AT-208G) is very gas-saturated and characterized by a strong smell of hydrogen sulphide and contains fluid escape structures. In the lower parts of the cores AT-206G and AT-208G, from the crater of the Ginsburg mud volcano, gas-hydrate crystals are found within the mud volcanic deposits.

One of the peculiarities of mud volcanic deposits of the Gulf of Cadiz, in contrast with mud breccias of the Eastern Mediterranean, the Black Sea, and the Norwegian margin, is their distinct stratification. In most cores containing mud breccia (AT-203G, AT-204G, AT-206G, AT-213G, and AT-214G) it is possible to distinguish from 3 to 8 individual layers, separated by sharp contacts. Mud breccia layer thickness rarely exceeds 0.5 m and in some cores is only 2-3 cm, implying a low level of recent mud volcanic activity with frequent expulsions of small volumes of mud. Another interesting feature of mud volcanic deposits of the Gulf of Cadiz, which is not very common for other regions of mud volcanism, is the intensive bioturbation in the upper parts of the flows. It probably can be explained by a specific mud breccia composition, perhaps enriched in organic matter, or by benthic faunal peculiarities of the region.

Facies VII:

Two cores in the EMF (AT-215G and AT-216G) and one core (AT-222G) from the northern part of the study area recovered a specific interval of relatively consolidated, greyish brown, structureless clay with fine grained terrigenous and foraminiferal admixture. The interval is very enriched in coral debris and contained rock clasts and brachiopod shell fragments. Its thickness varies from 20 to 40 cm. In AT-216G this interval overlay mud breccia with a sharp irregular contact and is covered by an upper pelagic marl with foraminifera and coral debris. In AT-222G the same horizon is observed between two mud breccia intervals. Core AT-215G, in an inferred mud volcano, penetrated only 30 cm of greyish brown, clayey interval rich in coral debris overlain by recent pelagic marl.

Detailed core study confirmed the relationship between Facies VII and mud volcanic processes. A possible explanation is that during quiescent periods of mud volcanic activity carbonate build-ups

develop on the mud volcanic edifice, which provides a hard substratum. Cold-water carbonate build-ups, known from the Rockall Trough, Porcupine Seabight (Hovland et al., 1994; Kenyon et al., 1998) and other areas in the North Atlantic are mainly found at the depths close to those where coral- debris rich sediments were recovered in the Gulf of Cadiz. Reactivation of mud volcanism processes lead to destruction of these new-formed carbonate build-ups. Their material mixes with mud breccia flows, forming the horizons with Facies VII. An abrupt change in ambient chemistry should lead to partial dissolution of carbonates, signs of which were observed during study of individual coral fragments.

Several cores recovered in the Gulf of Cadiz contain horizons of tube worms – *Pogonophora*. In AT-208G (Ginsburg mud volcano crater) there is a *Pogonophora*-rich layer within the uppermost part of mud volcanic deposits (7-10 cm bsf). In AT-206G and AT-217G (both from the crater of the Ginsburg mud volcano) and in AT-216G (the TTR mud volcano crater) horizons of *Pogonophora* were developed within upper pelagic marls overlying mud breccia. The *Pogonophora* layers are recently formed in the study area under conditions of active fluid seepage through the seafloor. In AT-207G (southern slope of the Ginsburg mud volcano) *Pogonophora* are abundant in the uppermost pelagic marl, and other evidence for fluid seepage - authigenic carbonate concretions - is found near the bottom of the core.

Two cores, taken from the southern (AT-210G) and northern (AT-212G) flanks of a small structure of assumed mud volcanic origin in the EMF, contain tabular siderite concretions, up to 7 cm in diameter, in the lower part of the recovered succession. This authigenic alteration in sediments could be also related to fluid venting in the area.

The crater of the Yuma mud volcano was also sampled with the TV-controlled grab (AT-209GR). Mud volcanic deposits, similar to those described above, and pelagic foraminiferal marl were recovered. Large rock clasts were preliminarily studied onboard and about 30 lithologies were described with the aim of characterizing the succession through which the mud volcano erupted. The most abundant among studied rock fragments are different sandstones, claystones, and poorly lithified marlstones.

Another TV-controlled grab sample was obtained from the crater of the Ginsburg mud volcano (AT-218GR). Beside mud volcanic deposits and recent pelagic sediments the recovery contained semi-consolidated brown clay with coral debris (similar to those recovered from AT-215G and AT-216G) and porous carbonate aggregates exceeding 0.5 m in size. These carbonate aggregates consisted of cemented corals, shell fragments and large claystone fragments. Possibly these aggregates are fragments of carbonate build-ups formed on the mud volcanic edifice under conditions of active hydrocarbon fluid seepage. Among rock fragments from the mud breccia, sandstone and claystone predominated.

Surficial clay mineral assemblages

D. DIXON

The cores that recovered mud breccia from the craters of mud volcanoes (AT-203, AT-204G, AT-206G, AT-213G, AT-214G, AT-215G, AT-216G and AT-217G) differ remarkably in clay mineral composition from the other cores taken in the near vicinity (Fig. 60). All these mud breccia cores exhibit a significantly increased smectite content (52-61%) (Fig. 61).

According to foraminifera studies of mud breccia from the craters, the extruded sediment is coming from as far down as Eocene and Miocene deposits (Sadkov and Ovsyannikov, 2000). This finding is consistent with the fact that Miocene deposits are very rich in smectite due to the volcanic regime operating at that time (Maldonado et al., 1999).

The surficial clay assemblages from the areas adjacent to the volcano craters exhibit a smectite content of 20 % almost uniformly throughout, this correlates with data from the deep Gulf of Cadiz where smectite contents of 17 and 22 % have been recorded (Grousset et al., 1988).

Only three cores were recovered from the northern Gulf of Cadiz, of these, two were sampled. One core was from the St. Petersburg mud volcano (AT-222G) and the other was from a channel levee

CLAY PERCENTAGES (areas)				CLAY MINERAL RATIOS (peak heights)			
	Sm	Ill	K+C		Sm/Ill	K+C/Ill	Sm/K+C
201G	20.67	60.15	19.17	201G	0.44	0.81	0.54
202G	23.56	58.66	17.78	202G	0.58	0.88	0.65
203G	61.85	23.64	14.50	203G	5.60	2.86	1.96
204G	55.23	30.31	14.46	204G	3.30	1.68	1.97
205G	41.07	42.86	16.07	205G	1.32	1.35	0.98
206G	56.88	25.51	17.61	206G	4.58	2.69	1.70
207G	20.22	58.74	21.04	207G	0.43	0.94	0.45
210G	21.13	59.33	19.54	210G	0.49	0.95	0.51
211G	20.77	58.26	20.97	211G	0.46	1.01	0.46
212G	27.53	50.95	21.52	212G	0.75	1.19	0.63
213G	58.32	29.95	11.73	213G	3.32	1.29	2.57
214G	52.38	34.53	13.09	214G	2.75	1.44	1.91
215G	22.38	57.83	19.80	215G	0.47	0.89	0.53
216G	21.01	60.37	18.63	216G	0.44	0.85	0.53
217G	55.98	28.99	15.02	217G	3.96	2.08	1.91
219G	26.05	55.09	18.86	219G	0.53	0.97	0.55
220G	27.90	55.52	16.58	220G	0.62	0.90	0.69
221G	27.41	54.26	18.33	221G	0.62	0.95	0.65
222G	40.47	39.88	19.65	222G	1.38	1.38	1.00
224G	26.49	45.52	27.99	224G	0.56	1.35	0.42

Sm = Smectite

Ill = Illite

K + C = Kaolinite + Chlorite

Figure 60. Gulf of Cadiz cores clay mineral data: percentages are calculated from XRD peaks values of the three most abundant clay types.

complex of a contourite channel formed by the Mediterranean Outflow Water (AT-224G). The St. Petersburg mud volcano core has a mineralogy almost identical to the core AT-205G, which was from the Ginsburg mud volcano. The second sampled core (AT-224G) exhibits an unusually high kaolinite+chlorite content (28 %) and also contains some mixed layer illite/smectite. Such an assemblage might indicate a significant input of terrigenous material and this fact is in an agreement with the location of the sampling site.

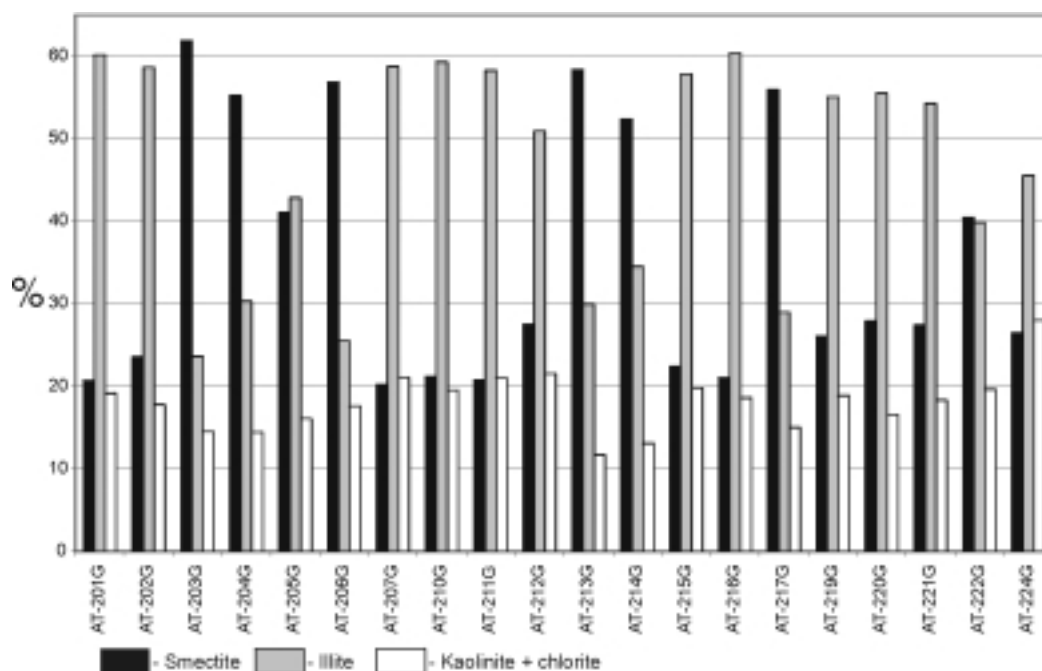


Figure 61. Clay mineralogy of the cores taken from the Gulf of Cadiz study area.

IV.1.5. Conclusions

The mud volcanoes we identified in this region are all located along the tectonically active Moroccan margin. Without deep multichannel seismic data, it is difficult to determine if emplacement of the mud volcanoes is tectonically controlled. In the WMF, the linearity of the ridges and a NW-SE trending lineament on the seafloor clearly suggest some type of fault controlled process. The present direction of tectonic compression in the region is NW-SE and several reverse and normal faults which deform Quaternary aged sediments in seismic line PSAT-121 attest to this tectonic stress. In addition, the mud volcanoes in the EMF tend to occur along a NW-SE line which could be coincidence or indicative of a fault controlled process

The mud volcanoes and diapirs we identified during this survey all fall in the region of olistostrome or accretionary wedge deposition first identified by Roberts (1970). Systematic westward movement of the Gibraltar arc is responsible for emplacement of the accretionary wedge/olistostrome during the Late Tortonian possibly supplying the sediments that make up the mud breccia complex we find in the gravity cores taken from the mud volcanoes. It is unclear when the mud diapirs and volcanoes first became active from the data we presently have. We are certain that these structures are at least Quaternary to Recent in age based on interpretation of seismic profiles which show deformation of adjacent stratigraphic units that are no older than Quaternary. Further investigations of the geochemistry of the sediment and pore waters obtained from the mud volcano gravity cores and detailed analysis of the mineralogy of the mud breccia clasts and rocks recovered from the mud volcanoes should shed some light on the genesis of this mud volcano province.

IV.2. MEDITERRANEAN UNDERCURRENT SHORT STUDY

N. H. KENYON, A. AKHMETZHANOV, M. IVANOV

Introduction

The aim of the short study was to obtain high resolution data from a channel formed by contour currents. There are two places on the European Margin where strongly flowing undercurrents pass through gateways that increase the speed of the flow and result in unusual sedimentary deposits. One is the Faeroe-Shetland Channel and its continuation, the Faeroe Bank Channel, which carry the Norwegian Sea Overflow water (NSOW). The approaches to the restricted part of the channel were

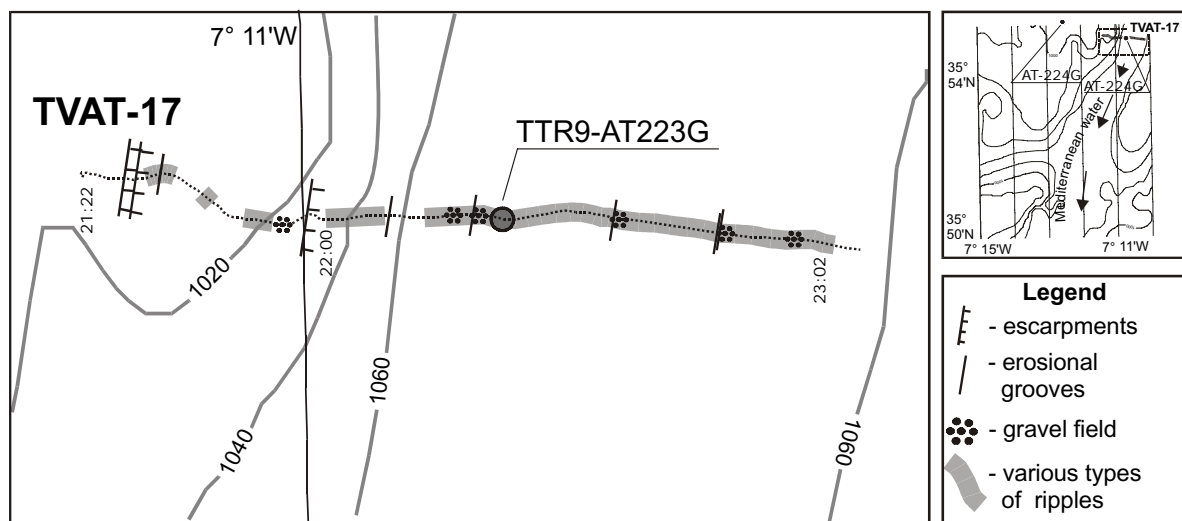


Figure 62. Interpretation of the underwater TV line TVAT-17 running across the Gil Eanes Channel cut by Mediterranean undercurrent water.

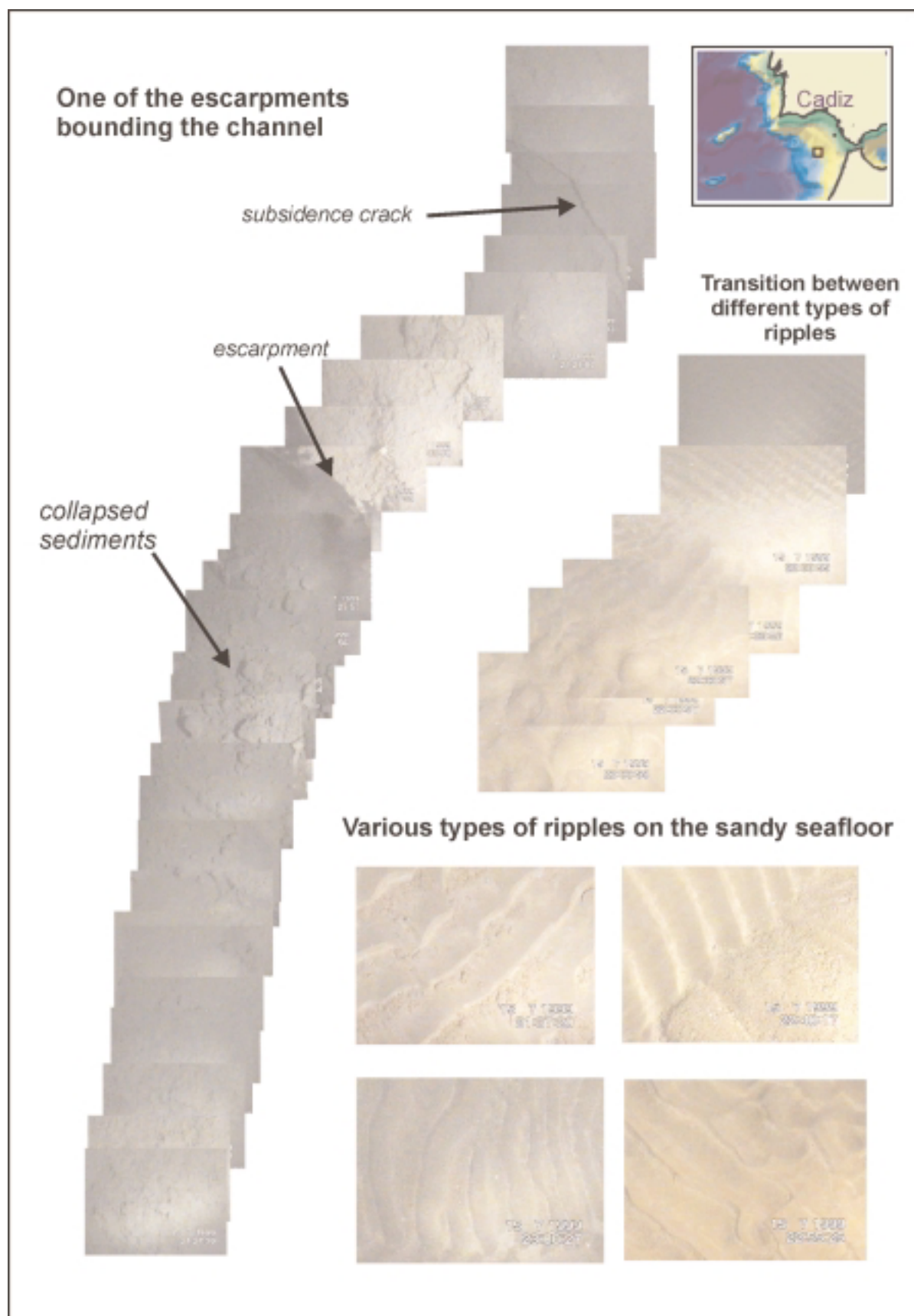


Figure 63. Stills from the video record TVAT-17 showing various seabed features.

investigated on TTR9, Leg 1, and the outflow area of the NSOW was investigated during TTR7, Leg 2 (Kenyon et al., 1998). The depositional processes of the Mediterranean Undercurrent where it exits from the Strait of Gibraltar have been studied extensively (Nelson et al., 1999) but there is one channel that is unusual and has been little studied. Rather than running alongslope with a bounding drift, as in the case of the well studied Faro Drift (which is further to the west), this channel carries a filament of the Undercurrent downslope. It is not guided at the present time by underlying topography but is on the top of a build up of sediment that is presumed to be laid down over a long period by the filament of the Undercurrent. It was first described by Kenyon and Belderson (1973) and it is here named the Gil Eanes Channel, after a celebrated navigator from this area.

GLORIA long range sidescan sonar data obtained in 1969 and 1970 showed the channel to be relatively straight with mud waves on its flanks. An air gun seismic profile had shown that it was not underlain by any significant diapiric ridge, unlike the ridge-guided downslope trending channels further to the west. A medium range sidescan sonar record, one of the first ever obtained in such water depths, showed what were thought to be sand waves on the channel floor (Kenyon & Belderson, 1973). The television profile, TVAT-17, was run to check out whether there is active sand transport down this channel.

TVAT-17

The profile starts at a depth of about 1010 m on the levee of the channel (Fig. 62). Silty-clayey bottom sediment has a smoothed surface and is intensively bioturbated. Down slope the profile crosses several escarpments a few meters high, which are believed to be formed by sediment failures where the channel wall is undercut by erosion near the base. Characteristic striations and fields of rippled sand seen on the flatter areas on the wall are also evidence for bottom current activity. Fields of rippled sand alternate with areas of smoothed silty-clayey seabed. Some gravel patches are observed. When the camera nears the base of the wall ripples become larger and have more irregular morphology. Below 1060 m the profile crosses the relatively flat channel floor. The record shows abundant sandy and gravelly material on the seafloor. Fields of ripples of various patterns are seen everywhere

Core No	Date	Time (GMT)	Latitude	Longitude	Cable length, m	Depth, m	Recovery, cm
TTR9-AT223G	15.07.99	16.52	35°54.678	07°10.688	998	971	2
TTR9-AT224G	15.07.99	18.10	35°55.138	07°12.575	915	888	242

Table 12.1 General information on the cores sampled from the Gil Eanes Channel in the Gulf of Cadiz.

(Fig. 63). The most common are large irregular ripples. The other common bedforms include fields of gravel with parallel ripples and erosional grooves. Formation of different types of bedforms is a function of current speed and type of sediment. Generally, for the mainly sandy sediment the following assemblage of bedforms is observed within the contourite channel: parallel symmetric ripples – parallel asymmetric ripples – transitional zone represented by several crisscrossing systems of ripples – large irregular ripples – gravel fields – erosional grooves. This assemblage is believed to reflect the pattern of current speed distribution within an individual stream of the bottom current, where the parallel symmetric ripples correspond to relatively low current speed and the erosional grooves to the highest speed.

Bottom samples

Samples obtained from the area confirm sidescan sonar and underwater TV observations. Only a small amount of well-sorted medium-coarse sand was retrieved from the thalweg of the channel at the station AT-223G and the gravity core AT-224G, taken from the levee, recovered a homogeneous sequence of well-sorted clayey silt.

V. ALBORAN AND SOUTH BALEARIC BASINS (Leg 3)

V. 1. OBJECTIVES AND GEOLOGICAL SETTING

M. COMAS AND M. IVANOV

Objectives

The Leg 3 of the TTR9 Programme was dedicated to geophysical survey and sea bottom sampling in selected sectors of the Alboran and South Balearic basins in the Western Mediterranean Sea (Fig. 64).

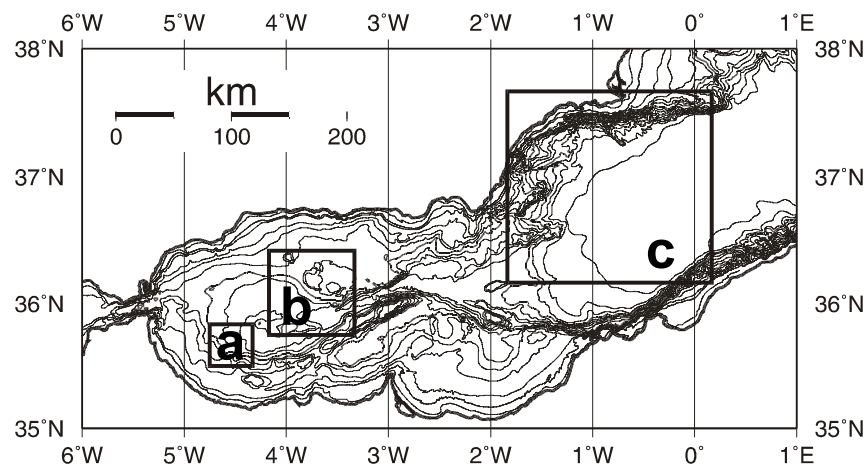


Figure 64. Bathymetry map of the Alboran and the South Balearic Seas showing sectors that were investigated during TTR-9 Leg 3. **a**- diapiric province in the southern Alboran Sea, **b** - dredging area in the northern Alboran Sea, **c** -South Balearic basin.

The main scientific objectives of Leg 3 were to investigate:

- 1) The nature and petro-structural characteristics of the basement of the basins. The basement of the Alboran basin is formed primarily of metamorphic complexes belonging to the Alboran Crustal Domain, the exhumed metamorphic core complexes of the Betic-Rifean cordilleras. The basement in the northern margins of the South Balearic basin, named the Palomares and the Mazarrón margins, was predicted to be formed of metamorphic rocks belonging to the Alpujarride or Nevado-Filabride complexes of the eastern Betic Cordillera.
- 2) The nature and age of volcanic edifices forming residual or structural highs within the basin. East of 4° W, broad areas of the top of the acoustic basement appear to be formed by volcanic rocks forming residual volcanic highs. Submarine volcanic edifices were expected to be the counterparts of Miocene volcanic rocks exposed in the Betic and Rifean chains.
- 3) The geometry of major tectonic lineaments and related faulting. Tectonic lineaments in the northern margins of the South Balearic basin are sites of seismogenic faults which are related to recent episodes of strike-slip, extensional or compressional tectonics.
- 4) The relationship between seafloor morphology and tectonics in actively deforming sectors. Submarine channeling, bedforms, sediment transport and slope instability are thought to be the surface expression of active faults, which have accounted for syn-sedimentary deformation of Plio-Quaternary to Recent sediments, as well as for seismogenic events.
- 5) The mud diapir province of the Alboran basin, and the possible development of mud-volcanoes at the top of the diapirs. The notable mud diapir province recognized in seismic profiling in the West Alboran basin is known to be formed of overpressured shales of early-to-middle Miocene age.

The mud diapirism relates to the middle Miocene extensional processes, but diapirism resumes by post-Messinian times and continues till the Holocene when it reaches and deforms the sea floor.

These objectives were planned to be met by the following activities:

- A reconnaissance of the selected sectors based on high resolution seismic reflection profiling and OKEAN long range sidescan sonar records. The aim was to collect information around seismogenic faults, the top of volcanic edifices and adjacent slopes, as well as the top of mud diapirs, and on the seismostratigraphy and structures of the latest Miocene to Holocene sequences.

- More detailed investigation by survey with the OREtech deep-towed sidescan sonar over selected sectors in the seafloor on the basis of OKEAN and seismic images. Further underwater TV recording and photography to be taken at suitable points.

- Sampling hard rocks cropping out at the sea floor by dredging submarine outcrops, and sampling sediments by gravity coring.

The area for investigations comprises selected sectors proposed by the TTR9 research team from the “Instituto Andaluz de Ciencias de la Tierra” (CSIC and University of Granada). TTR9 Leg 3 survey and investigations in the Alboran and South Balearic basins were of particular interest to address the scientific objectives of the Spanish project MAR98- 0981 (CICYT-CYTMAR), and meet the objectives of the named “BASACALB Leg” under this project.

Background and geological setting

The Neogene basins beneath the Alboran and South Balearic seas, just behind the Gibraltar Arc, correspond to the westernmost Mediterranean extensional basins. These basins are located within a Miocene arc-shaped thrust belt formed by the Betic (Southern Spain) and Maghrebian (Rif and Tell, in Morocco) Cordilleras. They originated by extension at the site of a former (late Cretaceous to Palaeogene) collisional orogen and developed within a convergence plate tectonic setting since the early Miocene.

The relevance of the Alboran and South Balearic basins and the surrounding mountain belts has to be considered for geodynamic reconstruction between African and Eurasian plates from the Cenozoic to Present. The possibilities that this land-locked scenario offer is to integrate marine surveys with geological and geophysical data from the surrounding mountain chains and thus maximize the value of any research that may test the predictions of the competing hypotheses for the origin and evolution of the western Mediterranean basins. Beside this, they are potential areas to address investigations of present-day crustal deformation in the region.

The Alboran and South Balearic seas were the site of a vigorous program of oil and gas exploration in the 1970's and 1980's and as a result, numerous seismic reflection profiles now exist from the basin, mostly from the Spanish and Moroccan margins. Most of these profiles are recorded out to 6 seconds two-way travel time and have been processed through stacking and migration. The seismic grid of commercial lines tie-in with 6 commercial boreholes; 4 on the Spanish side and 2 in the Moroccan shelf.

From the early 1990's several scientific surveys have been carried out in the region. These cruises have acquired significant geophysical data, including high resolution single channel and multi-channel seismic reflection profiling, multibeam bathymetry and sidescan sonar. Furthermore, specific geophysical investigations were dedicated to heat-flow distribution, and magnetic and gravity studies. Dives with the *Cyana* submersible sampled volcanic seamounts in the Alboran basin in 1994, and Leg 161 of the Ocean Drilling Program drilled in the Alboran and South Balearic basin in 1995 (Comas, Zahn, Klaus et al., 1996).

The Alboran Sea (about 400 km long and 200 km wide) has a maximum depth of less than 2000 m and exhibits a complex seafloor morphology, with several sub-basins, ridges, and seamounts. The Alboran Ridge, locally emergent at Alboran Island, and Alboran Trough are the more prominent linear reliefs that extend 180 km and trend obliquely (NE-SW) across the Alboran Sea. In the South Balearic basin water depth is up to 2600 m in the basin plain.

Geophysical data and modelling provide constraints on regional crustal thinning and configuration from the surrounding chains to the Alboran and South Balearic Seas (from 38 km in the Internal Betics to about 19-14 km beneath the central Alboran Sea) and suggest a steady W to E decrease in lithospheric thickness from the West Alboran basin to the South Balearic basin (from 60-90 km in the west to about 35-40 km in the east, at the transition to the South Balearic Sea (e.g. Torne and Banda, 1992; Watts et al., 1993; Polyak et al., 1996). There is no evidence for the existence of Cenozoic oceanic lithosphere in the Betic-Rif-Alboran region. Deep seismic data, however, suggest the presence of oceanic crust east of 1° W meridian in the South Balearic basin (Mauffret et al., 1987; Comas et al., 1995).

The basement of the Alboran basin is formed primarily of metamorphic complexes belonging to the Alboran Crustal Domain (the internal complexes of both the Betic and Rif Chains; composed of a syn- and post-metamorphic pre-Miocene polyphase thrust-stack. ODP Site 976 results confirmed that the Alboran Domain has N-S continuity beneath the Alboran Sea (Comas et al., 1997, 1996; Comas et al., 1999). East of 4° W most of the basement highs appear to consist of volcanic edifices, as revealed by dredging (Gierman et al., 1968) and diving data (Comas, *pers. comm.*). Nevertheless, the nature of the absolute basement in the eastern Alboran region and the South Balearic basin is uncertain.

Commercial ODP and DSDP drilling and correlation with the available seismic data provided information on the sedimentary cover in the Alboran and South Balearic basins. The older marine deposits overlying the basement beneath the Spanish Alboran margin are latest Aquitanian ?-Burdigalian in age, and consist of olistostromes containing clastic material and under-compacted shales. Middle to lower-upper Miocene deposits (Langhian and Serravallian / early Tortonian) consist of under-compacted shales at the base, passing upward into graded sand-silt-clay turbidites. Over-pressured material from these sediments forms the extensive diapir province in the West Alboran basin. Sediments from late Tortonian are formed of sandstone intervals that alternate with claystone and silty-clay beds, also corresponding to turbidite layers. Volcaniclastic levels intercalate throughout the middle and upper Miocene sequences. The Messinian deposits in the Alboran basin consist of marine siliciclastic or shallow carbonate facies, with occasional gypsum and anhydrite intervals. Messinian deposits have a nearly uniform maximum thickness of about 250 m (about 200 msec) across the entire Alboran Sea basin; furthermore, there exist wide areas in the basin lacking in Messinian sediments, probably due either to erosion or non deposition. A well-developed Messinian-evaporite (thick salt) sequence is absent, in contrast to the neighbouring South Balearic basin. Messinian evaporite developed in the South Balearic basin (salt domes beneath the abyssal plain), which thins towards the north and south margins and disappears towards the west towards the Alboran basin. No direct sample information exists about specific ages of pre-Messinian sediments in East Alboran and South Balearic basins. The Pliocene to Pleistocene sediments in the whole region consist mainly of pelagic deposits, fine-grained distal mud turbidites, hemipelagic clay, and scarce interbedded silt and sandstone turbidites. In the Alboran basin, the reflector that marks the base of the Plio-Quaternary sedimentary units corresponds to a strong erosional and locally angular unconformity, that correlates with the “M- reflector” – the top of the Messinian evaporites in the South Balearic basin and elsewhere in the Mediterranean (Ryan, Hsu et al., 1973; Comas et al., 1996).

The structure of the Alboran and South Balearic basins resulted from superimposed extensional and compressional tectonic stages. Rifting and progressive exhumation of the Alboran Domain took place from the late Oligocene to the early Miocene. Early stages of crustal stretching correlate with an early Miocene transgression (about 21-19 ma). A prominent middle to late Miocene rifting (from about 16-14 Ma to about 11-10 Ma) is identified in the seismic record of the West Alboran basin and has been constrained by ODP drilling. Generalized early Miocene and late-Serravallian- to-Tortonian magmatism, as well as notable mud diapirism in the West Alboran basin, have likely resulted from these extensional processes. This rifting, which is connected to large-scale extension detachments known in the Betics and Rif, ceased during the late Miocene (about 10 Ma ago). Patterns of Miocene extension, as well as areal distribution of metamorphic basement units and sedimentary sequences are consistent with an extensional detachment system to produce crustal thinning. Since the late Miocene, NE-SW

trending folds, NE-SW and NW-SE directed strike-slip faults, and tectonic inversions of former extensional faults caused a major contractive deformation in the region. Structures indicate a NNW/N directed compression during the Pliocene and Pleistocene. Post-Miocene tectonics caused a major reorganization of the whole region which resulted in prominent N-S shortening and uplifting of surrounding areas. Conspicuous wrench-fault lineaments at the southern margin of the South Balearic basin and at the limit between the Alboran and South Balearic basin, as well as significant NE-SW directed extension in both the West Alboran and the western South Balearic basins took place at these times. Messinian to Recent structures are consistent with late Neogene to Present Africa-Europe convergence plate kinematics and are thought to involve crustal boundaries (Comas et al., 1992; Jurado and Comas, 1992; Maldonado et al., 1992; Woodside & Maldonado, 1992; Watts et al., 1993; Comas and Soto, 1999; Comas et al., 1999).

V.2. ALBORAN BASIN (DIAPIRIC PROVINCE)

V.2.1. Seismic Data

M. COMAS, A. TALUKDER, J. WOODSIDE, A. VOLKONSKAYA

Seismic Line PS-170 MS

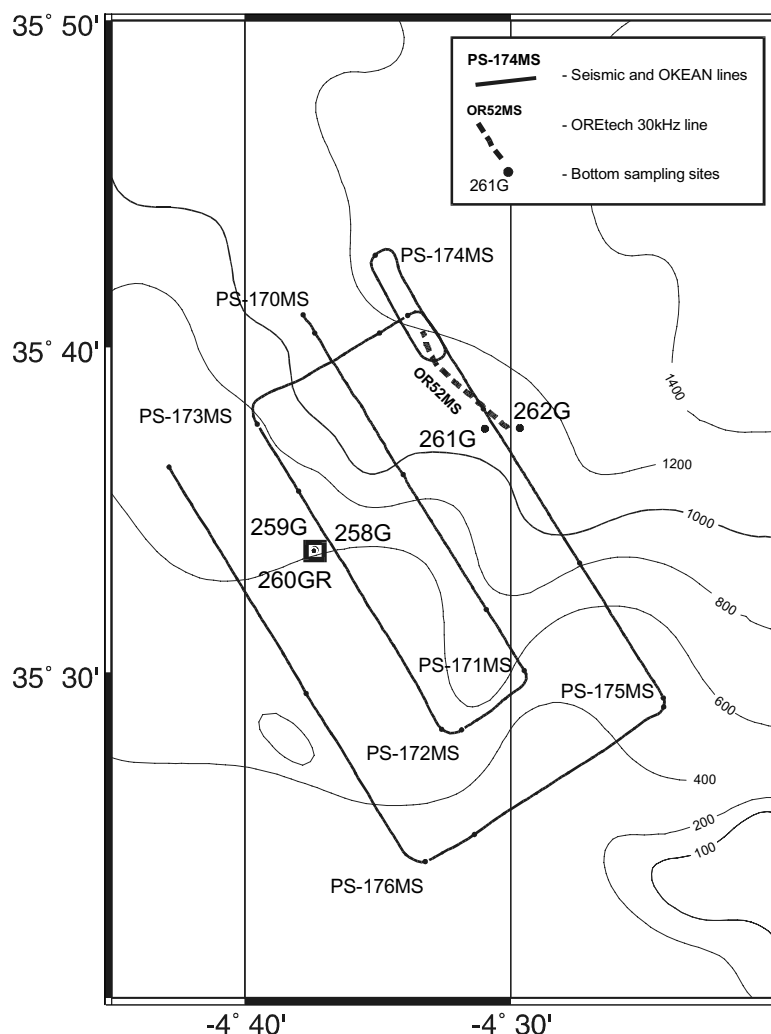


Figure 65. Location map of the southwestern Alboran Sea working area.

Profile PS-170 MS is 17.2 nm long and runs NNW-SSE in the West Alboran basin, across three mud diapir highs (Fig. 65). These diapirs deform the overlying sedimentary sequence, affecting the sea-bottom in two cases. Covering the mud diapirs, two seismostratigraphic units with distinctive seismic facies can be distinguished (Fig. 66). These units are characterized by strong parallel reflectors of variable amplitude, and locally they have lateral thickness variations and a wedge geometry. These two units are separated by a high amplitude reflector which corresponds to an erosional or angular unconformity (Fig. 66). The erosive character of this unconformity is clearly visible between shotpoints 40 to 160 (1600 ms TWT), 460 to 560 (1400 ms TWT), and from 920 to 1040 (1000 ms TWT). Both units cover the mud diapir highs with an onlap geometry (Fig. 66).

The uppermost unit (Unit I) is highly reflective with closely-spaced subparallel reflectors. It has a maximum thickness of 200 ms TWT. The lower unit (Unit II)

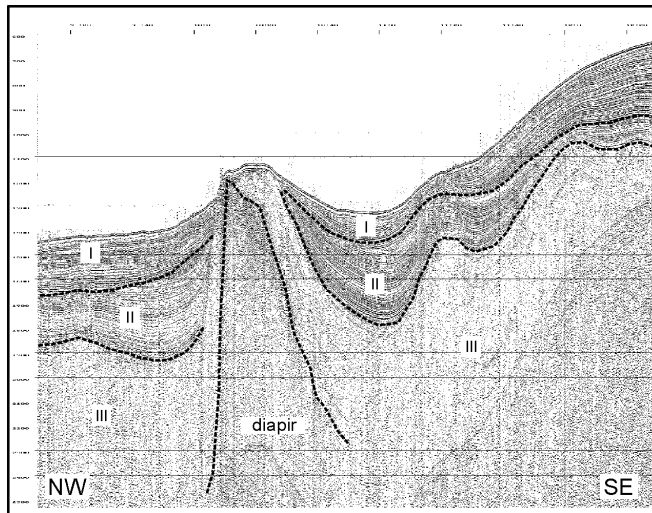


Figure 66. Seismic line PS 170 MS (from shotpoints 80 to 1080), showing the occurrence of three mud diapirs. The three seismic facies (I, II, and III) distinguished in the surveyed area are shown in the interpreted seismic line, together with their boundaries. Notice the erosive character of the boundary between Unit I and Unit II, and the upward doming of the seismic Units I to III coinciding with the top of the mud diapirs.

is in general less reflective and has more widely spaced high-amplitude reflectors. Several angular unconformities can be distinguished inside this unit. It has a variable thickness, ranging from 400 ms TWT to 200 ms TWT. Maximum thickness of Unit II is achieved between the diapirs (Fig. 66), decreasing in thickness towards the mud diapirs with an onlap geometry. Beneath Unit II scattered high amplitude reflectors can be distinguished (e.g. up to 2600 ms TWT at 560-680 shotpoints), which represent seismic unit III. A strong and discontinuous reflector appears up to 3000 ms TWT. On the basis of seismic correlation with nearby commercial multi-channel seismic profiles, this strong deep reflector probably corresponds to the Messinian unconformity (M-reflector) (Ryan et al., 1973; Jurado and Comas, 1992). The mud diapirs are represented by a seismic unit with no coherent internal reflections, locally with hyperbolae and high amplitude discontinuous reflections at the contact with

the sedimentary sequence (Fig. 66).

Units I to III are gently folded, the anticlines coinciding with mud diapirs. The largest diapir (shotpoints 300 to 560) reaches the seafloor and has a steep NW slope and a more gentle SE slope. Internally the largest diapir has at least one high angle normal fault, dipping southward. This fault cuts the top of the diapir and reaches the seafloor at shotpoint 370. The other two diapirs are smaller in size but do not disrupt Unit I, nevertheless this unit is always thinner over the diapirs. The diapir between shotpoints 740 and 830 cuts the base of Unit II and disturbs the layers above, producing differential uplift of the sea bottom.

At the SSE end of the profile the sea bottom rises and the layers dip NNW at a low angle.

Seismic Line PS-171 MS

Profile PS-171 MS is a 1.9 nm long line oriented ENE-WSW over the top of a mud diapir. In this seismic line we see the same three lithoseismic units as described in the previous line. The boundary between the units is concordant. The bottom of Unit I is between 1000 ms and 1200 ms TWT. Unit III appears below 1300 ms TWT. At shotpoint 80 a collapse structure occurs in Unit I. A strong reflection is found around shotpoint 120 at a depth of 1300-1400 ms TWT.

Seismic Line PS-172 MS

Profile PS-172 MS runs for 9.5 nm with a SE-NW trend over the top of two mud diapirs. One diapir is located at shotpoint 100 and connects laterally with the sampled Granada mud volcano. The lithoseismic units distinguished on this profile are similar to those units described previously (e.g. Seismic line PS-170 MS). The character of the unconformity at the base of Unit I is clearly seen at shotpoints 0 to 200, with an angular relationship and truncation of the reflectors of Unit II. Unit I has a minimum thickness of 150 ms TWT (e.g. at the southern end of the profile), increasing in thickness towards the mud diapir high, and reaching a thickness of up to 230 ms TWT on its southern flank (e.g. shotpoint 320). Unit II also increases in thickness towards the northwest, with a maximum thickness

of 480 ms TWT at the flank of the mud diapir (shotpoint 240) and a minimum thickness of 300 ms TWT (e.g. shotpoint 40). Unit III is almost transparent and only scarce reflectors can be distinguished in this profile (e.g. at 2000 ms TWT at shotpoint 80). The M-reflector is not clearly distinguished in this profile, although there are some scattered high amplitude reflectors at 2000 ms TWT at the southern end of the line (shotpoints 40-160).

The diapir seen at shotpoint 100 has caused an asymmetric anticline to develop above it, with a subvertical axial trace. This fold on top of the diapir affects reflectors mainly up to the base of the Unit I, decreasing in amplitude towards the top of Unit I. The northern diapir (between shotpoints 320 and 400) has subvertical faults at the flanks, which cut Unit II and the lower part of Unit I. There is a strong reflector inside Unit I which is folded and covers the diapir, indicating deposition of the uppermost part of the unit after faulting and during the latest stage of folding and/or rising of the diapir.

Seismic Line PS-173 MS

Profile PS-173 MS runs with a SW-NE trend and over a distance of 5 nm, on top of a mud diapir which outcrops locally. Seismic units I to III can be distinguished in the profile on the flanks of the mud diapir. Unit I is very thin (maximum thickness of 120 ms TWT) and partially covers the top of the diapir (thickness less than 20 ms TWT). Unit II appears only at the flanks of the mud diapir dipping outwards (maximum thickness of 280 ms TWT at shotpoint 0). Several internal angular unconformities can be distinguished inside Unit II, particularly at the northeastern flank of the diapir (shotpoint 250).

The flanks of the diapir are high-angle normal faults, which affect the whole sedimentary sequence, i.e. Unit I and II. This structure also affects the sea floor topography (Fig. 67) and causes a difference in the depth of Units I and II between the SW and NE flanks of the diapir (e.g. base of Unit I is located at 1200 and 1600 ms TWT, respectively). Unit II is tilted and has accommodation folds on both flanks of the mud diapir.

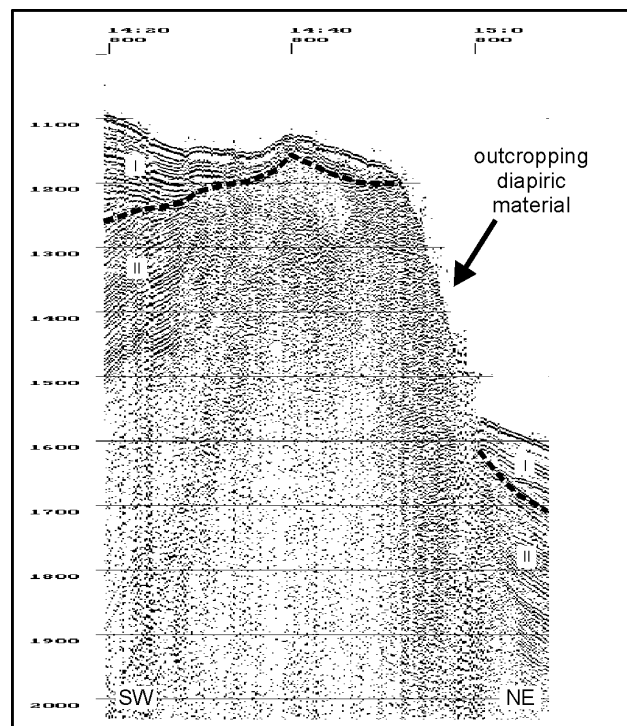


Figure 67. Seismic line PS 173 MS across a mud diapir high, outcropping at the sea floor. There is a change in depth of seismic units I and II on opposite sides of the diapir.

Seismic Line PS 174 MS

Profile PS-174 MS runs with a NW-SE trend for 14.35 nm. As in line PS-170 MS three anticlines can be observed, in two cases coinciding with mud diapirs.

The three units distinguished in the previous lines are also present in this seismic line. Unit I has a thickness of approximately 100 ms at the northwestern end of the seismic line and of 160 ms towards the southeast. Between shotpoints 80 and 180 it has a lenticular shape with highly reflective layers that change laterally to a transparent zone. At shotpoint 200 and 1700 ms TWT depth, there is a channel-like geometry that cuts into Unit II. This channel is part of the erosional event that produces the unconformity between Unit I and Unit II. This unconformity is evident also, and clearly erosive, between shotpoints 720 and 820.

Unit II has important thickness variations, ranging from 400 ms TWT in the synclinal axes, for example at shotpoints 120 or 680, to 120-to-50 ms in the anticlinal axes at shotpoints 760 or 960. It develops progressive angular unconformities in the fold limbs, with strong reflectors onlapping a less reflective bottom layer between shotpoints 680 and 740. In some areas the reflectors of this unit onlap the underlying Unit III.

Unit III has a uniform thickness of approximately 600 ms TWT, except in the limb of the fold between shotpoints 720 and 760 where its thickness decreases to about 200 ms TWT. Only a few scattered reflectors can be seen in this unit. The lower limit of the unit is a folded, continuous low amplitude reflector, that can be seen at a depth interval of 2300-2500 ms TWT. This reflector is interpreted as the Messinian (M) unconformity by correlation with nearby commercial seismic lines (Ryan et al., 1973; Jurado and Comas, 1992). The mud diapir between shotpoints 360 and 440 cuts all the seismic units, creating drag fold structures at the contact with the diapir. This diapir crops out on the sea bottom, producing a positive relief. Between shotpoints 700 and 820 there is an anticline over which all the seismic units are folded, producing uplift of the sea floor. The mud diapir between shotpoints 940 and 1020 intrudes into Units II and III, whereas Unit I remains undisturbed. The sea floor and the upper unit dip towards the northwest, from 600 to 1600 ms TWT.

Seismic Line PS-175 MS

Profile PS-175 MS runs with a NE-SW trend for a distance of 8.36 nm, crossing a mud diapir high (maximum elevation of 800 ms TWT depth at shotpoint 360). This mud diapir has an irregular topography with an associated minor high located at shotpoint 240 (1000 ms TWT). The top of the diapir is characterized by a strong and discontinuous package of irregular reflectors. Seismic units I and II can be both distinguished in the profile. Unit I has a maximum thickness of 350 ms TWT, decreasing towards the SW, showing a minimum thickness of 175 ms TWT on top of the mud diapir. The lower section of Unit I shows a remarkable lateral change in the seismic facies, decreasing its reflectivity towards the mud diapir high, where discontinuous and wavy reflectors are found. Unit II has a maximum thickness of 425 ms TWT at the northeastern end of the profile, decreasing towards the SW and disappearing on top of the mud diapir. Unit III cannot be distinguished clearly in the profile due to the occurrence of multiple reflections below 1100 ms TWT.

Seismic Line PS 176 MS

Profile PS 176 MS is a SE-NW line running for 14.7 nm, across the top of three mud diapirs. The southernmost diapir occurs between shotpoints 10 and 150. The top of the middle diapir is at shotpoint 430 and is approximately the same size as the diapir at shotpoint 80. The third diapir occurs at the end of the line (beginning at shotpoint 560) where it cuts all seismic units, reaching the seafloor. Several vertical faults cut the top of the two southernmost diapirs. These faults affect the three seismic units distinguished in this profile, which are similar to those units described previously (e.g. seismic line PS 170 MS). Faults produce a graben structure in the culmination of the two southernmost diapirs. The M-reflector is not clearly distinguishable in the profile.

All the units have their minimum thickness on top of the diapirs (250 ms TWT for Unit I and 350 ms TWT for Unit II). The two southernmost diapirs develop two anticlines with a subvertical axial trace, the southernmost one is symmetric and the northernmost one is asymmetric. Maximum thicknesses of units are observed in the syncline between both diapirs (400 ms TWT for Unit I and probably more than 450 ms TWT for unit II).

V.2.2. Sidescan Sonar Data

J. WOODSIDE, M. IVANOV, R. KOELEWIJN, I. ZELDENRUST AND P. SHASHKIN

The OKEAN records are most useful when used with the seismic and 3.5 kHz echo-sounder

records because the observed backscatter variations make more sense in this context. The area surveyed was not particularly deep, and covers an area of approximately 28 by 40 km between coordinates 35° 25' and 35° 45' N and from 4° 24' and 4° 45' W, with a gentle slope towards the north-north-east. The OKEAN profiles are 8 km wide and overlap each other. Most of the area is draped with a uniform sedimentation that provides a relatively uniform backscatter (Fig. 68). The deviations from this background level of backscatter are important. Artefacts on two of the short connecting lines

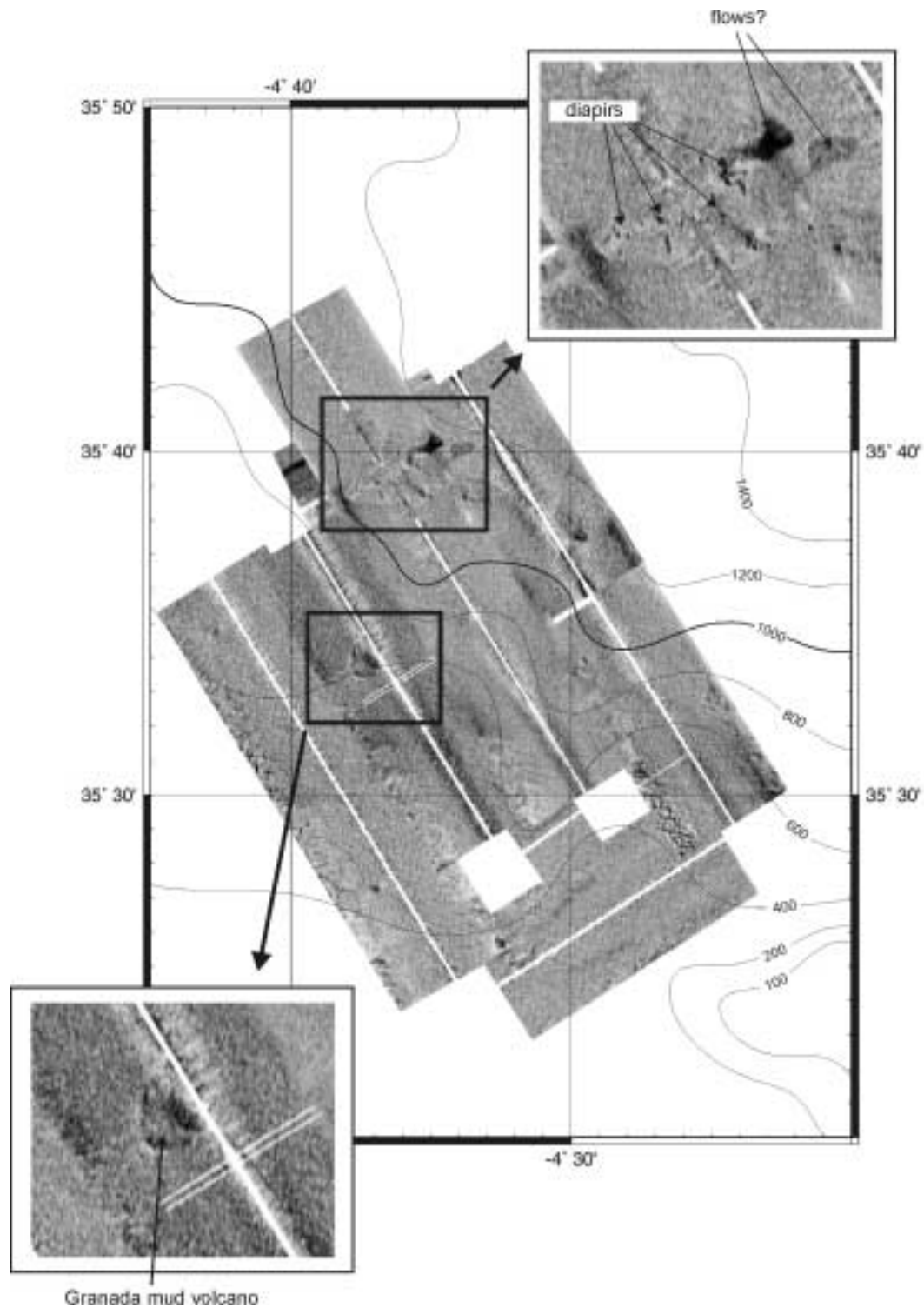


Figure 68. OKEAN mosaic from the southern Alboran basin.

(track-parallel striping on the starboard side of line PS-171, similar problems on the port side of PS-173) limit their usefulness but the rest of the data compensate for this.

Line PS-170 crosses three diapirs but the northwestern one is the most interesting on the OKEAN record. The upper surface of the diapir displays points and short lines of high backscatter, often in areas of slightly lower background backscatter. In several cases, shadows on the ship side of these features indicates that they may represent either the outer walls of depressions or positive features with current scouring around them. They may be associated with vents, in which case they could be concentrations of carbonate crusts. A 'flow-like' trace of high backscattering from two very high backscatter points widens down the slope of the diapir. This appears similar to mud flows observed on mud volcanoes elsewhere, with the high backscatter originating from rock clasts in the mud breccia. Further along the line (at 11:45) three similar high backscatter targets are observed on another mud diapir. Other variations in backscatter can be related to seafloor topography in general.

An elliptical feature on line PS-172 is defined by a low backscatter outer ring (contrasting with high backscatter on the inside of the outer ring), and an inner elliptical patch of high backscatter offset towards one side. A core made at this location (core TTR9-258G, see coring section) recovered mud breccia typical of material expelled under pressure at mud volcanoes. This location is near but not on one of the smaller diapirs but the seismic data suggest that a seep is present below it.

Line PS-174 displays several patches of moderately higher backscatter which could be interpreted as mud flows from diapirs. The backscatter is less for these patches than for that of line PS-170 (see above) suggesting either that they are older buried flows or are different in composition (e.g. smaller clasts). A small high backscatter point can be observed associated with one of these patches (at 16:42). Further along the line are four more high backscatter points similar to those seen on line PS-170 on top of the large diapir to the northwest and located in the same area as the three targets seen at 11:45 on line PS-170. A series of crescent-shaped features (shaped like dunes) is observed at the southwest corner of this OKEAN line but do not appear on the overlapping portion of line PS-175, suggesting that they are artefacts (e.g. interference patterns).

The final OKEAN line (PS-176), on the southwest slope of the basin, is remarkable only for several small circular patches of higher backscatter in a region of otherwise relatively uniform backscatter.

An OREtech deep tow sidescan and subbottom profiler line was terminated after only two hours of operation because of strong bottom currents at 90 degrees to the wind direction, making manoeuvring difficult and dangerous. Nevertheless, line OR-52MS provides a more detailed view of the northern flank of the largest diapir in the survey area. The base of the diapir and the lower flank show low but variable backscatter related possibly to the variable slope itself (there appear to be about 5 or 6 gentle terraces separated by slightly steeper areas) and different sediments on parts of the shelf with different slope angles. At the top of the slope, two oblique lineations on either side of the summit area indicate that the summit is a linear feature where it is crossed by the line. Backscatter is lower on the summit but increases toward the west where a number of the short lines of very high backscatter cross the summit at right angles. These high backscatter points are probably the same as those described for OKEAN lines PS-170 and PS-174. On the OREtech line, these features are clustered in a band crossing the summit obliquely in one area, and they appear to be related to depressions. The northwestern corner of the OREtech images shows, just off the summit, parallel bands of higher and lower backscatter with the same trend as the cluster of high backscatter targets. These may be related to slumping on the eastern side of the dome.

V.2.3. Bottom Sampling Results

J. FERNANDEZ SOLER, F. MARTINEZ-RUIZ, G. AKHMANOV, A. AKHMETZHANOV, A. STADNITSKAYA, E. KOZLOVA, A. SAUTKIN, L. MAZURENKO, D. OVSYANNIKOV, A. SADEKOV, I. BELENKAYA, E. SUSLOVA, AND D. GONCHAROV

Hard-rock dredging

Introduction

One of the most remarkable features of the Alborán area and the Betic and Rifian chains is the wide development of volcanic activity related to the formation and later evolution of the Alborán Sea. This activity is well exposed on land, and comprises several magmatic series, including tholeiitic dykes, complete calc-alkaline to ultrapotassic series of SE Spain, calc-alkaline to shoshonitic series in N Morocco, and a limited amount of alkaline basalts near Cartagena in Spain and in NE Morocco (e.g. Hernandez et al., 1987). The magmatism was produced in several cycles, ranging from > 27 Ma to 2.4 Ma (Bellon et al., 1983; Di Battistini et al., 1987). These “orogenic” series are usually related to subduction zones, but in the Alborán zone these rocks seem to develop instead in response to extensional tectonics after lithosphere thickening (Comas et al., 1999).

Although a large proportion of the magmatic products are now buried below the Alborán Sea, only limited information is available for these rocks, and so they are very poorly known. Studied samples include those from the Alborán Island, some samples from the Alborán Ridge, Yusuf Ridge and Al-Mansour Seamount, samples taken by the ODP Leg 161 (Hoernle et al., 1999) and some mentions of samples taken by dredging (Giermann et al., 1968) or recognised in commercial drilling. Thus, the main aims for the dredging were:

1. To recognise the existence and nature of the volcanic rocks, and the extent of the volcanic activity during the evolution of the Alborán basin.
2. To determine the age of the magmatic activity.
3. To study the petrological, geochemical and isotopic composition of the samples in order to determine the mechanisms of magma generation in such a peculiar geodynamic environment.

In addition, some of the dredging sites were intended to provide samples of the metamorphic basement of the Alborán basin, in order to determine the nature of the basement, and to study the mechanism and timing of the exhumation of the basement.

Dredge TTR9-263D

Dredge site 263D was on a topographic high situated between the Xauen Banc and the Alborán Ridge (Fig. 69). This zone, previously believed to be composed of outcropping basement rock, was suspected to also contain some volcanic rocks (Comas et al., 1999). Dredging was difficult due to the existence of widespread Mn-oxide and biogenic crust on the surface of the rocks. However, some pebbles of volcanic origin were recovered, in addition to abundant pieces of the Mn-biogenic crust.

The volcanic pebbles are all of andesitic composition, with phenocrysts of plagioclase and pyroxene as the main visible minerals, in a vitric groundmass. The degree of alteration is moderate to heavy in some of the samples. In the larger samples it is possible to see that these rocks are formed by a magmatic breccia, composed of heterometric clasts (more heavily altered) with typical curvilinear boundaries, immersed in a matrix of the same composition, although less altered, and commonly with jigsaw fitting of the clasts. This fragmentary facies indicates a degree of fragmentation due to rapid cooling and interaction with water, and is typical of the extrusion of intermediate-acidic lava domes in submarine environments. These rocks resemble macroscopically the basaltic andesites and pyroxene andesites existing in the nearby Ras Tarf in N Morocco and also with similar facies in the Cabo de Gata volcanic complex in SE Spain. This facies, which could be considered as acidic-intermediate hyaloclastic breccia, has also been recognized in the Yusuf and Al-Mansour areas in the eastern Alborán basin in a series of dives with the *Cyana* submersible.

Regarding the composition of these rocks, it is uncertain whether they are medium-K, calc-alka-

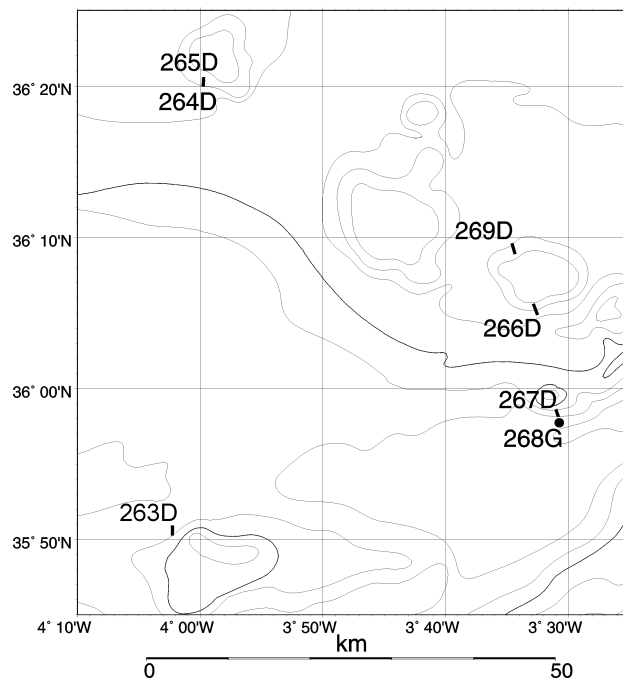


Figure 69. Bottom sampling locations on the northern Alboran basin margin.

line andesites, similar to the mentioned Ras Tarf or Cabo de Gata pyroxene andesites, or comparable to the low-K, basalt-to-andesite tholeiitic series existing in the Alborán Island, Yusuf and Al-Mansour seamounts.

TTR9-264D and TTR9-265D

This dredging site was intended to provide indications of the nature of a basement outcrop situated close to the high at ODP Site 976. As in the dredge 263D, recovery was poor due to the existence of extensive Mn-biogenic crusts and in fact the dredge was repeated twice (dredges 264D and 265D). In the second trial (265D) a large boulder of gneissic rock was obtained, in addition to abundant coral fragments, serpulid- and Mn crusts.

The sample (265D R-001) is a brownish to greenish gray gneissic rock (size: 33 x 21 x 10 cm) with K-feldspar, plagioclase, quartz, biotite, minor muscovite, tourmaline, fibrolite, and probable cordierite. The sample is a large fragment, sub-rounded in shape,

that has a very thin (< 1 mm) and continuous rim of Mn- and Fe-oxide. It is also covered partially by serpulids, corals, and ostreids. The irregularities at the sample surface are filled by fine-grained sediments. The sample probably corresponds to a fallen block on the slope of the basement high, as is revealed by its shape and the occurrence of a complete cover of oxide crust and biota colonization.

This sample has a penetrative fabric defined by a continuous foliation, marked by the orientation of mm-scale (< 2 mm in length) elongated blasts (e.g. K-feldspar, plagioclase, tourmaline, fibrolite) and platy minerals (biotite). There are also segregations (1-2 cm) of K-feldspar (also with plagioclase ?) that include biotite blasts with a larger size than in the matrix. Cordierite is also probably present in the matrix.

TTR9-266D

This dredging site was selected on the Djibouti Bank to find the nature of the exposed rocks, which were considered to be volcanic on the basis of the dredging samples taken by Giermann et al. (1968). The steepest slope was carefully selected, nevertheless, as in the two previous dredging sites the abundant coral and Mn crusts prevented sampling of the basement rocks and only one very small piece of a foliated shale was recovered. The rock (266D-R-01) is a grey to black, fine grained metamorphic rock, with mica and quartz. The sample shows a penetrative cleavage and a poorly developed lineation.

TTR9-267D

This site, situated on a very steep conic basement high (-680 m), SE of the Djibouti Bank, was recognised previously as a volcanic edifice by Giermann et al. (1968). The SE slope of this high was selected previously using the onboard profiling data. In spite of that, the dredge only recovered a few very small pieces of volcanic rock, in addition to very abundant muds and coral fragments.

Most of the volcanic samples (267D-V-001 and -003 to -007) are non vesicular, heavily altered andesites with a greenish, granular appearance due to the alteration of former pyroxene and plagioclase phenocrysts to a chlorite rich groundmass. Sample 267D-V-002 is peculiar in having a distinctive vesicular appearance. This rock also seems to contain hornblende, and has a smaller degree of alteration.

TTR9-269D

From this site, situated in the escarpment leading to the Alborán Channel, only a large amount of clayey foram ooze with shell fragments and spicules was recovered. No hard rocks from the basement, which is supposed to be of volcanic origin, were found.

Sediment cores

A total of four sites were selected for sampling on the mud diapir area in the southwestern Alboran basin (Fig. 65). The total recovery was 7.2 m. Sampling sites were chosen on the basis of the OKEAN mosaic images and seismic lines which showed structures corresponding to mud volcanoes, one of which has been named the Granada mud volcano (Tables 13 and 14). The extruded mud and mud breccia were cored at a water depth of 583 m and 580 m respectively in the two cores taken from the crater (258G and 259G). The eruptive products of Granada mud volcano consist of grey, poorly sorted, structureless, matrix supported mud breccia with coarse clasts of different lithologies with a prevalence of marlstone and claystone (Fig. 70). Preliminary results on the age of matrix and clasts indicate that the mud volcano material is not older than Paleocene. In core 258G mud volcanic deposits are blanketed with Holocene pelagic marl, light olive brown in colour and very enriched in planktonic foraminifers. Core 259G recovered only mud volcanic deposits. The succession was well stratified, several mud breccia flows were described with layer thickness varying from 3 cm to 0.5 m. Two inter-

The Alboran Sea

Core No	Date	Time, GMT	Latitude	Longitude	Cable length, m	Depth, m	Recovery
TTR9-258G	19.07.99	08:54	35°33. 719'	04° 37. 398'	590	583	144 cm
TTR9-259G	19.07.99	13:00	35°33. 761'	04° 37. 368'	587	580	119 cm
TTR9-260GR	19.07.99	14:39	35°33. 749'	04° 37. 400'	--	566	--
TTR9-261G	19.07.99	18:29	35°37. 493'	04° 30. 967'	1020	1003	247 cm
TTR9-262G	19.07.99	19:28	35°37. 509'	04° 29. 663'	1100	1086	210 cm
TTR9-263D	20.07.99	00:12	35°50. 926'	04° 02. 259'	1340	1267	0.5 m ³
		00:40	35°50. 270'	04° 02. 272'		1022	
TTR9-264D	20.07.99	21:31	36°20. 236'	03° 59. 728'	600	505	0.5 m ³
		21:55	36°20. 469'	03° 59. 711'		460	
TTR9-265D	20.21.07.99	23:33	36°19. 970'	03° 59. 756'	700	639	0.5 m ³
		00:37	36°20. 586'	03° 59. 713'		430	
TTR9-266D	21.07.99	07:13	36°04. 889'	03° 32. 509'	860	780	0.5 m ³
		08:27	36°05. 609'	03° 32. 863'		260	
TTR9-267D	21.07.99	11:12	35°57. 787'	03° 30. 660'	1600	1536	0.5 m ³
			35°58. 633'	03° 31. 023'		905	
TTR9-268G	21.07.99	13:43	35°57. 814'	03° 30. 655'	1600	1526	332 cm
TTR9-269D	21.07.99	16:08	36°09. 619'	03° 34. 592'	640	594	0.5 m ³
		17:08	36°08. 914'	03° 34. 345'		345	

The Balearic Basin

Core No	Date	Time, GMT	Latitude	Longitude	Cable length, m	Depth, m	Recovery
TTR9-270D	23.07.99	21:35	36°32. 736'	01° 37. 373'	1330	1240	0.5 m ³
		23:25	36°31. 931'	01° 37. 803'		891	
TTR9-271D	25.07.99	04:29	37°15. 341'	00° 45. 481'	2562	2514	0.1 m ³
		05:49	37°15. 864'	00° 44. 961'	2450	1987	
TTR9-272D	25.07.99	09:28	37°25. 234'	00° 46. 453'	1715	1580	0.1 m ³
		11:08	37°26. 041'	00° 46. 982'	1240	1050	
TTR9-273G	25.07.99	15:52	37°24. 164'	00° 18. 668'	2630	2534	170 cm
TTR9-274G	26.07.99	08:43	37°15. 959'	00° 02. 993'	2705	2635	465 cm
TTR9-275G	26.07.99	10:24	37°16. 365'	00° 03. 015'	2700	2656	439 cm
TTR9-276G	26.07.99	12:00	37°17. 971'	00° 06. 029'	2759	2724	71 cm

Table 13. General information on the cores sampled in the Alboran Sea and South Balearic basin.

Core No	Geographical Setting	Sedimentary Summary	Instrumentation	Acoustic Characteristics
TTR9-258G	Crater of the Granada mud volcano (at 13:46 on OKEAN sidescan sonar profile PR 172 MS)	Mud breccia covered by marl enriched in foraminifers	OKEAN sidescan sonar; 3.5 kHz profiler; Single channel high resolution seismic system	Very high backscattering on the sonar image
TTR9-259G	Crater of the Granada mud volcano (at 13:46 on OKEAN sidescan sonar profile PR 172 MS)	Mud breccia	The same set	Very high backscattering on the sonar image
TTR9-260GR	Crater of the Granada mud volcano (at 13:46 on OKEAN sidescan sonar profile PR 172 MS)	--	OKEAN sidescan sonar; 3.5 kHz profiler; Single channel high resolution seismic system; TV record	Very high backscattering on the sonar image
TTR9-261G	Hill on the slope (at 17:06 on OKEAN sidescan sonar profile PR 174 MS)	Homogeneous hemipelagic sediments	OKEAN sidescan sonar; 3.5 kHz profiler; Single channel high resolution seismic system	High backscattering on the sonar image
TTR9-262G	Flow of the Marrakech mud volcano (to the left at 17:11 on OKEAN sidescan sonar profile PR 174 MS)	Hemipelagic sediments with layers of slumped deposits and flow of mud breccia	The same set	Very high backscattering on the sonar image
TTR9-263D	Topographic high situated between the Xauen Banc and the Alboran Ridge (at 23:11-23:15 PR 10 MS 3.5 kHz profiler)	Homogeneous mud with black corals, warms and volcanic rocks	3.5 kHz profiler	Very steep slope without layering
TTR9-264D	A basement outcrop in the vicinity of ODP Site 976 (at PR 11 MS 3.5 kHz profiler)	Homogeneous mud with black corals, and 1 big block of the volcanic rocks	3.5 kHz profiler	Very steep slope without layering
TTR9-265D	A basement outcrop in the vicinity of ODP Site 976 (at PR 11 MS 3.5 kHz profiler)	Homogeneous mud with black corals, and 1 big block of the volcanic rocks	3.5 kHz profiler	Very steep slope without layering
TTR9-266D	Southern slope of the large hill on Djibuti Bank (at PR 13 MS 3.5 kHz profiler)	Homogeneous mud with black corals, and 1 big block of the volcanic rocks	3.5 kHz profiler	Very steep slope without layering
TTR9-267D	Southern slope of the small hill on the Djibuti Bank (at PR 14 MS 3.5 kHz profiler)	Homogeneous mud with black corals, and 1 big block of the volcanic rocks	3.5 kHz profiler	Very steep slope without layering
TTR9-268G	Base of southern small hill on the Djibuti Bank (at PR 14 MS 3.5 kHz profiler)	Hemipelagic sediments	3.5 kHz profiler	Very steep slope without layering
TTR9-269D	Northern slope of the Djibuti Bank (at PR 13 MS 3.5 kHz profiler)	Homogeneous mud	3.5 kHz profiler	Very steep slope without layering
TTR9-270D	Top of Maimonide Seamount (at 11:30 on the PS 186 MS)	Homogeneous mud	OKEAN sidescan sonar; 3.5 kHz profiler; Single channel high resolution seismic system	Steep slope
TTR9-271G	Steep slope of ridge, foot of Mazarron escarpment (at 14:14 on the PS 187 MS)	Pieces of volcanic rocks	The same set	Very steep slope
TTR9-272D	On Mazarron escarpment (at 0:50 on the PS 181 MS)	Pieces of volcanic rocks	The same set	Very steep slope without layering
TTR9-273G	Abyssal plain, northern part of the study area	Pelagic sediment	The same set	Flat area
TTR9-274G	Top of the salt diapir (1) (OR 53 MS)	Pelagic sediment	The same set	Small hill
TTR9-275G	Top of the salt diapir (1) (OR 53 MS)	Pelagic sediment	The same set	Dark patches on the small hill
TTR9-276G	Top of the salt diapir (2) (OR 53 MS)	Pelagic sediment	The same set	Small hill

Table 14. Sedimentological, acoustic and geological characteristics of sampling stations in the Alboran Sea and South Balearic basin.

vals (28-32 cm bsf and 42-58 cm bsf) were observed with structural peculiarities characteristic of redeposited mud volcanic deposits (Akhmanov and Woodside, 1998).

Core 261G was taken from a site characterized by high reflectivity on the OKEAN mosaic. A 247 cm recovery consisted of light pelagic marl, with abundant foraminifers and intensive bioturbation. No material which can cause a high reflectivity was obtained.

Core 262G was taken from a slope of an assumed mud volcanic edifice recorded as a high reflectivity spot on the OKEAN sidescan record. The uppermost 30 cm of recovery were represented by structureless, olive grey marl enriched in foraminifers. The lower boundary of the interval is very transitional. This pelagic marl is underlain by grey, structureless clay with abundant foraminifers and with numerous clasts of semi-consolidated claystone varying in size from 0.05 to 1 mm. Preliminary micropaleontological study of the interval showed the presence of microfossils of different ages (Eocene – Recent). The lowermost interval of the core consisted of slumped clayey sediments. Typical mud volcanic deposits were not recovered in this core. However the interval of clay with millimetre sized claystone clasts and the lowermost slumped clayey interval might be considered as a rare type of mud volcanic deposits. Something similar was described as a mud breccia by Staffini et al., (1993), working on mud volcanoes in the Eastern Mediterranean. On the other hand these sediments can be interpreted as mass wasting deposits.

One core (268G) was taken at the foot of the southern hill of the Djibuti Seamount, northeast of ODP Site 976 (Comas et al., 1995) (Fig. 69). Total recovery was 3.32 m. Pleistocene-Holocene sediments at this site mainly correspond to a very rich clay ooze with foraminifers. Occasional sandy layers are recognized about 2.5 m bsf. The uppermost interval (12 cm) corresponds to a brownish ooze richer in foraminifers with an oxidized appearance. Downcore, grey and olive grey intervals with occasional burrows are recognized. The bottom interval is more bioturbated. Along with normal pelagic sedimentation, slope processes resulted in slumping and mixing of sediments and in gravity flows.

Micropaleontological investigation of mud breccia from mud volcanic deposits of the Alboran mud volcano

A. SAUTKIN

Two cores (258G and 259G) recovered mud breccia from the previously unknown Granada mud volcano.

The mud breccia contains a variety of clasts of sedimentary rocks, represented by limestones, detrital limestones, clays, claystones, siltstones, marlstones and sandstones (Fig. 70).

Nannofossil dating of selected samples of rock clasts was done using a light microscope with a magnification of 1250x. Assemblages of calcareous nannofossils were studied in 39 samples of rock clasts and in 4 samples of matrix from the mud breccia.

The matrix assemblages of nannofossils express a wide range of geological ages. The species in the assemblages are rather abundant, poorly or moderately preserved and diversified. Dominant species include Upper Cretaceous coccoliths: *Micula decussata*, *Cribrosphaerella ehrenbergi*, *Predicosaera cretacea*, *Watznauria barnesae*. The Cenozoic, mainly Miocene-Pliocene, coccoliths (*Discoaster sp.*, *Discoaster deflandrei*, *Coccolithus pelagicus*, *Pontosphaera multipora*) and the Recent coccoliths (*Emiliania huxleyi*, *Gephyrocapsa sp.*, *Rhabdosphaera claviger*).

The rock assemblages do not have a high diversity of calcareous nannofossils species. The species in the rock clasts are poorly or moderately preserved, suggesting strong dissolution and disintegration of the calcareous nannofossils.

The majority of the rock clasts (27 samples) from the mud volcano are of Upper Cretaceous age. The most abundant species are *M. decussata*, *W. barnesae*, *C. ehrenbergi*, *Arkhangelskiella sp.*, *P. cretacea*, *Rhagodiscus angustus*, *Stradneria crenulata*, *Eiffelithus turriseiffelii*, *Tranalithus phacelosus*, *Gartnerago obliquum*, *Manivitella pemmadoides*, *Gloukolithus diplogrammus*. The common occurrence of *Arkhangelskiella sp.* in the rock clasts indicates an Upper Campanian- Maestrichtian age

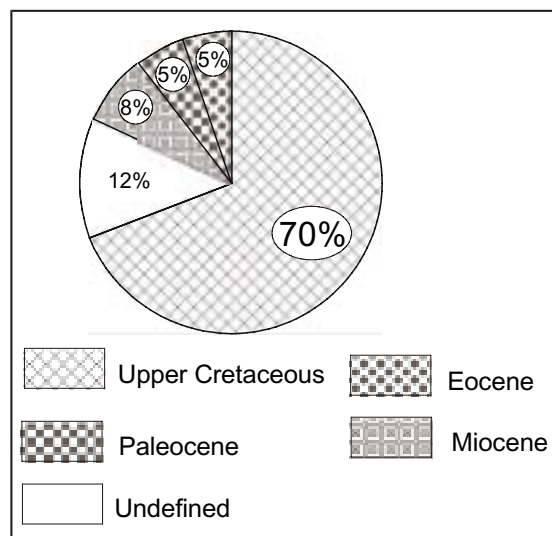


Figure 71. Inferred age of rock clasts from the mud breccia cores collected on the Granada mud volcano.

(CC18-CC26, Cretaceous coccolith zone). The presence of *Thierstenia ecclesiastica* and *G. obliquum* are indicative of a Turonian –Santonian age (CC10-CC19) (Table 15).

The Paleocene - Eocene species were observed in five samples of the rock clasts. In particular, taxa such as *Crusiplacolithus tenuis*, *Ellipsolithus bolii*, *Chiasmolithus consequetus*, *C. solitus*, *Neochiastozigus sp.*, *Discoaster multiradiatus*, *Toweius emines*, *Campylosphaera eodela* were identified in the samples. These taxa indicate a Paleocene-Early Eocene age (NP 4, NP9– NP10, Nannoplankton Paleogene zone) (Table 15).

Two samples of the rock clasts contain poorly preserved Neogene taxa of coccoliths and discoasters. *Discoaster* cf. *D. drugii*, *Discoaster* cf. *D. deflandrei*, *Helicosphaera* sp, *Coccolithus pelagicus*, *Pontosphaera multipora* were identified among them. These forms of discoasters suggest

[illegible]

Table 15. Summary information on lithology of rock clasts from mud breccia cores collected in the southwestern Alboran Sea area.

Miocene ages.

Such a variety of lithologies (Fig. 70) and wide range of geological ages (Fig. 71) for the rock fragments suggest a complicated structure for this mud volcanic region.

V.3. SOUTH BALEARIC BASIN: THE PALOMARES AND MAZARRÓN MARGINS

V.3.1. Seismic Data

M. COMAS, A. TALUKDER, J. WOODSIDE, A. VOLKONSKAYA

Seismic lines from the Palomares margin

The seismic lines PS-177 MS, PS-184 MS, and PS-185 MS on the Palomares margin are situated to the east of the onshore Vera basin and Cabo de Gata volcanic region (Fig. 72). This area represents the transition from the northern Alboran sea to the South Balearic basin. These lines are NNE-SSW oriented and cross two E-W submarine valleys and two NE-SW abrupt submarine highs. The two highs are associated with locally emergent acoustic basement. Sedimentary basins appear on both sides of these highs. Four main seismic units have been differentiated (Fig. 73):

Unit I, the stratigraphically highest, shows continuous reflectors which in some places, particularly on the uppermost part of this unit, become discontinuous with frequent hyperbola (e.g. shotpoint 1080 at 2800 ms TWTT on line PS-184 MS or at shotpoint 200 at 3200 ms TWTT on line PS-185 MS). This unit has a thickness of 200 ms TWTT on line PS-184 MS, reaching a depth of 3300 ms TWTT at shotpoint 160, of 2900 ms TWTT at shotpoint 1080, 2300 ms TWTT at shotpoint 160 and of 2700 ms TWTT at shotpoint 480. These depths are similar in all the lines. The base of Unit I is a continuous reflector with variable amplitude, showing in places an onlap geometry (e.g. shotpoints 2240 to 2320 on line PS-177 MS).

Unit II is fairly transparent with scattered reflectors, whereas in some areas high amplitude reflectors can be distinguished, as for example at shotpoints 160 at 3000 ms TWTT on line PS-177 MS. The base of the unit is marked by a high amplitude package of reflectors with a channel-like geometry (e.g. shotpoints 1040-1200 in PS-184 MS; 1280-1520 in PS-185 MS). This strong reflector occurs at variable depth along the same line, as can be seen for example between shotpoints 40 to 160 (at 3400 and 2900 ms TWTT in line PS-184 MS). The bottom of this unit is a general unconformity that corresponds to the Messinian (M) unconformity, seen in crossing commercial multi-channel seismic profiles. In general the reflectors of this unit onlap the underlying unit and the acoustic basement. The thickness of Unit II varies from 450 ms TWTT at shotpoints 120 or 480 on line PS-184 MS to nearly complete absence, pinching out on acoustic basement highs such as at shotpoints 1440 or 600 in line 184.

Unit III is a less reflective unit which locally has discontinuous reflectors cut at an angle by the Messinian unconformity. The base of this unit has not been identified in any of the three lines crossing the Palomares area.

The acoustic basement has a very reflective, disorganized fabric, with abundant hyperbola and an irregular upper surface. The acoustic basement highs are limited by faults with high angle straight fault scarps, and affect all the seismic units together with the sea floor, tilting their reflectors. Good examples of these faults can be seen on line 177 at shotpoints 345, 680, 1360-1400 and 1680; on line 184 at shotpoints 360, 520, 620, 1460, 140, 300 and 780; on line 185 at shotpoints 560, 750, 1760.

Two deep canyons incise the sea floor on seismic lines PS-177 MS (at shotpoints 950 and 2140) and PS-184 MS (shotpoints 940 and 600), corresponding respectively to Rambla Sopalmo and the Río Aguas Canyons (Fig. 74). They have sub-vertical walls and reach in places the base of Unit II (e.g. shotpoints 2120-2160 in line PS-177 MS).

Line PS-185 MS has some distinctive features not recognized in the other two lines, namely (i)

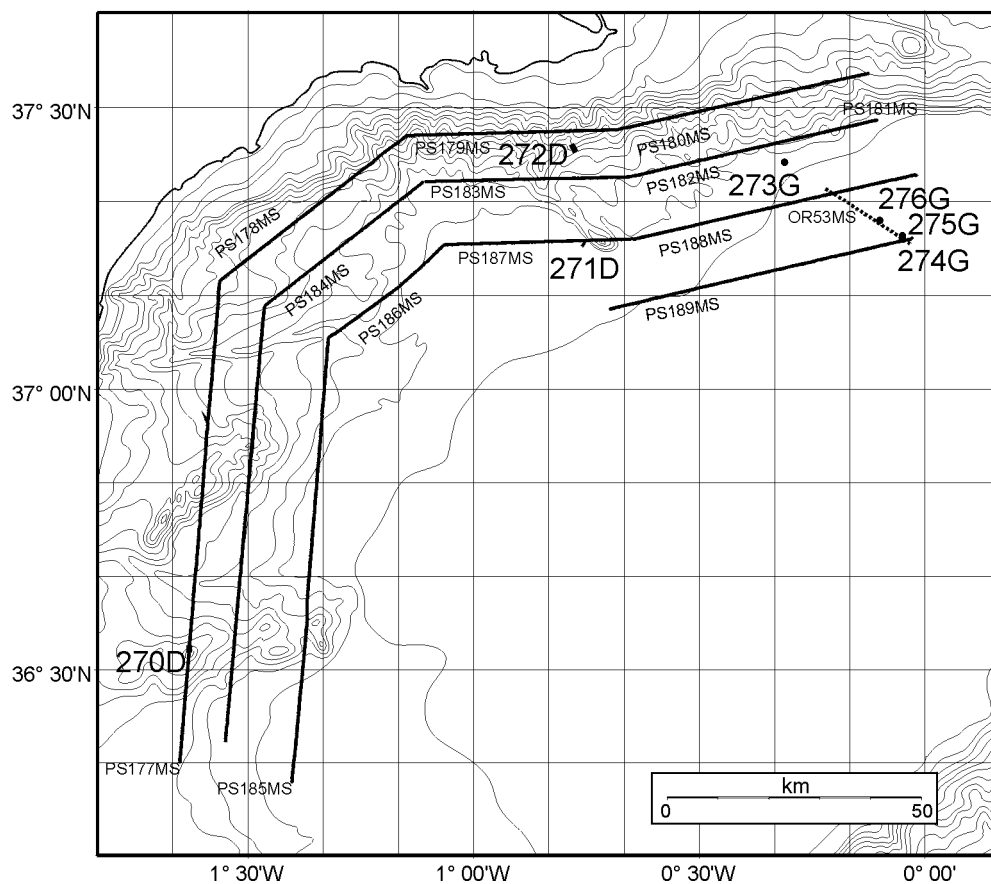


Figure 72. Location map of the Southern Balearic basin working area.

the existence of large planar areas in the basins not incised by canyons; (ii) the presence of two diapiric structures at shotpoints 320 and 1210; and (iii) the presence of a high-reflective, thin unit below Unit II and cut by the Messinian unconformity (e.g. at shotpoints 800 to 960, 1460 to 1760, and 1860 to 1960).

Seismic lines from the Mazarrón margin

The Mazarrón escarpment is an abrupt relief feature that connects the narrow Cartagena platform with the South Balearic abyssal plain. Six seismic lines parallel to the trend of the slope have been run (lines from PS-178 MS to PS-183 MS). Two of these lines (PS 178 MS and PS-183 MS) show the transition between the NNE-SSW Palomares Margin and the E-W Mazarrón escarpment. They show the proximal-distal variation in thickness of Pliocene to Recent units deposited along the margin of the South Balearic basin.

Three units can be distinguished in this transition:

Unit I is layered, with high reflectivity contrast with Unit II, and with alternating high- and low-reflective packages. Reflectivity increases gradually towards the south-western end of the profiles. The thickness of this unit changes laterally along the profiles, reaching its maximum values of 400 ms TWTT on line PS-183 MS, with an average value of 300 ms TWTT on line PS-178. The base of the unit is clearly erosive as can be seen at shotpoints 520 to 720 on PS-178 PS-and at shotpoints 440 to 560 on line PS-183 MS.

Unit II is transparent with low amplitude reflectors that are few and spaced out. It has a variable thickness with maximum values of 300 ms TWTT, whereas in other sectors it is absent (e.g. between shotpoints 840 and 1200 on line PS-178 MS). The base of Unit II is a high-amplitude package of reflectors that can be correlated with the M-reflector. The M reflector has a wavy geometry which may

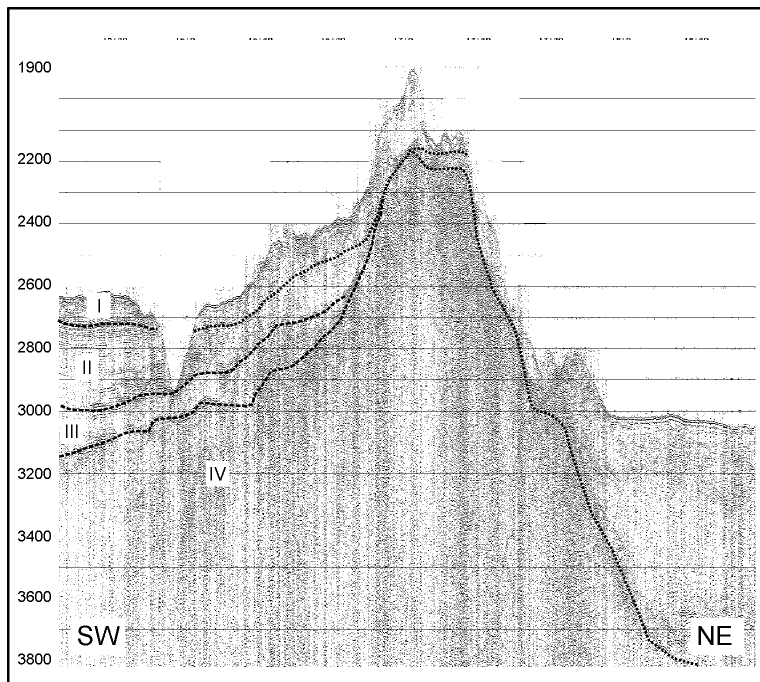


Figure 73. Sedimentary units in line PS 184MS on the Palomares margin (between shotpoints 960 and 1580).

be caused by tilting and folding, although the seismic lines have a poor resolution at these depths.

Unit III, situated immediately underneath the M reflector, has nearly transparent seismic facies with scarce and discontinuous reflectors.

The three units are affected by faulting and tilting. Most of these faults are high-angle normal faults with an apparent dip towards the NW, and in places associated antithetic faults are distinguished (e.g. at shotpoint 240 in line PS-178 MS). These faults also affect the sea floor topography and in some places they seem to control the occurrence and wall morphology of canyons and hills, as for example in the topographic high seen at shotpoint 50 on line PS-183 MS.

Four sub-parallel lines (PS-179 MS to PS-182 MS) continue further to the east, with an east-west direction, along the Mazarrón escarpment.

The two most northerly lines (PS-179 MS and PS-180 MS) run parallel to the coast line at a distance of 30 km from it. Deep gullies are seen, that produce an abrupt sea floor topography. On seismic line PS-179 MS only one seismic facies, with acoustic basement characteristics, has been observed. The gullies may be due to erosional and/or faulting processes. The western end of line PS-180 MS is analogous to line PS-179 MS although from shotpoint 200 towards the east, seismic units I and II appear. Seismic units I to III have a similar seismic character to those described in previous sections. Unit I and Unit II have an average thickness of 150 ms and 100 ms respectively (e.g. shotpoint 800). Seismic Units I and II cover the gullies in the acoustic basement although they are affected by erosional or tectonic processes in the canyons. An important canyon (Cañón del Negrete) with a depth of 400 ms is seen around shotpoint 500. This canyon can also be recognized in the southern line (PS 181 MS), partially filled by sediments, at shotpoint 960.

Lines PS-182 MS and PS-181 MS run parallel to lines PS-179 MS and PS-180 MS respectively, at a distance of 5 nm. Seismic units I and II also appear in these lines, affected together with the sea floor by faulting and erosion. They can be seen on line PS-182 MS, between shotpoints 0 and 480 where Unit I and II have a thickness of 100 and 300 ms respectively. At shotpoint 180 they are cut by a high angle planar fault that affects the sea floor, lowering it 300 ms. Between shotpoints 180 and 480, on the footwall of the previously mentioned fault, the sea floor is gullied and Unit I seems to be eroded. At shotpoint 480 there is a fault that produces an abrupt escarpment of 600 ms, that limits the western side of a prominent basement high. At shotpoint 960 there is a canyon, partially filled by high amplitude horizontal reflectors. There are frequent gullies affecting the sea floor between shotpoints 640 and 880, that generate hyperbolae that mask the seismic facies.

Line PS-181 MS is also crossed by frequent gullies and canyons. The canyons are filled with high amplitude, short, parallel reflectors, that produce hyperbolae at the ends, for example at shotpoints 560, 640, 1180, 1240 and 1300. Neither the M reflector nor basement can be seen on this seismic line. Unit I has different seismic facies than in other places, with wavy, scattered reflectors.

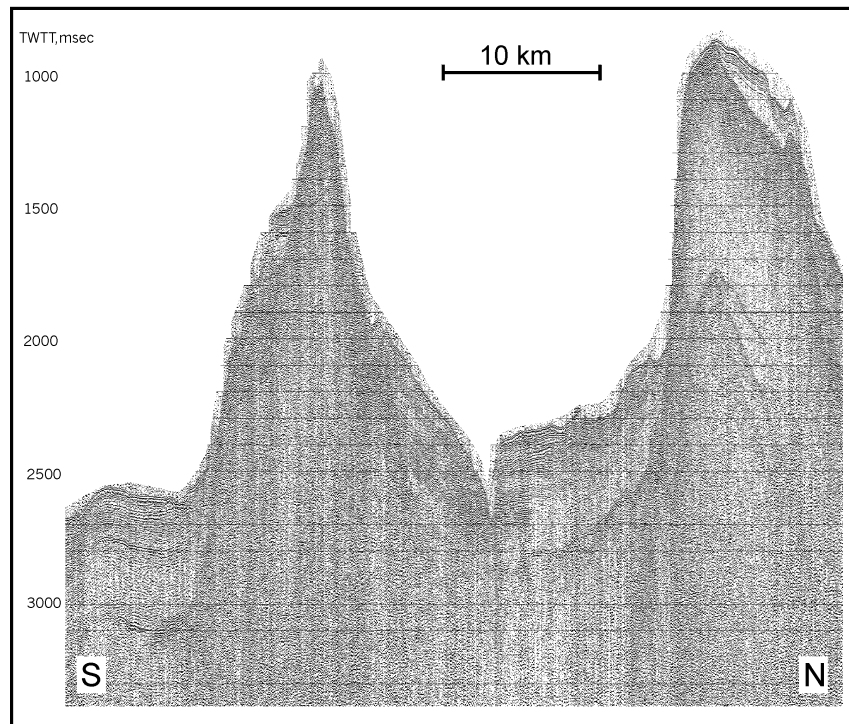


Figure 74. Steep Rio Aguas Canyon in the upper slope of the Palomares margin, line PS177MS (between shotpoints 2040 to 2320).

Seismic lines from the abyssal plain of the South Balearic basin

Four seismic lines with WSW-ENE to W-E trend (PS-186 MS to PS-189 MS), sub-parallel to the lines along the Mazarrón escarpment, show a seismic image of the shallower areas of the abyssal plain at the north-western margin of the South Balearic basin. The transition from the Mazarrón escarpment towards the abyssal plain corresponds to an abrupt change in the dip of the slope.

Seismic units I to III can also be distinguished in these lines, with a similar seismic character to those described in previous sections (e.g. see Mazarrón escarpment section). However, there is an increase in thickness and some other geometrical differences between units, together with the presence of abundant diapirs (Fig. 75), compared with the Mazarrón escarpment.

Unit I and II fill synclinal structures on the flanks of the diapirs, with maximum thickness of 800 ms TWT (e.g. shotpoints 1360 in line PS-188 MS, and 160 in line PS-187 MS) decreasing and even disappearing towards the top of the diapirs (e.g. shotpoints 1420-1520 in PS-188 MS, and 320-440 in PS-189 MS). Several progressive angular unconformities can be seen inside Unit I in the flanks of some diapirs (e.g. at shotpoint 1400 in PS-188 MS). The canyons incising the Mazarrón escarpment produce large (approx. 15 km wide) fan-like deposits on the South Balearic abyssal plain, as seen in profile PS-188 MS (between shotpoints 0 to 320) where a sedimentary wedge with chaotic, wavy and strong reflectors and occasional discontinuous sub-horizontal reflectors pinches out towards the channel levees (e.g. shotpoint 240).

The most conspicuous characteristic of this area is the occurrence of a large diapiric province. The diapirs reach the sea floor in places, such as many of the diapirs in line PS-189 MS (e.g. at shotpoints 360-440, 1200-1240, 1440-1480, and 1640). The progressive unconformities in Unit I together with the uplift of the ends of Unit II, provide evidences for a continuous rise of the diapirs during the deposition of Unit I and Unit II. Below some of the diapirs a group of highly reflective reflectors rise upwards (e.g. at shotpoints 1160-1280 and 1440-1520 on line PS-189 MS). This structure is certainly formed by the higher seismic velocity of the upper diapir material (probably salt) with respect to the nearby sediments.

Basement is seen in highs and locally emerges forming steep residual topographic crests. These

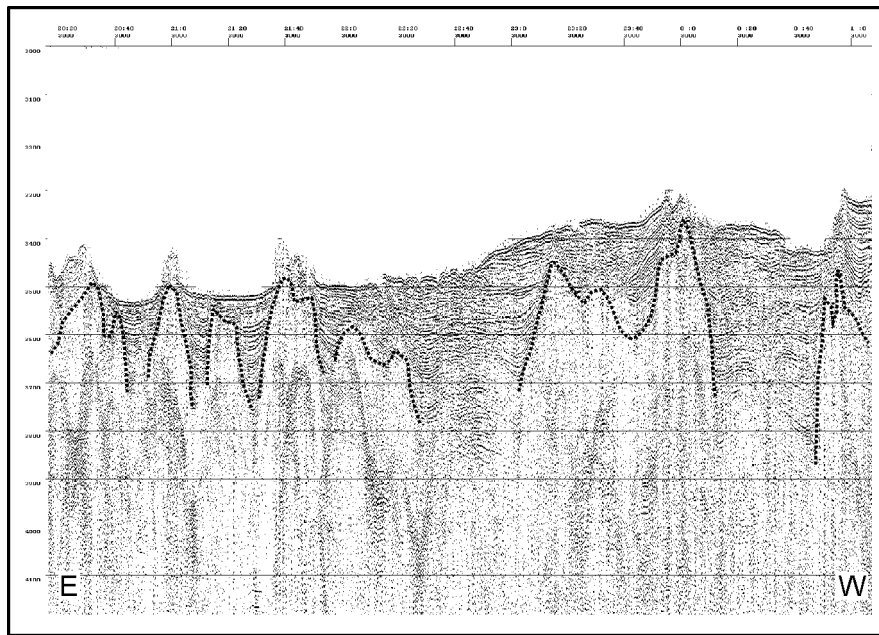


Figure 75. Salt diapirs in the south Balearic basin, line PS189MS (shotpoints 808-1520).

basement highs are bounded by high-angle normal faults which cut up to the M unconformity (e.g. at shotpoints 240-280 in PS-186 MS and 720-840 in PS-187 MS). One of these highs was dredged at site TTR9-271D.

V.3.2. Sidescan Sonar Data

J. WOODSIDE, M. IVANOV, R. KOELEWIJN, I. ZELDENRUST AND P. SHASHKIN

This margin can be divided into two general areas (Fig. 76). One is the Palomares margin which is dominated by the Maimonide Ridge and the Abubacer volcanic highs and by two major canyons, and the other is the ENE-WSW trending Mazarron margin, south of Cartagena, which is dominated by active mass wasting. The OKEAN lines were run close enough to permit the making of a mosaic (Fig. 76). This OKEAN data is very useful in aiding the interpretation of the seismic lines in this geologically complicated area. Because the lines are generally parallel to the continental slope, where the seafloor has high relief and other topographic variations, the OKEAN lines provide continuity of surface features between lines and indicate where seismic side echoes may originate.

OKEAN Line PS-177 is representative of the region of large NE-SW structural ridges and deeply incised canyon systems. The canyons do not appear to be very impressive on the OKEAN lines because they cross them almost perpendicularly. Thus, the sidescan does not register strong backscatter from the walls of the canyons. The southernmost canyon is associated on land with the Rambla de San Jose. It is crossed at about 06:40 where its presence is characterized by some minor variations in backscatter across the OKEAN image. The larger canyon associated on land with the Rambla Sopalmu, Río Aguas, and Río Almanzora shows up better because of larger local variations in backscatter across the image between 09:56 and 10:15. These variations are generally small points of high backscatter in patches of slightly higher background backscatter. The impression is of larger debris in the channel and exposure on the flanks. On the west side of the sidescan image there are lines of higher backscatter which are probably associated with either the thalweg of the channel, where coarser sediments would be expected, or with the flank of the channel, possibly as a result of failures along the relatively steep channel walls.

The Maimonide Ridge is crossed on OKEAN Line PS-177 between 05:00 and 06:10. The rough-

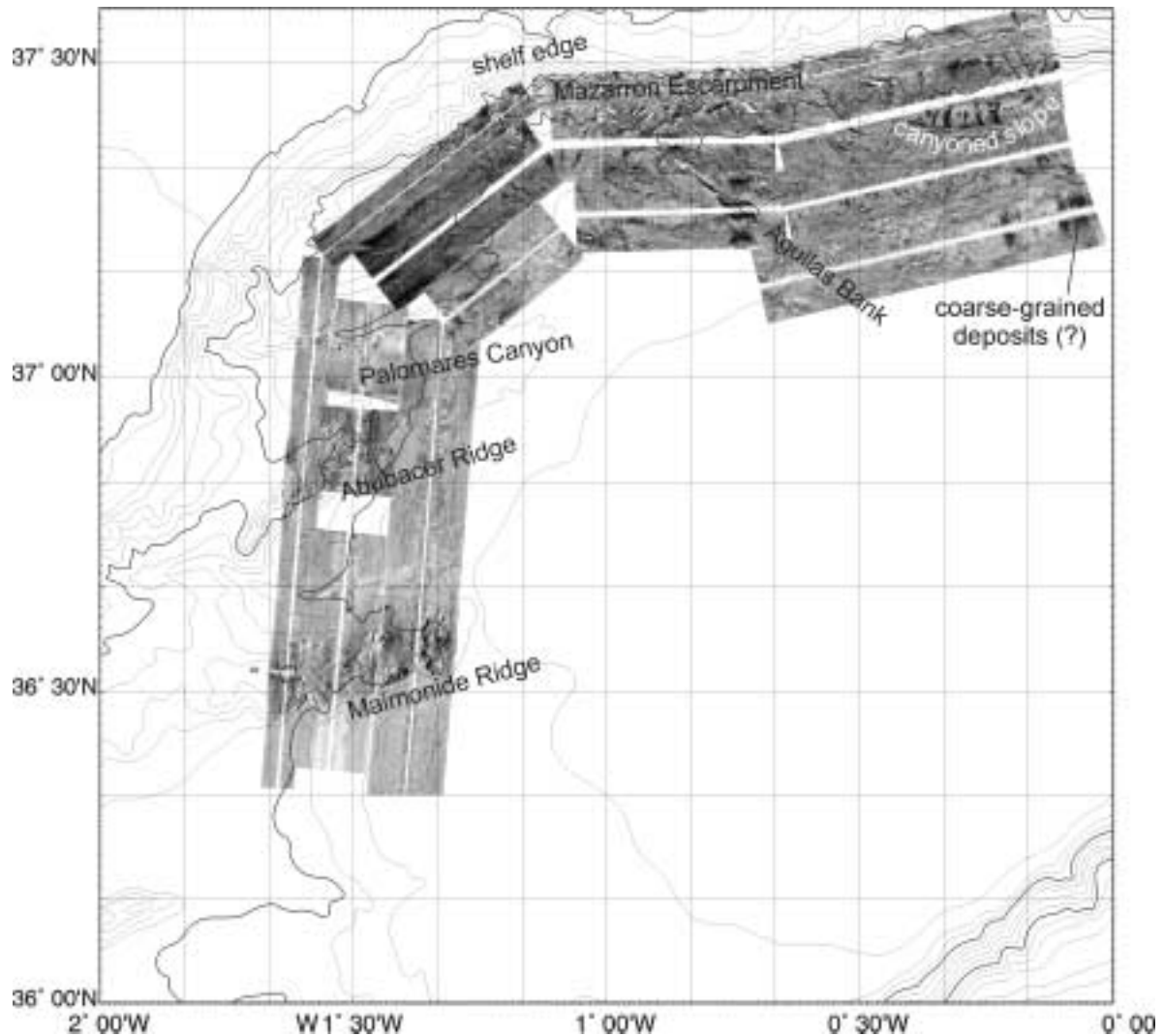


Figure 76. OKEAN mosaic from the Palomares margin (South Balearic basin).

ly east-northeast trend of the ridge is apparent. Definition of the ridge is principally from traces of high and low backscatter along both sides of it and elevated backscatter on the surface in between. The traces of high and low backscatter, for example on the southeast flank between 05:10 and 05:30, are probably irregular channels down the southern flank of the ridge. The very high backscatter is from the outer sides of the channels, with shadows from the inner sides. At 05:30 the channels can be seen to go to the top of the ridge. On the north side, the base of the ridge is defined by an irregular trace of high backscatter contrasting with the relatively uniform moderate backscatter from the sediments to the north. Some of the high backscatter points are probably larger rocks or small scale volcanic outcrops on the surface of the ridge.

The Abubacer Ridge displays a very abrupt and linear southern margin in the OKEAN record from line PS-177, as expected from the seismic line. An irregular trace of high backscatter crosses the OKEAN image obliquely from about 07:35 to about 08:00. The orientation is east-northeast/west-southwest. The more easterly part of the escarpment appears to have two steps separated by steeper slopes. Some traces of slightly higher backscatter in the sediments to the south suggests debris flows or talus trains from the southern escarpment. The upper surface of the structure is smoother in appearance than the Maimonide Ridge, probably on account of the sedimentary drape observed on the seismic profile. The structure rises to the west along a step near the crossing of the line. Rock falls from higher up to the west are seen in a flow to the lower eastern part at 08:00. A few points of high backscatter on the western part may be caused by larger rocks or by parts of the basement projecting

out of the sediments. To the east, another step downward can be seen about 5 km from the center line. The northern flank of the structure is not as well defined in the OKEAN record as the southern flank, indicating that it is not as abrupt, and that there is probably sedimentary drape on it. The northern edge of Abubacer at about 08:45 seems to be more clearly indicated to the east (than to the west) where several channels appear to be incised, giving short north-south trending pairs of high and low backscatter marking the outer and inner sides of the grooves respectively.

The northern part of the survey, south of the Mazarrón escarpment and Cartagena area, was surveyed in three sections, each with a slightly different character. The westernmost zone is transitional between the southern part of the survey area just described for line PS-177 and the complicated eastern region. The mouth of the channel emerging from the canyon for the Rio Aguas is imaged on PS-186 near the southwest end. Patchy higher and lower backscatter occurs along an east-west belt, probably as a result of deposits of poorly sorted material from the canyon. To the north of the canyon is a low ridge which is observed crossing the west end of both PS-178 and PS-183 in an east-west direction. Further to the northeast there is a large slide deposit crossing both line PS-178 and PS-183 on the OKEAN mosaic. The slide is difficult to see on PS-178 but occurs between 13:30 and 13:45. The scar from the slide is visible on the northwest side of line PS-178, as a series of steps in the slope defined by high backscatter (within Cañón de Mazarrón). Downslope, on OKEAN line PS-183, the slide is a slightly elevated zone of higher backscatter, probably as a result of coarser debris. To the northeast end of PS-178 the upper continental slope becomes more complicated with what appears to be short, ENE-WSW, tributary canyons to Mazarrón Canyon cut into a promontory (14:00), and traces of southeastward directed downslope debris trails (e.g. within a valley between 14:00 and 14:10). These canyons feed into a broader canyon (Cañón de Mazarrón) which can be seen cutting perpendicularly across line PS-183. On the northwest side of PS-183 there is a prominent but narrow canyon feeding into the larger canyon from the nose of a promontory. Large high backscatter points on the nose of the promontory may be erosional scars or large rock blocks.

OKEAN line PS-179 is dominated by erosional processes at the shelf edge. In places the shelf edge is visible (from 15:30 to the end of the line at 17:35) as an irregular line of promontories and embayments defined by the high backscatter of a short sharp escarpment. Beyond the scarp to the north slumps are beginning to form (between 16:00 and 16:35) where the incipient slump scar shows a sediment draped step dropping down to the south. At 16:30 and 17:05 recent slumps appear to have spread sediment over the irregular seafloor producing a smoother surface. Slumps along the upper slope are in evidence from the arcuate (concave downslope) traces of inferred listric faulted units of sediment between 14:45 and 15:30 and at 17:00, 17:12, 17:25, and 17:30 on PS-179. The sediment moves from the shelf into broad upper slope areas which funnel into narrower canyons downslope. The canyons are separated by relatively sharp ridges which are defined as the apex of chevron-patterned erosional gullies (e.g. at 16:13, 16:33, 16:47, 16:57). The erosional gullies feed downslope into the canyons. The processes of erosion and transport of sediments appear to be very active, to produce such distinct and significant relief and to leave such large debris on the seafloor, as is apparent on the western half of lines PS-182 and PS-187 and near the join between PS-187 and PS-188.

In the OKEAN mosaic, the downslope channels appear to consolidate in several channels defined by higher backscatter traces on lines PS-182, PS-181, and to a lesser extent further south on lines PS-187 and PS-188. Good examples of this are on the west end of PS-182 and on the east end of PS-181. The high-backscatter traces of the south-southwest directed channels on the west end of PS-182 appear to connect up-slope erosional areas with the southeast directed Cañón de Tiñoso. In the east of the area (especially on OKEAN line PS-181), channels radiate southward from an embayment and promontory (between 20:00 and 20:50 on OKEAN line PS-180) as straight traces of high backscatter (between about 22:30 and 23:00). These downslope channels start upslope at high backscatter scars on the promontory and stop abruptly at the basin floor. Smaller channels to the west on PS-181 do not have as high backscatter. These channels curve toward the east as they approach the basin floor, crossing PS-181 at 01:00, at about 00:30 (Cañón de Espada) and at 00:00 for a broader channel from a small scarp half way up the slope. Cañón de Espada is more pronounced and, from the high backscatter at a

bend to the east, has a very well defined south bank. To the south of the channel are patches of mixed high and low backscatter suggestive of deposits from large mass flows.

The basin floor itself is represented to the south on OKEAN lines PS-187, 188, and 189 by a mottled pattern of lighter and darker backscatter in the middle of the grey scale range. This is possibly slightly hummocky topography from the sediments deposited from the slope or facies variations caused by sorting variations in the sediments (e.g. with coarser sediments ponded in the slightly deeper areas and finer sediments on more elevated areas such as salt diapirs).

A ridge extends towards the southeast from the base of the slope, crossing line PS-182 at about 03:00 and line PS-187 at about 14:30. The ridge shows up well on the OKEAN mosaic because of high backscatter from the southwestern flank (on OKEAN line PS-187) and shadow from the same flank as seen on its continuation into OKEAN line PS-182. On OKEAN line PS-187 there is a larger and higher area of the ridge visible above the seafloor. Here there is strong backscatter from most of the top of the ridge. To the south of this end of the ridge is seafloor with a higher backscatter, which might be interpreted as caused by coarse material eroded from the ridge.

V.3.3. Bottom Sampling Results

J. FERNANDEZ SOLER, F. MARTINEZ-RUIZ, G. AKHMANOV, A. AKHMETZHANOV, A. STADNITSKAYA, E. KOZLOVA, A. SAUTKIN, L. MAZURENKO, D. OVSYANNIKOV, A. SADEKOV, I. BELENKAYA, E. SUSLOVA, AND D. GONCHAROV

Hard-rock dredging

Dredge TTR9-270D

This sampling site was selected on top of the Maimonide seamount, whose volcanic origin was suggested by the existence of positive aeromagnetic anomalies (Galdeano & Ciminale, 1987). In spite of the careful selection of a steep slope, by combining the information provided by the seismic lines collected during the cruise and the 3.5 kHz profiler, the dredge extracted a large amount of sticky mud sediments in which only three very small pieces (< 3 cm) of glassy vesicular rocks were recovered (samples 270D-R-01 and 270D-R-02). The rocks are very fresh and composed almost exclusively of a black, pumiceous glass, devoid of recognisable crystals. Due to the lack of visible minerals, the classification of the rock and its relation to other volcanic series in the Alborán Domain should await further chemical analyses.

Dredge TTR9-271

This sampling site, situated at the base of the Mazarrón escarpment, was selected on the slope of a small high that emerges from the South Balearic abyssal plain. The objective was to recognise whether this point is a protruding section of the basement that is observed immediately to the north, in the Mazarrón escarpment, or whether it is a volcanic high, in which case the goal was to get a sample of the South Balearic oceanic crust. A dredge sampler with a wider recovery net was used, in order to avoid the complete filling of the net with sticky muds such as those found in the last dredges.

Three lithic pieces were recovered and some coral-rich crust pieces. There are laminated micrites surrounded the pebbles and replacing some of the coral branches. The lithic fragments are very rounded. One of them is a carbonate (dolomite?) rock, almost completely covered by corals, and the other two are plutonic-looking rocks (altered granitoids). The correlation of the carbonate rocks with the metamorphic series outcropping onland just to the north, in the Cartagena Sector, is clear. Regarding the granitoid rocks, there is not an equivalent lithology in the nearby Betic mountains. The only lithologies that seem to be macroscopically similar to these samples are found as isolated plutonic pebbles included as xenoliths in the Cabo de Gata volcanic rocks, but further petrological and geochemical study is needed to verify this relationship.

Dredge TTR9-272D

A dredge sample on the slope of the Mazarrón escarpment was made to identify the nature of the rocks that outcrop along the prominent ridges of this topographic feature, which have been well observed with the OKEAN and seismic data. Four pieces of rock were recovered. All of them,

although partially concealed by Fe-Mn crusts, seem to correspond to cataclastic fine-grained breccias composed of an irregular aggregate of lithic fragments. The composition of these clasts (slates, carbonate rocks, etc.) correlates well with the lithologies found onland to the north, in the Cartagena and Mazarrón areas. The cataclastic nature is easily reconciled with the faulting origin of the Mazarrón escarpment which is obvious in the bathymetric, OKEAN and seismic data.

Sediment cores

A total of four sites were chosen for coring to study sedimentary facies and depositional processes in the South Balearic basin and to sample slopes and domes of salt diapirs (Fig. 72).

Core 273G, taken on the abyssal plain in the northeastern part of the study area, consisted mainly of light pelagic marl with abundant foraminifers. In the middle part the core is a horizon of consolidated oxidized marl. This horizon appeared to be some kind of “hard-ground” and probably its formation reflects an abrupt change in depositional environment in the region.

Core 274G, taken from the top of one of salt diapirs, consisted mainly of pelagic marl with several turbiditic layers composed of normally graded silt and sand. In the lower part of the core there is a 10 cm thick sapropelic layer. No visible evidence of active salt diapirism is noted.

Core 275G was taken from slope of the diapir dome sampled in previous station. A recovery of more than 4 metres was represented by intercalation of carbonate and clayey-carbonate sediments with numerous thin silty and sandy turbiditic deposits. The lowermost interval was intensively disturbed with several microfaults. These dislocations might appear in response to salt diapir growth.

Core 276G sampled the top of the other salt diapir. The core has intercalations of marl and thin turbidite layers. Visible evidence of salt diapiric processes is not observed.

V.4. CONCLUSIONS

M. COMAS, A. AKHMETZHANOV, M. IVANOV

Data obtained during Leg 3 will shed more light on the structure and composition of the Alboran Sea basement. The character of the recent sedimentation pattern is mainly controlled by complex seabed topography, climate and neotectonics. In the deeper parts of the basin, where carbonate-rich pelagic sediments dominate, the bases of volcanic edifices and basement highs are areas of accumulation of turbidites and mass wasting deposits.

The area of clay diapirs development on the southern margin of the basin was comprehensively studied. Two mud volcanoes and several diapirs were discovered and sampled. Further studies of retrieved deposits will allow better understanding of the sedimentary succession in this area.

The tectonic nature of the Mazarrón escarpment in the southern Balearic basin has been further confirmed.

The seismic data showed a broad development of salt diapirs on the Balearic abyssal plain. The survey allowed mapping of their distribution and establishment of their morphology and relations to the host sedimentary succession.

REFERENCES

- Abrantes, F., Baas, J., Haflidason, H., Rasmussen, T., Klitgaard, D., Loncaric, N. and Gaspar, L., 1998. **Sediment fluxes along the Northeastern European Margin: inferring hydrological changes between 20 and 80 kyr.** *Marine Geology*, 152, 7-23.
- Akhmanov, G.G. and Woodside J.M., 1998. **Mud volcanic samples in the context of the Mediterranean Ridge mud diapiric belt.** In: Robertson, A.H.F., Emeis, K.-C., Richter, C. and Camerlenghi, A. (Eds.), *Proc. ODP, Sci. Results*, 160, College Station, TX (Ocean Drilling Program), 597-605.
- Bellon, H., Bordet, P. and Montenat, C., 1983. **Chronologie du magmatisme neogene des Cordilleres Betiques (Espagne meridionale).** *Bulletin de la Société Géologique de France*, 25, 205-218.
- Biscaye, P.E., 1965. **Mineralogy and sedimentation of recent deep-sea clay in the Atlantic Ocean and adjacent seas and oceans.** *Geological Society of America Bulletin*, 76, 803-832.
- Blankenship, C. L., 1992. **Structure and palaeogeography of the External Betic Cordillera, southern Spain.** *Marine and Petroleum Geology*, 9, 256-264.
- Boldreel, L.O. and Andersen, M.S., 1993: **Late Paleocene to Miocene compression in the Faroe-Rockall area.** In: J.R. Parker (Ed), *Petroleum Geology of Northwest Europe. The Geological Society*, London, 1025-1034.
- Broecker, W.S., 1994. **Massive iceberg discharges as triggers for global climate change.** *Nature*, 372, 421-424.
- Clark, J.D., Kenyon, N.H. and Pickering, K.T., 1992. **Quantitative analysis of the geometry of submarine channels: implications for the classification of submarine fans.** *Geology*, 20, 633-636.
- Comas, M. and Soto, J.I., 1999. **Brittle deformation in the metamorphic basement at Site 976; implications for middle Miocene extensional tectonics in the western Alboran basin.** *Proc. ODP, Sci. Results*, 161, College Station, TX (Ocean Drilling Program), 331-344.
- Comas, M., Platt, J.P., Soto, J.I. and Watts, A.B., 1999. **The origin and tectonic history of the Alboran basin; insights from Leg 161 results.** *Proc. ODP, Sci. Results*, 161, College Station, TX (Ocean Drilling Program), 555-580.
- Comas, M., Zahn, R., Klaus, A., 1995. **Mediterranean Sea II.** (Science Operator Report Leg 161), *JOIDES Journal*, 21(3), 20-25.
- Comas, M.C., Dañobeitia, J.J., Alvarez Marron, J. and Soto, J.I., 1997. **Crustal reflections and structure in the Alboran basin: Preliminary results of the ESCI-Alboran survey.** *Rev. Soc. Geol. España*, 8, 76-88.
- Comas, M.C., Garcia-Duenas, V. and Jurado, M.J., 1992. **Neogene tectonic evolution of the Alboran basin from MCS data.** *Geo-Marine Letters*, 12, 157-164.
- Comas, M.C., Zahn, R., Klaus, A. and Shipboard Scientific Party, 1996. **Leg 161- Western Mediterranean.** *Proc. ODP, Init. Repts.*, 161:College Station, TX (Ocean Drilling Program), 1023 pp.
- Damuth, J.E., Flood, R.D., Kowsmann, R.O., Belderson, R.H., and Gorini, M.A., 1988. **Anatomy and growth pattern of Amazon deep-sea fan as revealed by long-range sidescan sonar (GLORIA) and high-resolution seismic studies.** *American Association of Petroleum Geologists Bulletin*, 72, 885-911.
- Dewey, J.F., Helman, M.L., Turco, E., Hutton, D.H.W. and Knott, S.D., 1989. **Kinematics of the western Mediterranean.** In: Coward, M. (Ed) *Alpine Tectonics*. Spec Publ. Geol. Soc. London, 45, 265-283.
- Di Battistini, G., Toscani, L., Iaccarino, S. and Villa, I.M., 1987. **K/Ar ages and the geological setting of calc-alkaline volcanic rocks from Sierra de Gata, SE Spain.** *Neues Jahrbuch für Mineralogie*, 8, 369-383.
- Flynn, J.A., Bally, A.W. and Wu, S., 1996. **Emplacement of a passive-margin evaporitic allochthon in the Betic Cordillera of Spain.** *Geology*, 24, 1, 67-70.
- Galdeano, A. and Ciminale, M., 1987. **Aeromagnetic evidence for the rotation of Sardinia (Mediterranean Sea): comparison with the paleomagnetic measurements.** *Earth and Planetary Science Letters*, 82, 193-205.
- Gardner, J.V. and Kidd, R.B., 1987. **Sedimentary processes on the Northwestern Iberian Continental Margin viewed by long-range sidescan sonar and seismic data.** *Journal of Sedimentary Petrology*, 57, 397-407.
- Gardner, J.M., 2000. **Morphology of seafloor mud volcanoes on the Moroccan continental margin.** *Geophysical Research Letters*, (Submitted).
- Geosphere-biosphere coupling: Carbonate mud mounds and cold water reefs.** International Conference and Sixth Post-Cruise Meeting of the Training-through-Research Programme, Gent, Belgium, 7-11 February 1998. *IOC Workshop Report*, 143, UNESCO, 1998.
- Giermann, G., Pfannenstiel, M. and Wimmenauer, W., 1968. **Relations entre morphologie tectonique et volcanisme en mer d'Alboran (Mediterranee occidentale).** *C. R. Somm. Soc. Geol. France*, 4, 116-118.

- Grousset, F.E., Joron, J.L., Biscaye, P.E., Latouche, C., Treuil, M., Maillet, N., Faugeres, J.C. and Gonthier, E., 1988. **Mediterranean outflow through the Strait of Gibraltar since 18,000 years B.P.: mineralogical and geochemical arguments.** *Geo-Marine Letters*, 8, 25-34.
- Hansen, B., Østerhus, S., 2000. **North Atlantic--Nordic Seas exchanges.** *Progress in Oceanography*, 45(2), 109-208.
- Hernandez, J., de Larouziere, F.D., Bolze, J. and Bordet, P., 1987. **Le magmatisme neogene betico-rifain et le couloir de décrochement trans-Alboran.** *Bulletin de la Société Géologique de France*, 3, 257-267.
- Hoernle, K., van den Bogaard, P., Duggen, S., Mocek, B. and Garbe-Schönberg, D., 1999. **Evidence for Miocene subduction beneath the Alboran Sea: $^{40}\text{Ar}/^{39}\text{Ar}$ dating and geochemistry of volcanic rocks from Holes 977A and 978A.** *Proc. ODP, Sci. Results*, 161, College Station, TX (Ocean Drilling Program), 357-374.
- Hovland, M., Croker, P.F. and Martin, M., 1994. **Fault-associated seabed mounds (carbonate knolls?) off western Ireland and north-west Australia.** *Marine and Petroleum Geology*, 11, 232-246.
- Jurado, M.J. and Comas, M.C., 1992. **Well log interpretation and seismic character of the Cenozoic sequence in the Northern Alboran Sea.** *Geo-Marine Letters*, 12: 129-136.
- Kenyon N.H., Ivanov M.K. and Akhmetzhanov A.M. (eds), 1998. **Cold water carbonate mounds and sediment transport on the Northeast Atlantic margin. Preliminary results of geological and geophysical investigations during the TTR-7 cruise of R/V Professor Logachev in co-operation with the CORSAIRES and ENAM 2 programmes.** *IOC Technical Series*, 52, 178 pp.
- Kenyon, N.H., 1987. **Mass-wasting features on the continental slope of northwest Europe.** *Marine Geology*, 74(1/2), 57-77.
- Kenyon, N.H., Belderson, R.H., 1973. **Bedforms of the Mediterranean undercurrent observed with sidescan sonar.** *Sedimentary Geology*, 9, 77-99.
- Kenyon, N.H., Ivanov, M.K. and Akhmetzhanov, A.M. (eds.), 1999. **Geological Processes on the Northeast Atlantic margin.** *IOC Technical Series*, 54, UNESCO, 141 pp.
- Kenyon, N.H. and Millington, J., 1995. **Contrasting deep-sea depositional systems in the Bering Sea.** In: Pickering, K.T., Hiscott, R.N., Kenyon, N.H., Ricci Lucchi, F., Smith, R.D.A. (eds). *Atlas of deep water environments: architectural style in turbidite systems.* London, Chapman & Hall, 196-202.
- Limonov, A.F., Kenyon, N.H., Ivanov, M.K. and Woodside J.M. (eds.), 1995. **Deep sea depositional systems of the Western Mediterranean and mud volcanism on the Mediterranean Ridge. Initial results of geological and geophysical investigations during the Forth UNESCO-ESF 'Training through Research' Cruise of R/V Gelendzhik (June-July 1994).** *UNESCO Reports in Marine Science*, 67, 171 pp.
- Maldonado, A. and Comas, M. C., 1992. **Geology and geophysics of the Alboran Sea: An introduction.** *Geo-Marine Letters*, 12, 61-65.
- Maldonado, A. and Somoza, L., 1997. **La zona de fractura Azores-Gibraltar y las cadenas Béticas en el Golfo de Cadiz. Evolucion Geologica.** Abstr. 2nd Congress Margen continental Iberico Atlantico. Univ. Cadiz, 71-72.
- Maldonado, A., Campillo, A.C., Mauffret, A., Alonso, B., Woodside, J. and Campos, J., 1992. **Alboran Sea Late Cenozoic tectonic and stratigraphic evolution.** *Geo-Marine Letters*, 12, 179-186.
- Maldonado, A., Somoza, L. and Pallarés, L., 1999. **The Betic orogen and the Iberian—African boundary in the Gulf of Cádiz: geological evolution (central North Atlantic),** *Marine Geology*, 155, 9-43.
- Mauffret, A., El-Robrini, M. and Genesseeux, M., 1987. **Indice de la compression recente en mer Méditerranée; un bassin losangique sur la marge nord-algerienne.** *Bulletin de la Société Géologique de France*, 3, 1195-1206.
- Moros, M., Endler, R., Lackschewitz, K.S., Wallrabe-Adams, H-J., Mienert, J. and Lemke, W., 1997. **Physical properties of Reykjanes Ridge sediments and their linkage to high-resolution Greenland Ice Sheet Project 2 ice core data.** *Paleoceanography*, 12, 687-695.
- Mougenot, D. 1985. **Progradation on the Portuguese continental margin: interpretation of seismic facies.** *Marine Geology*, 69, 113-130.
- Mougenot, D., Kidd, R.B., Mauffret, A., Gagnauld, H., Rothwell, R.G. and Vanney, J.R., 1984. **Geological interpretation of combined Seabeam, Gloria and seismic data from Porto and Vigo seamounts, Iberian continental margin.** *Marine Geophysical Researches*, 6, 329-363.
- Mougenot, D., Vanney, J.-R., Mauffret, A. and Kidd, R.B., 1986. **Les montagnes sousmarines de la marge continentale nord-portugaise: morphologie et evolution structurale.** *Bulletin de la Société Géologique de France*, 8, 401-412.
- Nelson, C.H., Baraza, J., Maldonado, A., Rodero, J., Escutia, C. and Barber, Jr., J.H., 1999. **Influence of the Atlantic inflow and Mediterranean outflow currents on Late Quaternary sedimentary facies of the**

- Gulf of Cadiz continental margin.** *Marine Geology*, 155, 99-129.
- Nielsen, T.H., Waagstein, R., Rasmussen, J. and Larsen, B., 1981: **Marine seismic investigation of the shelf around the Faeroe Islands.** *Danm. Geol. Unders.*, 101-109.
- Polyak, B.G., Fernandez, M., Khutorsky, M.D., Soto, J.I., Basov, I.A., Comas, M.C., Khain, V. Ye., Alonso, B., Apagova, G.V., Mazurova, I.S., Negrodo, A., Tochitsky, V.O., de la Linde, J., Bogdanov, N.A. and Banda, E., 1996. **Heat flow in the Alboran Sea (the Western Mediterranean).** *Tectonophysics*, 263, 191-218.
- Roberts, D.G. and Kidd, R.B., 1984. **Sedimentary and structural patterns on the Iberian Continental Margin: an alternative view of continental margin sedimentation.** *Marine and Petroleum Geology*, 1, 37-48.
- Roberts, D.G., 1970. **The Rif-Betic orogen in the Gulf of Cadiz.** *Marine Geology*, 9, 31-37.
- Rodero, J., Pallares, L. and Maldonado, A., 1999. **Late Quaternary seismic facies of the Gulf of Cadiz Spanish margin: depositional processes influenced by sea-level change and tectonic controls.** *Marine Geology*, 155, 13 -56.
- Ryan, W.B.F., Hsu, K.J., Nesteroff, W.D., Pautot, G., Wezel, F.C., Lort, J.M., Cita, M.B., Maynz, W., Stradner, H. and Dumitrica, P., 1973. **Initial Reports of the Deep Sea Drilling Project, 13**, Washington (U.S. Gov. Printing Office), 1447 pp.
- Sadekov, A.Y. and Ovsyannikov, D.O., 2000. **Age of rock clasts from the Yuma mud volcano breccia on the basis of foraminiferal study (Gulf of Cadiz, NE. Atlantic).** In: Geological processes on European Continental Margins (TTR-9 Post-Cruise Conference) Abstracts, University of Granada.
- Sanz de Galdeano, C. and Vera, J.A., 1992. **Stratigraphic record and palaeogeographic context of Neogene basins in the Betic Cordillera, Spain.** *Basin Research*, 4, 21-36.
- Srivastava, S. P., Schouten, H., Roest, W.R., Klitgord, K.D., Kovacs, L.C., Verhoef, J. and Macnab, R., 1990. **Iberian plate kinematics: a jumping plate boundary between Eurasia and Africa.** *Nature*, 344, 756-759.
- Staffini, F., Spezzaferri, S. and Aghib, F., 1993. **Mud diapirs of the Mediterranean Ridge: sedimentological and micropaleontological study of the mud breccia.** *Riv. It. Paleont. Strat.*, 99, 225-254.
- Stoker, M.S., 1995. **The influence of glacial sedimentation on slope-apron development on the continental margin off northwest Britain.** In: Scrutton R. A., Stoker, M.S., Shimmield, G.B. and Tudhope, A.W. (eds). *The Tectonics, Sedimentation and Palaeoceanography of the North Atlantic region. Geological Society, London, Special Publications*, 90, 159-177.
- Torne, M. and Banda, E., 1992. **Crustal thinning from the Betic Cordillera to the Alboran Sea.** *Geo-Marine Letters*, 12, 76-81.
- Vanney, J-R. and Mougenot, D., 1990. **A gouf-type canyon, the Canhao da Nazare (Portugal).** *Oceanologica Acta*, 13, 1-14 & bathymetric chart scale 1:150,000.
- Vogt, P.R., Gardner, J. and Crane, K., 1999. **The Norwegian-Barents-Svalbard (NBS) continental margin: Introducing a natural laboratory of mass wasting, hydrates, and ascent of sediment, pore water, and methane.** *Geo-Marine Letters*, 19, 2-21.
- Vorren, T.O.; Laberg, J.S., Blaume, F., Dowdeswell, J.A., Kenyon, N. H., Mienert, J., Rumohr, J. and Werner, F., 1998. **The Norwegian-Greenland Sea continental margins; morphology and late Quaternary sedimentary processes and environment.** *Quaternary Science Reviews*, 17, 273-302.
- Waagstein, R. and Rasmussen, J., 1975: **Glacial erratics from the seafloor south-east of the Faeroe Islands and the limit of glaciation.** *Annal. Societ. Scient. Faeroensis (Frydskaparrit)*, 23, 101-119.
- Watts, A.B., Platt, J.P. and Buhl, P., 1993. **Tectonic evolution of the Alboran Sea basin.** *Basin Research*, 5, 153-177.
- Wilson, R.C. L., Hiscott, R.N., Willis M.G. and Gradstein, F.M., 1989. **The Lusitanian basin of West-Central Portugal: Mesozoic and Tertiary tectonic, stratigraphy, and subsidence history.** In: Tankard, A.J., Balkwill, H.R. (eds), *Extensional tectonics and stratigraphy of the North Atlantic margins. AAPG Mem.* 46, 341-361.
- Woodside, J.M. and Maldonado, A., 1992. **Styles of compressional neotectonics in the Eastern Alboran Sea.** *Geo-Marine Letters*, 12, 111-116.

IOC Technical Series No. 56
Annexe I - page 1

R/V Professor Logachev

CRUISE TTR-9

CORE TTR9-AT-CORE 144 G

Location:

Upper part of the slump

Latitude:

61°24.98' N

Longitude:

04°43.28' W

Date:

15/06/99 07:04 GMT

Water Depth:

575 m

Recovery:

174 cm

SUBSAMPLING CODES:

AGE:

Sedimentology

Geochemistry

1- Collection

6- Gas

2- Grain size

7- TOC

3- Mineralogy

8- Fluor.

4- X-ray

9- Bitum

5- Thin sections

10- Pore water

H- Holocene

LP- Late Pleistocene

EP- Early Pleistocene

LITHOLOGY	Colour	Structure	Age	Section	Samples		Depth, cm	Magnetic Susceptibility (CGS units)
					Sediment	GeoChem		
<div><div>SAND: Greyish brown, coarse. Upwardcoarsening interval</div><div>SANDY SILTY CLAY: Dark grey, structureless.Upper boundary is gradual; lower boundary issharp</div><div>SANDY CLAY: Grey, structureless. Occasional drop stones and shell fragments (mud flow?)</div></div>	5Y 4/2	↑			1	1	0	
	2.5Y 3/0	●		1	1	50		
	2.5Y 3/0	●		2	1	100		
		●		3			150	

R/V Professor Logachev CRUISE TTR-9

CORE TTR9-AT-CORE 145G

Location: Mass flow/channel setting

Latitude: 61°24.05' N Longitude: 04°40.31' W

Date: 15/06/99 09:05 GMT

Water Depth: 695 m

Recovery: 259 cm

SUBSAMPLING CODES:

AGE:

Sedimentology

Geochemistry

- 1- Collection
- 2- Grain size
- 3- Mineralogy
- 4- X-ray
- 5- Thin sections

- 6- Gas
- 7- TOC
- 8- Fluor.
- 9- Bitum
- 10- Pore water

H- Holocene
LP- Late Pleistocene
EP- Early Pleistocene

LITHOLOGY

Colour

Structure

Age

Section

Samples

Sediment

GeoChem

Depth, cm

Magnetic Susceptibility
(CGS units)

SAND: Light brown, coarse, in clayey matrix. Occasional drop stones

SANDY SILTY CLAY: Light brown, structureless

SILTY CLAY: Grey, structureless with sandy admixture. Numerous drop stones chaotically distributed along the interval (diameter from 0.4cm to 1 cm). Occasional shell fragments

2.5Y 4/2

2.5Y 3/0

1

2

1

3



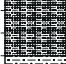
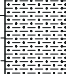
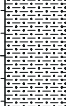
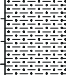
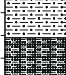
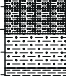
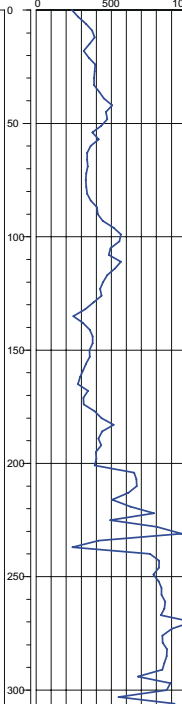
4

5

1

1

1

R/V Professor Logachev CRUISE TTR-9					CORE TTR9-AT-CORE 146G					
Location:		Mid/lower part of the slump								
Latitude:		61°22.96' N Longitude: 04°34.73' W								
Date:		15/06/99 11:53 GMT								
Water Depth:		867 m								
Recovery:		309 cm			<div>SUBSAMPLING CODES:</div> <div><div>Sedimentology</div><div>Geochemistry</div></div> <div><div>1- Collection 2- Grain size 3- Mineralogy 4- X-ray 5- Thin sections</div><div>6- Gas 7- TOC 8- Fluor 9- Blum 10- Pore water</div></div> <div>AGE: H- Holocene LP- Late Pleistocene EP- Early Pleistocene</div>					
LITHOLOGY		Colour	Structure	Age	Section	Samples		Depth, cm	Magnetic Susceptibility (CGS units)	
						Sediment	GeoChem			
      	SAND: Brownish, fine grained in clayey matrix, structureless, water saturated	5Y 4/2				1	1	0		
	SILTY SANDY CLAY: Greenish, structureless, occasional burrows filled with slightly darker material. The lower boundary is oblique and faint	5Y 4/1			1					50
	SILTY CLAY: Dark grey, structureless, bioturbated. Burrows are filled with coarser material with shell debris	5Y 3/2			2	1				100
										150
	SILTY SANDY CLAY: Greyish brown, structureless with significant admixture of coarse sand and abundant shell debris. Numerous drop stones chaotically distributed along the interval (diameter from 0.4 cm to 1 cm). Mud flow	2.5Y 3/2			3	3 1				200
	SILTY CLAY: Dark grey with less sandy admixture, structureless. Few patches of different lithology represented by sand/silt clayey matrix. Sandy admixture decreases down the interval. Mud flow	5Y 3/1			4	1				250
	CLAY: Grey, with silty admixture, brownish patches filled by silty clay. Mud flow				5					300
	SILTY CLAY: Grey with sandy admixture, structureless, abundant drop stones and shell debris	2.5Y 3/0								

Core log TTR-9-AT-146G

R/V Professor Logachev CRUISE TTR-9 CORE TTR9-AT-CORE 148G

Location: Lower part of the slump

Latitude: 61°16.79' N Longitude: 04°29.37' W

Date: 15/06/99 16:14 GMT

Water Depth: 1043 m

Recovery: 349 cm

SUBSAMPLING CODES:

Sedimentology
1- Collection
2- Grain size
3- Mineralogy
4- X-ray
5- Thin sections

Geochemistry
6- Gas
7- TOC
8- Fluor.
9- Bitum.
10- Pore water

AGE:
H- Holocene
LP- Late Pleistocene
EP- Early Pleistocene

LITHOLOGY

Colour

Structure

Age

Section

Samples

Sediment

GeoChem

Depth, cm

Magnetic Susceptibility (CGS units)

The figure is a stratigraphic log of Core TTR9-AT-CORE 148G. It displays various parameters against depth (0 to 350 cm). The lithology column on the left describes the sediment types and their characteristics. The color column shows the color of the sediment at different depths. The structure column indicates the sedimentary structures. The age column shows the age of the sediment. The section column shows the section of the core. The samples column shows the sample numbers. The depth column shows the depth in centimeters. The magnetic susceptibility column shows the magnetic susceptibility in CGS units.

LITHOLOGY	Colour	Structure	Age	Section	Samples	Depth, cm	Magnetic Susceptibility (CGS units)
SANDY CLAY: Brownish, watersaturated with coarse sand fragments up to 2 mm. Coarser upwards. Rich in forams	2.5Y 4/2	~			1	0	~
CLAY: Yellowish brown, consolidated	2.5Y 5/2	~		1	1	~	~
SAND: Brownish, coarse in clayey matrix. Lower boundary is gradational	5Y 3/1	~			1	~	~
CLAY: Yellowish brown, structureless with irregular lower boundary	5Y 4/1	~		2	1	~	~
SILTY CLAY: Dark grey, disturbed, with patches of watersaturated clayey sediment rich in foraminifera and shell fragments	2.5Y 3/0	~		3	3	~	~
SILTY CLAY: Dark grey, with much of terrigenous admixture and foraminifera. Shell debris. Several patches (up to 10 cm in diameter) with darker silty clay. Several drop stones. Debris flow	2.5Y 4/2	~		4	3	~	~
SILTY CLAY: Light grey, structureless, rich in foraminifera	2.5Y 4/2	~		5	3	~	~
MARL: Light grey, bioturbated, rich in foraminifera. Lower boundary is sharp and irregular due to bioturbation	2.5Y 4/2	~		6	3	~	~
SILTY CLAY: Grey, bioturbated. Burrows are filled with sediment from the above interval	2.5Y 4/2	~		6	3	~	~
CLAY: Dark grey, homogeneous with numerous drop stones and occasional shell fragments. Mud flow	2.5Y 4/2	~		6	3	~	~

Core log TTR-9-AT-148G

R/V Professor Logachev CRUISE TTR-9	CORE TTR9-AT-CORE 149G
-------------------------------------	------------------------

Location: Lower part of the slump

Latitude: 61°14.85'N Longitude: 04°33.64'W

Date: 15/06/99 18:18 GMT

Water Depth: 1032 m

Recovery: 384 cm



SUBSAMPLING CODES:

Sedimentology

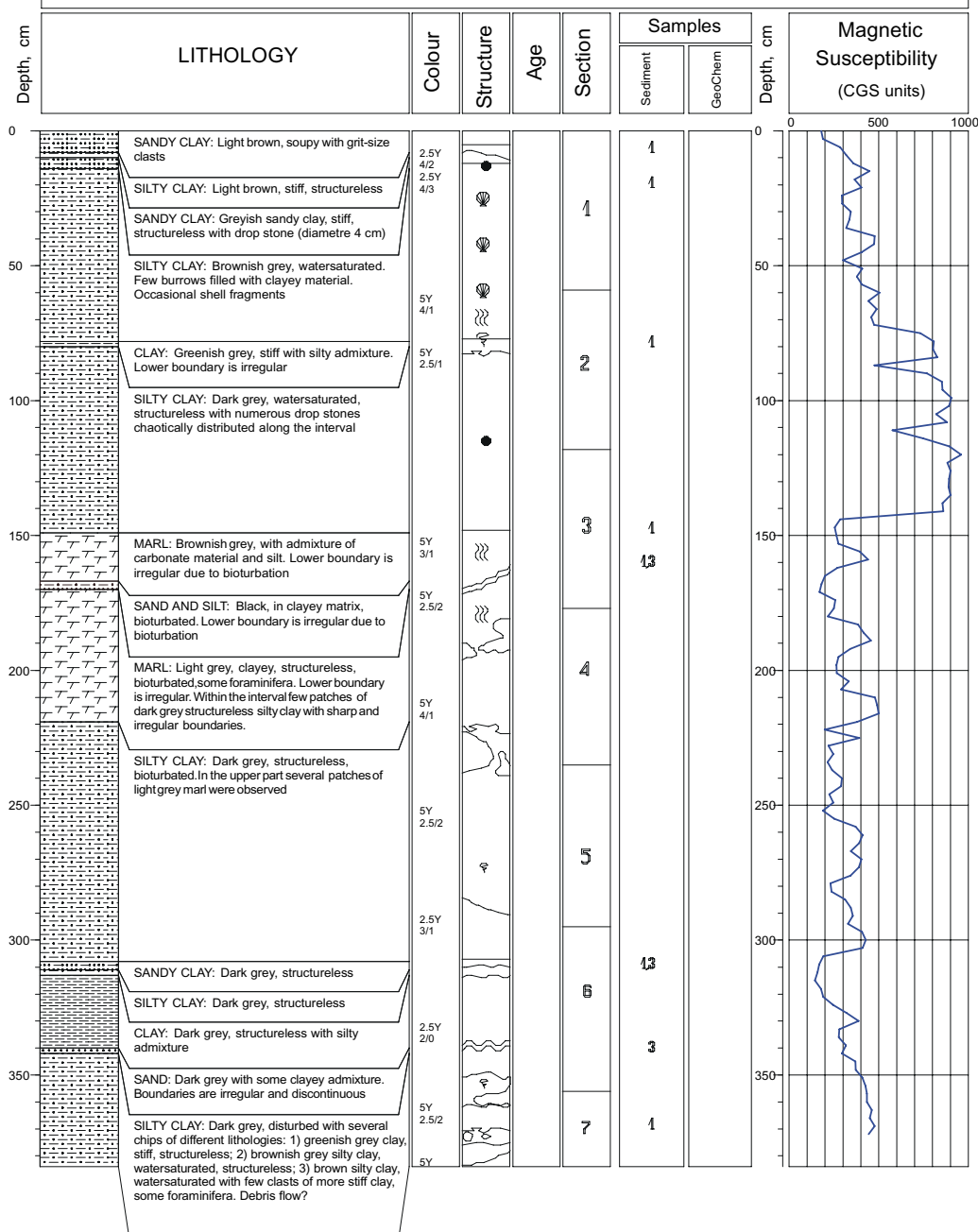
- 1- Collection
- 2- Grain size
- 3- Mineralogy
- 4- X-ray
- 5- Thin sections

Geochemistry

- 6- Gas
- 7- TOC
- 8- Fluor.
- 9- Bitum
- 10- Pore water


AGE:

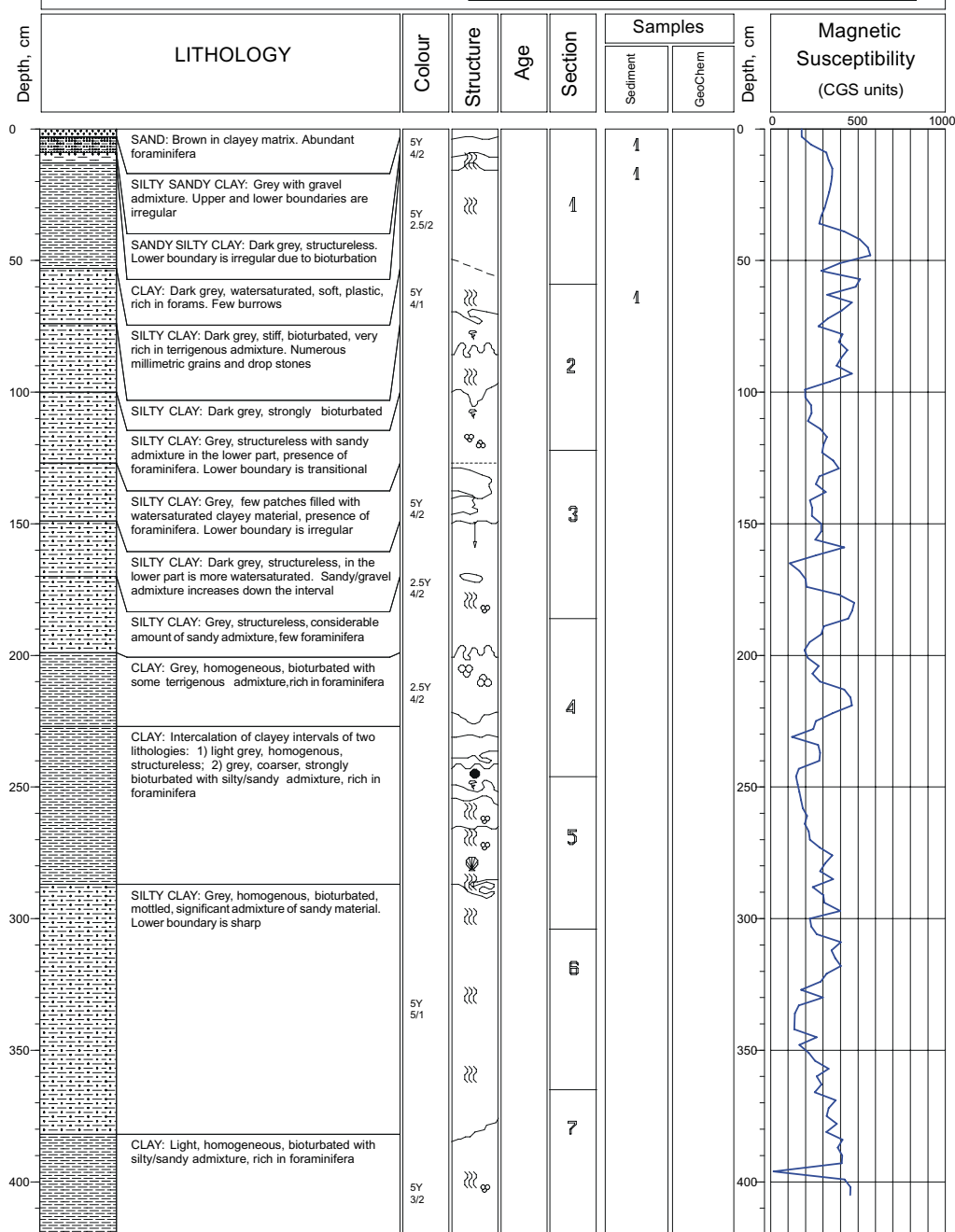
- H- Holocene
LP- Late Pleistocene
EP- Early Pleistocene



Core log TTR-9-AT-149G

R/V Professor Logachev CRUISE TTR-9 CORE TTR9-AT-CORE 150G

Location:	Lower part of the slump			
Latitude:	61°14.01' N	Longitude: 04°35.57' W		
Date:	15/06/99 19:22 GMT			
Water Depth:	1020 m			
Recovery:	421 cm			
		SUBSAMPLING CODES:	AGE:	
		Sedimentology	Geochemistry	
		1- Collection	6- Gas	H- Holocene
		2- Grain size	7- TOC	
		3- Mineralogy	8- Fluor.	LP- Late Pleistocene
		4- X-ray	9- Bitum	
		5- Thin sections	10- Pore water	EP- Early Pleistocene



Core log TTR-9-AT-150G

R/V Professor Logachev CRUISE TTR-9 CORE TTR9-AT-CORE 153G
Location: Slump area with bottom current indications

Latitude: 60°41.69' N **Longitude:** 05°02.51' W

Date: 19/06/99 02:02 GMT

Water Depth: 916 m

Recovery: 406 cm

SUBSAMPLING CODES:
Sedimentology

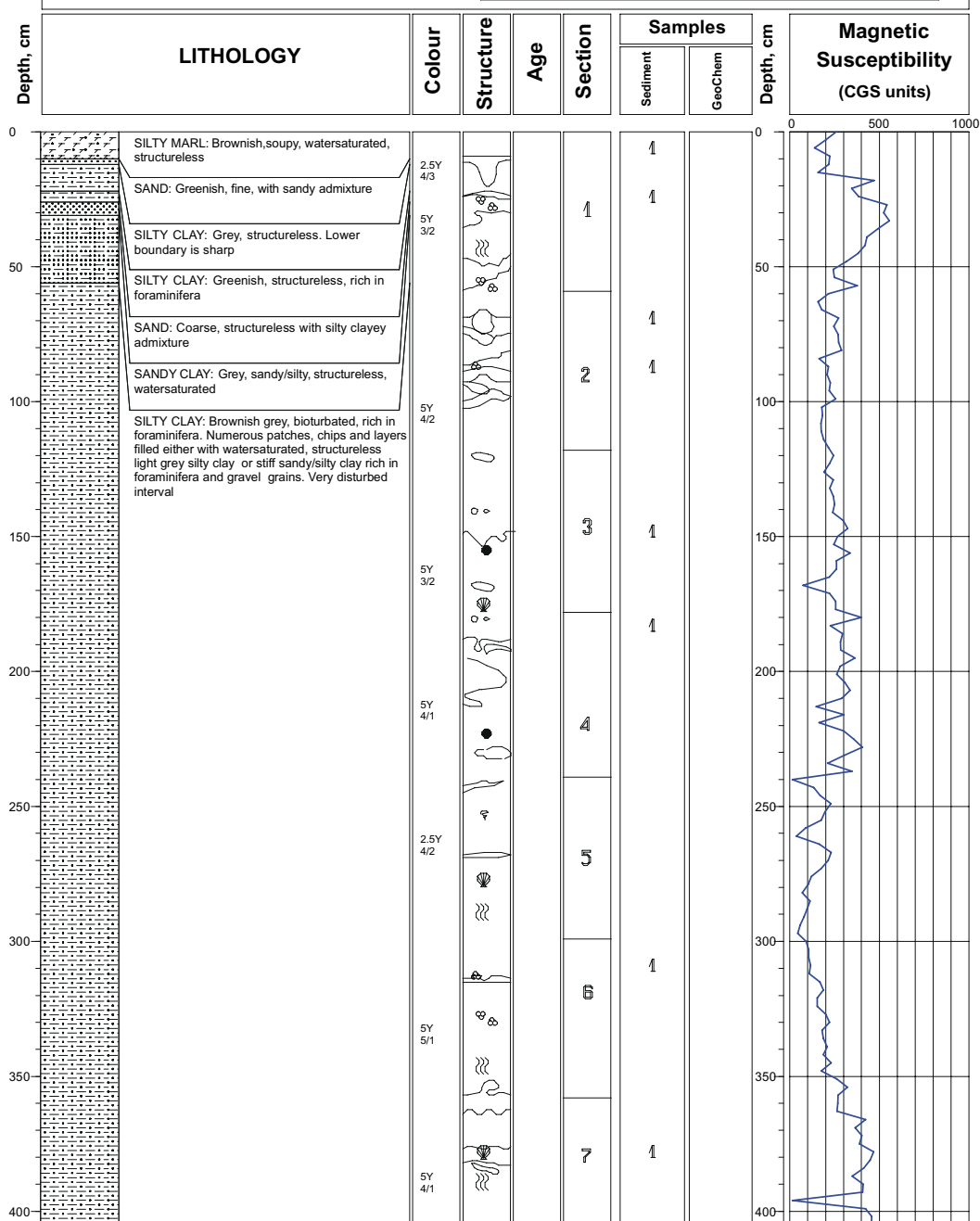
- 1- Collection
- 2- Grain size
- 3- Mineralogy
- 4- X-ray
- 5- Thin sections

Geochemistry

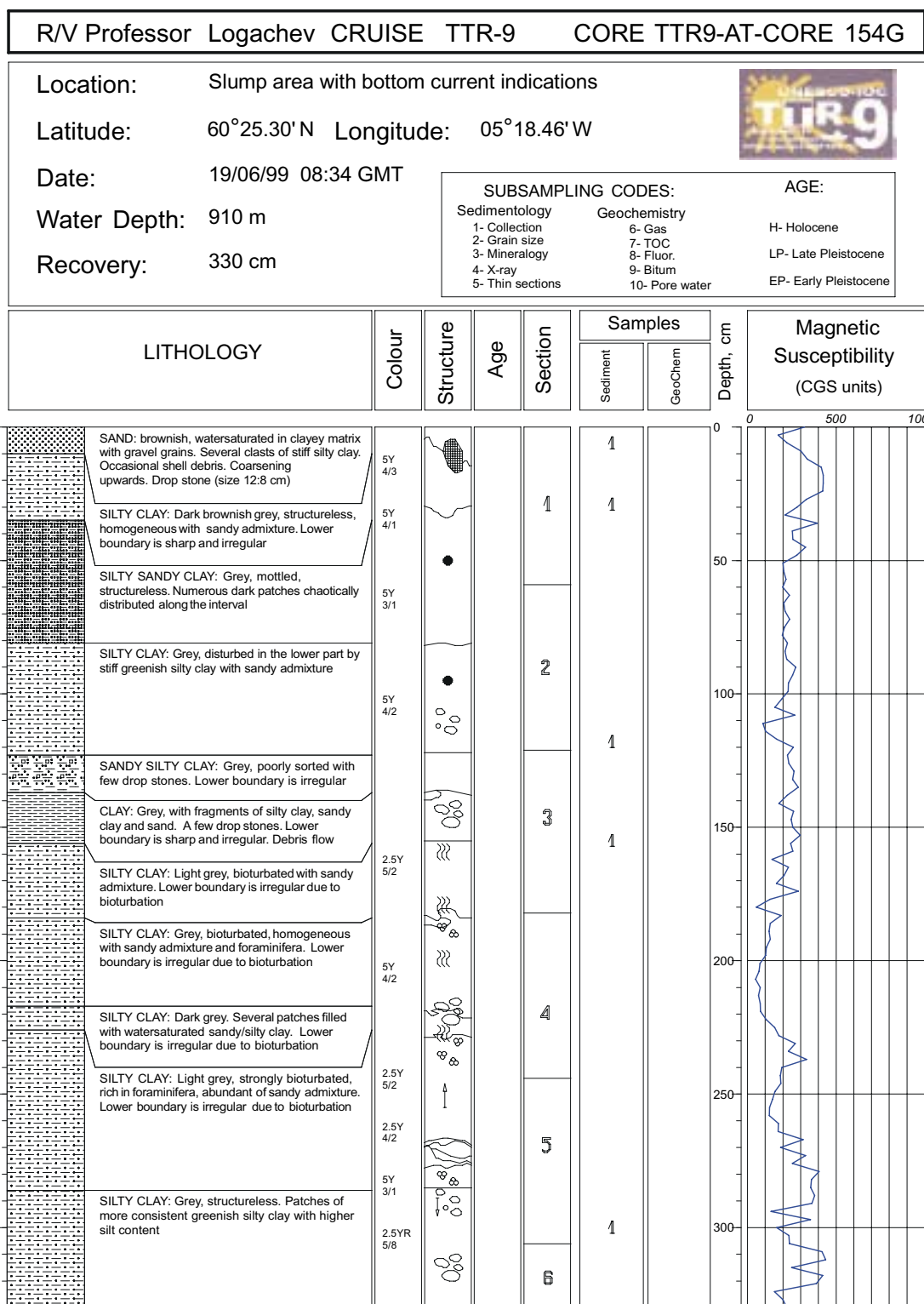
- 6- Gas
- 7- TOC
- 8- Fluor.
- 9- Bitum
- 10- Pore water

AGE:

- H- Holocene
- LP- Late Pleistocene
- EP- Early Pleistocene



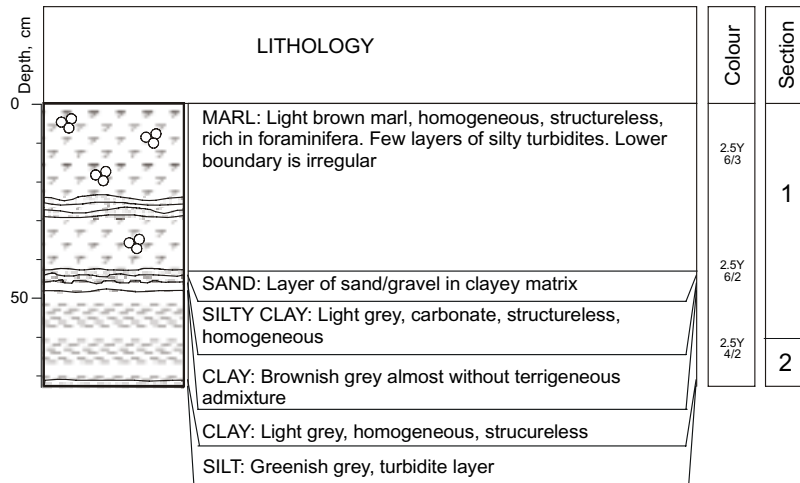
Core log TTR-9-AT-153G



Core log TTR-9-AT-154G

R/V Professor Logachev CRUISE TTR-9 CORE TTR9 - AT - 195G

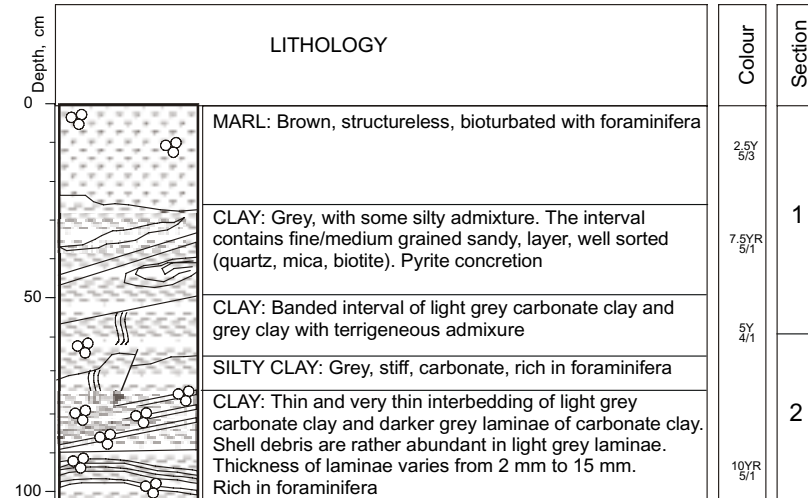
Location: Shelf on the broad Dom Carlos Valley,
to the west of Porto Seamount
Latitude: 40°36.98' N **Longitude:** 10°36.52' W
Date: 05/07/99 16:36 GMT
Water Depth: 4469 m **Recovery:** 73 cm



Core log TTR-9-AT-195G

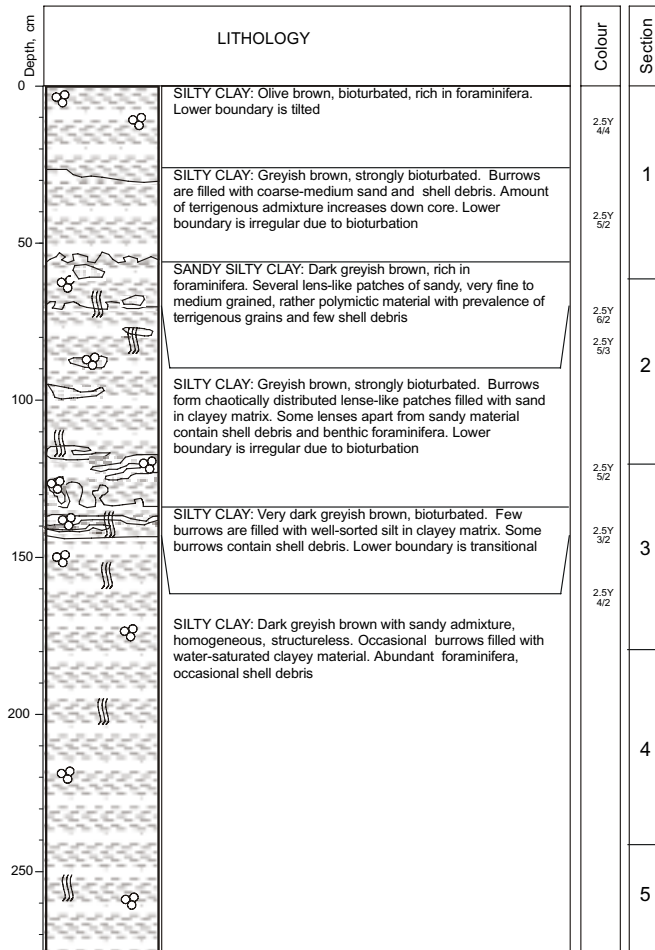
R/V Professor Logachev CRUISE TTR-9 CORE TTR9 - AT- 197G

Location: Dom Carlos Valley
to the east of Vasco da Gama Seamount
Latitude: 40°37.76' N **Longitude:** 11°00.75' W
Date: 06/07/99 23:52 GMT
Water Depth: 4800 m **Recovery:** 103 cm



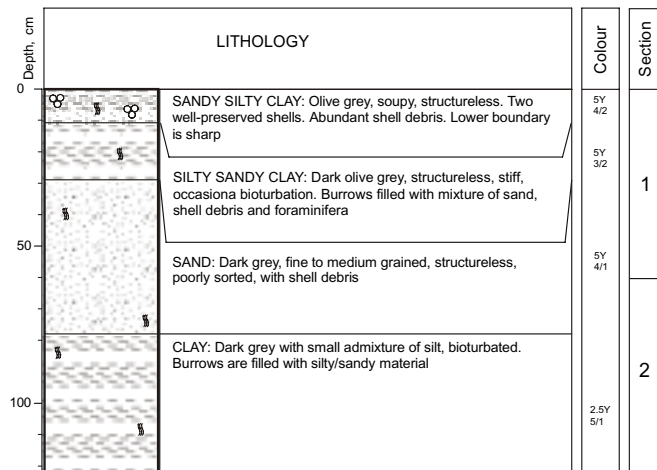
Core log TTR-9-AT-197G

R/V Professor Logachev CRUISE TTR-9 CORE TTR-9 - AT - 198G		
Location:	Upper slope to the southwest of the Estremadura Spur, a flat area between canyons on the Lisbon margin	
Latitude:	38°41.85' N	Longitude: 10°01.82' W
Date:	08/07/99 20:20 GMT	
Water Depth:	1045 m	Recovery: 276 cm



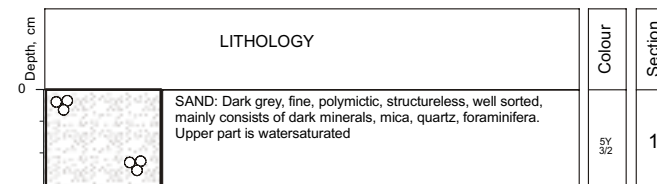
Core log TTR-9-AT-198G

R/V Professor Logachev CRUISE TTR-9 CORE TTR-9 - AT - 199G		
Location:	Flat area on Lisbon margin, to the West of Lisbon canyon	
Latitude:	38°31.15' N	Longitude: 09°30.58' W
Date:	08/07/99 23:23 GMT	
Water Depth:	143 m	Recovery: 122 cm



Core log TTR-9-AT-199G

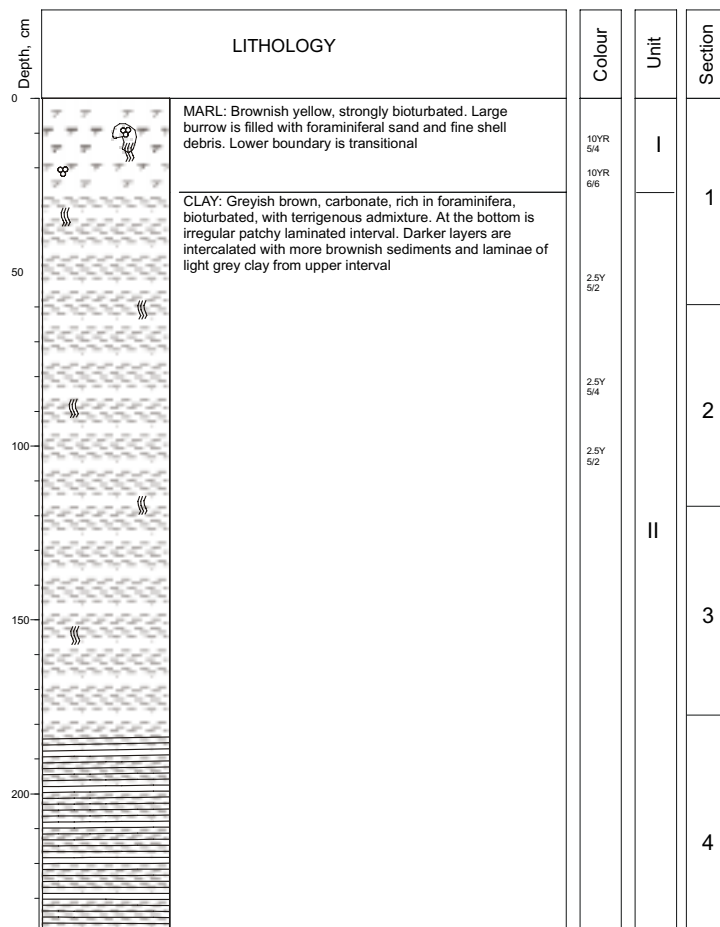
R/V Professor Logachev CRUISE TTR-9 CORE TTR-9 - AT - 200G		
Location:	Upper continental slope to the South of Setubal canyon	
Latitude:	38°04.80' N	Longitude: 09°08.98' W
Date:	09/07/99 02:32 GMT	
Water Depth:	502 m	Recovery: 31 cm



Core log TTR-9-AT-200G

R/V Professor Logachev CRUISE TTR-9 **CORE TTR9 - AT - 201G**

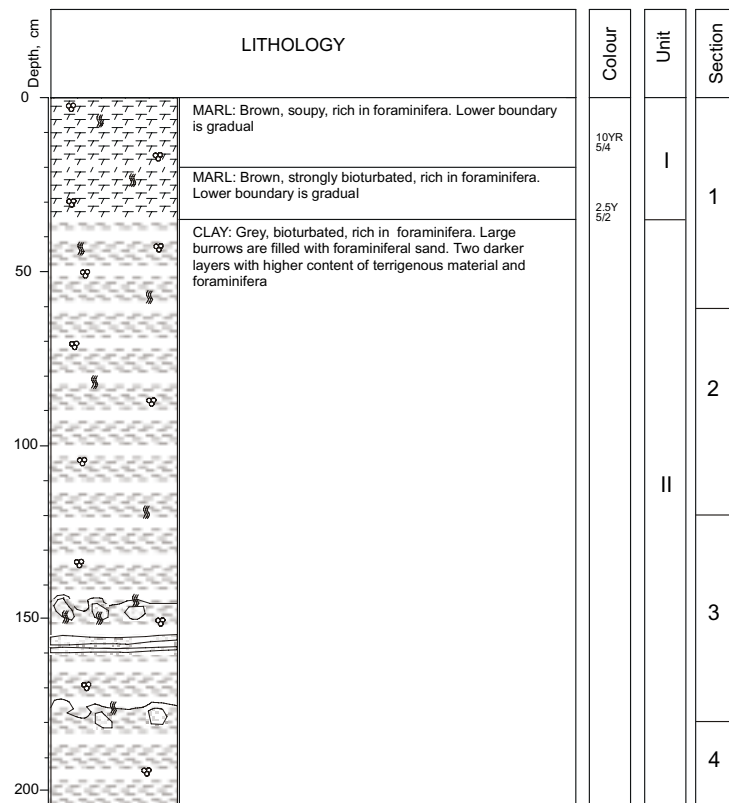
Location: Plain to the North of Yuma mud volcano
Latitude: 35°27.31' N **Longitude:** 07°06.52' W
Date: 11/07/99 08:44 GMT
Water Depth: 1064 m **Recovery:** 239 cm



Core log TTR-9-AT-201G

R/V Professor Logachev CRUISE TTR-9 **CORE TTR9 - AT - 202G**

Location: Northern flank of the Yuma mud volcano
Latitude: 35°26.32' N **Longitude:** 07°06.38' W
Date: 11/07/99 09:58 GMT
Water Depth: 1147 m **Recovery:** 205 cm

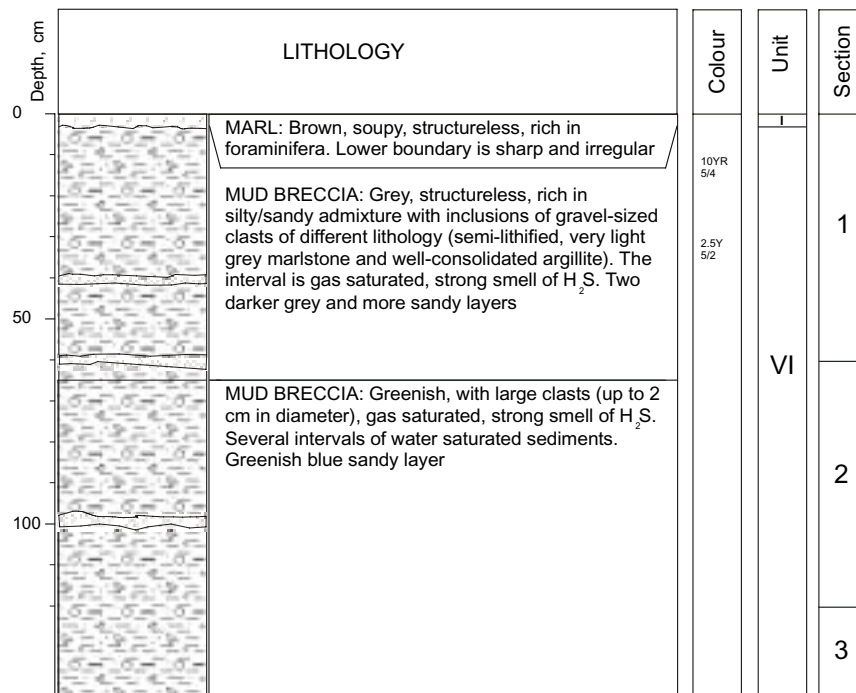


Core log TTR-9-AT-202G

ANNEXE I. CORE LOGS (LEG 2, Gulf of Cadiz)

R/V Professor Logachev CRUISE TTR-9 **CORE TTR9 - AT - 203G**

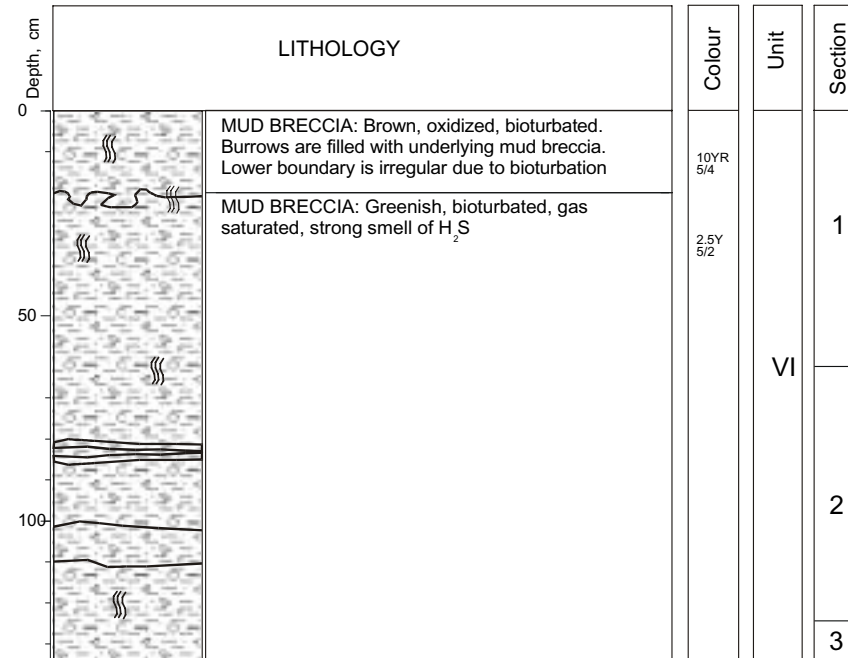
Location: Main crater of the Yuma mud volcano
Latitude: 35°25.39' N **Longitude:** 07°06.03' W
Date: 11/07/99 10:54 GMT
Water Depth: 964 m **Recovery:** 142 cm



Core log TTR-9-AT-203G

R/V Professor Logachev CRUISE TTR-9 **CORE TTR9 - AT - 204G**

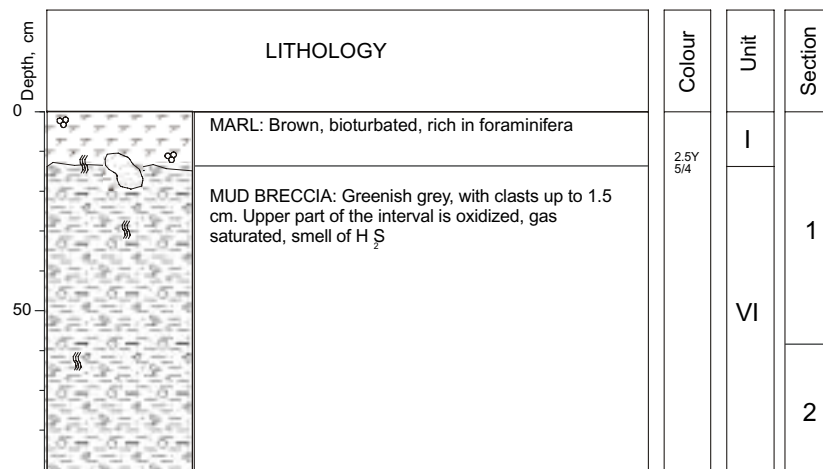
Location: Small crater of the Yuma mud volcano
Latitude: 35°25.01' N **Longitude:** 07°05.58' W
Date: 11/07/99 11:45 GMT
Water Depth: 983 m **Recovery:** 134 cm



Core TTR-9-AT-204G

R/V Professor Logachev CRUISE TTR-9 **CORE TTR9 - AT - 205G**

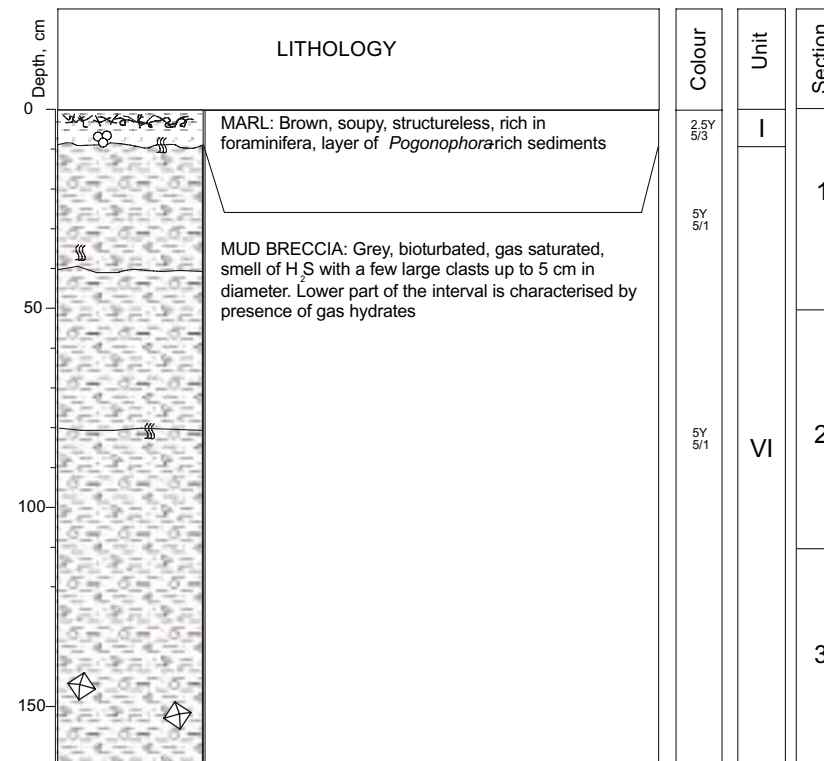
Location: Mud flow of the Ginsburg mud volcano
Latitude: 35°22.96' N **Longitude:** 07°05.76' W
Date: 11/07/99 13:05 GMT
Water Depth: 1040 m **Recovery:** 91 cm



Core log TTR-9-AT-205G

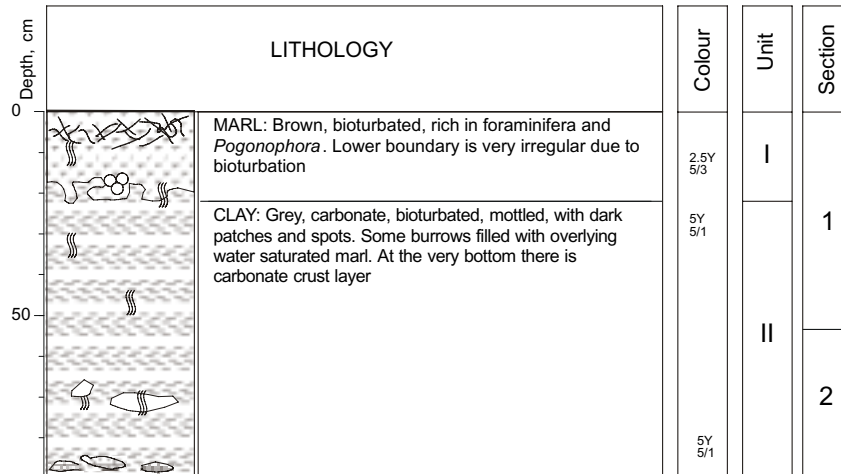
R/V Professor Logachev CRUISE TTR-9 **CORE TTR9 - AT - 206G**

Location: Crater of the Ginsburg mud volcano
Latitude: 35 22.39' N **Longitude:** 07 05.35' W
Date: 11/07/99 13:47 GMT
Water Depth: 912 m **Recovery:** 165 cm



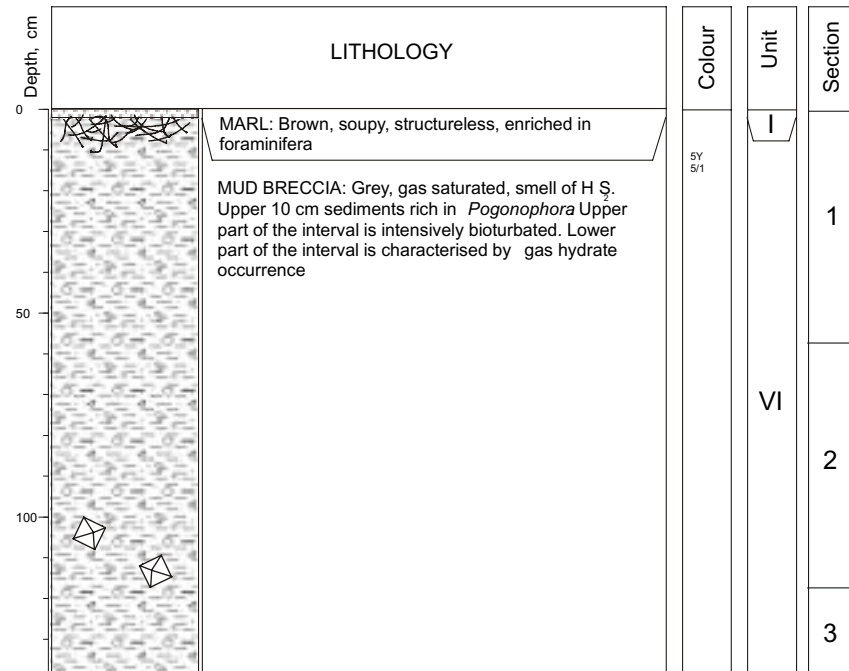
Core log TTR-9-AT-206G

R/V Professor Logachev CRUISE TTR-9 CORE TTR9 - AT - 207G			
Location:	Southern slope of the Ginsburg mud volcano		
Latitude:	35°21.56' N	Longitude:	07°05.10' W
Date:	11/07/99 14:33 GMT		
Water Depth:	1140 m	Recovery:	89 cm



Core log TTR-9-AT-207G

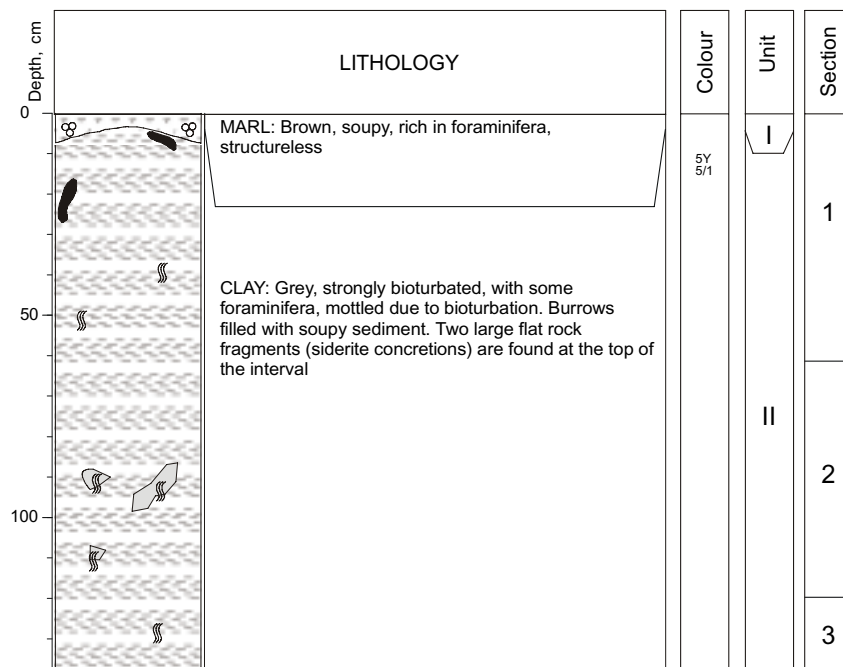
R/V Professor Logachev CRUISE TTR-9 CORE TTR9 - AT - 208G			
Location:	Crater of the Ginsburg mud volcano		
Latitude:	35°22.39' N	Longitude:	07°05.32' W
Date:	11/07/99 15:27 GMT		
Water Depth:	911 m	Recovery:	138 cm



Core log TTR-9-AT-208G

R/V Professor Logachev CRUISE TTR-9 **CORE TTR9 - AT - 210G**

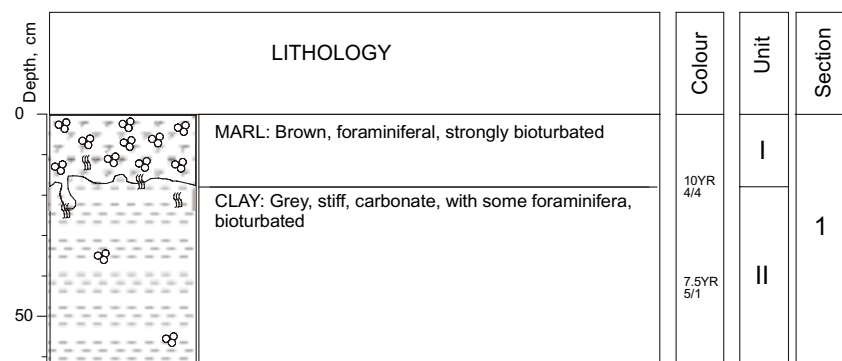
Location: Southern flank of assumed mud volcano in the Eastern Moroccan field
Latitude: 35°26.21' N **Longitude:** 06°46.47' W
Date: 12/07/99 22:37 GMT
Water Depth: 517 m **Recovery:** 138 cm



Core log TTR-9-AT-210G

R/V Professor Logachev CRUISE TTR-9 **CORE TTR9 - AT - 211G**

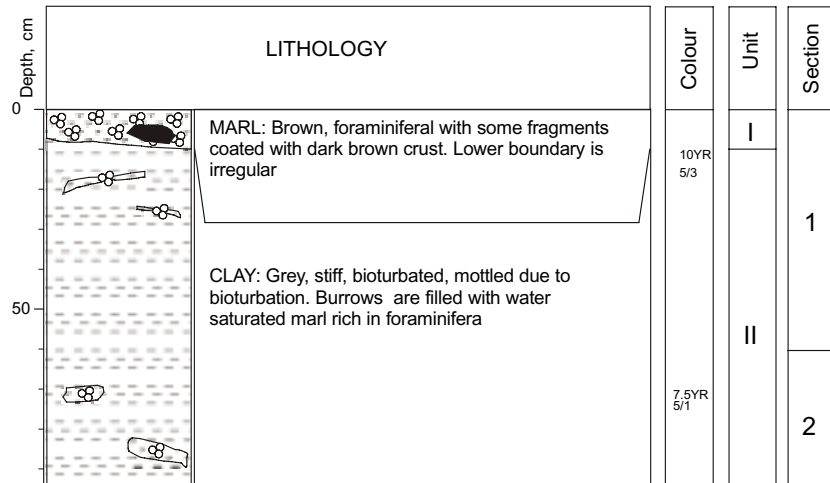
Location: Southern flank of assumed mud volcano in the Eastern Moroccan field
Latitude: 35°25.89' N **Longitude:** 06°45.78' W
Date: 12/07/99 23:21 GMT
Water Depth: 540 m **Recovery:** 62 cm



Core log TTR-9-AT-211G

R/V Professor Logachev CRUISE TTR-9 **CORE TTR9 - AT - 212G**

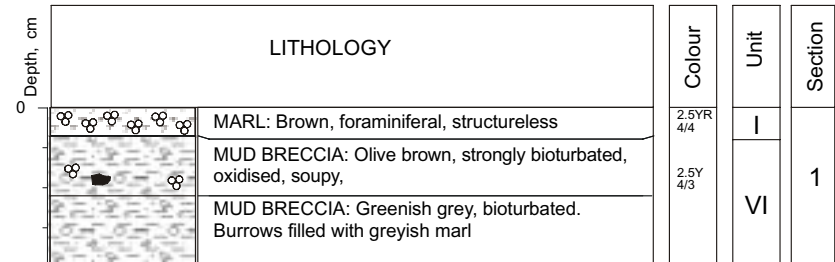
Location: Northern flank of assumed mud volcano in the Eastern Moroccan field
Latitude: 35°26.44' N **Longitude:** 06°46.46' W
Date: 13/07/99 00:39 GMT
Water Depth: 503 m **Recovery:** 94 cm



Core log TTR-9-AT-212G

R/V Professor Logachev CRUISE TTR-9 **CORE TTR9 - AT - 213G**

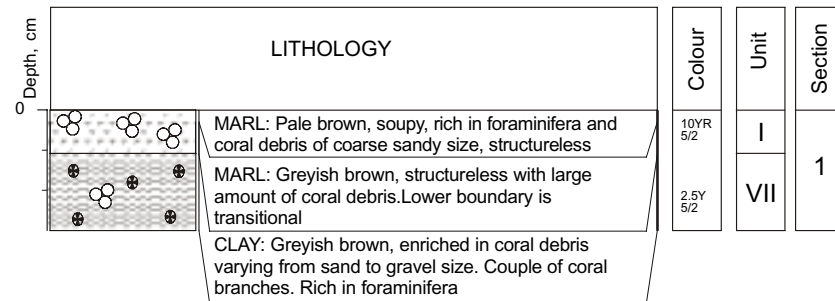
Location: Crater of the Kidd mud volcano
Latitude: 35°25.60' N **Longitude:** 06°44.10' W
Date: 13/07/99 01:46 GMT
Water Depth: 502 m **Recovery:** 39 cm



Core log TTR-9-AT-213G

R/V Professor Logachev CRUISE TTR-9 **CORE TTR9 - AT - 215G**

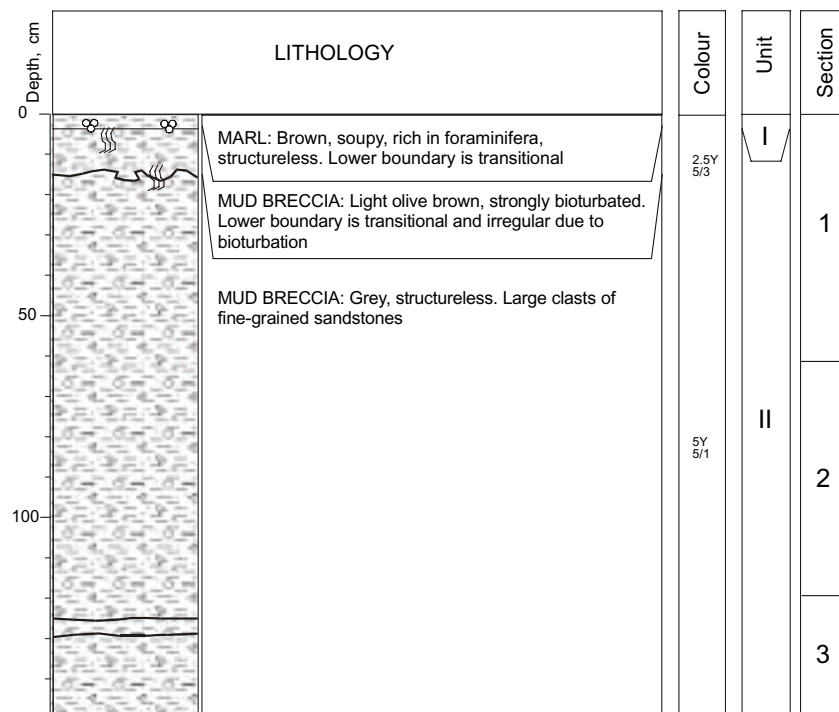
Location: Crater of assumed mud volcano in the Eastern Moroccan field
Latitude: 35°22.01' N **Longitude:** 06°51.90' W
Date: 13/07/99 13:36 GMT
Water Depth: 596 m **Recovery:** 30 cm



Core log TTR-9-AT-215G

R/V Professor Logachev CRUISE TTR-9 **CORE TTR9 - AT - 214G**

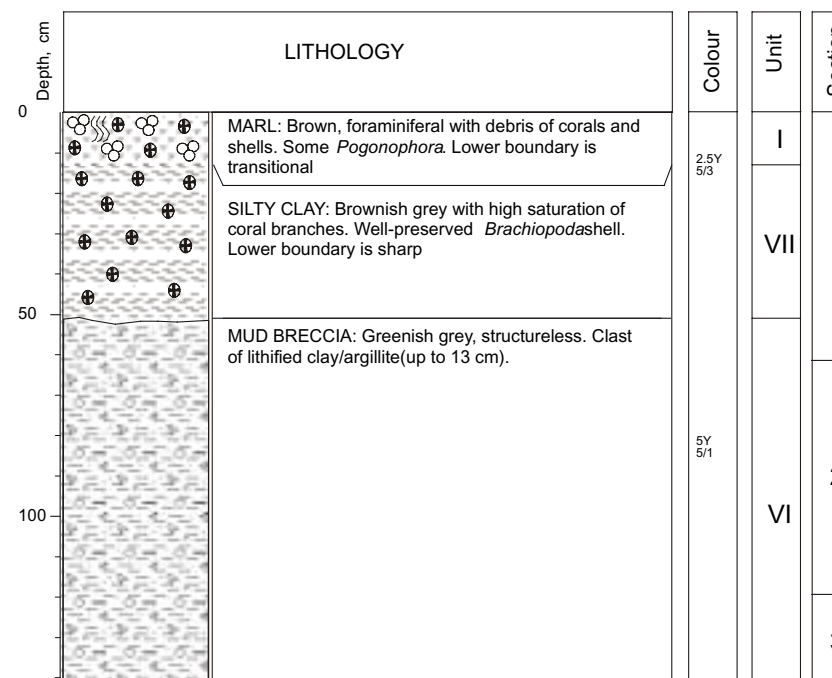
Location: Crater of the Adamastor mud volcano
Latitude: 35°21.92' N **Longitude:** 06°45.55' W
Date: 13/07/99 11:35 GMT
Water Depth: 511 m **Recovery:** 149 cm



Core log TTR-9-AT-214G

R/V Professor Logachev CRUISE TTR-9 **CORE TTR9 - AT - 216G**

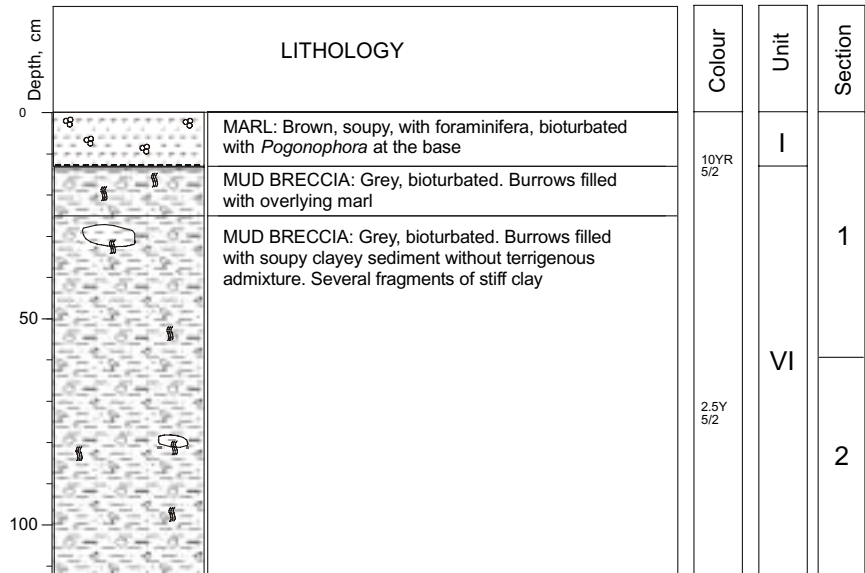
Location: Crater of the TTR mud volcano
Latitude: 35°22.29' N **Longitude:** 06°55.62' W
Date: 13/07/99 14:47 GMT
Water Depth: 721 m **Recovery:** 142 cm



Core log TTR-9-AT-216G

R/V Professor Logachev CRUISE TTR-9 CORE TTR9 - AT - 217G

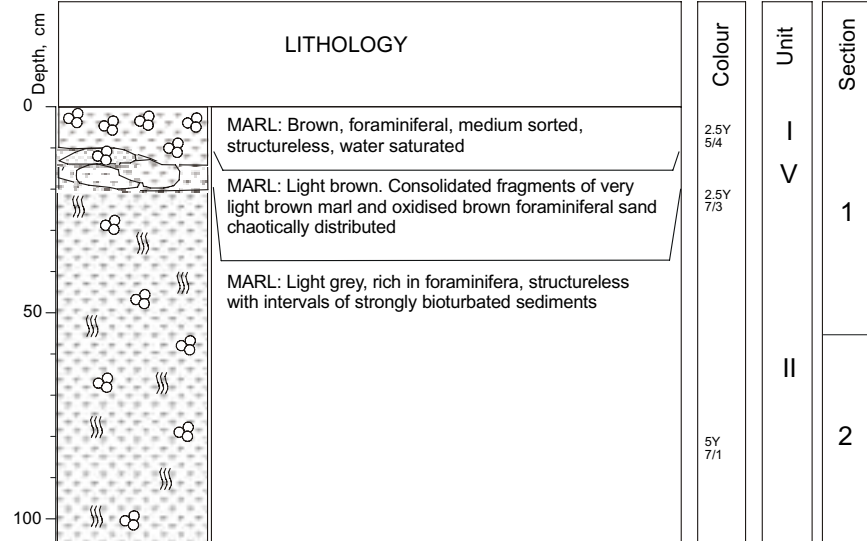
Location: Crater of the Ginsburg mud volcano
Latitude: 35°22.22' N **Longitude:** 07°05.38' W
Date: 13/07/99 21:18 GMT
Water Depth: 918 m **Recovery:** 112 cm



Core log TTR-9-AT-217G

R/V Professor Logachev CRUISE TTR-9 CORE TTR9 - AT - 220G

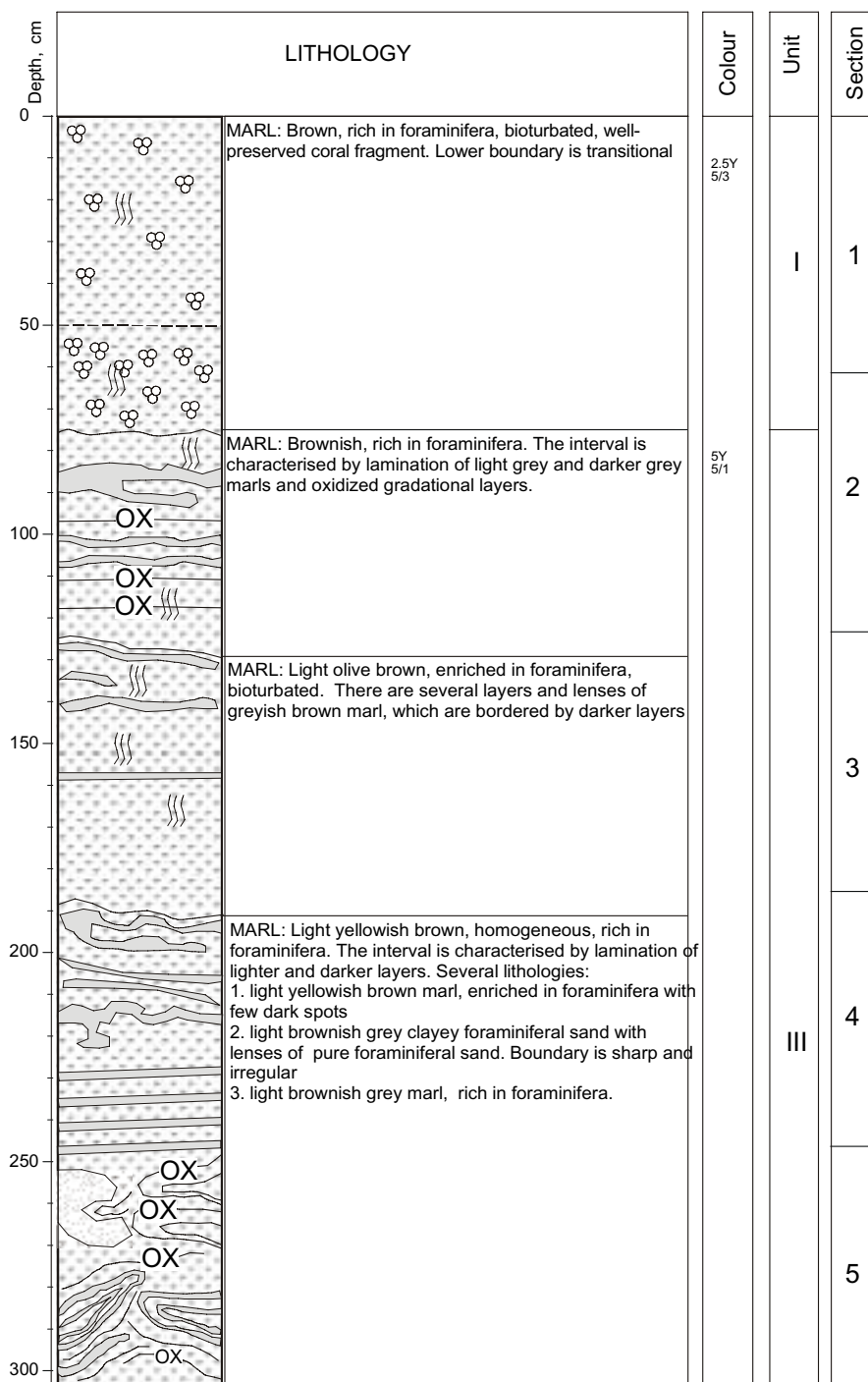
Location: Ridge in the Western Moroccan field
Latitude: 35°26.50' N **Longitude:** 07°40.86' W
Date: 14/07/99 18:38 GMT
Water Depth: 1504 m **Recovery:** 106 cm



Core log TTR-9-AT-220G

R/V Professor Logachev CRUISE TTR-9 CORE TTR9 - AT - 219G

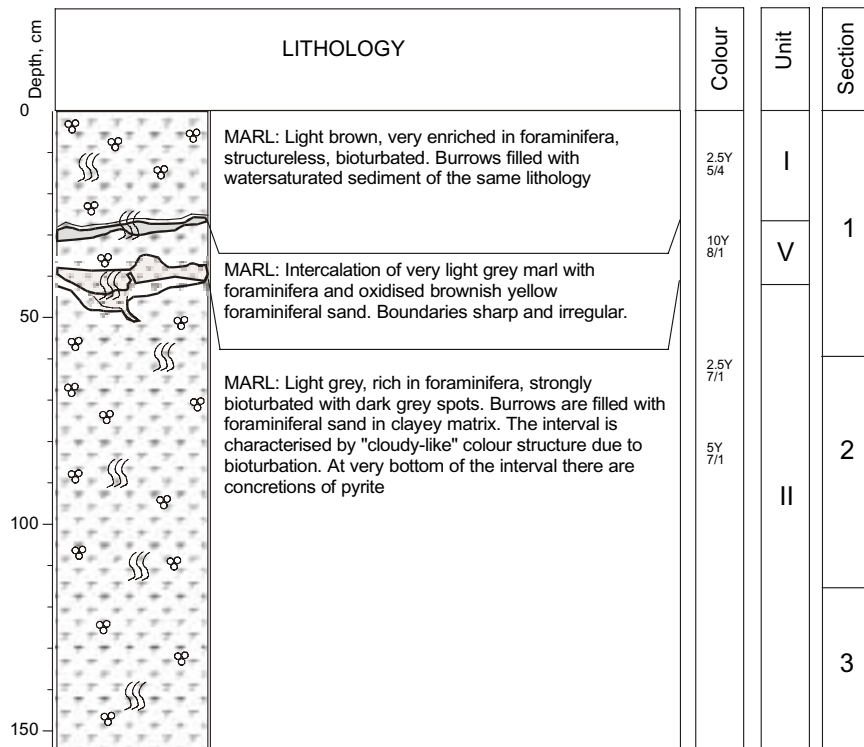
Location: Ridge in the Western Moroccan field
Latitude: 35°23.55' N **Longitude:** 07°41.17' W
Date: 14/07/99 16:45 GMT
Water Depth: 1508 m **Recovery:** 304 cm



Core log TTR-9-AT-219

R/V Professor Logachev CRUISE TTR-9 **CORE TTR9 - AT - 221G**

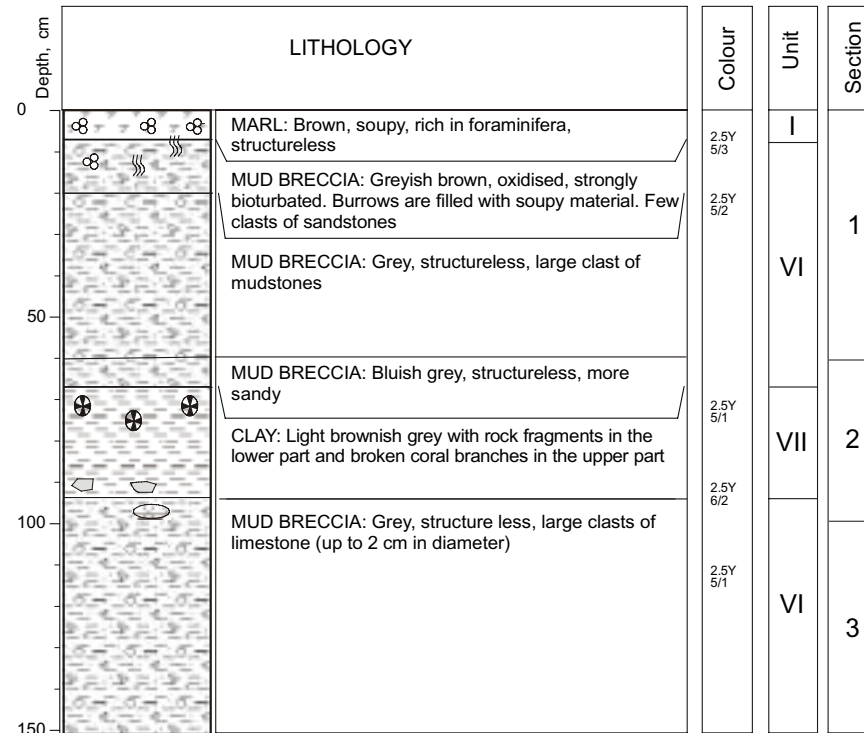
Location: Ridge in the Western Moroccan field
Latitude: 35°23.74' N **Longitude:** 07°48.41' W
Date: 14/07/99 20:36 GMT
Water Depth: 1682 m **Recovery:** 155 cm





Core log TTR-9-AT-221G

R/V Professor Logachev CRUISE TTR-9 **CORE TTR9 - AT - 222G**

Location: Crater of the St.-Petersburg mud volcano
Latitude: 35°53.75' N **Longitude:** 07°02.44' W
Date: 15/07/99 12:36 GMT
Water Depth: 879 m **Recovery:** 151 cm



Core log TTR-9-AT-222G

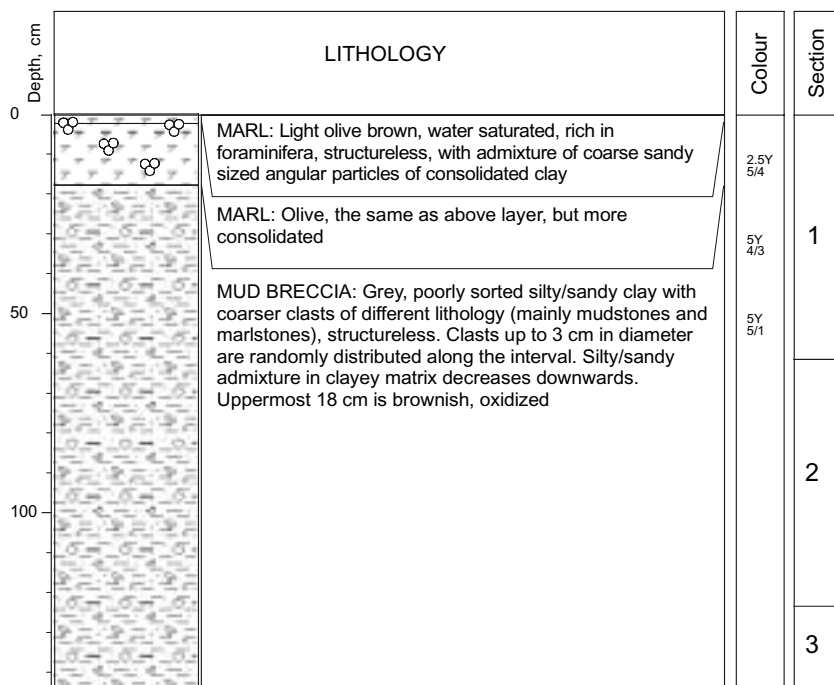
R/V Professor Logachev CRUISE TTR-9				CORE	TTR9 - AT- 224G																						
Location:		The Gil Eanes Channel levee																									
Latitude:		35°55.14' N		Longitude:			07°12.58' W																				
Date:		15/07/99 18:10 GMT																									
Water Depth:		888 m																									
Recovery:		242 cm			<table><tr><th colspan="2">SUBSAMPLING CODES:</th><th>AGE:</th></tr><tr><td>Sedimentology</td><td>Geochemistry</td><td></td></tr><tr><td>1- Collection</td><td>6- Gas</td><td>H- Holocene</td></tr><tr><td>2- Grain size</td><td>7- TOC</td><td></td></tr><tr><td>3- Mineralogy</td><td>8- Fluor.</td><td>LP- Late Pleistocene</td></tr><tr><td>4- X-ray</td><td>9- Bitum</td><td></td></tr><tr><td>5- Thin sections</td><td>10- Pore water</td><td>EP- Early Pleistocene</td></tr></table>		SUBSAMPLING CODES:		AGE:	Sedimentology	Geochemistry		1- Collection	6- Gas	H- Holocene	2- Grain size	7- TOC		3- Mineralogy	8- Fluor.	LP- Late Pleistocene	4- X-ray	9- Bitum		5- Thin sections	10- Pore water	EP- Early Pleistocene
SUBSAMPLING CODES:		AGE:																									
Sedimentology	Geochemistry																										
1- Collection	6- Gas	H- Holocene																									
2- Grain size	7- TOC																										
3- Mineralogy	8- Fluor.	LP- Late Pleistocene																									
4- X-ray	9- Bitum																										
5- Thin sections	10- Pore water	EP- Early Pleistocene																									
<div>LITHOLOGY</div> <div></div>																											
<div>CLAYEY SILT: Olive, watersaturated, with foraminifera, well sorted</div>																											
<div>CLAYEY SILT: Olive grey, well sorted with foraminifera and shell fragments. At the very bottom there are several burrows filled with soupy clayey sediment</div>																											
<div></div>																											
<div></div>																											
<div></div>																											
<div></div>																											
<div></div>																											
<div></div>																											
<div></div>																											
<div></div>																											
<div></div>																											
<div></div>																											
<div></div>																											
<div></div>																											
<div></div>																											
<div></div>																											
<div></div>																											
<div></div>																											
<div></div>																											
<div></div>																											
<div></div>																											
<div></div>																											
<div></div>																											
<div></div>																											
<div></div>																											
<div></div>																											
<div></div>																											
<div></div>																											
<div></div>																											
<div></div>																											
<div></div>																											
<div></div>																											
<div></div>																											
<div></div>																											
<div></div>																											
<div></div>																											
<div></div>																											
<div></div>																											
<div></div>																											
<div></div>																											
<div></div>																											
<div></div>																											
<div></div>																											
<div></div>																											
<div></div>																											
<div></div>																											
<div></div>																											
<div></div>																											
<div></div>																											
<div></div>																											
<div></div>																											
<div></div>																											
<div></div>																											
<div></div>																											
<div></div>																											
<div></div>																											
<div></div>																											
<div></div>																											
<div></div>																											
<div></div>																											
<div></div>																											
<div></div>																											
<div></div>																											
<div></div>																											
<div></div>																											
<div></div>																											
<div></div>																											
<div></div>																											
<div></div>																											
<div></div>																											
<div></div>																											
<div></div>																											
<div></div>																											
<div></div>																											
<div></div>																											
<div></div>																											
<div></div>																											
<div></div>																											
<div></div>																											
<div></div>																											
<div></div>																											
<div></div>																											
<div></div>																											
<div></div>																											
<div></div>																											
<div></div>																											
<div></div>																											
<div></div>																											
<div></div>																											
<div></div>																											
<div></div>																											
<div></div>																											
<div></div>																											
<div></div>																											
<div></div>																											
<div></div>																											
<div></div>																											
<div></div>																											
<div></div>																											
<div></div>																											
<div></div>																											
<div></div>																											
<div></div>																											
<div></div>																											
<div></div>																											
<div></div>																											
<div></div>																											
<div></div>																											
<div></div>																											
<div></div>																											
<div></div>																											
<div></div>																											
<div></div>																											
<div></div>																											
<div></div>																											
<div></div>																											
<div></div>																											
<div></div>																											
<div></div>																											
<div></div>																											
<div></div>																											
<div></div>																											
<div></div>																											
<div></div>																											
<div></div>																											
<div></div>																											
<div></div>																											
<div></div>																											
<div></div>																											
<div></div>																											
<div></div>																											
<div></div>																											
<div></div>																											
<div></div>																											
<div></div>																											
<div></div>																											
<div></div>																											
<div></div>																											
<div></div>																											
<div></div>																											
<div></div>																											
<div></div>																											
<div></div>																											
<div></div>																											
<div></div>																											
<div></div>																											
<div></div>																											
<div></div>																											
<div></div>																											
<div></div>																											
<div></div>																											
<div></div>																											
<div></div>																											
<div></div>																											
<div></div>																											
<div></div>																											
<div></div>																											
<div></div>																											
<div></div>																											
<div></div>																											
<div></div>																											
<div></div>																											
<div></div>																											
<div></div>																											
<div></div>																											
<div></div>																											
<div></div>																											
<div></div>																											
<div></div>																											
<div></div>																											
<div></div>																											
<div></div>																											
<div></div>																											
<div></div>																											
<div></div>																											
<div></div>																											
<div></div>																											
<div></div>																											
<div></div>																											
<div></div>																											
<div></div>																											
<div></div>																											
<div></div>																											
<div></div>																											
<div></div>																											
<div></div>																											
<div></div>																											
<div></div>																											
<div></div>																											
<div></div>																											
<div></div>																											
<div></div>																											
<div></div>																											
<div></div>																											
<div></div>																											
<div></div>																											
<div></div>																											
<div></div>																											
<div></div>																											
<div></div>																											
<div></div>																											
<div></div>																											
<div></div>																											
<div></div>																											
<div></div>																											
<div></div>																											
<div></div>																											
<div></div>																											
<div></div>																											
<div></div>																											
<div></div>																											
<div></div>																											
<div></div>																											
<div></div>																											
<div></div>																											
<div></div>																											
<div></div>																											
<div></div>																											
<div></div>																											
<div></div>																											
<div></div>																											
<div></div>																											
<div></div>																											
<div></div>																											
<div></div>																											
<div></div>																											
<div></div>																											
<div></div>																											
<div></div>																											
<div></div>																											
<div></div>																											
<div></div>																											
<div></div>																											
<div></div>																											
<div></div>																											
<div></div>																											
<div></div>																											
<div></div>																											
<div></div>																											
<div></div>																											
<div></div>																											
<div></div>																											
<div></div>																											
<div></div>																											
<div></div>																											
<div></div>																											
<div></div>																											
<div></div>																											
<div></div>																											
<div></div>																											
<div></div>																											
<div></div>																											
<div></div>																											
<div></div>																											
<div></div>																											
<div></div>																											
<div></div>																											
<div></div>																											
<div></div>																											
<div></div>																											
<div></div>																											
<div></div>																											
<div></div>																											
<div></div>																											
<div></div>																											
<div></div>																											
<div></div>																											
<div></div>																											
<div></div>																											
<div></div>																											
<div></div>																											
<div></div>																											
<div></div>																											
<div></div>																											
<div></div>																											
<div></div>																											
<div></div>																											
<div></div>																											
<div></div>																											
<div></div>																											
<div></div>																											
<div></div>																											

Core log TTR-9-224G

ANNEXE I. CORE LOGS (LEG 3, Western Mediterranean Sea)

R/V Professor Logachev CRUISE TTR-9 **CORE TTR-9 - 258G**

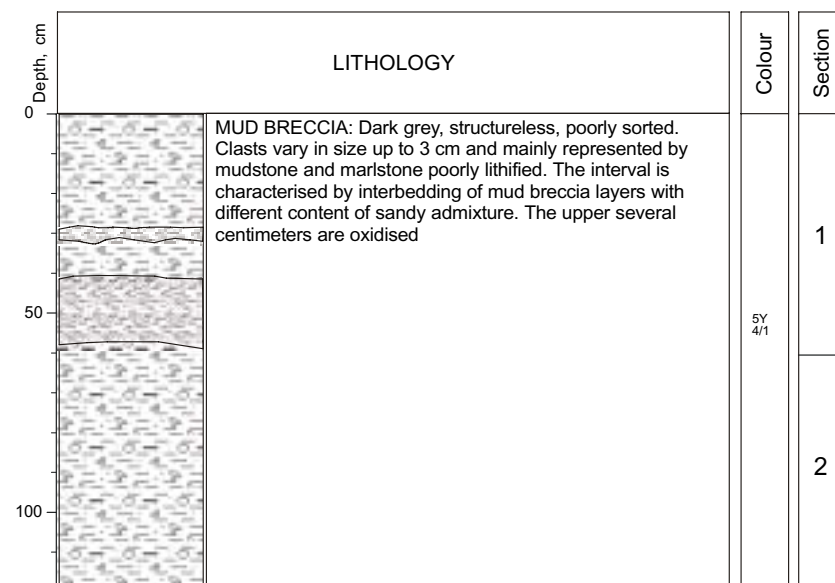
Location: Crater of the Granada mud volcano
Latitude: 35°33.72' N **Longitude:** 04°37.40' W
Date: 19/07/99 08:54 GMT
Water Depth: 583 m **Recovery:** 144 cm



Core log TTR-9-258G

R/V Professor Logachev CRUISE TTR-9 **CORE TTR-9 - 259G**

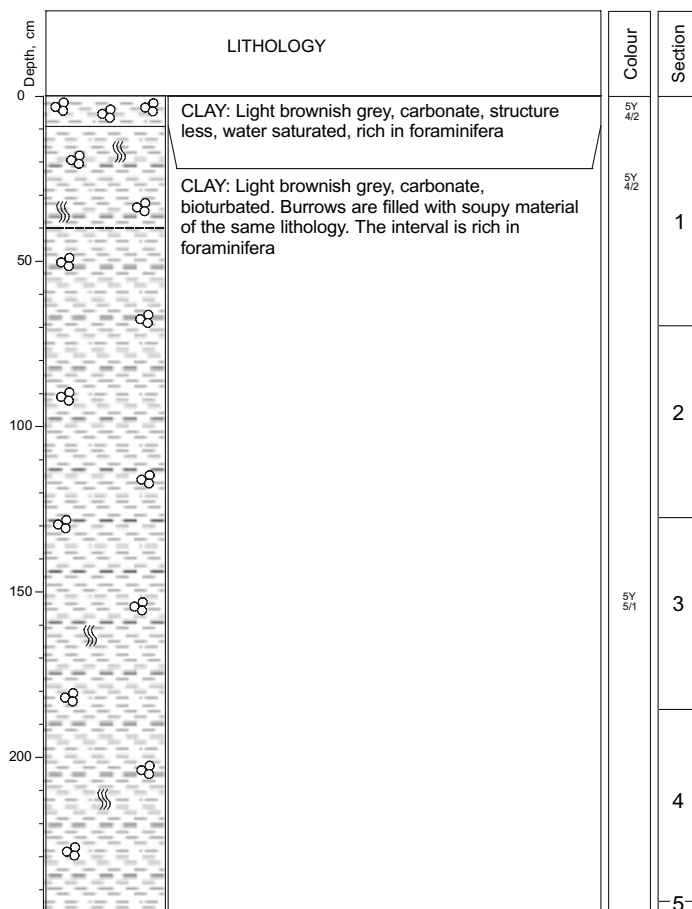
Location: Crater of the Granada mud volcano
Latitude: 35°33.76' N **Longitude:** 04°37.37' W
Date: 19/07/99 13:00 GMT
Water Depth: 580 m **Recovery:** 119 cm



Core log TTR-9-259G

R/V Professor Logachev CRUISE TTR-9 CORE TTR-9 - 261G

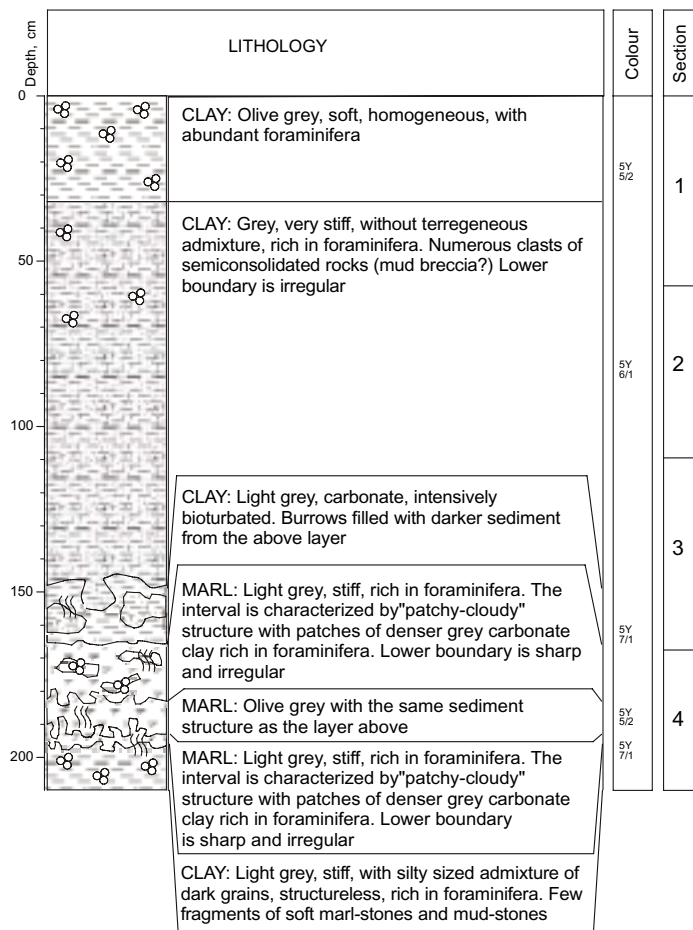
Location: Assumed mud volcano
Latitude: 35°37.49' N **Longitude:** 04°30.97' W
Date: 19/07/99 18:29 GMT
Water Depth: 1003 m **Recovery:** 247 cm



Core log TTR-9-261G

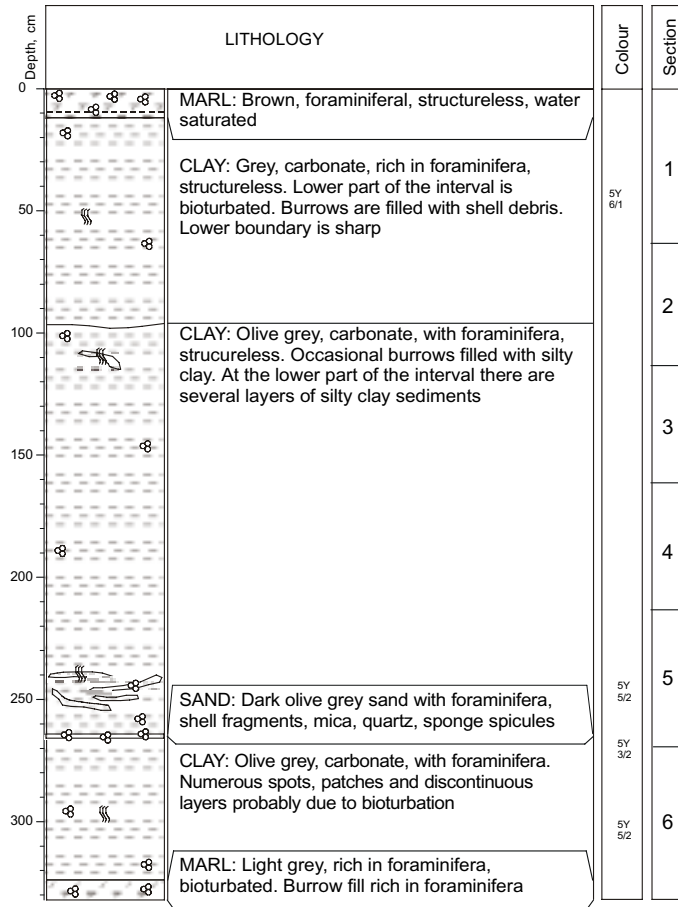
R/V Professor Logachev CRUISE TTR-9 CORE TTR-9 - 262G

Location: Flow of the assumed mud volcano
Latitude: 35°37.51' N **Longitude:** 04°29.66' W
Date: 19/07/99 19:28 GMT
Water Depth: 1086 m **Recovery:** 210 cm



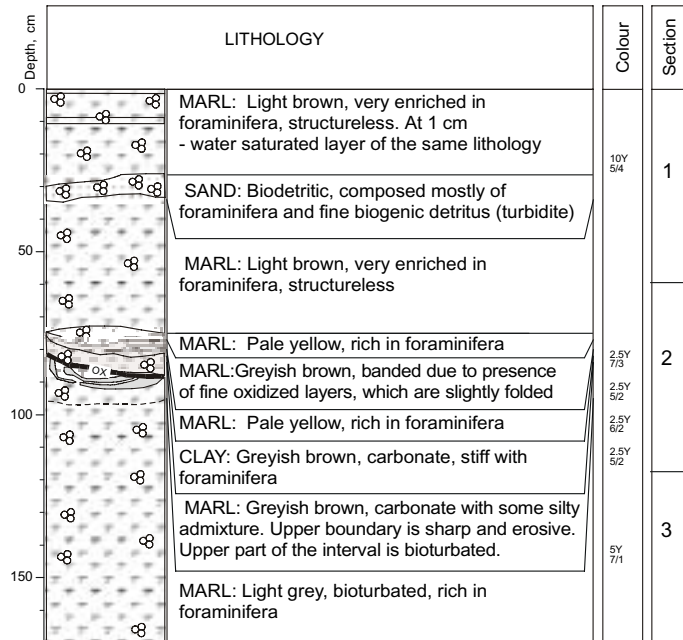
Core log TTR-9-262G

R/V Professor Logachev CRUISE TTR-9		CORE TTR-9 - 268G
Location:	Bottom of southern foot of the Djibuti Seamount	
Latitude:	35°57.81' N	Longitude: 03°30.66' W
Date:	21/07/99	
Water Depth:	1526 m	Recovery: 332 cm



Core log TTR-9-268G

R/V Professor Logachev CRUISE TTR-9		CORE TTR-9 - 273G
Location:	NE part of the study area	
Latitude:	37°24.16' W	Longitude: 00°18.67' N
Date:	25/07/99	
Water Depth:	2534 m	Recovery: 170 cm



Core log TTR-9-273G

R/V Professor Logachev CRUISE TTR-9

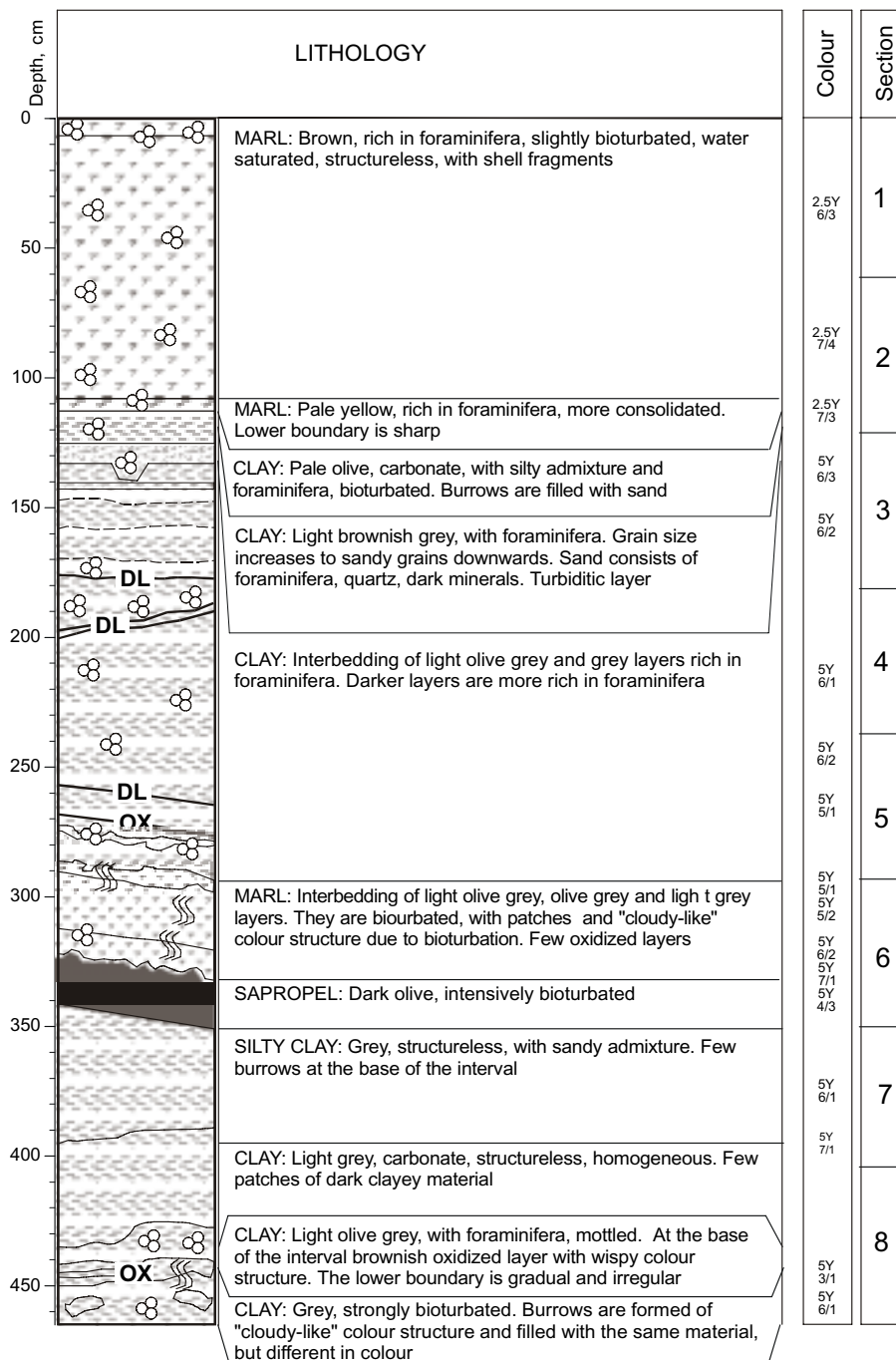
CORE TTR-9 - 274G

Location: Top of salt diapir 1, the NE part of the study area

Latitude: 37°15.96' N **Longitude:** 00°02.99' W


Date: 26/07/99

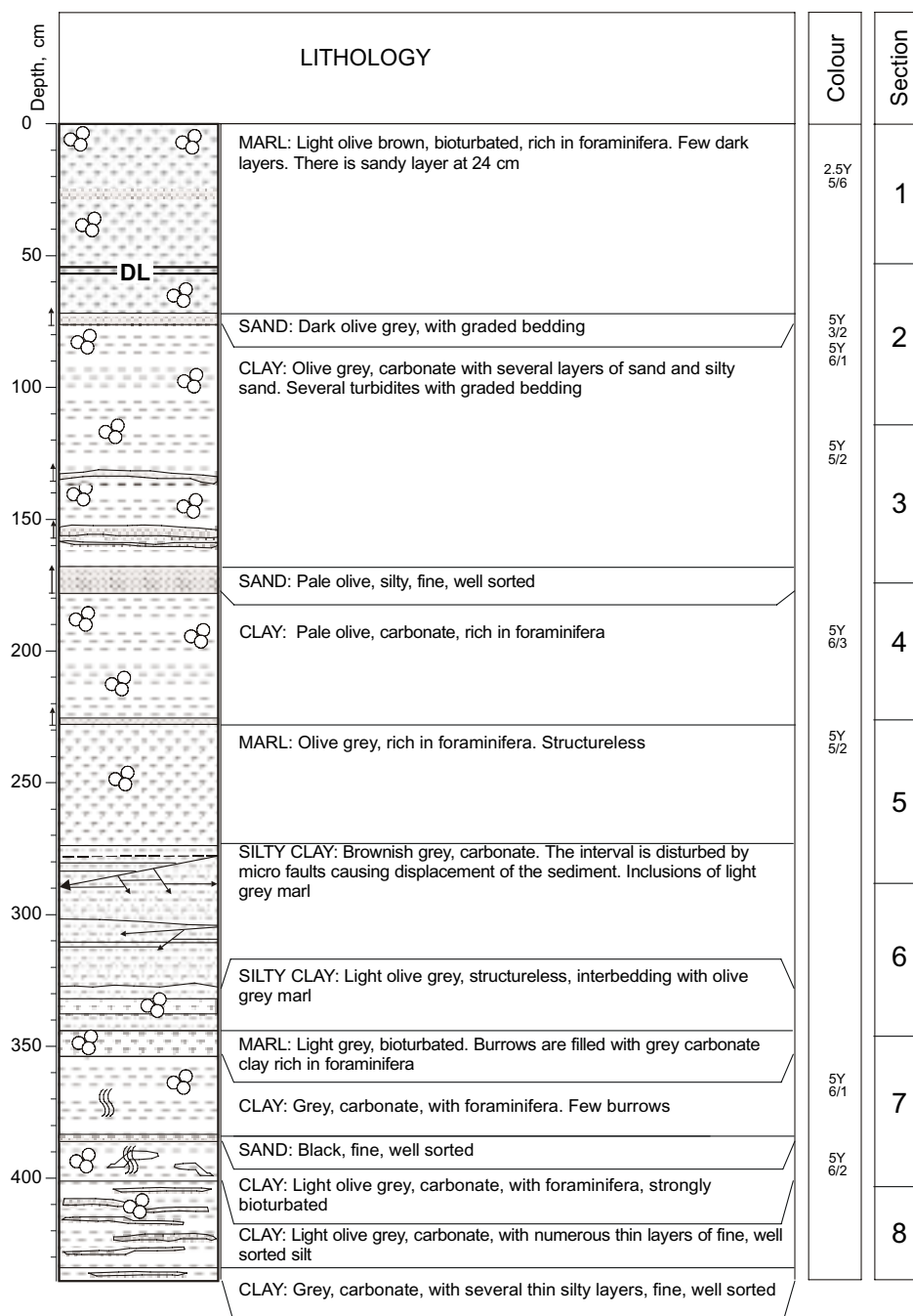
Water Depth: 2587 m **Recovery:** 465 cm



Core log TTR-9-274G

R/V Professor Logachev CRUISE TTR-9 CORE TTR-9 - 275G

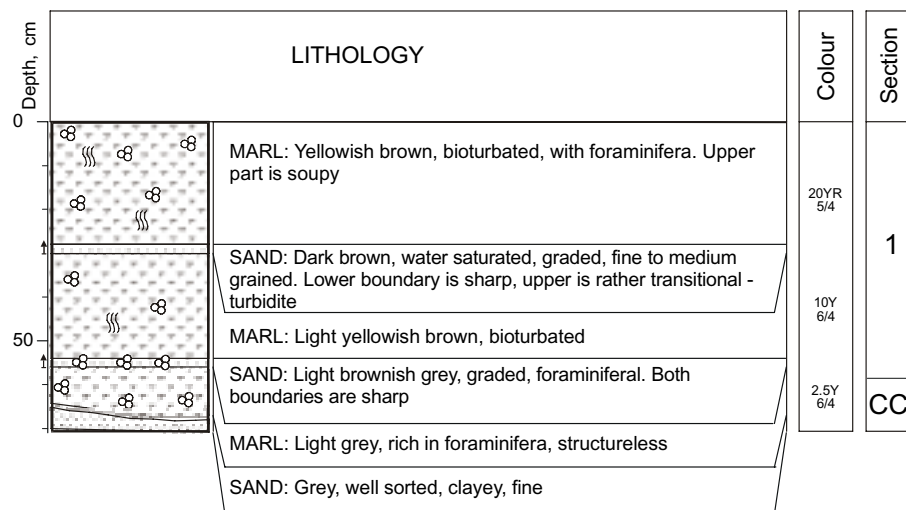
Location:	Slope of the diapir 1, the NE of the study area		
Latitude:	37°16.37' N	Longitude: 00°03.02' W	
Date:	26/07/99		
Water Depth:	2608 m	Recovery: 439 cm	



Core log TTR-9-275G

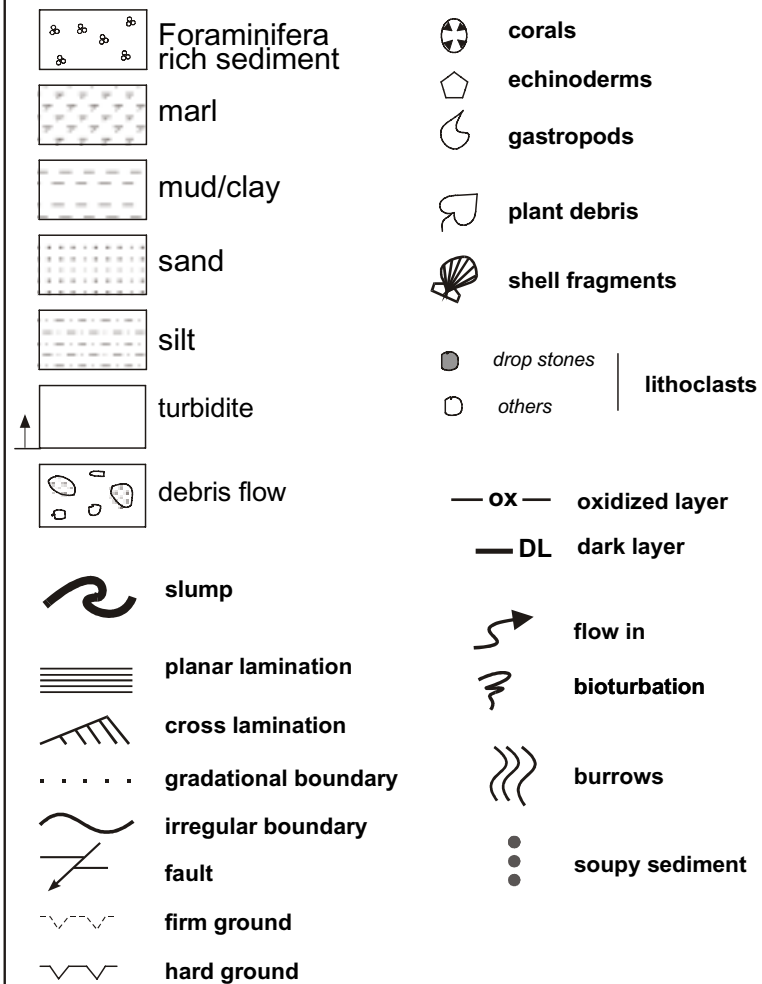
R/V Professor Logachev CRUISE TTR-9 CORE TTR-9 - 276G

Location: Top of the salt diapir 2, the NE part of the study area
Latitude: 37°17.97' N **Longitude:** 00°06.03' W
Date: 26/07/99
Water Depth: 2674 m **Recovery:** 71 cm



Core log TTR-9-276G

LEGEND



ANNEXE II. LIST OF TTR-RELATED REPORTS

- Limonov, A.F., Woodside, J.M. and Ivanov, M.K. (eds.), 1992. **Geological and geophysical investigations in the Mediterranean and Black Seas. Initial results of the "Training through Research" Cruise of R/V Gelendzhik in the Eastern Mediterranean and the Black Sea (June-July 1991).** *UNESCO Reports in Marine Science*, 56, 208 pp.
- Limonov, A.F., Woodside, J.M. and Ivanov, M.K. (eds.), 1993. **Geological and geophysical investigations of the deep-sea fans of the Western Mediterranean Sea. Preliminary report of the 2nd cruise of the R/V Gelendzhik in the Western Mediterranean Sea, June-July, 1992.** *UNESCO Reports in Marine Science*, 62, 148 pp.
- "Training-Through-Research" Opportunities Through the UNESCO/TREDMAR Programme. Report of the first post-cruise meeting of TREDMAR students. Moscow State University, 22-30 January, 1993.** *MARINF*, 91, UNESCO, 1993.
- Limonov, A.F., Woodside, J.M. and Ivanov, M.K. (eds.), 1994. **Mud volcanism in the Mediterranean and Black Seas and Shallow Structure of the Eratosthenes Seamount. Initial results of the geological and geophysical investigations during the Third UNESCO-ESF "Training-through-Research" Cruise of RV Gelendzhik (June-July 1993).** *UNESCO Reports in Marine Science*, 64, 173 pp.
- Recent Marine Geological Research in the Mediterranean and Black Seas through the UNESCO/TREDMAR programme and its 'Floating University project, Free University, Amsterdam, 31 January-4 February 1994. Abstracts.** *MARINF*, 94, UNESCO, 1994.
- Limonov, A.F., Kenyon, N.H., Ivanov, M.K. and Woodside J.M. (eds.), 1995. **Deep sea depositional systems of the Western Mediterranean and mud volcanism on the Mediterranean Ridge. Initial results of geological and geophysical investigations during the Fourth UNESCO-ESF 'Training through Research' Cruise of R/V Gelendzhik (June-July 1994).** *UNESCO Reports in Marine Science*, 67, 171 pp.
- Deep-sea depositional systems and mud volcanism in the Mediterranean and Black Seas. 3rd post-cruise meeting, Cardiff, 30 January - 3 February 1995. Abstracts.** *MARINF*, 99, UNESCO, 1995.
- Ivanov, M.K., Limonov, A.F. and Cronin, B.T. (eds.), 1996. **Mud volcanism and fluid venting in the eastern part of the Mediterranean Ridge. Initial results of geological, geophysical and geochemical investigations during the 5th Training-through-Research Cruise of R/V Professor Logachev (July-September 1995).** *UNESCO Reports in Marine Science*, 68, 127pp.
- Sedimentary basins of the Mediterranean and Black Seas. 4th Post-Cruise Meeting, Training-through-Research Programme. Moscow and Zvenigorod, Russia, 29 January-3 February. Abstracts.** *MARINF*, 100, UNESCO, 1996.
- Woodside, J.M., Ivanov, M.K. and Limonov, A.F. (eds.), 1997. **Neotectonics and Fluid Flow through Seafloor Sediments in the Eastern Mediterranean and Black Seas. Preliminary results of geological and geophysical investigations during the ANAXIPROBE/TTR-6 cruise of R/V Gelendzhik, July-August 1996. Vols. 1, 2.** *IOC Technical Series*, 48, UNESCO, 226 pp.
- Gas and Fluids in Marine Sediments: Gas Hydrates, Mud Volcanoes, Tectonics, Sedimentology and Geochemistry in Mediterranean and Black Seas. Fifth Post-cruise Meeting of the Training-through-Research Programme and International Congress, Amsterdam, The Netherlands, 27-29 January 1997.** *IOC Workshop Report*, 129, UNESCO, 1997.
- Geosphere-biosphere coupling: Carbonate Mud Mounds and Cold Water Reefs. International Conference and Sixth Post-Cruise Meeting of the Training-through-Research Programme, Gent, Belgium, 7-11 February 1998.** *IOC Workshop Report*, 143, UNESCO, 1998.
- Kenyon, N.H., Ivanov, M.K. and Akhmetzhanov, A.M. (eds.), 1998. **Cold water carbonate mounds and sediment transport on the Northeast Atlantic Margin.** *IOC Technical Series*, 52, UNESCO, 178 pp.
- Kenyon, N.H., Ivanov, M.K. and Akhmetzhanov, A.M. (eds.), 1999. **Geological Processes on the Northeast Atlantic Margin.** *IOC Technical Series*, 54, UNESCO, 141 pp.
- Geological Processes on European Continental Margins. International Conference and Eighth Post-cruise Meeting of the Training-Through-Research Programme, University of Granada, Spain, 31 January - 3 February 2000.** *IOC Workshop Report*, 168, UNESCO, 2000.

IOC Technical Series

No.	Title	Languages
1	Manual on International Oceanographic Data Exchange. 1965	(out of stock)
2	Intergovernmental Oceanographic Commission (Five years of work). 1966	(out of stock)
3	Radio Communication Requirements of Oceanography. 1967	(out of stock)
4	Manual on International Oceanographic Data Exchange - Second revised edition. 1967	(out of stock)
5	Legal Problems Associated with Ocean Data Acquisition Systems (ODAS). 1969	(out of stock)
6	Perspectives in Oceanography. 1968	(out of stock)
7	Comprehensive Outline of the Scope of the Long-term and Expanded Programme of Oceanic Exploration and Research. 1970	(out of stock)
8	IGOSS (Integrated Global Ocean Station System) - General Plan Implementation Programme for Phase 1.1971	(out of stock)
9	Manual on International Oceanographic Data Exchange - Third Revised Edition. 1973	(out of stock)
10	Bruun Memorial Lectures. 1971	E, F, S, R
11	Bruun Memorial Lectures. 1973	(out of stock)
12	Oceanographic Products and Methods of Analysis and Prediction. 1977	E only
13	International Decade of Ocean Exploration (IDOE), 1971-1980. 1974	(out of stock)
14	A Comprehensive Plan for the Global Investigation of Pollution in the Marine Environment and Baseline Study Guidelines. 1976	E, F, S, R
15	Bruun Memorial Lectures, 1975 - Co-operative Study of the Kuroshio and Adjacent Regions. 1976	(out of stock)
16	Integrated Ocean Global Station System (IGOSS) General Plan and Implementation Programme 1977-1982.1977	E, F, S, R
17	Oceanographic Components of the Global Atmospheric Research Programme (GARP). 1977	(out of stock)
18	Global Ocean Pollution: An Overview. 1977	(out of stock)
19	Bruun Memorial Lectures - The Importance and Application of Satellite and Remotely Sensed Data to Oceanography. 1977	(out of stock)
20	A Focus for Ocean Research: The Intergovernmental Oceanographic Commission - History, Functions, Achievements. 1979	(out of stock)
21	Bruun Memorial Lectures, 1979: Marine Environment and Ocean Resources. 1986	E, F, S, R
22	Scientific Report of the Intercalibration Exercise of the IOC-WMO-UNEP Pilot Project on Monitoring Background Levels of Selected Pollutants in Open Ocean Waters. 1982	(out of stock)
23	Operational Sea-Level Stations. 1983	E, F, S, R
24	Time-Series of Ocean Measurements. Vol. 1.1983	E, F, S, R
25	A Framework for the Implementation of the Comprehensive Plan for the Global Investigation of Pollution in the Marine Environment. 1984	(out of stock)
26	The Determination of Polychlorinated Biphenyls in Open-ocean Waters. 1984	E only
27	Ocean Observing System Development Programme. 1984	E, F, S, R
28	Bruun Memorial Lectures, 1982: Ocean Science for the Year 2000. 1984	E, F, S, R
29	Catalogue of Tide Gauges in the Pacific. 1985	E only
30	Time-Series of Ocean Measurements. Vol. 2. 1984	E only

(continued on inside back cover)

No.	Title	Languages
31	Time-Series of Ocean Measurements. Vol. 3. 1986	E only
32	Summary of Radiometric Ages from the Pacific. 1987	E only
33	Time-Series of Ocean Measurements. Vol. 4. 1988	E only
34	Bruun Memorial Lectures, 1987: Recent Advances in Selected Areas of Ocean Sciences in the Regions of the Caribbean, Indian Ocean and the Western Pacific. 1988	Composite E, F, S
35	Global Sea-Level Observing System (GLOSS) Implementation Plan. 1990	E only
36	Bruun Memorial Lectures, 1989: Impact of New Technology on Marine Scientific Research. 1991	Composite E, F, S
37	Tsunami Glossary - A Glossary of Terms and Acronyms Used in the Tsunami Literature. 1991	E only
38	The Oceans and Climate: A Guide to Present Needs. 1991	E only
39	Bruun Memorial Lectures, 1991: Modelling and Prediction in Marine Science. 1992	E only
40	Oceanic Interdecadal Climate Variability. 1992	E only
41	Marine Debris: Solid Waste Management Action for the Wider Caribbean. 1994	E only
42	Calculation of New Depth Equations for Expendable Bathymetographs Using a Temperature-Error-Free Method (Application to Sippican/TSK T-7, T-6 and T-4 XBTs). 1994	E only
43	IGOSS Plan and Implementation Programme 1996-2003.1996	E, F, S, R
44	Design and Implementation of some Harmful Algal Monitoring Systems. 1996	E only
45	Use of Standards and Reference Materials in the Measurement of Chlorinated Hydrocarbon Residues. 1996	E only
46	Equatorial Segment of the Mid-Atlantic Ridge. 1996	E only
47	Peace in the Oceans: Ocean Governance and the Agenda for Peace; the Proceedings of <i>Pacem in Maribus</i> XXIII, Costa Rica, 1995. 1997	E only
48	Neotectonics and fluid flow through seafloor sediments in the Eastern Mediterranean and Black Seas - Parts I and II. 1997	E only
49	Global Temperature Salinity Profile Programme: Overview and Future. 1998	E only
50	Global Sea-Level Observing System (GLOSS) Implementation Plan - 1997. 1997	E only
51	L'état actuel de l'exploitation des pêcheries maritimes au Cameroun et leur gestion intégrée dans la sous-région du Golfe de Guinée (<i>underpreparation</i>)	F only
52	Cold water carbonate mounds and sediment transport on the Northeast Atlantic Margin. 1998	E only
53	The Baltic Floating University: Training Through Research in the Baltic, Barents and White Seas - 1997. 1998	E only
54	Geological Processes on the Northeast Atlantic Margin (8th training-through-research cruise, June-August 1998. 1999	E only
55	Bruun Memorial Lectures, 1999: Ocean Predictability. 2000	E only
56	Multidisciplinary Study of Geological Processes on the North East Atlantic and Western Mediterranean Margins (9th training-through-research cruise, June-July 1999). 2000	E only